Spatially correlated structural disorder phenomena in zinc-rich alloys

Dissertation

zur

Erlangung des Doktorgrades

der Naturwissenschaften

(Dr. rer. nat.)

dem

Fachbereich Chemie

der Philipps-Universität Marburg

vorgelegt von

Partha Pratim Jana

aus Tamluk,India

Marburg/Lahn 2011

This work was carried out from November 2007 to April 2011 at the Department of Chemistry, Philipps University, Marburg under the supervision of Prof. Dr. B. Harbrecht.

Vom Fachbereich Chemie
der Philipps-Universität Marburg als Dissertation am 26.07.2011 angenommen.

Erstgutachter	Prof. Dr. B. Harbrecht
Zweitgutachter	Prof. Dr. W. Massa

Tag der mündlichen Prüfung am 25.08.2011

To my beloved parents and brother

Table of Contents

Page

1 Introduction **1**

2 Experiment **7**

2.1 Starting materials for syntheses 8

2.2 Synthesis 8

2.2.1 Solid state synthesis 8

2.2.2 Flux method 8

2.3 Phase analyses and data processing 9

2.3.1 Powder X-ray diffraction 9

2.3.2 Single crystal X-ray diffraction 10

2.3.3 Energy dispersive X-ray analyses and scanning electron microscopy 11

2.4 Physical properties 12

2.4.1 Thermal analyses 12

2.4.2 Magnetic susceptibility 12

2.4.3 Electrical conductivity 13

3.1 Introduction to the binary system Cr-Zn 15

3.2 Introduction to the binary system Au-Zn 17

3.3 Introduction to the binary system Pd-Zn 19

4 The crystal structure of $CrZn_{17-\delta}$ ($-0.8 \leq \delta \leq 1.7$)-a cluster approach, disorder phenomena and some physical properties **21**

4.1 Introduction 21

4.2 Synthesis and morphological features 23

4.3 Single crystal structure analysis 24

4.4 Phase analyses and physical properties 25

4.5 Structural characteristics 33

4.6 Summary 43

5 Spatially correlated structural disorder phenomena in γ-brass related complex zinc-rich alloys $(M,Cr)Zn_n$, (M = Au, Pd) 45

5.1 Introduction 45

5.2 Spatially correlated structural disorder phenomena in γ-brass related complex zinc-rich alloys (Au,Cr)$Zn_{n;}$ n = 10.2–6.4 48
5.2.1 Introduction 48
5.2.2 Synthesis and morphological features 48
5.2.3 Single crystal structure determination 49
5.2.4 Phase analysis and physical properties 50
5.2.5 Structural characteristics 62
5.2.6 Summary 76
5.3 Spatially correlated structural disorder phenomena in γ-brass related complex zinc-rich alloys (Pd,Cr)$Zn_{n,}$ n = 14.8-12.3 79
5.3.1 Introduction 78
5.3.2 Solid state synthesis 78
5.3.3 Single crystal structure determination 79
5.3.4 Phase analysis and physical properties 80
5.3.5 Structural characteristics 88
5.3.6 Summary 93

6 Structural chemistry of ternary γ-brass type phases in the Au-Pd-Zn system 95
6.1 Introduction 95
6.2 Ternary γ-brass phases in the Au-Pd-Zn system 97
6.2.1 Syntheses and characterization 97
6.2.2 Single crystal structure determination 97
6.2.3 Phase analyses and physical properties 98
6.2.4 Structural characteristics 102
6.2.5 Summary 107
. 6.3 Structural chemistry of ternary γ'-phases in the Au-Pd-Zn system 108
6.3.1 Solid state synthesis 108
6.3.2 Single crystal structure determination 108
6.3.3 Phase analyses and physical properties 109
6.3.4 Structural characteristics 117

6.3.5 Summary 127
7 Spatially correlated structural disorder phenomena in complex zinc-rich alloys (Au,Ru)$Zn_{n;}$ n = 10.7-3.2 129
7.1 Introduction 129
7.2 Synthesis and morphological features 130
7.3 Single crystal structure determination 130
7.4 Phase analysis 131
7.5 Structural characteristics 136
7.6 Summary 147
8 Summary 149
9 Zusammenfassung 154
Appendix 160
References 206

Chapter 1

Introduction

Intermetallic compounds have broad industrial application and richly varied structural chemistry, electronic structures, and physical properties (electronic, magnetic, thermal and mechanical). [1-9] From the very beginning of the civilization, the properties of the metals and the intermetallic compounds have been used, so that these materials were always associated with human culture. In the last 20 years a large number of intermetallic compounds have been synthesized and their study has given much information about structure-property relationship. [3]

Intermetallic compounds are divided into the following three groups:

•The Laves phases are alloys of the composition AB_2 ($r_A < r_B$). They form close-packed structures.

•The Zintl-phase compounds with an electro-positive cation and a polymeric anion.

•The Hume-Rothery phases.

An important component of many intermetallics is the transition element zinc. [10-13] Zinc -rich-phases deserve exceptional chemical interest due to its intricate phase relations and structural complexity.

Hume-Rothery listed four factors of importance regarding the electronic structure of alloys: [14]

(a) the difference between the electronegativities of the two metals,

(b) a tendency for elements near the end of the short periods and B subgroups to complete their octet of electrons and a similar tendency to fill the d shell in later transition elements,

(c) orbital type restrictions in structures with certain type of hybrid bonding and

(d) the formation of definite crystal structures at characteristic e/a ratio. [15]

Hume-Rothery pointed out the importance of e/a ratio in controlling the phase stability and the phase boundaries in brass-like alloys. [16-18] According to Hume-Rothery, brass-like alloys occur at a certain ratio of number of valence electrons to atom (e/a), i.e.

valence electron concentration (*vec*). Such alloys are known as Hume-Rothery alloys or electron compounds. This particular type of intermetallics is formed by noble metals and group 2, 12-15 elements.

In the Cu-Zn system, at different compositions five different phases (i.e. α-, β-, γ-, ε- and η- brass) have been characterized. These phases pass through the intermetallic compounds which are very important to explain the different type of intermetallic compounds. With the increase of addition of Zn (*hcp*) in the *fcc* lattice structure of Cu, the following changes occur gradually.

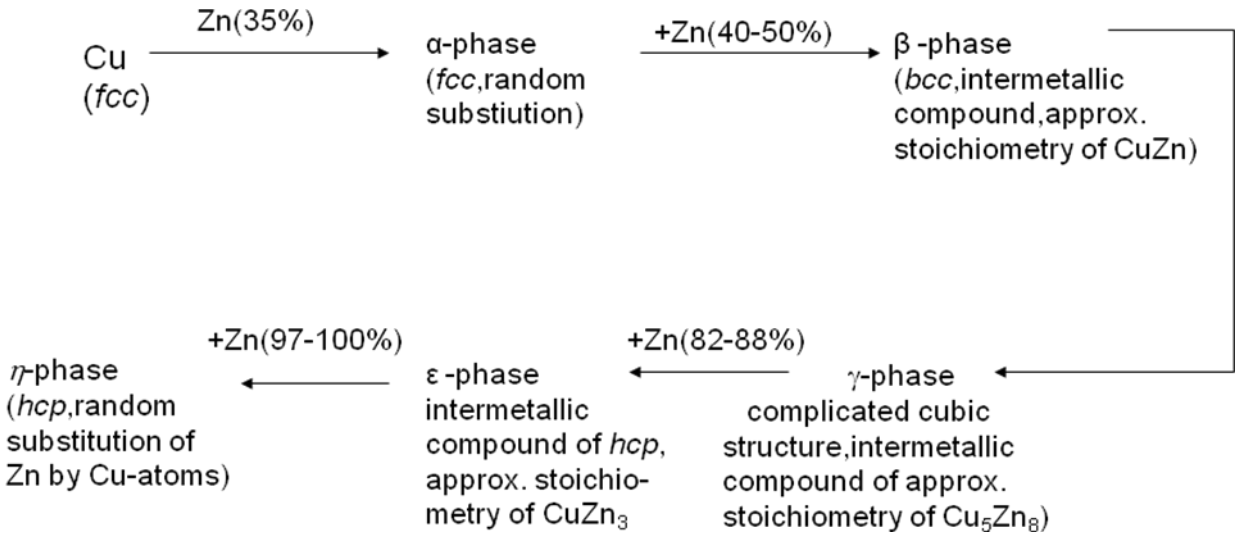

The α- and η-phases are considered as primary solid solutions in the parent metals. [19]

In the Cu-Zn system, β-, γ- and ε- brass phases appear at (e/a) ratios of 21/14, 21/13 and 21/12, respectively. In many other systems of binary alloys similar phases are found. The β-phases CuZn, Cu_3Al and Cu_5Sn adopts the *bcc* W-type structure and stabilized at the ratio of 21/14 (e/a) irrespective of the structural distributions and nature of the components.

In some systems, instead of the β-phase, a complex structure similar to β-manganese [19,20] appears at a ratio 21/14 (e. g.Ag_3Al, [21] CoZn [22]).

The γ-brass phases are regarded as structurally most complex Hume-Rothery phase in the brass-like system. A prominent example of γ-brass is Cu_5Zn_8. [23] It forms a hierarchical structural variant of β-brass like structure and consists of so-called γ-brass cluster (introduced by Bradley and Thewlis) having 26 atoms. [23]

The Hume-Rothery rule was extended by various investigators specially Westgern, Phragmén, Bradley and Thewlis. [24,25] They showed that in the various alloy systems the β-, γ-, ε- phases occur at or near to (e/a) ratios of 21/14, 21/13, 21/12, respectively.

The theoretical significance of the Hume-Rothery rule and the quantum mechanical treatment in the brass-like system has been discussed by Mott and Jones. [26,27]

The Jones theory was the first attempt of the application of quantum mechanics to the mechanism of underlying e/a-scaled stabilization of the crystal structures in the brass-like system. Such stabilization has been explained in terms of a lowering of the kinetic energy of the valence electrons associated with a reduction of density of states at the Fermi level. [15,27,28-32] Such a reduction is expected at a given *vec* value for that type of structure which has energetically favorable flat portions at the Fermi surface, due to the contacts between the free electron Fermi sphere of diameter $2k_F$ with a suitable set of Brillouin zones, characterized by the reciprocal lattice vector K_{hkl}. As a result, the strength of the stabilizing Fermi-Brillouin zone interaction correlates directly with valence electron concentration.

The γ-phases presently attract most attention due to their structural complexity and challenge the understanding of the underlying stabilization mechanism. [33,34] Morton, by electron microscopy studies, revealed that the γ-brass regions of Cu-Zn, [35] Ni-Zn [36] and Pd-Zn [37] do not only accommodate the γ-brass phase but also a bundle of structurally related, complex phases with lower symmetry than that of the γ-phase. These studies showed two types of inversion antiphase domain structures (IAPD), which have a long periodic regular domain structure. Among these two IAPD structures the striped structure has a periodicity of 70 Å. The triangular structure has a periodicity of about 2000 Å (Fig.1.1). Morton showed that a correlation between the length of the longest crystallographic axis and the valence electron concentration

(Fig.1 1 b).The lowering of symmetry is associated with striped dark and light contrast variations occurring along one of the face diagonal direction of the cubic γ-brass type structure. [38] Similar kind of super-structures were also observed in the Al-Cu [39,40] and Al-Cr [41] system.

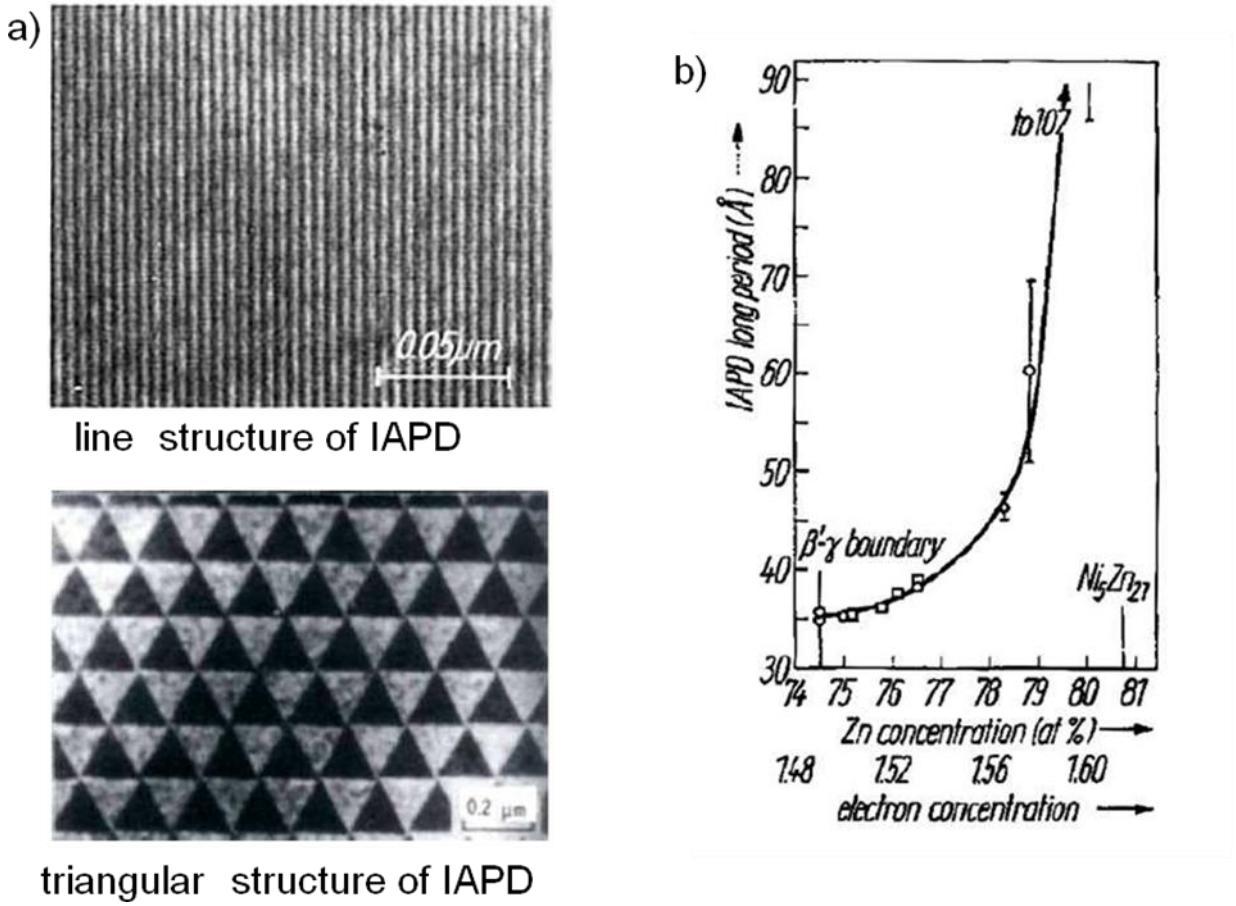

Figure 1.1: a) Top: bright-field image of the planar anti-phase domain structure.
Bottom: dark field image of the triangular IAPD structure. [37]
b) A graph showing the variation of the planar IAPD with composition and with valence electron concentration. [36]

To elucidate the crystal structure of these γ-brass or γ-brass related phases among the complex metallic alloys (CMA), we studied the Cr-Zn binary system. The Cr-Zn binary system has previously been studied by many researchers. [42-51] They identified two phases: $CrZn_{13}$ and $CrZn_{17}$.

We reinvestigated the γ-brass related phase in the zinc-rich part of the Cr-Zn system as a consequence of our investigations on expressions of structural complexity in intermetallic systems. In order to gain an insight into expressions, cause and mechanism and structure-property relationship for such phases, we studied the impact of substitution of chromium and zinc by 2nd or 3rd row transition elements on the evolution of the structure of ternary derivatives of $CrZn_{\sim 17}$.The research performed in this dissertation is the impact of gold or palladium on $CrZn_{\sim 17}$. We have chosen gold or palladium for substitution because of its strong scattering contrast compared to that of chromium and zinc. This fact may permit distinguishing the atomic site of gold or palladium by the results of X-ray diffraction experiment. Comprehensive studies by single crystal X-ray diffraction experiments on several specimens in highly differentiated ternary Au-Cr-Zn and Pd-Cr-Zn alloys reveal the existence, phase width, phase stability and structural characteristics associated with spatial correlation among all kinds of disorders in Zn-rich ternary phases.

To get an insight into the structure-composition-property relationship among complex metal-rich phases, we have also concentrated on ternary or pseudobinary Hume-Rothery-based systems. This work is motivated by the discovery $Pd_{2+x}Zn_{11-x}$ [52,53] phases in the γ-brass region i.e. approximately between 75 and 85 atom % Zn. The zinc-richest phase accommodates the cubic γ-brass structure, but as the Pd concentration increases, these phases show extraordinary periodicities along a single direction that provide approximants to potentially one dimensional quasi-periodic structure. [53,54] On account of these backgrounds, we investigated the gold substituted $Pd_{2+x}Zn_{11-x}$ to understand how substitution of Pd and Zn by Au atoms can influence the structural stability and chemical compositions of γ-brass phases related to $Pd_{2+x}Zn_{11-x}$. No phase has been reported in the Pd-Zn-Au ternary system to date.

Recently, in the Ru-Zn system, $Ru_{21+\delta}Zn_{261-\delta'}$ ($0 \leq \delta \leq 5$ and $0 \leq \delta' \leq 9$), [55] the congener of large hexagonal $FeZn_{10}$ [56] has been structurally identified. In order to get a better understanding into the structure-composition relationship of such phases, we investigated the effect of substitution of ruthenium and zinc by gold on the evolution of the structure of substituted $Ru_{21+\delta}Zn_{261-\delta'}$.

The physical property determination of the synthesized materials was one of the goals of this work. Thermal stability, magnetic properties and electrical properties of the synthesized materials and their variations with composition have been studied.

Chapter 2

Experiment

2.1 Starting materials for syntheses

The starting materials were obtained from commercial sources. The materials with their sources which were used for syntheses are gathered together in the Table 2.1.

Table 2.1: Starting material for the syntheses

Elements	Form	Purity[%]	Source
chromium	pieces	99.995	Alfa, Aldrich
gold	granules	99.99	ABCR
palladium	powder	99.9	ABCR
ruthenium	powder	99.8	ABCR
zinc	granules	99.9999	Chempur

2.2 Synthesis

2.2.1 Solid state synthesis

All the syntheses were carried out in evacuated quartz glass ampoules with an external diameter of 0.8 cm. The samples were prepared from the elements on a 200-300 mg scale. The metals were sealed in previously out-gassed quartz glass ampoules under a reduced argon pressure of 0.5 Pa. The reactions were carried out in a program-controlled electric furnace after setting up the temperature. To avoid eventual loss of zinc due to evaporation, the reactants were kept at a lower temperature than the rest of the ampoule. The samples were finally cooled to ambient temperature either by turning off the furnace or by quenching in a water bath.

2.2.2 Flux method

Flux method is a simple method [57,58] of crystal growth where the components of the desired substance are dissolved in a solvent (flux). Molten metals [59,60] and metal halides [10,61] are used as solvents for the growth of a variety of compounds and exploratory syntheses of new intermetallic materials. It takes place in a crucible made of non-reactive metal such as tantalum, niobium or other non-reactive elements. Crucibles are normally sealed in evacuated quartz glass ampoules or reactions take place in controlled atmosphere furnaces.

A saturated solution is prepared by keeping the constituents of the desired crystal and the flux at a temperature slightly above the saturation temperature long enough to form a complete solution. Then the crucible is cooled in order to cause the desired crystal to precipitate.

The advantages of the flux method are as follows:

-The crystals are grown out of a solvent that reduces the melting temperature of the desired compound.

-Excess flux could be easily removed by dissolving or by applying an external force, such as centrifugation.

-Crystal growth is relatively fast.

A disadvantage is that most flux method syntheses produce relatively small crystals. This method was successfully applied for the syntheses of compounds at the zinc - rich side. Here, excess Zn was used as as self-flux and excess zinc is separated after the completion of the reaction in the form of few tiny ductile globules next to the brittle phase of silvery lustre.

.

2.3 Phase analyses and data processing

2.3.1 Powder X-ray diffraction

All the samples were examined by X-ray powder diffractometry to check the purity of single-phased samples, to determine the adjacent phases and to identify new phases. The powder diffraction patterns were recorded by a X' Pert MPD diffractometer ($Cu_{K\alpha}$ = 1.5406 Å, 40kV, 40mA) made by Philips operating in Bragg-Brentano geometry using a secondary monochromator (Graphite). The powders were evenly distributed in a single crystal silicon plate. All the diffractograms were recorded between $5 < 2\theta < 90^{O}$ at room temperature. The calculation of the theoretical diffraction patterns and the data collection and processing were performed with the X' Pert software package [62]- supplied by the Pan analytical company. The diffraction profiles of single or multiphase samples were quantitatively analyzed by a Rietveld method with use of X' Pert Plus software. Positional parameters as obtained from the single crystal X - ray structure determination were used as starting parameters for the profile fit. The qualities of the refinements were analyzed by a graphically represented difference curve and R-values. The Bragg R-value (R_B) and the unweighted profile R-value (R_P) are used for accuracy of refinement. The weighted profile R-value (R_{wP}) is therefore a measure of the quality of the entire fit. The definition of the R values (residuals) are given as follows

$$R_{\mathrm{B}} = \frac{\sum \left| I_{ko} - I_{kc} \right|}{\sum I_{ko}}$$

$$R_P = \frac{\sum | y_{io} - y_{ic} |}{\sum y_{io}}$$

$$R_{wP} = \sqrt{\frac{\sum w_i (y_{io} - y_{ic})^2}{\sum w_i y^2_{io}}}$$

Here, I_{ko} *and* I_{kc} are the measured and calculated intensities of reflection k, y_{io} and y_{ic} are measured and the calculated intensities, w_i is the weighting factor on a point i of the diffractogram.

2.3.2 Single crystal X-ray diffraction

Single crystal X-ray diffraction method was used for the unknown structures determination and confirmation of structural aspects for known structures. The crystals were selected from a crushed product and then mounted on top of glass fibres capillaries of 0.2 mm diameter using silicon grease. The diffraction intensities of crystals were collected on a Stoe Image Plate Diffraction System, IPDS-I or IPDS-II using graphite monochromated $Mo_{K\alpha}$ radiation (λ = 0.71073 Å) at room temperature. The data collection and processing on the IPDS diffractometer was performed using programs supplied by Stoe [63]:

Expose: [63] For data collection

Cell :[63] To obtain the unit cell dimensions

Integrate : [63] For data reduction

For the structural determination the following programs were used:

XPREP: Cell reduction and determination of possible space groups on the basis of systematic extinctions

SHELX-97 : [64]: For structure solution and refinement

SUPERFLIP : [65]: For structure solution

The measured intensities were corrected for Lorentz and polarization effects and further numerical absorption correction was performed by using the X-SHAPE and X-RED programs. [66,67]

The definition of the R-values (residuals) are given as follows

$$R_1 = \frac{\sum_{hkl} \| F_o | - | F_c \|}{\sum_{hkl} | F_o |}$$

$$wR_2 = \sqrt{\frac{\sum_{hkl} w.(F_o^2 - F_c^2)^2}{\sum_{hkl} w.(F_o)^2}}$$

$$S = \frac{\sum_{hkl} w.(F_o^2 - F_c^2)^2}{m - n}$$

S represents the goodness of fit, where, m = number of reflections, n = number of parameters. The difference m-n gives the overdetermination of the structure. For a correct structure with a suitable weighting scheme, S will have a value close to one. [68]

2.3.3 Energy dispersive X-ray analyses and scanning electron microscopy

A scanning electron microscope (CS-4DV, CAM Scan 20 kV) equipped with an EDS (Energy Dispersive X-Ray Spectroscopy) with SiLi detector (Thermo Noran Instruments, Pt-L, Zn-L) was used to obtain a pictorial representation of the studied objects and to determine the approximate elemental composition of a sample. The analysis was carried out with the Voyager program [69] from Thermo Noran.

2.4 Physical properties

2.4.1 Thermal analysis

Thermo-chemical analyses were performed by employing a differential scanning calorimeter operating in the temperature range 670-1370 K (DSC setsys 16/18 Setaram, Pt/Rh thermocouple). The differential scanning calorimetry is a fingerprint technique that provides information about chemical reactions, phase transitions, and structural changes occurring in a sample during heating and cooling cycles. Usually 30-40 mg samples were pressed to pellets of 0.3 cm in diameter and then placed into small hand-made silica ampoules of external diameter of 0.5 cm. The silica ampoules were sealed under a reduced pressure. The length of the sample container was reduced to ≈ 1.5 cm to suppress incongruent vaporization of Zn. An empty silica container of similar size was used as a reference. The experiments were carried out under argon atmosphere at constant pressure. To ensure reproducibility of the thermal events the experiments were usually repeated twice at heating and cooling rates of 10 K min^{-1}.

2.4.2 Magnetic Susceptibility

The magnetic susceptibility measurements were performed on a SQUID (Superconducting Quantum Interference Device; MPMS, Quantum Design, San Diego) magnetometer from 1.8-330 K at a constant magnetic field (1-5 Tesla). Field dependent measurements were carried out on selected samples between 5 K and room temperature. About 200-300 mg of the substance was used for each measurement. The data were corrected for magnetic contributions from the sample holder manufactured from gelatine.

The molar susceptibilities χ_{mol} of the samples were calculated as follows

$$\chi_{mol} = \frac{M \cdot m_{mol}}{H \cdot \rho} \; m^3 \; mol^{-1}$$

M: magnetic moment [A m^{-1}] ρ: density of the sample [kg m^{-3}]

H: magnetic field [A m^{-1}] m_{mol}: molar weight of the sample [kg mol^{-1}]

Generally, the susceptibility is the sum of different contributions:

$$\chi_{mol} = \chi_{mol}^{para} + \chi_{mol}^{Tip} + \chi_{mol}^{dia}$$

χ_{mol} = molar susceptibility

χ_{mol}^{para} =T – dependent paramagnetic contribution

χ_{mol}^{Tip} =T – independent paramagnetic contribution

χ_{mol}^{dia} =T – independent diamagnetic contribution

2.4.3 Electrical conductivity

The electrical resistance of microcrystalline samples was measured in the temperature range 30-300 K under vacuum using a closed-cycle He cryostat and a temperature controller (Lake Shore). The electrical resistivities were determined by applying a four-point probe method in the d. c. mode. The four Cu wires were attached to a rod-like sample using silver epoxy paste. Contact distances and the cross sectional areas of the rod-like sample were determined using a light microscope. The voltage was measured (Hewlett Packard) at a constant current (Advantest) of 20 m A, respectively.

A constant current I was applied across two electrodes while the potential across the two others was measured. The electrical resistance R can be calculated according to Ohm's law,

$$R = \frac{U}{I}$$

According to this method the resistivity 'ρ' of the sample is a function of the resistance R and the thickness of the sample. The conductivity is the reciprocal of the resistivity,

$$\rho = \frac{U}{I} \cdot \frac{A}{d}$$

Where:

U = Potential difference between the inner electrodes [V]

I = constant current applied between the outer electrodes [A]

A = Area of the sample [m^2]

d = distance between the two inner electrodes [m].

Chapter 3

3.1 An introduction to the binary system Cr-Zn

The Cr-Zn binary system has been studied by many researchers, but, a complete phase diagram over the entire composition range has not yet been established. Only the zinc-rich part of this system is reviewed by Moser and Heldt, [42] showing the existence of two intermetallic compounds $CrZn_{13}$ and $CrZn_{17}$.

The information about $CrZn_{\sim 17}$ was first mentioned by Henry Le Chatelier [43] and was confirmed later by many investigators. [42,44-51] The crystal structure of $CrZn_{17}$ was first proposed by Hanemann [49] to be based on a hexagonal lattice (a = 1.2916 nm and c = 3.0562nm.) which eventually turned out to be correspondence to a rhombohedral setting of a cubic lattice as revealed by $a_o = a_c(2\sqrt{2})$, $b_o = a_c/\sqrt{3}$, $c_o = a_c/2$.

The $CrZn_{13}$ phase was first reported by Hartmann *et al*. [46] The recent review of this binary partial phase diagram developed by Reumont and Perrot [45] included the $CrZn_{13}$ (ζ phase) as an equilibrium phase. However, the stability of $CrZn_{13}$ was questioned by Hansen [70] stating that, the raw Cr material used by Hartmann *et. al*. contain 1.5% Fe which could have altered the outcome of the experiments. In spite of thorough and systematic study, Brown [71] was unable to prepare a substantial quantity of $CrZn_{13}$ for analyses, therefore suggested that $CrZn_{13}$ phase might be metastable. Tang and Yu [44] concluded that the $CrZn_{17}$ phase was the only intermetallic phase in the binary Cr-Zn system after carefully conducted experiments. The list of known structures in the Cr-Zn binary system is summarized in the Table 3.1.1. The phase diagram of the Cr-Zn binary system is shown in Fig. 3.1.1.

Table 3.1.1: Cr-Zn crystal structure data

Phase	Pearson symbol	Space group	Structure type
Cr	*cI*2	*I*m-3m	W
~$CrZn_{13}$	(a)	-	$Zn_{13}Co$
~$CrZn_{17}$	(b)	-	-
Zn	*hP*2	*P*6_3/mmc	Mn

(a) Monoclinic, (b) Hexagonal

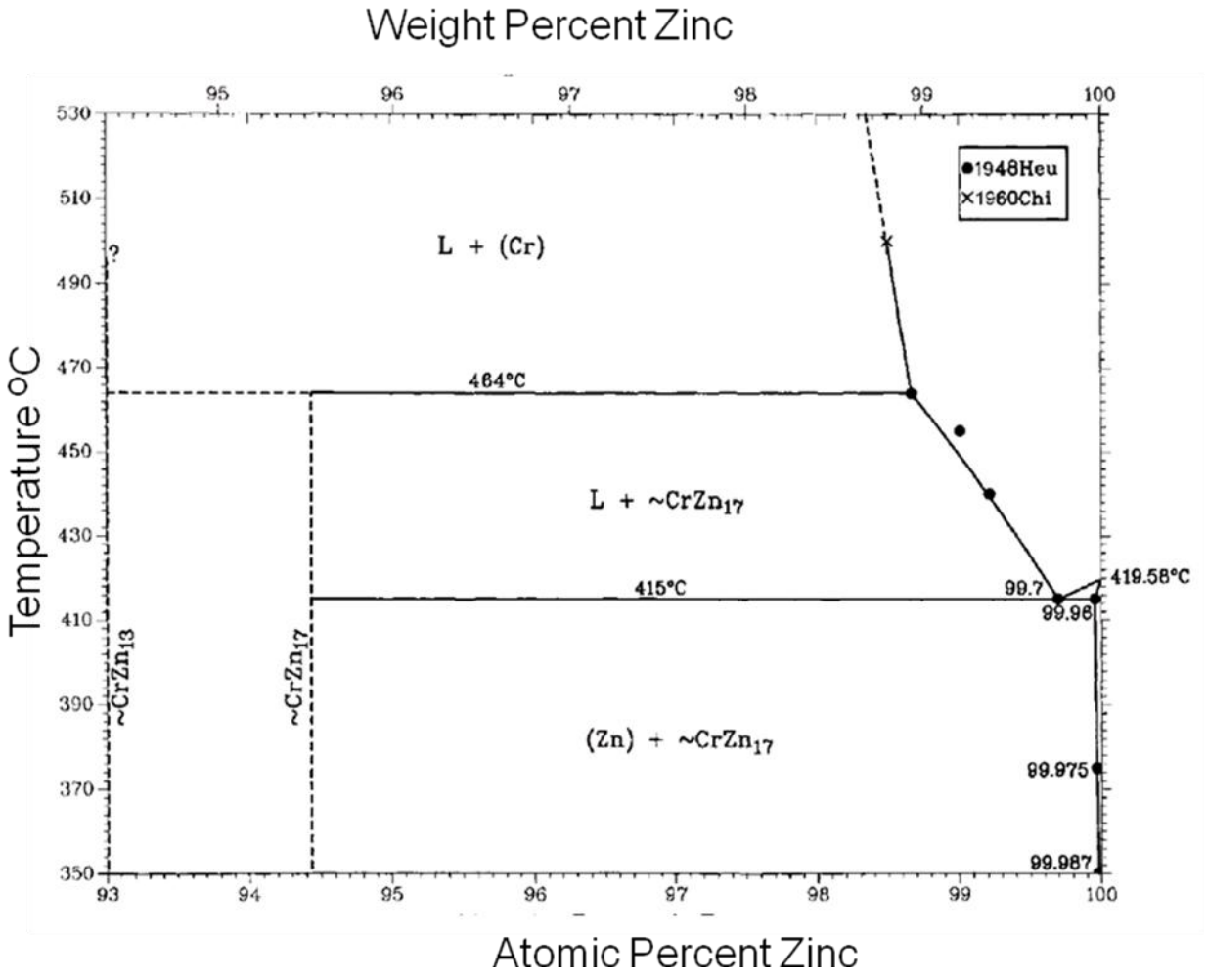

Fig. 3.1.1: Phase diagram of the Zn-rich part of the Cr-Zn system [1992 Mos].

3.2 An introduction to the binary Au-Zn system

The phase diagram of the Au-Zn binary system was reviewed by Okamoto and Massalski [72] based on the reported phase boundaries from different sources. [73–77] Several intermetallic phases in this system are reported [78-89]. Structures of these phases are listed in the Table 3.2.1 and details of the boundaries of these phases are available in the phase diagram (Fig. 3.2.1) by Okamoto and Massalski [72]. New data were reported by Prasad *et al*., [90] and Ipser and Krachler, [91] and Liu *et al*. [92]

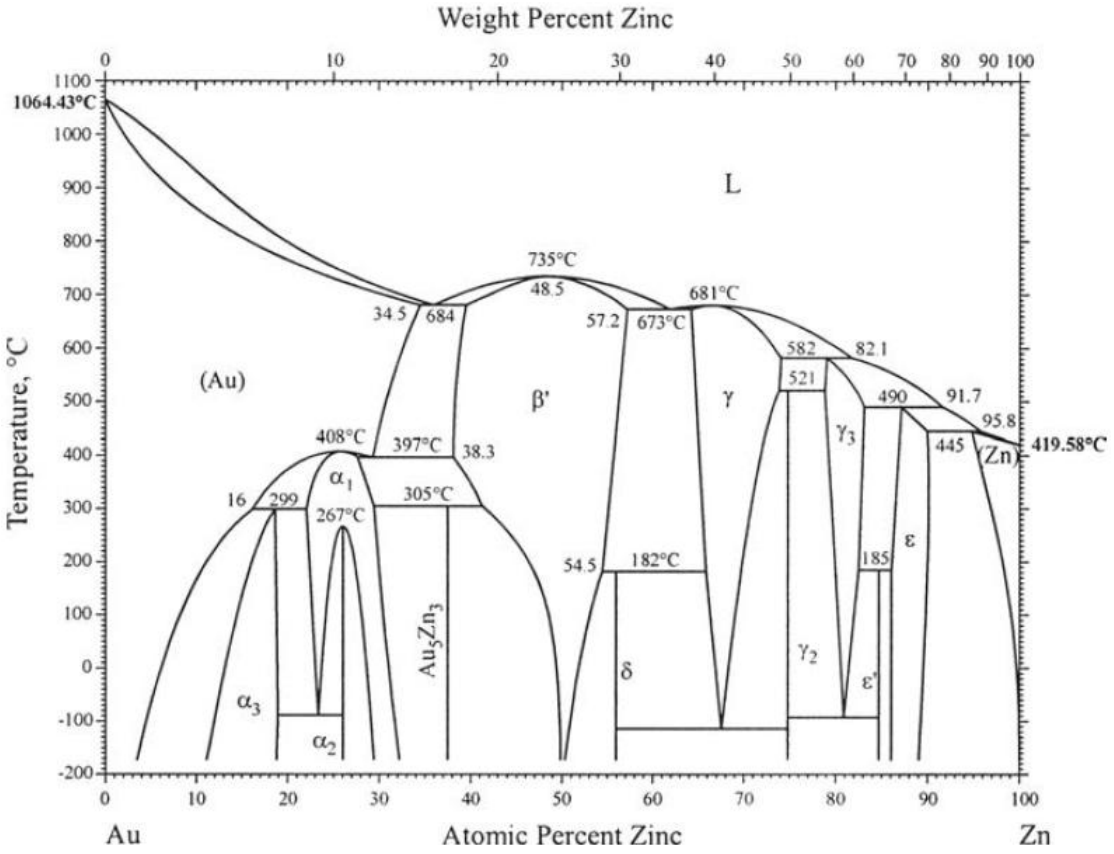

Fig. 3.2.1: Au-Zn Phase diagram [Okamoto & Massalski]

Table 3.2.1: Au-Zn crystal structure data

Phase	Pearson symbol	Space group	Structure type
Au	*cF*4	*F*m-3m	Cu
$Au_{3.25}Zn_{0.75}$ [78]	*oP*96	*P*nmn	Cu_3Pd
$Au_{0.78}Zn_{0.22}$ [79]	*cF*4	*F*m-3m	Cu
Au_3Zn [78]	*oS*32	*C*mce	-
Au_3Zn [78,81]	*tI*64	$I4_1$/acd O2	Ag_3Mg
Au_5Zn_3 [80]	o*I*128	*I*bam	-
AuZn [82-87]	*cP*2	*P*m-3m	CsCl
$AuZn_3$ [75,88]	*cP*32	*P*m-3n	UH_3
$Au_{0.12}Zn_{0.88}$ [75]	*hP*2	$P6_3$/mmc	Mg
$Au_{0.05}Zn_{0.95}$ [89]	*hP2*	$P6_3$/mmc	Mg
$Au_{0.04}Zn_{0.96}$ [75]	*hP*2	$P6_3$/mmc	Mg
Zn	*hP*2	*P*6_3/mmc	Mg

3.3 An introduction to the binary Pd-Zn system

Experimental work to clear up the phase equilibria has been done by Köster *et al*. [93] and Nowotny *et al*. [94] (thermal analysis, metallographic observations, X-ray diffractography). Alasafi *et al*. [95] have identified a metastable phase $PdZn_2$. All the results from the above mentioned investigations have been taken by Massalski [96] to construct a phase diagram (Fig. 3.3.1).

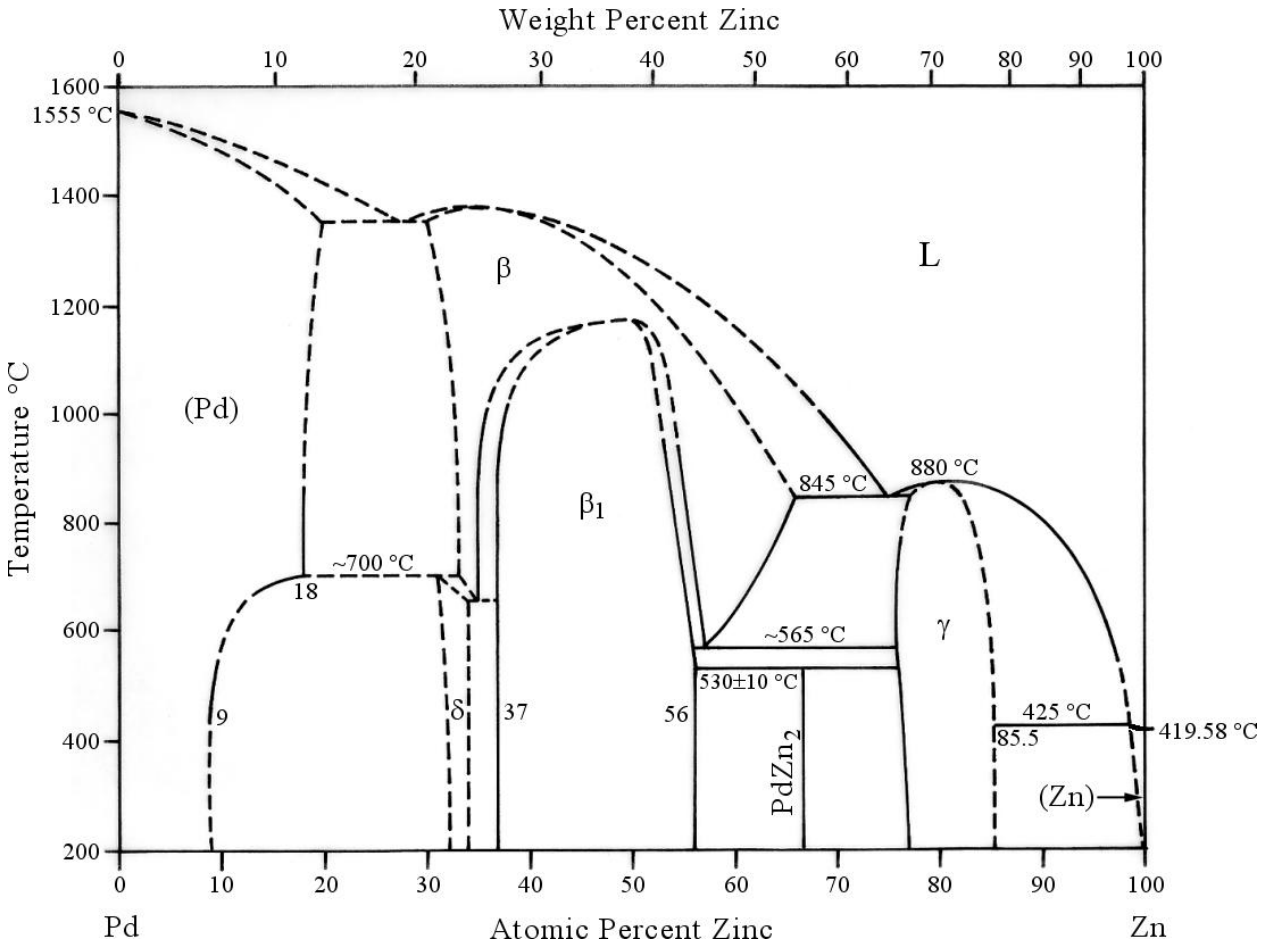

Figure 3.3.1: Phase diagram for the Pd-Zn system according to Massalski.[96]

A series of γ-brass related structure in the Zn-rich portion of the Zn-Pd phase diagram is investigated by single-crystal diffraction method. Single-crystal X-ray diffraction allowed for the identification for six phases in $Zn_{1-x}Pd_x$ ($0.15 < x < 0.25$) with zinc concentration

ranging from approximately 75% to 85. [53,97] Among these six phases, two structures formulated as $Zn_{81.9(6)}Pd_{18.1}$ (an alternative formulation-$Pd_{2.35}Zn_{10.65}$) and $Zn_{75.7(7)}Pd_{24.3}$ have been fully refined using the conventional space groups, *I*-43m and *C*mce, respectively. [53] They correspond to the limiting composition of the γ-brass region of the Pd-Zn phase diagram but show distinctly different crystal structures. The phase richest in zinc adopts the cubic γ-brass structure, but as the Pd content increase, these phase show extraordinary periodicity along a single direction that provides approximants to potentially one-dimentional quasi-periodic structures. [53,54,98] Recently some of these complex structures were solved by superspace group strategies. [99] The list of known structures in the Pd-Zn binary system are summarized in the Table 3.3.1.

Table 3.3.1: Pd-Zn crystal structure data

Phase	Pearson symbol	Space group	Structure type
Pd	*cF*4	*F*m-3m	Cu
$Pd_{0.82}Zn_{0.18}$ [94]	*cF*4	*F*m-3m	Cu
Pd_2Zn [102]	*oP*12	*P*nma	Co_2Si-b
PdZn [86,100,101]	*tP*2	*P*4/mmm	CuTi
$Pd_{0.8}Zn_{1.2}$ [94]	cP2	P*m-3m*	CsCl
$Pd_{2.67}Zn_{5.33}$ [95]	*hP*2	*C*mmm	-
$Pd_{2.35}Zn_{10.65}$ [53,52,94]	*cI*52	*I*-43m	Cu_5Zn_8
$Pd_{24.3}Zn_{75.7}$ [53]	*oC*276	*C*mme	-
Zn	*hP*2	$P6_3/mmc$	Mg

Chapter 4

The crystal structure of $CrZn_{17-\delta}$ ($-0.8 \leq \delta \leq 1.7$)-a cluster approach, disorder phenomena, and some physical properties

4.1 Introduction

Cr-Zn alloy coatings are of particular interest in hot-dip galvanizing of steel due to the higher corrosion resistance at reduced thickness, in comparison to that of pure zinc. [103-106] Corrosion protective properties of the coatings are closely related to phase's composition. Several important characteristics, such as formability, [107] adhesion to the substrate, [108,109] and hardness [105] demand the necessity of the determination of the crystal structure and spatial distribution of phases within the coating.

Productive approaches to the rationalization of the structural chemistry of a fairly large group of intermetallics hark back to Hume-Rothery's recognition that the average number of valence electrons per atom, also termed valence electron concentration (*vec*), is the decisive factor, both for the sequence of phases and the structural outcome in valence electron-poor intermetallic systems with $1 < vec < 2$. [16,18] The most complicated structures are found for *vec* values close to 21/13. They are accommodated in and close to the γ-phase field of brass-like systems. The most prominent example of γ-brass is Cu_5Zn_8. It forms a hierarchical structural variant of β-CuZn and consists of so-called γ-clusters having 26 atoms. [110,111] Note that the term cluster used in this context merely expresses the spatial arrangement of prudently chosen groups of atoms which are considered to be useful for unravelling complicated

intermetallic structures often containing hundreds of atoms in the unit cell. That such a partitioning of crystal structures can become a mind-provoking task has been repeatedly demonstrated, e.g., in efforts to uncover relations between distinct complex intermetallic structures each of which-at first glance-appears to be unique. [112] Other illustrative examples are the structures of quasicrystals, [113] approximants, [114] and particular complex alloys [115-119] with up to > 23 000 atoms per unit cell. [120]

A multitude of intermetallic systems accommodate γ-brass-type and/or structurally related phases. The γ-cluster is built up by four atomic shells: an inner tetrahedron (IT), an outer tetrahedron (OT), an octahedron (OH) and a distorted cuboctahedron (CO) and complies with discrete quadruples of distorted icosahedra about IT atoms enclosing a common IT, then also called Pierce cluster. [121] A similar, yet expanded cluster consisting of 34 atoms forms a quadruple of icosahedra about the OT atoms. Each of the four icosahedra shares with an enclosed IT one of its faces. Clusters of this size partially interpenetrate. [122] Several variations of γ- and γ-related structures have been reported:

(i) Electronic distortions or specific chemical ordering in the shells can be associated with a reduction of rotational symmetry from c*I* to h*R* or translation symmetry from cI to cP. Examples are $Al_5Cu_{8,}$ [123] Al_8Cr_5, [124] and Ir_7Zn_{19}. [125]

(ii) Significantly, more complex and modulated structures of some Cd-, [126] and Zn-rich phases [99] have recently been revealed. Their lattice parameters are metrically related according to $a_o = a_c$, $b_o = \sqrt{2}\, a_c$, $c_o = 1/3\ n\ a_c$ with n = 5, 8, 13, 18, 21, 31 bearing a close resemblance to the respective cubic γ-brass-type phase with lattice parameter a_c. [38]

(iii) Further modifications are known, giving rise to the formation of 2a x 2a x 2a superstructures. They usually have $F\bar{4}3m$ space group symmetry and contain 392-448 atoms per unit cell. These structures can be partitioned into four distinct clusters, each arranged according to the motif of a cubic close packed arrangement. The motifs are shifted relatively to each other like atoms and octahedral and tetrahedral voids in fcc Cu.

On account of these backgrounds, we reinvestigated the γ-brass related phase of composition $CrZn_{17-\delta}$ ($-0.8 \leq \delta \leq 1.5$) in the zinc rich part of the Cr-Zn system as a consequence of our investigations on expressions of structural complexity in intermetallic system. Single crystal X-ray diffraction studies of various samples throughout the homogeneity range of the phase reveals a relation among occupation of disordered sites and essential structural characteristics associated with the variation of the valence electron concentration in a structurally complex Hume-Rothery phase.

4.2 Synthesis and morphological features

$CrZn_{17-\delta}$ is accessible in a reactive flux from the elements in previously evacuated quartz glass ampoules under autogenously generated Zn pressure in the temperature range 695-740 K, i.e. above the melting point of Zn and below the decomposition temperature of $CrZn_{17-\delta}$. Crystals were grown by slow cooling of the melt over a period of 8 d.

The samples were prepared from the elements, chromium: 99.995% (Aldrich); zinc: 99.9999% (Chempur) on a 200-300 mg scale. The metals were sealed in small, previously out-gassed fused silica ampoules (length: 3 cm, diameter: 0.8 cm) under a reduced argon pressure of about 0.5 Pa. The molar fraction x_{Cr} of the mixtures was systematically varied between 0.03 and 0.08. The ampoules were heated up to 1273 K at a rate of 200 K h^{-1}, kept at this temperature for 2 h, then cooled down to 703 K during a period of 4 h (142.5 K h^{-1}), and eventually annealed at this temperature for 5 days. Hereafter, the samples were quenched either in cold water or cooled to room temperature. Zinc loss due to vaporization was essentially suppressed by keeping the volume of the reaction container small and by placing the starting materials at the less hot side of the tube. Samples richer in Zn than $CrZn_{17-\delta}$ contained excess zinc in form of few tiny ductile globules next to the brittle binary phase of silvery lustre. In some cases, crystals of hexagonal, plate-like shapes are formed (c.f. Fig. 4.1).

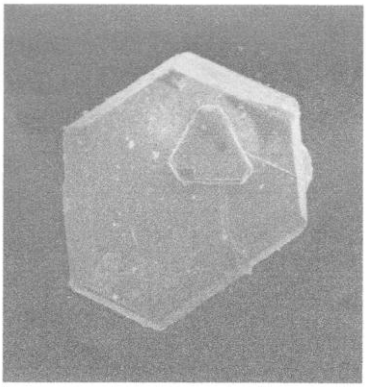

Figure 4.1: Scanning electron micrograph of a regular form crystal of $CrZn_{17.00}$.The size of the crystal is 309x276 μm.

4.3 Single crystal structure analysis

In order to get reliable information about the homogeneity range of the γ-brass related zinc-rich phase, four distinct single crystals ranging from $0.03 \leq x_{Cr} \leq 0.08$ were studied by means of single crystal X-ray diffraction. Crystal 1 (C1) was selected from the sample richest in chromium having nominal composition $x_{Cr} = 0.08$ and crystal 3 (C3) from a samples containing zinc droplets as a minor component. Crystal 2 (C2) with medium Zn-content was taken from a sample with nominal composition $x_{Cr} = 0.05$. The diffraction intensities were measured with an imaging plate diffraction system (IPDS, Stoe, Cie $Mo_{K\alpha}$, graphite monochromator). [63] The intensities could conclusively be indexed on the basis of a 1.8 nm large *F*-centred cubic unit cell. The data sets were corrected for Lorentz and polarization effects. A numerical absorption correction based on the size and shape of the crystal was applied to the data. [66,67] The structure was solved in the acentric space group $F\bar{4}3m$ (216) by applying direct methods and refined by minimizing differences in F^2 with a full-matrix least-square algorithm. [64] The possible positions of missing zinc atoms were taken from difference Fourier synthesis maps. At this stage the structure refinement converged at $R(F) = 0.15$. Further improvement of the calculations was achieved by partially replacing chromium for zinc on those Zn sites which showed higher displacement parameters with respect to normal in a first step,

assuming those sites to be fully occupied. On the other hand metal sites exhibiting conspicuously large displacement parameters were checked for partial occupancy and positional disorder. Atoms for which the refined occupancy factors deviated by less than twice the standard from unity were reset to unity in the final refinement cycles. Local structural disorder phenomena were recorded by introducing split positions. All disordered sites were refined with uncoupled occupation parameters except those which were assumed to be partly occupied by both components for reasons of good match between the starting composition and EDS analyses on one side and the composition as determined by diffraction on the other side. Each structure was checked for possible twinning by inversion and its absolute configuration. Anisotropic displacement parameters of the atoms were taken into account except for those at few positional disordered sites. The final refinement including an extinction correction and a proper weighting scheme yields R(*F*) values between 0.038 and 0.047. Details concerning the data collection, atomic coordinates, equivalent isotropic displacement parameter and anisotropic displacement parameters are listed in the Table 4.1, 4.2 and 4.3. Further details of the crystal structure determination are given in the appendix (A2, A3 and A4).

4.4 Phase analyses and physical properties

The homogeneity range of $CrZn_{17-\delta}$ was studied by means of preparative methods, X-ray diffraction and calorimetric measurements. Single crystal X-ray structure and EDS analyses are essentially in accord with the previously postulated composition $CrZn_{17}$, [47-49] though the phase definitely exhibits a discernible homogeneity range extending over the range $0.053 \leq x_{Cr} \leq 0.062$, i.e., from $CrZn_{15.3}$ to $CrZn_{17.8}$. In spite of the weak scattering contrast between Cr and Zn, the composition determined by X-ray diffraction agrees acceptably with the results of 24 EDS analyses from crystals of the Cr- and Zn-rich phase boundaries, $CrZn_{15.9(1.5)}$ and $CrZn_{17.8(6)}$.

Table 4.1: Crystallographic and technical data for the single crystal structure refinement for $CrZn_{15.34}$ (C1), $CrZn_{17.50}$ (C2), $CrZn_{17.81}$ (C3)

chemical formula	$Cr_{1.54}Zn_{23.62}$(C1)	$Cr_{1.36}Zn_{23.79}$(C2)	$Cr_{1.33}Zn_{23.69}$(C3)
Pearson symbol	*cF*402.6	*cF*402.4	*cF*400.3
x_{Cr}	0.0612	0.0540	0.0532
crystal system; space group type; Z	cubic; $F\bar{4}3m$ (No.216); 16		
a/pm[a]	1824.90(10)	1828.46(2)	1828.50(10)
V/10^6 pm^3 [a]	6077.4(6)	6113.0(1)	6113.4(6)
ρ_{calcd}/g cm^{-3}	7.102	7.067	7.031
μ/mm^{-1}	37.495	37.412	37.233
crystal color	silvery with metallic luster		
data collection			
crystal size/mm^3	0.12x0.10x0.08	0.10x0.10x0.08	0.08x0.06x0.04
diffractometer	IPDS (Stoe & Cie.)		
radiation	$Mo_{K\alpha}$		
monochromator	Graphite		
distance crystal-IP/mm	40	80	70
T/K	293(2)	293(2)	293(2)
φ_{min}-φ_{max}/^{o}	0-210	0-180	0-180
$\Delta\varphi$	1	1	1
$2\theta_{max}$/^{o}	65.9	63.64	64.92
reflns measured	22908	18492	19756
index range	-27≤*h*≤27 -26≤*k*≤27 -27≤*l*≤27	-26≤*h*≤27 -27≤*k*≤27 - 27≤*l*≤27	-27≤*h*≤27 -27≤*k*≤27 -27≤*l*≤27
completeness of data set	0.997	1.000	0.997
Data reduction/ absorption correction	IPDS-Software,[63] X-RED[66]/numerical, X-SHAPE[67]		
unique reflns	1185	1086	1146
R_{int}	0.1814	0.1349	0.0708
structure solution, refinement			
structure solution	direct methods, SHELXS-97[64]		
structure refinement	full-matrix least squires on F^2 (SHELXL-97[64])		
no. reflns used	1185	1086	1146
no. variables	82	80	80
observed reflns (F_o>4σ(F_o))	829	831	1034
R(*F*) (F_o>4σ(F_o))	0.0388	0.0461	0.0348
R(*F*) (all data)	0.0694	0.0695	0.0411
weighting factor k_1/k_2 [b]	0.0215/0	0.0269 /0	0.0226/141.5312
wR (F^2)(all data)	0.0697	0.0696	0.0630
GOF (F^2)	0.970	0.926	1.096
extinction coefficient	0.000009(3)	0.000035(3)	0.000031(4)
$\Delta\rho_{min}/\rho_{max}$/10^{-6}epm^{-3}	-1.545/1.628	-1.449/1.142	-1.093/1.766

[a] Parameters determined by use of powder diffraction data.[b] Weighting scheme: $1/\omega=\sigma^2(F_O^2)+(k_1.P)^2+k_2.P$ with $P = ⅓(\max(F_O^2,0) + .2F_c^2)$.

Table 4.2: Structural data for $CrZn_{15.34}$ (C1), $CrZn_{17.50}$ (C2), $CrZn_{17.81}$ (C3)

Cluster	Atom	Site		*x*	*y*	*z*	SOF	*U*eq[a]/pm^2
Z(1)	Zn10	4a	CC	0[b]	0	0	0.64(3)	150(2)
							0.78(3)	180(2)
							0.85(2)	168(14)
	Zn11	16e	IT	0.0532(3)	*x*	*x*	0.332(14)	280(3)
				0.0527(5)			0.245(14)	290(4)
				0.0524(5)			0.140(10)	260(5)
	M12	16e	OT	0.91560(8)	*x*	*x*	0.68(4)	122(8)
				0.91533(8)			0.89(5)	142(9)
				0.91541(6)			0.92(3)	138(5)
	Zn13	24f	OH	0.16462(19)	0	0	1	372(6)
				0.16280(19)				337(6)
				0.16090(13)				290(4)
	Zn15	48h	CO	0.15505(8)	*x*	0.02187(9)	1	270(3)
				0.15456(8)		0.02279(10)		259(4)
				0.15387(6)		0.02359(7)		270(3)
Q(2)	Cr20	4c	CC	1/4	1/4	1/4	0.90	60(2)
							1	115(14)
								82(7)
	Zn21	48h	IT	0.3211(2)	*x*	0.3491(4)	0.246(8)	350(4)
				0.3216(2)		0.3489(3)	0.240(8)	220(3)
				0.32152(17)		0.3486(2)	0.250(6)	249(19)
	Zn22	16e	OT	0.16565(9)	*x*	*x*	0.919(13)	258(9)
				0.16624(11)			0.893(16)	319(13)
				0.16650(8)			0.855(12)	329(9)
	Zn23	24g	OH	0.0935(4)	1/4	1/4	0.43(2)	250(3)
				0.0947(6)			0.34(3)	270(4)
				0.0947(5)			0.266(17)	270(3)
	Zn23´	48h	OH´	0.2224(4)	*x*	0.3918(4)	0.238(11)	320(3)
				0.2215(4)		0.3907(4)	0.248(12)	330(3)
				0.2226(3)		0.3910(3)	0.254(8)	330(2)
	Zn23´´	48h	OH´´	0.2759(11)	*x*	0.1101(12)	0.062(9)	170(8)
				0.2743(9)		0.1095(9)	0.114(13)	260(6)
				0.2741(4)		0.1102(5)	0.135(8)	200(3)
	Zn25	48h	CO	0.07511(9)	*x*	0.26490(9)	1	326(4)
				0.07460(9)		0.26468(9)		291(4)
				0.07422(6)		26436(6)		271(3)
H(3)	Zn30	4c	CC	1/2	1/2	1/2	1	242(12)
								211(13)
								223(8)
	Zn32	16e	OT	0.41220(8)	*x*	*x*	1	205(5)
				0.41190(9)				200(6)
				0.41182(6)				188(4)
	Zn34	48h	CO	0.04839(6)	*x*	0.65291(10)	1	209(3)
				0.04848(6)		0.65252(10)		199(3)
				0.04846(4)		0.65250(7)		194(2)
	Zn35	16e	OT	0.19130(6)	*x*	0.51724(8)	1	220(3)
				0.19168(7)		0.51642(9)		217(4)
				0.19194(5)		0.51616(6)		210(2)
T(4)	Cr42	16e	OT	0.64857(10)	*x*	*x*	1	98(5)
				0.64815(11)				105(6)
				0.64839(7)				97(4)
	Zn43	24g	OH	0.64337(11)	1/4	1/4	1	174(4)
				0.64284(12)				175(4)
				0.64286(8)				164(3)
	Zn45	48h	CO	0.10583(6)	*x*	0.77706(8)	1	229(3)
				0.10547(7)		0.77681(9)		231(4)
				0.10537(5)		0.77702(6)		215(2)

[a] *U*eq is defined as one third of the trace of orthogonalized U_{ij} tensor, [b] structural data given in the top, middle and bottom lines refer to crystal C1, C2 and C3, respectively, [c] SOF(Zn), SOF(Cr)=1-SOF(Zn).

4.3: Anisotropic thermal displacement parameters

Table 4.3.1: Anisotropic thermal displacement parameters U_{ij} (pm^2) for $CrZn_{15.34}$ (C1)

Atom	U_{11}	U_{22}	U_{33}	U_{23}	U_{13}	U_{12}
Zn10	150(2)	U_{11}	U_{11}	0	0	0
Zn11	280(3)	U_{11}	U_{11}	30(2)	U_{23}	U_{23}
M12	122(8)	U_{11}	U_{11}	0(5)	U_{23}	U_{23}
Zn13	652(19)	232(7)	U_{22}	31(9)	0	0
Zn15	283(5)	U_{11}	244(7)	-76(5)	U_{23}	67(6)
Cr20	60(2)	U_{11}	U_{11}	0	0	0
Zn21	320(3)	U_{11}	400(5)	-200(3)	U_{23}	20(2)
Zn22	258(9)	U_{11}	U_{11}	-25(7)	U_{23}	U_{23}
Zn25	386(6)	U_{11}	206(8)	80(5)	U_{23}	160(8)
Zn30	242(12)	U_{11}	U_{11}	0	0	0
Zn32	205(5)	U_{11}	U_{11}	19(6)	U_{23}	U_{23}
Zn34	156(4)	U_{11}	315(8)	1(3)	U_{23}	-51(5)
Zn35	222(4)	U_{11}	218(7)	4(4)	U_{23}	11(6)
Cr42	98(5)	U_{11}	U_{11}	-3(6)	U_{23}	U_{23}
Zn43	174(9)	174(6)	U_{22}	-57(7)	0	0
Zn45	272(5)	U_{11}	145(6)	46(4)	U_{23}	31(6)

Table 4.3.2: Anisotropic thermal displacement parameters U_{ij} (pm^2) for $CrZn_{17.50}$ (C2)

Atom	U_{11}	U_{22}	U_{33}	U_{23}	U_{13}	U_{12}
Zn10	180(2)	U_{11}	U_{11}	0	0	0
Zn11	290(4)	U_{11}	U_{11}	50(3)	U_{23}	U_{23}
M12	142(9)	U_{11}	U_{11}	-18(6)	U_{23}	U_{23}
Zn13	561(18)	225(8)	U_{22}	52(10)	0	0
Zn15	281(5)	U_{11}	213(8)	-87(5)	U_{23}	70(7)
Cr20	115(14)	U_{11}	U_{11}	0	0	0
Zn21	230(3)	U_{11}	220(4)	-97(19)	U_{23}	-10(2)
Zn22	319(13)	U_{11}	U_{11}	-47(9)	U_{23}	U_{23}
Zn25	338(6)	U_{11}	199(9)	75(5)	U_{23}	107(8)
Zn30	211(13)	U_{11}	U_{11}	0	0	0
Zn32	200(6)	U_{11}	U_{11}	5(7)	U_{23}	U_{23}
Zn34	153(4)	U_{11}	290(9)	10(4)	U_{23}	-51(5)
Zn35	213(5)	U_{11}	226(8)	7(5)	U_{23}	18(6)
Cr42	105(6)	U_{11}	U_{11}	-28(7)	U_{23}	U_{23}
Zn43	172(11)	176(6)	U_{22}	-55(8)	0	0
Zn45	276(5)	U_{11}	141(7)	40(4)	U_{23}	17(7)

Table 4.3.3: Anisotropic thermal displacement parameters U_{ij} (pm^2) for $CrZn_{17.81}$ (C3)

Atom	U_{11}	U_{22}	U_{33}	U_{23}	U_{13}	U_{13}
Zn10	168(14)	U_{11}	U_{11}	0	0	0
Zn11	260(5)	U_{11}	U_{11}	50(4)	U_{23}	U_{23}
M12	138(5)	U_{11}	U_{11}	-6(4)	U_{23}	U_{23}
Zn13	446(11)	212(5)	U_{22}	52(10)	0	0
Zn15	284(4)	U_{11}	241(5)	-100(4)	U_{23}	96(5)
Cr20	82(7)	U_{11}	U_{11}	0	0	0
Zn21	245(19)	U_{11}	260(3)	-116(13)	U_{23}	18(14)
Zn22	329(9)	U_{11}	U_{11}	-81(6)	U_{23}	U_{23}
Zn25	315(4)	U_{11}	182(5)	58(3)	U_{23}	99(8)
Zn30	223(8)	U_{11}	U_{11}	0	0	0
Zn32	188(4)	U_{11}	U_{11}	4(4)	U_{23}	U_{23}
Zn34	151(3)	U_{11}	281(6)	7(3)	U_{23}	-51(4)
Zn35	210(3)	U_{11}	210(5)	2(3)	U_{23}	8(4)
Cr42	97(4)	U_{11}	U_{11}	-16(4)	U_{23}	U_{23}
Zn43	165(7)	163(4)	U_{22}	-44(5)	0	0
Zn45	256(3)	U_{11}	132(4)	42(3)	U_{23}	13(4)

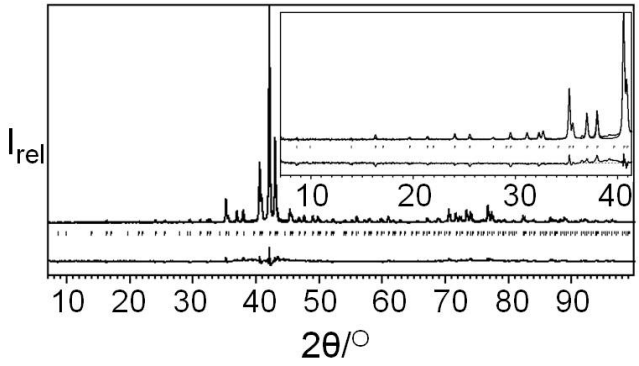

Figure 4.2: X-ray powder diffractogram of $Cr_{1.36}Zn_{23.79}$ (x_{Cr} = 0.0540) together with the profile fit, the difference spectrum and the Bragg positions. Insert shows low angle Rietveld profile fit; $Cu_{K\alpha,}$ a = 1828.46 (2) pm; R_B = 0.0628, R_P = 0.0974.

All samples were examined by use of X-ray powder diffractometer (X´PERT MPD, Philips). The diffraction patterns were quantitatively analyzed by the Rietveld method. [62,127,128] Positional parameters as obtained from single crystal X-ray structure determination were used as starting parameters for the profile fit. The lattice parameters listed in the Table 4.1 were determined from three diffractograms of samples close to the chromium-rich (x_{Cr} = 0.061) and zinc-rich (x_{Cr} = 0.053 and 0.054) phase boundaries, respectively. Relevant data concerning the refinement are given in the figure (Fig. 4.2)

caption. The residuals for the final refinement cycles affirm single phase products and the plausibility of the structures.

Thermal analyses and subsequent XPRD measurements confirm [45, 48] that the phase melts incongruently according to, e.g., $CrZn_{17.5}$ (s) → Cr (s) + 17.5 Zn (l) at 743 K (onset, maximum: 757 K), c.f. Fig. 4.3. The decomposition temperature changes barely with composition: $CrZn_{15.3,}$ the phase at the Cr-rich boundary, was found to melt at 745 K. A pre-melting feature evolving at approx. 702 ± 3 K showed up in DTA runs of differently composed samples. We suggest that this thermal effect is associated with a discontinuous increase of structural disorder upon heating prior to melting, yet a proof is still lacking. Recrystallization of $CrZn_{17-\delta}$ appears to be kinetically inhibited at the chosen cooling rate of 10 K min^{-1}. The shift of the exothermic effect to 682 K upon cooling is due to solidification of Zn (T_m = 693 K). The phase forms again after annealing at 723 K for 30 min.

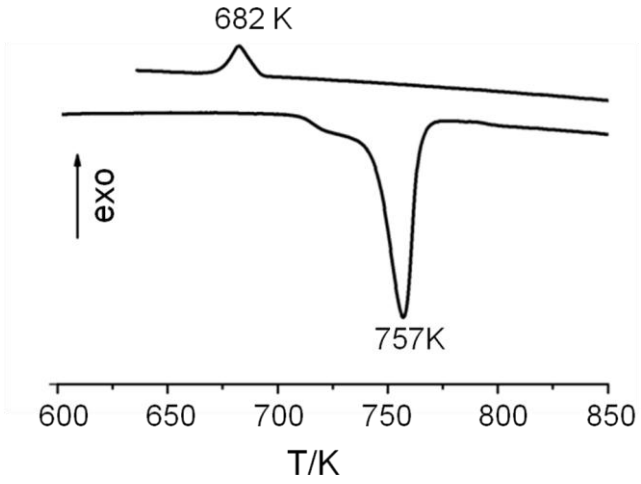

Figure 4.3: Thermo-chemical analysis of $Cr_{1.36}Zn_{23.79}$ (x_{Cr} =0.0540). Shown is the thermal stability ranges of cubic γ-brass related phase in the Cr-Zn binary system.

According to the graphs of the susceptibility-temperature product χT versus T and 1/χ versus T (Fig. 4.4), $CrZn_{17-\delta}$ is essentially a Pauli paramagnet-in spite of its richness in zinc [122,129,130] A positive temperature independent molar susceptibility χ_{TIP} varies

between 5.50(1) and 5.20(2) 10^{-11} m^3mol^{-1} (c.f. Table 4.4). Moreover, an additional T-dependent paramagnetic contribution is indicated by a slight hyperbolic increase of the susceptibility with decreasing temperature. Opposed to the T-independent part of the susceptibility, the T-dependent contribution alters significantly with composition, both with respect to the value of the effective magnetic moment and the Weiss temperature(Θ). If we attribute the localized magnetic moment exclusively to Cr we obtain 0.11(1) μ_B, Θ = -41(2) K for $CrZn_{15.3}$ and 0.16(1) μ_B, Θ = -84(2) K for $CrZn_{17.8}$. Although we hesitate to give an interpretation for the quantities of the moments and Weiss temperature, we conclude that the temperature dependent part of the susceptibility of $CrZn_{17-\delta}$ may be used as a sensitive measure of the Cr content. Magnetisation measurements at constant temperature and variable field disclosed a weak non-linear behaviour, also at ambient temperature. The cause of the small hysteretic effect shown in the insert of Fig. 4.4 needs additional clarification.

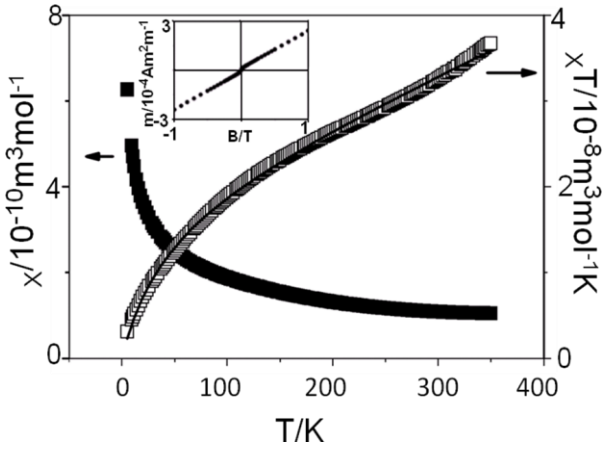

Figure 4.4: Magnetic susceptibility of $Cr_{1.54}Zn_{23.62}$ (x_{Cr} = 0.0612) at 1 T. The insert shows the field dependent magnetization at 298K.

Numerical data concerning the thermal, magnetic and electrical properties of $CrZn_{17-\delta}$ are summarised in the Table 4.4.

Table 4.4: Data concerning the thermal, magnetic and electrical properties of $CrZn_{17-\delta}$

parameters		$CrZn_{15.3}$	$CrZn_{17.5}$
thermal	T_{mp} / K	700 (2)	703 (2)
	T_m / K (onset)	745 (2)	743 (2)
magnetic	$\chi_{TIP}/10^{-10}$ m^3 mol^{-1}	5.50(1)	5.20(2)
	μ_{eff} / μ_B	0.11(1)	0.16(1)*
	Θ / K	41(2)	84 (2)
resistivity	ρ_{300}/mΩcm	0.94	

Table 4.4: DTA data, temperature independent part of the susceptibility χ_{TIP}, effective magnetic moments μ_{eff} per Cr atom, Weiss temperatures of two compositionally distinct samples, (the value signed by * refers to $CrZn_{17.8}$); resistivity ρ of $CrZn_{15.3}$ at 300 K.

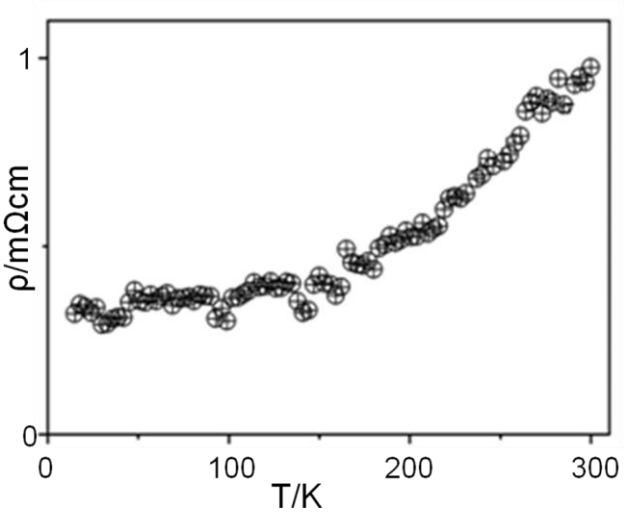

Figure 4.5: Resistivity ρ of single phase $Cr_{1.54}Zn_{23.62}$ (x_{Cr} = 0.0612) between 15 K and 300 K.

Measurements of the electrical resistance at constant current and variable temperature (15-300 K) identify $CrZn_{15.3}$ as a moderate metallic conductor (Fig. 4.5). The resistivity

steadily increases with temperature from 0.33 mΩcm at 15 K to 0.94 mΩ cm at 300 K. The measurements of a second sample containing chromium in excess corroborate the findings: 0.37 mΩcm (15 K) and 0.82 mΩcm. Thus, the resistivity at 300 K is approx. two orders of magnitude larger than that of the elements, $\rho_{Zn,\ 293}$ = 5.8 μΩ cm, $\rho_{Cr\ 297}$ = 12.5 μΩ cm. [42] Enhanced resistivities are typical for brass-type phases as the mechanism of stabilisation of Hume-Rothery phases implies a reduction of the electron concentration at the Fermi level and, hence, a reduction of the numbers of charge carriers.

4.5 Structural characteristics

$CrZn_{17-\delta}$ forms a complex, partly disordered $(2a_\gamma)^3$ structural derivative of a γ-brass related phase with lattice parameter a_γ and Pearson symbol *cI*52*.* A γ-brass related phase, in turn, can be regarded as a $(3a_{bcc})^3$ superstructure of the elemental bcc-type structure with ordered vacancies. Accordingly, the structure of $CrZn_{17-\delta}$ represents a further variant of the elemental bcc-structure of order 6^3 = 216. [122] $CrZn_{17-\delta}$ crystallises in the acentric cubic space group $F\bar{4}3m$ (216) with approximately 400-403 atoms per unit cell. The change of the lattice parameter (Table 4.1) with composition conforms to the difference in the molar atomic volumes of the two constituents, $-V_{Zn}$ = 9.2x10^3 cm^3mol^{-1}, $-V_{Cr}$ = 7.2 x 10^3 cm^3mol^{-1} Complex structures of this type are favourably analysed by decomposing them into either condensed or interpenetrating clusters [131] - also called nested polyhedral units, [132] which are grouped around the 16 high symmetry points per unit cell. They are equivalent with those of the atoms and voids in fcc Cu-type structure. Such a partitioning of the structure assures that the composition of the phase results from summing up the composition of the constituting clusters. We note that the term cluster in this context differs from its meaning in other areas of chemistry as it addresses merely topological aspects of a group of atoms chosen by considering symmetry. Chemical bonding is not explicitly respected. The outcome of this cluster concept is a clear description of the atomic arrangement of structurally complex intermetallic phases. Moreover, it strikingly discloses element-specific

structural dissimilarities between γ-brass related structures having more than 400 atoms in the unit cell.

The four constitutive clusters are grouped about the symmetry points: 0 0 0, ¼ ¼ ¼, ½ ½ ½, and ¾ ¾ ¾. Hence, each cluster type is arranged according to the motif of cubic close packed spheres. There are 4 x 4 clusters per unit cell. We shall address each cluster type by a capital letter indicating its position, i.e., Z for 0, Q for ¼, H for ½, and T for ¾. [133] Furthermore, the clusters will be differentiated by a set of three or four atomic shells composing the clusters. The shells are congruent with various Platonic and Archimedean solids. Each shell corresponds to a distinct crystallographic site and is identified by two capital letters. CC designates atoms occupying a high symmetry site, IT those occupying the vertices of an inner tetrahedron. Accordingly, OT stands for outer tetrahedron, TT for truncated tetrahedron which is also called Friauf polyhedron, and CO for cuboctahedron. Furthermore, we numerate atoms of a given cluster according to their distance from the centre of the cluster. To give an example, Z Zn12 atoms constitute the second shell (OT) of cluster 1 grouped around 0 0 0, ½ ½ 0 etc.

As previously found for Pt_5Zn_{21} [129] and $Ir_{7+7\delta}Zn_{97-4\delta}$ [122] the atomic arrangement of $CrZn_{17-\delta}$ can be subdivided into two partial structures of similar size and different composition. One part of the structure is built up by H and T clusters and completely ordered, hence, compositionally invariant throughout the homogeneity range of the phase. The second partial structure comprising the Z and Q clusters is partly disordered and variable in composition. The clusters of each partial structure form a replica of a sphalerite-type network, yet in a hierarchic version since clusters replace atoms. The partial structures are separated by half the length of lattice parameter a. The two networks interpenetrate mutually and contactless. The various cluster types are depicted in Fig. 4.6.

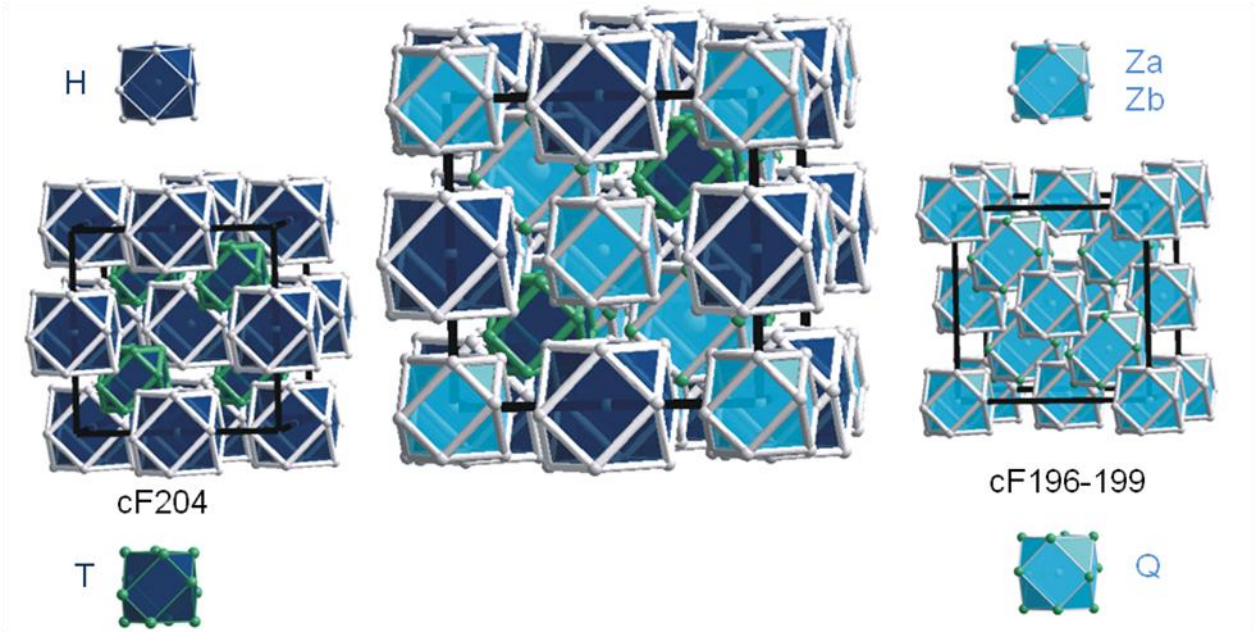

Figure 4.6: Crystal structure of $Cr_{1.36}Zn_{23.79}$ (x_{Cr} = 0.0540) depicted as a mutually interpenetrating diamond-like arrangement of clusters at around high symmetry points of the *F*-centered cubic unit cell. The clusters are represented by idealized cuboctahedron shells, which are color coded regarding their affirmation with either the compositionally invariant (dark-blue, c*F*204) substructure or variable (sky-blue, c*F*196-199) substructure.

The compositionally invariant partial structure: The H cluster of the compositionally invariant partial structure consists of a central Zn30, a TT shell of 12 Zn34 with 4 additional OT Zn32 above the hexagonal faces of the truncated tetrahedron. The Zn_{17} units are enclosed by 12 CO Zn35, resulting in a clean Zn_{29} α-Mn-type cluster. Though this monoatomic Zn_{29} cluster is certainly stabilised by bonding interactions with atoms of the surrounding clusters we conclude, that the Z, Q, and T clusters of $CrZn_{17-\delta}$ form a suitable matrix stabilising Zn_{29} nuclei of α-Mn-type structure. The second cluster is built up by 22 atoms and grouped about T. The largest portion of the Cr content of the compound, Cr42, is segregated on OT sites around T. 6 OH Zn43 bisect the edges of the Cr42 OT. Twelve surrounding Zn45 CO complement the $NiTi_2$-type Cr_4Zn_{18} cluster (Fig. 4.7) representing the domain of the $CrZn_{17-\delta}$ structure richest in Cr. Accordingly, the composition of the ordered substructure is Cr_4Zn_{47}.

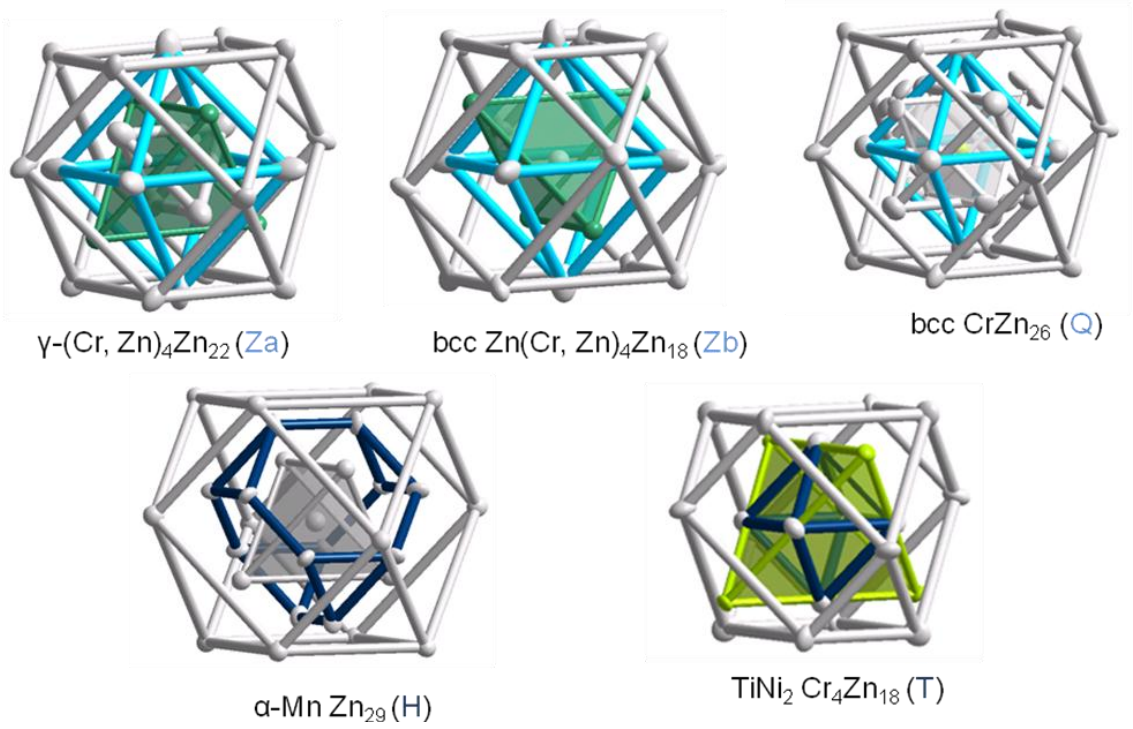

Figure 4.7: Representation of five symmetrically and topologically distinct clusters found in the crystal structures of $Cr_{1.36}Zn_{23.79}$ (x_{Cr} = 0.0540). All atoms are displayed by their anisotropic thermal displacement ellipsoid (75% probability, crystal 2). Ellipsoids representing sites with mixed Cr/Zn occupation are shown in sea green, Cr in lime, and Zn in light grey, respectively. The clusters are numbered consecutively along the body diagonal starting with the disordered γ/bcc-type cluster Z (1) placed about the origin. Each cluster is identified by its symbol and composition. The chosen color code indicates the distinction of clusters constituting a substructure of constant (dark-blue) and variable (sky-blue) composition.

The compositionally variable partial structure: The second partial structure is formed by the Z and Q clusters. It varies in composition between $Cr_{2.2}Zn_{47.5}$ and $Cr_{1.3}Zn_{47.8}$. The variation of composition is accompanied by various disorder phenomena. Difference Fourier analyses reveal three specifiable kinds of disorder typical for many structurally complex alloys:

(i) Random vacancies due to partly occupied sites

(ii) substitution disorder, i.e. mutual substitution of the two components on specific sites

(iii) positional disorder ascertainable by introducing split positions

The Z cluster consists of partly occupied Zn10 CC and Zn11 IT sites, of OT sites being statistically occupied by Cr and Zn, Zn13 OH, and an outer Zn15 CO shell. The clear correlation between the independently refined occupation factors f(CC) = 1-f(IT), (c.f. Table 4.2) can be rationalized by assuming that either a defect bcc-type clusterCr_xZn_{23-x} ($0.3 < x < 1.3$) with shell sequence CC, OT, OH, CO or a γ-type cluster Cr_xZn_{26-x} ($0.3 < x < 1.3$) (IT, OT, OH, CO) is situated about Z. The fraction of the γ-cluster is given by $0.33 \geq f(Zn11) \geq -0.14$, and that of the defect bcc cluster by 1 -f(Zn11). Hence, too short distances d(Zn10-Zn11) do not occur (c.f. Table 4.2). The composition obtained by assuming mixed, i.e., disorder type II instead of partial, i.e., disorder type I occupation of the Z OT site agrees very well with the starting composition and the results of the EDS analyses. The disorder in the Z cluster can be classified as type II, yet not only limited to a specific crystallographic site but, additionally to a set of sites.

At first glance, a much more puzzling factor is the disorder of Cr20 centring the Q cluster. It appears questionable whether or not random vacancies exist at CC in the Cr-rich phase. Zn 21 IT is threefold split leading to a TT shell with physically impossible short, but uncritical distances because of the fact that, only ~ 3 out of 12 Zn21 positions per cluster are occupied. Zn22 OT also exhibits also random vacancies slightly increasing in concentration (8–15 %) parallel with the overall Zn content of the phase. Moreover, only a fraction (43–27%) of OH Zn23 positions are occupied, other OH atoms take two symmetrically uncoupled two fold split positions OH’ and OH’’. Independent refinement of the fractional occupancies result in the relation f(Zn23) + 2 x f(Zn23’) + 2 f(Zn23’’) ≈ 1 indicating that all six and not more OH positions per cluster are occupied. Twelve Zn25 CO form the outermost shell. Slightly increased displacement parameters are a relict of the disorder in the interior. The heavily disordered cluster Q is depicted in Fig. 4.8.

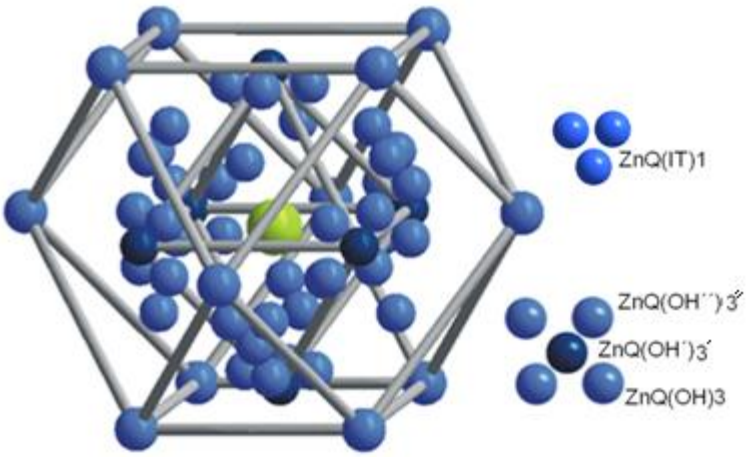

Figure4.8: Representation of a heavily disordered Q cluster about ¼ ¼ ¼, the patterns of disorders-IT (right, top) and OH (right, bottom).

Two additional correlations between site occupancy factors f (c.f. Table 4.2) provide evidence, that the various disorder phenomena in various shells are interrelated: f(IT,Zn21) ≈ f(OH', Zn23'), f(Zn22) + f(Zn23'') ≈ 1. So far, the coherence in disorder concerns only Zn sites of cluster Q. As the systematic change in disorder on the Zn sites is an implication of the varying Cr content, some kind of information transfer has to take place from those Cr to Zn sites, which vary with composition. The change in Cr content is essentially confined to the mixed occupied OT site of cluster Z. The parallel increase of the site occupancy factors f(Z,Zn12), the Zn fraction at OT in cluster Z, and 1-f(Q,Zn23), a measure of the positional disorder of OH atoms in cluster Q, indicates such an interrelation between the compositional changes in the various cluster types of the compositionally variable partial structure. A crystallographic meaningful chemical formula for the phase ensues by the sum of the composition of the two complementary substructures. Accordingly, the homogeneity range extends from $Cr_{5.3}Zn_{94.8}$ to $Cr_{6.2}Zn_{94.5}$. If we assume that the phase is stabilized by the Hume-Rothery mechanism, i.e., if we take for Cr -4 e and for Zn 2 e into account, we obtain values ranging from 1.681-1.633 for the valence electron concentration per atom. Noteworthy, the value of the phase at the Cr-rich boundary is close to the expected ideal value of γ-phases 21/13 = 1.615.

Extended Clusters: All clusters discussed so far are sheathed by an exterior CO shell. A closer inspection of the atomic arrangements in giant γ-brass-type related structures reveals that, there are further atoms similar far apart from the cluster centre as the CO atoms forming or complementing a further shell comprising 28 atoms. The four extended clusters are shown in Figure 4.9. Some characteristics of the clusters and shells are summarised in the Table 4.5.

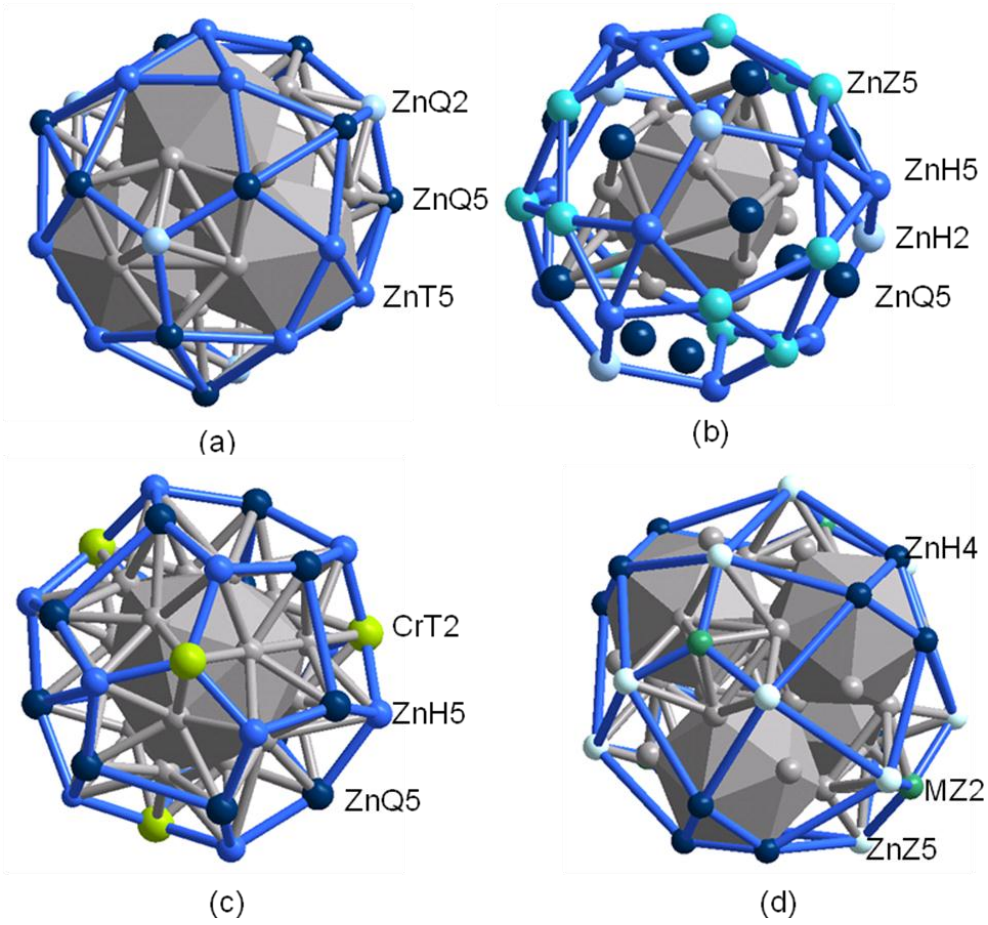

Figure 4.9: Cluster structures (a)-(d).Representation of 28 atoms polyhedra around high symmetry points. ((a),(b) clusters are located around 0 0 0 and ¼ ¼ ¼; (c), (d) clusters are built around ½ ½ ½ and ¾ ¾ ¾ respectively). Constituting zinc atoms of 28-atoms polyhedra has been shown by blue, chromium by lime and Cr/Zn mixed occupied site by sea green. Zinc atoms of the above mentioned polyhedra from different sites have been recognized by the variation of the concentration of blue color.

The Z cluster is depicted as a γ-cluster in Fig 4.9 a. Twelve CO Zn15 atoms are shown in light grey, 12 additional T Zn45 (light blue) extend the γ-cluster to the typical 38 atom quadruple of icosahedrons grouped around an interior Z IT highlighted in Fig 4.9 a. Twelve T Zn45, 12 Q Zn25 (dark teal) and 4 Q Zn 22 (pale blue) form the outer shell representing a tetrated dodecahedron TD, $3^{16}5^{12}$ with equal number of faces and vertices. At the zinc-rich border of the homogeneity range the cluster contains only a small fraction of Cr atoms (0.3) per cluster. Hence, if the phase width were fractionally extended to Cr_5Zn_{93}, we may anticipate an unseen Zn_{51} ($Zn@Zn_4@Zn_6@Zn_{12}@Zn_{28}$) cluster, a possible nucleus for a metastable modification of elemental zinc.

If we neglect splitting of atomic positions and random vacancies, the heavily disordered cluster Q can be approximated by a fragment of the W-type bcc structure. Fig. 4.9 b emphasizes the coordination about a central Cr20 given by 4 Zn21, 4 Zn22, and 6 Zn23. Twelve CO Zn25 situated above the rhombic faces form the Archimedean dual of the Catalan rhombic dodecahedron. The ensuing 28 atoms, 12 CO Zn35 (light blue), 12 Z Zn15 (Aqua), and 4 H Zn32 (pale blue), form a tetrated dodecahedron confining the extended $CrZn_{54}$ cluster.

Next we turn to the two extended clusters of the compositionally invariant partial structure. The extended H cluster is perfectly ordered. Its composition is $Zn_{41}Cr_4$. The outer 28 atoms, given by 12 H CO Zn35, 12 Q Zn25, and 4 T Cr42, cap the 28 triangulated faces of the interior deltahedral Zn_{17} unit as emphasized by grey tinge in Fig. 4.9 c. Hence, the outer shell conforms to the dual of the Friauf polyhedron which is described by the formula $5^{12}6^4$. It designates the enclosing polygons of the exterior and the vertex configuration of the interior polyhedron. The principle of duality holds also for the next atomic shell formed by 12 T CO Zn45 and 4 Q IT Zn21. Consequently, the configuration of these atoms conforms to a second, enlarged self-similar Friauf polyhedron with its vertices located above the 16 faces of the $5^{12}6^4$ fullerene cage. The additional 16 atoms extend the 28 atom polyhedron to a 44 atom polyhedron enclosed by 84 triangles. A particular outcome of this building principle based on triangulation and

duality is a clean tetrahedral close-packed Cr_4Zn_{57} H cluster composed of 28+28+24+60 = 140 slightly distorted, space-filling M_4 tetrahedra. The fourth $NiTi_2$-type cluster does not adhere to this principle, because an octahedral arrangement of atoms is incompatible with tetrahedral close packing as typical for Frank-Kasper phases. The expansion of the H cluster by 12 H TT Zn34 (dark teal) imports a quadruple of icoshedra that is accentuated by tinge as shown in Fig. 4.9 d. Each of the four icosahedra is condensed to a triangular face of an octahedron built up by 6 OH Zn43. The 28 atom shell is round out by 12 Z Zn15 (light turquoise) and 4 Z M12 (sea green). 4 x 3 Z CO Zn15 form a $3^4 6^4$ truncated tetrahedron TT, 4 x 3 Z TT Zn34 are located above the 4 hexagons of the TT, and 4 Q M12 above the triangles of the TT, 28 polygons, namely 12 kites, 12 trapezoids and 4 triangles, form the periphery of the extended $Cr_4M_4Zn_{42}$ T cluster. Needless to say, different to the smaller 22-29 atom clusters, the extended clusters interpenetrate; thus, contain information of the total structure. The configuration of the exterior 28 atoms shell depends both on the nature of the adjacent smaller clusters and their orientation in space.

Table 4.5: Description of 28-atoms polyhedral about the special sites Z, Q, H, T

Cluster	Sub-shell	Vertex configuration	Polyhedral formula
Z(1)	Q2	5^3	Tetrated dodecahedron
	Q5	$5^2.3^2$	$3^{16}.5^{12}$
	T5	5.3.5.3	
Q(2)	Z5	5.3.5.3	Tetrated dodecahedron
	H5	$5^2.3^2$	$3^{16}.5^{12}$
	H2	5^3	
H(3)	T2	5^3	Fullerene
	Q5	6.5^2	$5^{12}.6^4$
	H5	6.5^2	
T(4)	Z2	4^3	$3^4.4^{24}$
	H4	4.4.4.3	
	Z5	4.4.4.4	

This last chapter deals with a comparison of the structures of the two congeneric phases $CrZn_{17-\delta}$ and $MoZn_{20.4}$. [134] According to the classical Hume-Rothery concept the structure of brass-type phases is assumed to be decisively controlled by the valence

Table 4.6: Minimum (d_{min}), maximum (d_{max}) and mean interatomic distances (<d>) and coordination numbers (C.N.) for $CrZn_{15.34}$ (C1), $CrZn_{17.50}$ (C2), $CrZn_{17.81}$ (C3)

Cluster	Atoms	Site	C1 d_{min}-d_{max} <d> (pm)	C.N.	C2d_{min}-d_{max} <d> (pm)	C.N	C3d_{min}-d_{max} <d> (pm)	C.N.
Z(1)	Zn10	CC	266.8-300.4 <287.0>	10	268.2-297.7 <285.9>	10	267.9-294.2 <283.7>	10
	Zn11	IT	245.3-274.6 <263.2>	12	243.1-272.6 <262.3>	12	240.3-271.0 <260.7>	12
	M12	OT	258.8-266.8 <263.1>	13	258.9-268.2 <263.3>	13	258.7-267.9 <262.7>	13
	Zn13	OH	245.3-300.4 <275.4>	13	243.1-297.7 <275.1>	13	240.3-295.2 <274.1>	13
	Zn15	CO	263.8-299.9 <277.8>	12	264.0-302.3 <278.5>	12	263.3-302.0 <278.5>	12
Q(2)	Cr20	CC	257.6-285.6 <272.2>	14	258.8-284.0 <271.4>	14	258.3-284.0 <271.1>	14
	Zn21	IT	254.8-336.5 <281.9>	12	255.4-335.5 <282.0>	12	254.4-334.4 <282.0>	12
	Zn22	OT	251.9-302.1 <274.3>	13	251.4-298.1 <274.5>	13	250.4-298.3 <274.2>	13
	Zn23	OH	252.6-285.6 <266.5>	9	253.0-284.0 <266.3>	9	252.3-284.0 <266.2>	9
	Zn23´	OH´	242.6-320.2 -	12	242.5-322.1 -	12	242.2-319.3 -	12
	Zn23´´	OH´´	240.2-310.3 -	11	242.9-310.7 -	11	244.5-311.1 -	11
	Zn25	CO	256.0-322.1 <281.7>	12	257.7-323.9 <282.6>	12	259.2-324.7 <283.0>	12
H(3)	Zn30	CC	277.5-305.7 <298.7>	16	279.0-305.7 <299.1>	16	279.3-305.7 <299.1>	16
	Zn32	OT	261.8-284.7 <278.2>	11	260.4-285.5 <278.8>	11	260.6-285.5 <279.0>	11
	Zn34	CO	249.8-305.7 <274.7>	12	250.7-305.7 <275.0>	12	250.6-305.7 <275.2>	12
	Zn35	OT	242.6-328.8 <285.0>	14	242.5-329.0 <285.7>	14	242.2-329.2 <286.1>	14
T(4)	Cr42	OT	258.7-263.8 <260.9>	12	257.9-265.9 <261.8>	12	258.5-266.7 <262.1>	12
	Zn43	OH	261.9-276.3 <273.4>	12	263.6-277.3 <274.7>	12	263.0-277.6 <274.7>	12
	Zn45	CO	258.8-302.2 <278.7>	12	258.9-304.4 <279.9>	12	258.7-304.1 <280.3>	12

electron concentration implying that pairs of elements of the same groups irrespective of other distinctive atomic factors are expected to produce the same structure. Indeed, while the chemistry of 3d and 4d block elements frequently differs significantly due to differences in bonding capabilities of the corresponding nd states, the structures of $CrZn_{17-\delta}$ and $MoZn_{20.4}$ share many features in spite of the compositional distinctions and the complexity of the structures. Common features are: (i) The clusters are the

same in both structures. The composition of the ordered partial structure is M_4Zn_{47} for each compound. (ii) Though different in composition the cluster types of the disordered structures are the same as well. Structural differences concern: (i) The cluster types at Z of $MoZn_{20.4}$ are clean Zn clusters, i.e., defect bcc-Zn_{23} (f = 0.35) and γ-Zn_{26} (f = 0.65). (ii) An additional reduction of the Mo compared to the Cr content is due to substitution disorder at Q CC. Consequently *vec* is significantly larger: 1.720. (iii) No positional disorder is reported for the Mo compound. We conclude that in spite of a close structural resemblance the enormous complexity of these large cell structures provides room for element specific structural differentiations.

4.6 Summary

The crystal structure of the zinc-rich phase $CrZn_{17-\delta}$ first mentioned by Henry Le Chatelier in 1895 [47] has been analysed for three distinct compositions including the phases at the Cr-rich (δ = 1.7) and Zn-rich (δ = -0.8) boundaries.

The structure represents a 2a x 2a x 2a superstructure of a γ-brass related structure with approximately 400 atoms in the cubic unit cell. Partitioning of the structure into various clusters grouped around the 16 high symmetry points reveals that the structure can be subdivided into two partial structures, arranged like two non-intersecting zinc blende type nets which are shifted relatively to each other by half a lattice parameter a/2. One partial structure comprising clean α-Mn-type Zn_{29} and $NiTi_2$-type Cr_4Zn_{18} clusters is ordered and compositionally invariant over the homogeneity range. Its complement is significantly richer in Zn, $Cr_{1.3}Zn_{47.8}$-$Cr_{2.2}Zn_{47.5}$, and disordered. Three types of disorder can be differentiated: random vacancies, substitution and positional disorder.

Correlations can be identified between disorder parameters of affected sites indicating a spatial coherence between the various disorder phenomena. Since the atomic distances change usually less than 2 pm we assume that band electronic factors control the correlation.

The valence electron concentration per atom is-at least at the Cr-rich boundary-very close 21/13 as expected for the *vec*-controlled structure formation of γ-phases. The structure is isopointal to that of congeneric $MoZn_{20.4}$. Though the two structures are very similar in many respects, the enormous structural complexity as expressed by the large unit cell and numerous symmetrically inequivalent crystallographic sites provides room for noticeable element specific structural differentiation.

$CrZn_{17-\delta}$ is a moderate metallic conductor, exhibits week temperature-dependent paramagnetic properties, and, essentially in accord with previous reports, [45,48] melts incongruently at 743-745 K.

Chapter 5

Spatially correlated structural disorder phenomena in γ-brass related complex zinc-rich alloys (M,Cr)Zn_n; (M = Au,Pd)

5.1 Introduction

In contrast to the long-standing history of some intermetallics, pioneering studies in the field of Hume-Rothery phases [16,18] were not conducted before the beginning of the nineteenth century. According to the present knowledge, Hume-Rothery phases are formed between a suitable element of group 2, 12-14 and transition elements which preferably are noble metals. They mostly display medium to large homogeneity ranges and are specified by idealized composition.

Within the sequence of brass-like Hume-Rothery phases the γ-brass phases are of particular interest among the intermetallic compounds because of their structural complexity and stabilization mechanism. γ-brass phases are a special kind of intermetallic compound in which the formation of a particular structure does not depend on any element-specific property of chemical constituents, but an element-specific particular value of the valence electron concentration (*vec*) or electron/atom (e/a) ratio which was first identified by Hume-Rothery. γ-brass phases achieve their stability by the lowering of kinetic energy of the valence electron associated with a reduction of density of state at the Fermi level. Such reduction is achieved due to the interaction between the Fermi surface of radius k_F and the Brillouin zone characterized by a reciprocal lattice vector. [135,136] A prominent example of γ-brass is Cu_5Zn_8. [110, 111] The unit cell contains

two formula units with a lattice parameter, a ≈ 900 pm in the body centre cubic space group $I\bar{4}3m$. The atomic arrangement of γ-brass phase can be generated by β-brass phase by starting from a 3 x 3 x 3 superstructure of the bcc packing of atoms followed by removing two atoms from the resulting 54-atom supercell (one from the corner, one from the center of the supercell), then shifting the remaining atomic sites to the resulting coordinates. [137] By several experimental and theoretical means, it has been shown for γ-brass phases, *vec* value is 21/13 per atom. There are several recent reports on the prototype of Cu_5Zn_8 for different transition metals combined (M = Ni, Rh, Ir) [11,138,139] with zinc holding composition $M_2Zn_{11.}$

Some transition metal-zinc systems accommodate bundle-wise phases of bewildering composition and structural complexity. [53,54,126,140,141] Among complex crystalline phases, the structure most closely related to γ-brass is a 2a x 2a x 2a superstructure of γ-brass related Hume-Rothery phase previously termed as “cubic giant cell structure”. [142,143] These phases occur in several binary systems, such as $Fe_{22}Zn_{78,}$ [144] $MoZn_{20.44,}$ [134] $Pt_5Zn_{21,}$ [129] and $Ir_{7+7\delta}Zn_{97-11\delta.}$ [122] In spite of structural and compositional difference, these cubic giant cell structures can be uniformly visualized by decomposing them into four symmetrically independent structural units each consisting of 22-29 atoms centering around the high symmetry points of the cell, i.e. : (0 0 0), (¼ ¼ ¼), (½ ½ ½), (¾ ¾ ¾).

Recently, we have structurally identified the congener of γ-brass Cu_5Zn_8 in the Cr-Zn system, $CrZn_{17-\delta}$ ($-0.8 \leq \delta \leq 1.7$) [145] exhibiting more than 400 atoms per unit cell. In order to gain an insight into expressions, cause and mechanism and structure-property relationship for such phases, we studied the impact of substitution of chromium and zinc by 2nd or 3rd row transition elements on the evolution of the structure of ternary derivatives of $CrZn_{17-\delta}$.

We have chosen gold or palladium for substitution because of its strong scattering factor compared to that of chromium and zinc. This fact may permit distinguishing the atomic sites of gold or palladium by the results of X-ray diffraction experiment.

As part of a research programme, we explore the Au-Cr-Zn and Pd-Cr-Zn system to understand how substitution of monovalent Au atoms or zerovalent Pd atoms for

divalent Zn and/or tetravalent (negative) Cr could influence the structural stability and chemical compositions of 2a x 2a x 2a superstructure of γ-brass related phase $CrZn_{17-\delta}$.

According to the classical Hume-Rothery concept the structures of γ-brass-type phases is assumed to be decisively controlled by the valence electron concentration irrespective of the nature of constituting elements. Indeed, the chemistry of 4d (e.g. Pd) and 5d (e.g. Au) transition-elements differs significantly due to differences in bonding capabilities of the corresponding nd states. So end of this chapter deals with a comparison of the structures of $CrZn_{17-\delta}$: Au and $CrZn_{17-\delta}$: Pd.

5.2 Spatially correlated structural disorder phenomena in γ-brass related complex zinc-rich alloys $(Au,Cr)Zn_n$; n = 10.2-6.4

5.2.1 Introduction

Subject of discussion, herein, is the impact of gold on $CrZn_{17-\delta}$. Comprehensive studies by single crystal X-ray diffraction experiments on several specimens in highly differentiated ternary Au-Cr-Zn alloys reveal the existence, phase width and structural characteristics associated with spatial correlation among all kinds of disorders in γ-brass related phases formulated as $(Au,Cr)Zn_n$, n = 10.2-6.4.

5.2.1 Synthesis and morphological features

About fifteen reactions were carried out with different Au/Cr ratio in $(Au_xCr_{1-x})Zn_{\sim 10}$ starting from the pure elements: Au (99.99%, ABCR), Cr (99.995%, Aldrich) Zn (99.9999%, Chempur). Samples of precisely weighted metals (ca.0.3 g) are loaded and sealed in previously out-gassed, fused silica ampoules (3 cm long, 0.8 cm in diameter) under a reduced argon pressure of about 0.5 Pa. The metals were heated at a rate of 194.4 K h^{-1} up to 1273 K at which the ampoules were kept for 2 h. Hereafter, the temperature was reduced to 703 K at a rate of 114K h^{-1} and annealed at this temperature for 5 days. The samples were either quenched in cold water or cooled to ambient temperature. To avoid eventual loss of zinc due to evaporation, the reactants were kept at a lower temperature than the rest of the ampoule. Products obtained from these reactions were silvery, brittle ingots and were found to be stable in air. In most cases, small amounts of gaseous zinc sometimes re-condenses into few tiny globules in close contact to the regular, brittle, silvery, lustrous metallic products. In some cases crystals have hexagonal shape. (Fig. 5.2.1)

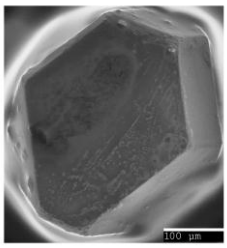

Figure 5.2.1: Scanning electron micrograph of a regular form of a crystal of $Au_{4.59}Cr_{4.85}Zn_{91.33}$

5.2.2 Single crystal structure determination

Eleven single crystals ranging from $0.02 \leq x_{Au} \leq 0.10$ were selected from different Au–Cr–Zn reactions were studied by X-ray means. Among all the samples studied, three crystals are discussed in detail herein. Further crystallographic details of other specimens are listed in the appendix. Crystal 1 (C1) was selected from a sample poorest in gold having $x_{Au} = 0.026$ and crystal 10 (C10) was selected from a sample richest in gold content having $x_{Au} = 0.097$. Crystal 4 (C4) having a medium Au–content was taken from a sample of nominal composition $x_{Au} = 0.038$, because the sample starting with the composition, Au starts to substitutes Zn on the M23 site in addition to the M12 site and specimens with $x_{Au} \geq 0.038$, the M12 site becomes fully occupied by Au. The diffraction intensities were recorded with an imaging plate diffraction system IPDS (Stoe & Cie) working with $Mo_{K\alpha}$ radiation. [63] The intensities could be indexed on the basis of a 1.8 nm large *F*-centered cubic unit cell. The measured intensities were corrected for Lorentz and polarization effects and were further corrected for absorption by using STOE X-SHAPE and X-RED program. [66,67] The structures were solved in the acentric space group $F\bar{4}3m$ (No. 216) by applying direct methods and refined using the SHELX-97 program package based on full-matrix least-square refinements. [64] The possible position of missing zinc atoms was taken from difference Fourier synthesis maps. At this stage the structure refinement converged at R (F) < 0.17. Further

improvement of the calculations was achieved by partially replacing chromium and/or zinc by gold on the site which showed lower displacement parameters with respect to normal, assuming those sites to be fully occupied by mutual substitution of the two components. On the other hand, those metal sites having relatively large thermal displacement parameters were checked for partial occupancy and positional disorder. Atoms for which the refined occupancy factors deviated by less than twice the standard from unity were reset to unity in the final refinement cycles. Local structural disorder phenomena were recorded by introducing split positions. All the disorder sites were refined with non-coupled occupation parameters except the ones showing mixed occupancy. Each structure was checked for possible twinning by inversion and its absolute configuration by making use of a possible violation of Friedel's law due to anomalous dispersion effect. The anisotropic displacement parameters of all the atoms except a few positional disordered sites were refined. The final refinement including an extinction correction and a proper weighting scheme yields R(*F*) values between 0.032 and 0.054. Further details concerning the crystallographic data and structure determination (for C1, C4, C11) are gathered in the Table 5.2.1. Positional and occupational parameters together with the equivalent displacement parameters (U_{eq}) are given in the Table.5.2.2 and 5.2.3. Further details of the crystal structure investigations can be obtained from the appendix (from A8 to A43).

5.2.3 Phase analysis and physical properties

The homogeneity range and constitutions of cubic γ-brass phases in the Au–Cr–Zn systems were examined by means of preparative methods, calorimetric measurements and X-ray diffraction, and EDS analyses.

Chemical composition determined by EDS and X-ray single crystal refinement shows an extended homogeneity range over $0.026 \leq x_{Au} \leq 0.097$ and $0.063 \leq x_{Cr} \leq 0.039$, i.e., from $Au_{2.6}Cr_{6.4}Zn_{91.7}$ to $Au_{10.0}Cr_{4.0}Zn_{89.0}$. Composition evaluated by EDS and X-ray single crystal refinements agrees well. The loaded composition for different preparation,

Table 5.2.1: Crystallographic and technical data for the single crystal structure refinements of $Au_{2.63}Cr_{6.36}Zn_{91.68}$ (C1), $Au_{3.79}Cr_{5.37}Zn_{91.75}$ (C4), $Au_{10.00}Cr_{4.00}Zn_{89.00}$ (C11)

	C1	C4	C11
crystallographic data			
chemical formula	$Au_{2.63}Cr_{6.36}Zn_{91.68}$	$Au_{3.79}Cr_{5.37}Zn_{91.75}$	$Au_{10.0}Cr_{4.0}Zn_{89.0}$
Pearson symbol	*cF*402.7	*cF*403.6	*cF*412
x_{Au}	0.026	0.038	0.0971
crystal system			
space group type; Z	cubic; $F\bar{4}3m$ (No.216); 4		
a/pm[a]	1828.8(2)	1832.8(1)	1843.0(1)
$V/10^6$ pm^3 [a]	6116.4(1)	6156.7(6)	6259.8(4)
ρ_{calcd}/g cm^{-3}	7.431	7.577	8.484
μ/mm^{-1}	42.499	44.818	57.309
crystal color	silvery with metallic luster		
data collection			
crystal size/mm^3	0.10x0.09x0.06	0.10x0.10x0.08	0.06x0.04x0.04
diffractometer	IPDS (Stoe & Cie.)		
radiation	$Mo_{K\alpha}$		
monochromator	graphite		
distance crystal-IP/mm	40	40	90
T/K	293(2)	293(2)	293(2)
φ_{min}-φ_{max}/^{o}	0-100	0-100	0-180
$\Delta\varphi$	1	1	1
$2\theta_{max}$/^{o}	66.12	66.00	66.66
reflns measured	11136	11212	19837
index range	-28≤*h*≤27	-16≤*h*≤27	-28≤*h*≤25
	-24≤*k*≤27	-27≤*k*≤27	-28≤*k*≤28
	-14≤*l*≤28	- 21≤*l*≤28	-25≤*l*≤23
completeness of data set	0.991	0.997	0.988
data reduction/ absorption correction	IPDS-software,[63] X-RED[66]/numerical, X-SHAPE[67]		
unique reflns	1191	1198	1242
R_{int}	0.1292	0.0990	0.0719
structure solution, refinement			
structure solution	direct methods, SHELXS-97 [64]		
structure refinement	full-matrix least squires on F^2 (SHELXL-97[64])		
no. reflns used	1191	1198	1442
no. variables	80	80	64
observed reflns (F_o>4σ(F_o))	1072	1129	1240
R(*F*) (F_o>4σ(F_o))	0.0518	0.0494	0.0279
R(*F*) (all data)	0.0570	0.0525	0.0323
weighting factor k_1/k_2 [b]	0.0850/348.3745	0.0666 /607.0464	0.0323/361.0367
wR (F^2)(all data)	0.1500	0.1287	0.0744
GOF (F^2)	1.093	1.076	1.194
extinction coefficient	0.000094(15)	0. 00042(3)	0.000020(5)
$\Delta\rho_{min}/\rho_{max}$/10^{-6}epm^{-3}	-1.981/2.707	-2.094/2.608	-3.509/2.503

[a] Parameters determined by use of powder diffraction data. [b] Weighting scheme: $1/\omega=\sigma^2(F_O^2)+(k_1.P)^2+k_2.P$ with $P = ⅓(\max(F_O^2,0) + .2F_c^2)$.

Table 5.2.2: Structural data for $Au_{3.79}Cr_{5.37}Zn_{91.68}$ (C1), $Au_{3.79}Cr_{5.37}Zn_{91.75}$ (C4), $Au_{10.0}Cr_{4.0}Zn_{89.0}$ (C11)

Cluster	Atom	Site		*x*	*y*	*z*	SOF	*U*eq[a]/pm^2
Z(1)	Zn10	4a	CC	0[b]	0	0	0.78(5)	230(3)
							0.57(4)	240(4)
							0	-
	Zn11	16e	IT	0.0544(6)	*x*	*x*	0.27(2)	340(5)
				0.0551(3)			0.49(2)	320(3)
				0.05331(7)			1	161(4)
	M12	16e	OT	0.91381(4)	*x*	*x*	0.659(10)	165(4)
				0.91348(3)			0.908(10)	145(3)
				0.91346(2)				116(1)
	Zn13	24f	OH	0.1604(3)	0	0	1	389(9)
				0.1672(4)				532(14)
				0.18458(13)				208(4)
	Zn15	48h	CO	0.15489(10)	*x*	0.02327(13)	1	291(5)
				0.15595(10)		0.02307(13)		276(5)
				0.15489(6)		0.02425(8)		207(3)
Q(2)	Cr20	4c	CC	1/4	1/4	1/4	1	123(12)
								117(12)
							0	-
	Zn21	16e	IT	-	-	-	0	-
				-	-	-	0	-
				0.31800(13)			1	296(6)
	Zn21´	48h	IT´	0.3214(4)	*x*	0.3487(5)	0.252(11)	320(3)
				0.3215(3)		0.3474(5)	0.231(10)	260(3)
							0	-
	Zn22	16e	OT	0.16625(12)	*x*	*x*	0.92(2)	284(13)
				0.16602(12)			0.90(2)	251(13)
				0.16990(9)			1	202(4)
	Zn23	24g	OH	0.0943(5)	1/4	1/4	0.49(3)	390(3)
				0.0913(4)			0.439(15)	300(3)
							0	-
	Au23			-	-	-	0	-
				0.0913(4)			0.027(15)	300(3)
				0.07979(3)			1	180(1)
	Zn23´	48h	OH´	0.2214(6)	*x*	0.3894(7)	0.216(15)	350(4)
				0.2224(6)		0.3901(7)	0.208(14)	350(4)
							0	-
	Zn23´´	48h	OH´´	0.2746(12)	*x*	0.1132(15)	0.052(12)	90(9)
				0.2759(17)		0.112(2)	0.059(14)	280(13)
							0	-
	Zn25	48h	CO	0.07457(13)	*x*	0.26494(13)	1	334(6)
				0.07571(13)		0.26568(14)		339(6)
				0.08389(6)		0.27100(8)		239(3)
H(3)	Zn30	4c	CC	1/2	1/2	1/2	1	248(14)
								223(13)
								257(10)
	Zn32	16e	OT	0.41196(11)	*x*	*x*	1	230(6)
				0.41235(11)				204(6)
				0.41481((7)				186(4)
	Zn34	48h	CO	0.04836(7)	*x*	0.65218(12)	1	226(4)
				0.04827(7)		0.65214(11)		207(4)
				0.04802(5)		0.65323(8)		197(3)
	Zn35	16e	OT	0.19125(9)	*x*	0.51634(12)	1	248(5)
				0.19072(9)		0.51686(11)		235(5)
				0.18897(6)		0.52448(8)		209(3)
T(4)	Cr42	16e	OT	0.64844(12)	*x*	*x*	1	132(6)
				0.64859(12)				117(6)
				0.64901(8)				91(4)
	Zn43	24g	OH	0.64315(15)	1/4	1/4	1	205(5)
				0.64351(14)				185(5)
				0.64511(9)				152(3)

Zn45	48h	CO	0.10615(9) 0.10671(9) 0.10825(5)	*x*	0.77574(11) 0.77508(10) 0.77590(7)	1	257(5) 233(5) 189(3)

[a] *U*eq is defined as one third of the trace of orthogonalized U_{ij} tensor. [b] structural data given in the top to bottom lines refer to crystals C1,C4, C11 respectively. [c] SOF(Au), SOF(Cr)=1-SOF(Au).

Table 5.2.3.1: Anisotropic thermal displacement parameters U_{ij} (pm^2) for $Au_{2.63}Cr_{6.36}Zn_{91.68}$ (C1)

Atom	U_{11}	U_{22}	U_{33}	U_{23}	U_{13}	U_{12}
Zn10	230(3)	U_{11}	U_{11}	0	0	0
Zn11	340(5)	U_{11}	U_{11}	130(4)	U_{23}	U_{23}
M12	165(4)	U_{11}	U_{11}	-7(2)	U_{23}	U_{23}
Zn13	680(3)	244(9)	U_{22}	66(11)	0	0
Zn15	301(7)	U_{11}	271(10)	-83(6)	U_{23}	82(8)
Cr20	123(12)	U_{11}	U_{11}	0	0	0
Zn21´	320(3)	U_{11}	340(5)	-110(2)	U_{23}	0(3)
Zn22	284(13)	U_{11}	U_{11}	-48(8)	U_{23}	U_{23}
Zn25	390(8)	U_{11}	221(9)	66(7)	U_{23}	145(9)
Zn30	248(14)	U_{11}	U_{11}	0	0	0
Zn32	230(6)	U_{11}	U_{11}	16(7)	U_{23}	U_{23}
Zn34	192(5)	U_{11}	294(9)	9(4)	U_{23}	-56(6)
Zn35	250(6)	U_{11}	245(9)	13(5)	U_{23}	5(7)
Cr42	132(6)	U_{11}	U_{11}	-17(6)	U_{23}	U_{23}
Zn43	226(12)	194(7)	U_{22}	-56(8)	0	0
Zn45	303(7)	U_{11}	167(8)	27(5)	U_{23}	120(7)

Table 5.2.3.2: Anisotropic thermal displacement parameters U_{ij} (pm^2) for $Au_{3.79}Cr_{5.37}Zn_{91.75}$ (C4)

Atom	U_{11}	U_{22}	U_{33}	U_{23}	U_{13}	U_{12}
Zn10	240(4)	U_{11}	U_{11}	0	0	0
Zn11	320(3)	U_{11}	U_{11}	80(2)	U_{23}	U_{23}
M12	145(3)	U_{11}	U_{11}	-11(2)	U_{23}	U_{23}
Zn13	1110(4)	240(10)	U_{22}	55(13)	0	0
Zn15	290(7)	U_{11}	247(9)	-75(6)	U_{23}	80(8)
Cr20	117(12)	U_{11}	U_{11}	0	0	0
Zn21´	240(3)	U_{11}	280(5)	-100(3)	U_{23}	30(2)
Zn22	251(13)	U_{11}	U_{11}	-28(8)	U_{23}	U_{23}
Zn25	382(9)	U_{11}	253(10)	88(7)	U_{23}	161(10)
Zn30	223(13)	U_{11}	U_{11}	0	0	0
Zn32	204(6)	U_{11}	U_{11}	8(7)	U_{23}	U_{23}
Zn34	172(5)	U_{11}	279(9)	4(4)	U_{23}	-48(6)
Zn35	234(6)	U_{11}	236(9)	14(5)	U_{23}	17(7)
Cr42	117(6)	U_{11}	U_{11}	-10(7)	U_{23}	U_{23}
Zn43	201(11)	177(7)	U_{22}	-46(8)	0	0
Zn45	262(6)	U_{11}	143(8)	29(4)	U_{23}	9(7)

Table 5.2.3.3: Anisotropic thermal displacement parameters U_{ij} (pm^2) for $Au_{10.0}Cr_{4.0}Zn_{89.0}$ (C11)

Atom	U_{11}	U_{22}	U_{33}	U_{23}	U_{13}	U_{12}
Zn11	161(4)	U_{11}	U_{11}	23(4)	U_{23}	U_{23}
Au12	116(1)	U_{11}	U_{11}	-9(1)	U_{23}	U_{23}
Zn13	220(8)	202(5)	U_{22}	16(7)	0	0
Zn15	213(4)	U_{11}	196(6)	-44(3)	U_{23}	-32(5)
Zn21	296(6)	U_{11}	U_{11}	143(8)	U_{23}	U_{23}
Zn22	202(4)	U_{11}	U_{11}	27(4)	U_{23}	U_{23}
Au23	135(2)	202(2)	U_{22}	-15(2)	*0*	*0*
Zn25	258(4)	U_{11}	203(6)	19(3)	U_{23}	-4(6)
Zn30	257(10)	U_{11}	U_{11}	0	0	0
Zn32	186(4)	U_{11}	U_{11}	11(4)	U_{23}	U_{23}
Zn34	165(3)	U_{11}	262(6)	-11(3)	U_{23}	-52(4)
Zn35	225(4)	U_{11}	178(6)	33(3)	U_{23}	-16(5)
Cr42	91(4)	U_{11}	U_{11}	-2(4)	U_{23}	U_{23}
Zn43	176(7)	140(4)	U_{22}	-25(5)	0	0
Zn45	221(4)	U_{11}	123(5)	21(3)	U_{23}	-12(4)

the corresponding refined compositions from single crystal X-ray diffraction experiments, and EDS analyses for selected crystalline specimens are summarized in the Table 5.2.4.

Table 5.2.4: A summary of loaded and obtained compositions from single crystal X-ray diffraction and EDS analyses for selected crystalline specimens

Loaded composition	Crystal designation	Refined composition	EDS composition
$Au_{2.5}Cr_{7.5}Zn_{90.7}$	C1	$Au_{2.6}Cr_{6.4}Zn_{91.7}$	$Au_{2.4(1)}Cr_{6.7(8)}Zn_{91.5(8)}$
$Au_{2.3}Cr_{6.9}Zn_{91.5}$	C2	$Au_{2.8}Cr_{6.2}Zn_{91.7}$	$Au_{2.7(1)}Cr_{4.8(10)}Zn_{93.1(10)}$
$Au_{2.7}Cr_{6.4}Zn_{91.4}$	C3	$Au_{3.3}Cr_{5.7}Zn_{91.6}$	$Au_{3.2(6)}Cr_{5.6(4)}Zn_{91.9(10)}$
$Au_{3.8}Cr_{5.3}Zn_{91.8}$	C4	$Au_{3.8}Cr_{5.4}Zn_{91.8}$	$Au_{4.0(4)}Cr_{6.3(7)}Zn_{90.4(10)}$
$Au_{3.7}Cr_{5.5}Zn_{91.7}$	C4a	$Au_{3.8}Cr_{5.3}Zn_{91.8}$	$Au_{3.7(6)}Cr_{5.0(5)}Zn_{92.1(6)}$
$Au_{4.6}Cr_{4.6}Zn_{91.6}$	C5	$Au_{4.6}Cr_{4.9}Zn_{91.3}$	$Au_{5.5(8)}Cr_{5.0(2)}Zn_{90.2(10)}$
$Au_{4.6}Cr_{4.9}Zn_{91.3}$	C6	$Au_{5.2}Cr_{4.7}Zn_{91.9}$	$Au_{5.1(2)}Cr_{4.3(2)}Zn_{92.4(3)}$
$Au_{5.2}Cr_{5.2}Zn_{92.2}$	C7	$Au_{5.6}Cr_{4.6}Zn_{92.3}$	$Au_{6.6(13)}Cr_{4.9(1)}Zn_{90.9(13)}$
$Au_{6.5}Cr_{2.8}Zn_{92.6}$	C8	$Au_{6.2}Cr_{4.5}Zn_{91.2}$	$Au_{6.2(7)}Cr_{4.4(7)}Zn_{91.2(10)}$
$Au_{7.5}Cr_{1.9}Zn_{93.7}$	C9	$Au_{7.7}Cr_{4.3}Zn_{91.0}$	$Au_{7.0(5)}Cr_{3.7(10)}Zn_{92.3(6)}$
$Au_{7.9}Cr_{4.3}Zn_{90.4}$	C10	$Au_{7.9}Cr_{4.3}Zn_{90.4}$	$Au_{7.6(6)}Cr_{4.4(8)}Zn_{91.0(6)}$
$Au_{10.0}Cr_{4.0}Zn_{89.0}$	C11	$Au_{10.0}Cr_{4.0}Zn_{89.0}$	$Au_{9.1(3)}Au_{4.1(8)}Zn_{89.8(6)}$
$Au_{10.0}Cr_{4.0}Zn_{89.0}$	C11a	$Au_{10.0}Cr_{4.0}Zn_{89.0}$	$Au_{9.7(8)}Cr_{3.5(8)}Zn_{89.8(8)}$
$Au_{10.0}Cr_{4.0}Zn_{89.0}$	C11b	$Au_{10.0}Cr_{4.0}Zn_{89.0}$	$Au_{9.7(8)}Cr_{3.5(8)}Zn_{89.8(8)}$

The sample with nominal composition $Au_{10.0}Cr_{4.0}Zn_{89.0}$ coexists with a competing binary phase of approximate composition $AuZn_7$ [75] (ε-phase, space group $P6_3/mmc$, prototype Mg) as observed by EDX and analysis and X-ray powder diffraction experiment. According to EDS (9 data points) the competing binary phase has an average composition of $Au_{12.0(4)}Zn_{87.3(6)}$. Specimens with $x_{Au} \leq 0.026$ show a strong tendency to form multiply twinned face-centered cubic lattices of a ~1.8 nm large *F*-centered cubic unit cells.

A Rietveld refinement [62,127,128] was performed on a single phase sample containing x_{Au} = 0.026 (x_{Cr} = 0.063), x_{Au} = 0.051 (x_{Cr} = 0.046), and x_{Au} = 0.097 (x_{Cr} = 0.039), respectively. Positional parameters of the single crystal X-ray structure determination were used as starting parameters for the refinements against bulk sample X-ray powder data. A profile fit is shown in Fig. 5.2.2, Fig. 5.2.3, and Fig. 5.2.4, respectively.

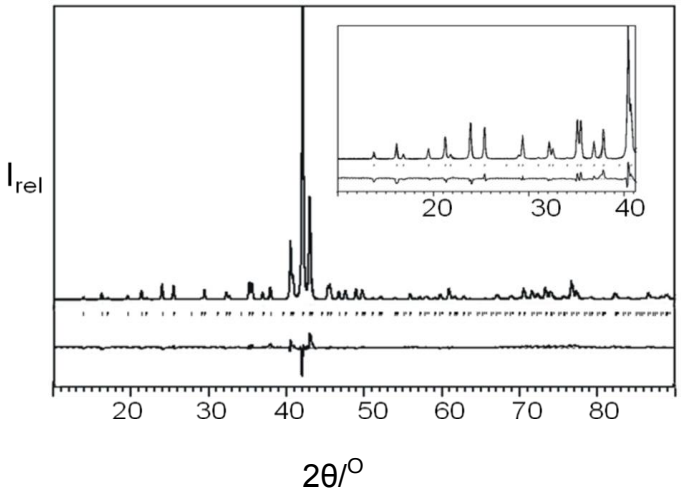

Figure 5.2.2: Observed and calculated X-ray powder diffractogram of $Au_{2.63}Cr_{6.36}Zn_{91.68}$ over the 2θ range 10-90° together with the profile fit, the difference spectrum and the Bragg positions. Insert shows low angle Rietveld profile fit; $Cu_{K\alpha,}$ a = 1828.8 (2) pm; R_B = 0.0587, R_P = 0.0681.

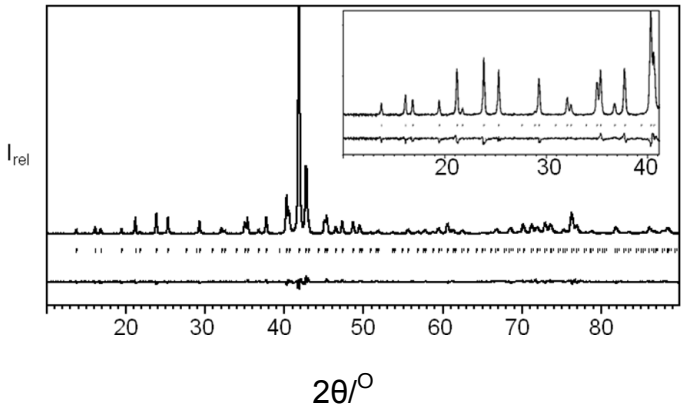

Figure 5.2.3: Observed and calculated X-ray powder diffractogram of $Au_{5.15}$ $Cr_{4.73}Zn_{91.93}$ over the 2θ range 10-90^O together with the profile fit, the difference spectrum and the Bragg positions. Insert shows low angle Rietveld profile fit; $Cu_{K\alpha,}$ a = 1836.5 (1) pm; R_B = 0.0279, R_P = 0.0513.

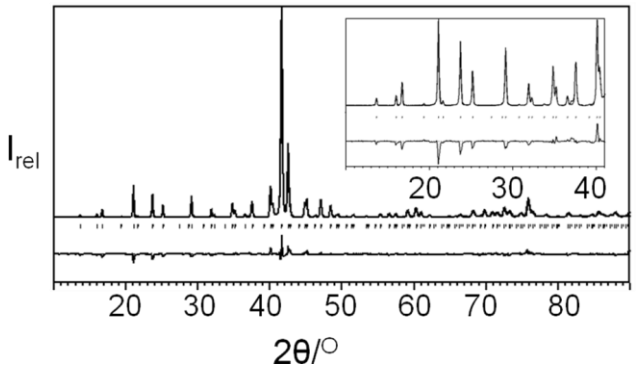

Figure 5.2.4: Observed and calculated X-ray powder diffractogram of $Au_{10.0}Cr_{4.0}Zn_{89.0}$ over the 2θ range 10-90^O together with the profile fit, the difference spectrum and the Bragg positions. Insert shows low angle Rietveld profile fit; $Cu_{K\alpha,}$ a = 1843.0(1) pm; R_B = 0.05643, R_P = 0.06277.

The relevant data concerning the refinements are given in the figure caption. Four diffraction patterns in the 2θ range 7-41° are shown in the Fig. 5.2.5. Progressively substitution of Cr and Zn by Au is reflected in a modified intensity modulation becoming most obvious for some low angle diffraction intensities (c.f. Fig. 5.2.5).

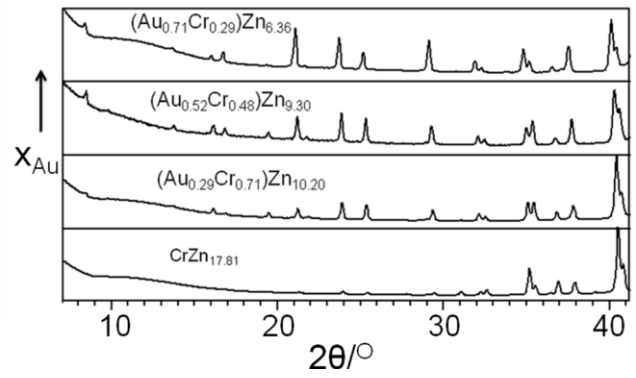

Figure 5.2.5: X-ray powder diffraction patterns in the 2θ range 7-41° observed for $CrZn_{17.81}$, $Au_{2.63}Cr_{6.36}Zn_{91.68}$, $Au_{5.15}Cr_{4.73}Zn_{91.93}$ and $Au_{10.0}Cr_{4.0}Zn_{89.0}$.

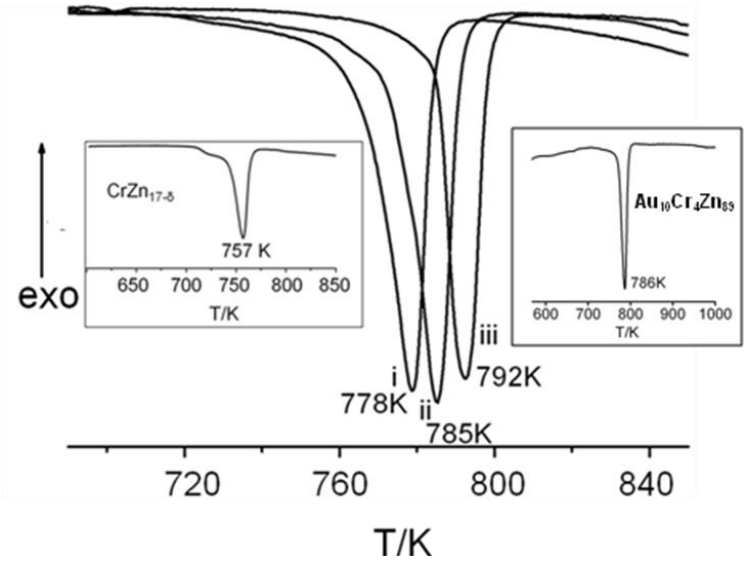

Figure 5.2.6: Thermo-chemical analysis of $Au_{2.63}$ $Cr_{6.36}$ $Zn_{91.68}$ (i), $Au_{3.80}Cr_{5.33}Zn_{91.75}$ (ii), $Au_{7.69}Cr_{4.30}$ $Zn_{91.03}$ (iii). Transformation from solid to liquid is shown for different samples of the Au-Cr-Zn system. Insert (left) shows the thermal stability range of $CrZn_{17-\delta}$ and (right) shows the thermal stability of $Au_{10}Cr_4Zn_{89}$.

The decomposition temperatures change according to compositions of the phase throughout the homogeneity range. The peak maxima shift towards higher temperature with increase of gold content the homogeneity range as in Fig. 5.2.6. Phase of Au-Cr-Zn

system resist to recrystallize at a chosen cooling rate of 10 K h^{-1}. The phase does not reform even after 12 h annealing prior to the melting of the corresponding sample.

Table 5.2.5.1: Onset temperatures and peak maxima concerning DTA measurement of single phase samples in Au-Cr-Zn system

	Melting point (T_m)	
x_{Au}	Onset (K)*	Peak maxima (K)
0.026	753	778
0.038	758	785
0.075	768	792
0.097	762	786

* The onset is the point of intersection of the tangent drawn at the point of greatest slope on the leading edge of the peak with the extrapolated base line.

Magnetic properties and resistivity: Molar magnetic susceptibilities of polycrystalline samples(x_{Au} = 0.026, x_{Au} = 0.032, x_{Au} = 0.055, x_{Au} = 0.061, x_{Au} = 0.075 and x_{Au} = 0.097) were recorded with a SQUID magnetometer in the temperature range 1.8-300 K at a magnetic flux density of 1-5 Tesla. The data were recorded for magnetic contributions from the sample holder made of gelatine. The diamagnetic contributions of the sample holder were subtracted from the data. Depending on the composition of the phase the magnetic behavior reaches from a resulting paramagnetic on the Cr-rich edge to diamagnetic on the Au-rich edge. On the edges, we can clearly explain the overall magnetic properties by diamagnetic contributions and additionally Curie-Weiss like contributions. Depending on the nature of two parts, materials behave either paramagnetic or diamagnetic (Fig. 5.2.7.1 & Fig. 5.2.7.2). Samples with intermediate composition could not be described this way, they behave mainly diamagnetic and temperature independent. For the five samples the temperature independent susceptibility $\chi_0 x10^{-11}$ m^3 mol^{-1} values amounted to -5.2 (6), -1.5 (3), -10.0 (1), -14.0 (7), -17.3 (2) and -6.0 (1), respectively. The negative values indicate that the Pauli paramagnetism is overcompensated by the core diamagnetism of the respective

compounds. Numerical data regarding magnetic properties are summarized in the Table 5.2.5.2.

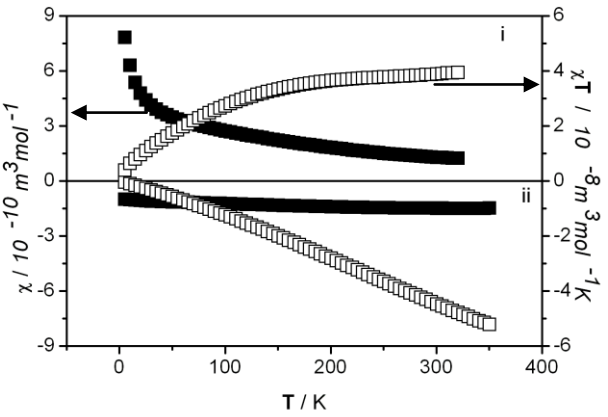

Figure 5.2.7.1: Magnetic susceptibility as a function of temperature for $Au_{2.63}$ $Cr_{6.36}$ $Zn_{91.68}$ (i) and $Au_{7.69}Cr_{4.30}$ $Zn_{91.03}$ (ii) at 5 T.

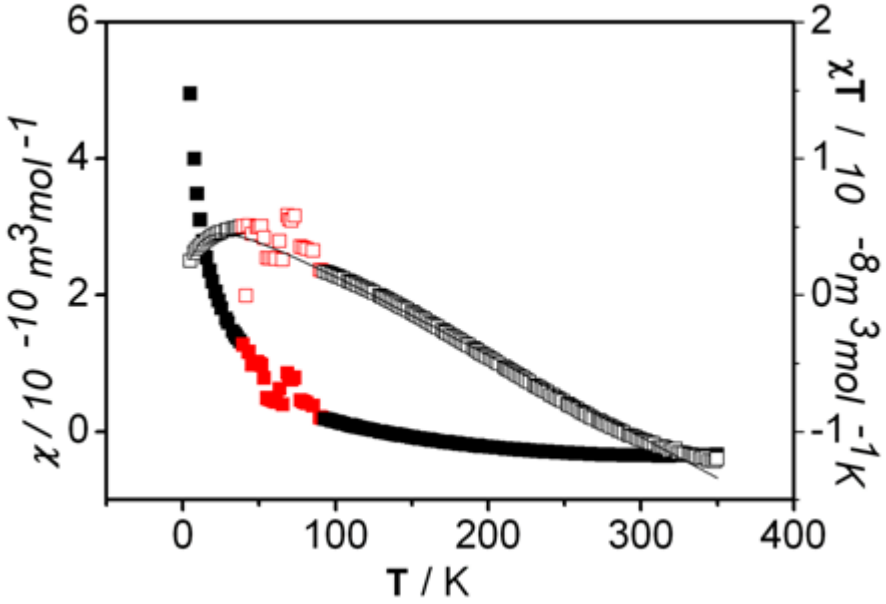

Figure 5.2.7.2: Magnetic susceptibility as a function of temperature for Au_{10} Cr_4 Zn_{89} at 1 T.

Table 5.2.5.2: A summary of magnetic data for selected crystalline specimens

Composition	χ_0 (10^{-11} m^3 mol^{-1})	μ_{eff} (μB)	θ (K)	B (T)
$Au_{2.36}Cr_{6.36}Zn_{91.68}$	-5.2(6)	0.90(2)	-149(8)	5
$Au_{3.26}Cr_{5.74}Zn_{91.57}$	-1.5(3)	0.86(1)	-123(3)	1
$Au_{5.62}Cr_{4.57}Zn_{92.25}$	-10.0(1)	linear fit	-	5
$Au_{6.19}Cr_{4.50}Zn_{921.19}$	-14.0(7)	linear fit.	-	5
$Au_{7.69}Cr_{4.30}Zn_{91.03}$	-17.3(2)	0.30(2)	-116(15)	5
$Au_{10}Cr_4Zn_{89}$	-6.0(1)	0.36(1)	-9(1)	1

χ_{Tip} = Temperature independent molar susceptibility
μ_{eff} = Effective magnetic moment
θ = Weiss temperature
B = Magnetic flux density

Electrical resistivity at constant current and variable temperature (30-300K) changes barely with the composition of the ternary phases. Au-poor sample with nominal composition x_{Au} = 0.026 exhibits weak metallic conducting property (i-a). Samples richest in Au with nominal composition x_{Au} = 0.068 and x_{Au} = 0.077 show moderate metallic behavior with increasing resistivity for increasing temperature (Fig. 5.2.8 (v-c) & (vi-c)). Samples having a medium Au-content (x_{Au} = 0.038, x_{Au} =0.046, and x_{Au} = 0.055) resistivities steadily decrease with temperature from 30K to 300K (Fig. 5.2.8 (ii-b), (iii-b) and (iv-b)). Furthermore, $Au_{10}Cr_4Zn_{89}$ shows resitivity ρ steadily growing from 0.33 mΩcm (30K) to 0.45 mΩcm (300K) (Fig.5.2.8 (vii-d)). Data concerning the electrical properties of the Au-Cr-Zn system are listed in the Table 5.2.5.3.

The resistivities of the Au-Cr-Zn ternary phases at 300 K are nearly two orders of magnitude higher than that of the constituting elements–$\rho_{Zn,\ 293K}$ = 5.8 μΩ cm, $\rho_{Cr,293K}$ = 12.5 μΩ cm, $\rho_{Au,293K}$ = 2.44 μΩ cm.

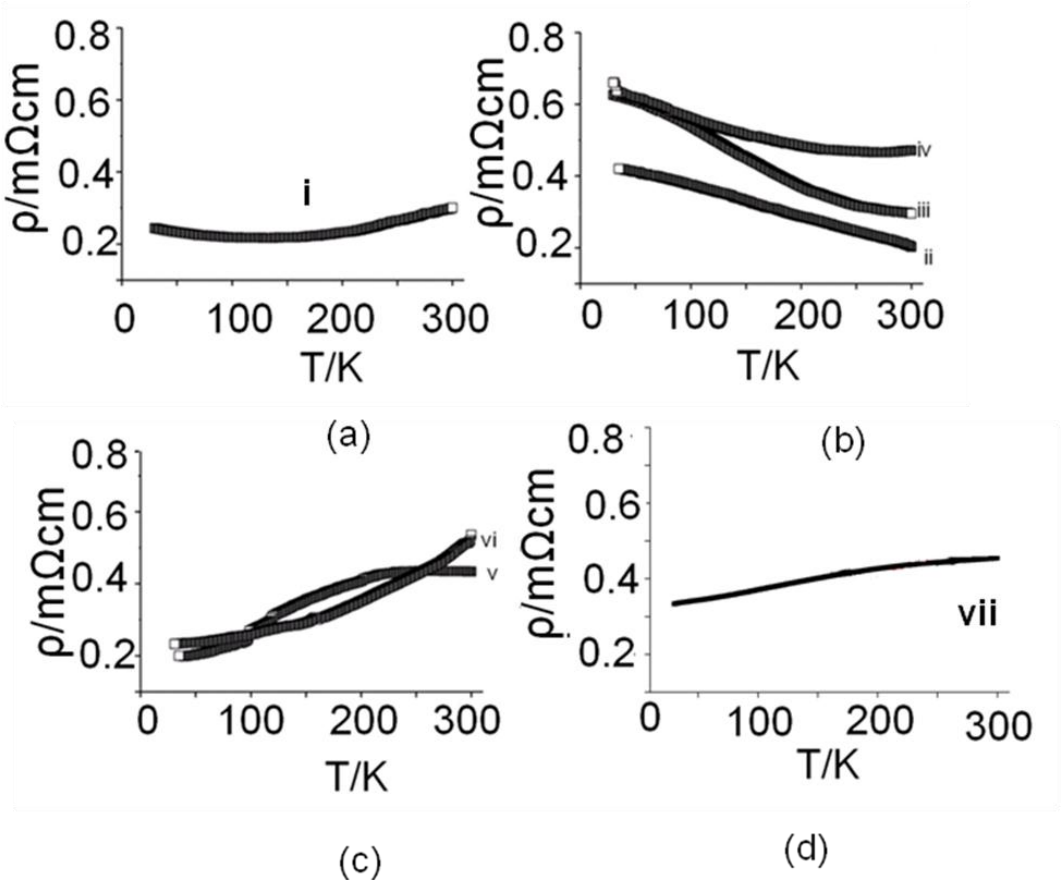

Figure 5.2.8: Resistivities ρ of single phase samples $Au_{2.63}$ $Cr_{6.36}$ $Zn_{91.68}$ (i-a), $Au_{3.80}$ $Cr_{5.37}$ $Zn_{91.75}$ (ii-b), $Au_{4.59}Cr_{4.85}Zn_{91.33}$ (iii-b), $Au_{5.62}Cr_{4.57}Zn_{92.25}$ (iv-b), $Au_{6.88}Cr_{4.53}Zn_{90.13}$ (v-c), $Au_{7.88}Cr_{4.29}Zn_{90.42}$ (vi-c) and $Au_{10}Cr_4Zn_{89}$ (vii-d) between 30-300 K.

Table 5.2.5.3: A summary of resistivity data for the selected crystalline specimens

	x_{Au}	ρ_{30K} (mΩcm)	ρ_{300K} (mΩcm)
a (i)	0.026	0.24	0.30
b (ii)	0.038	0.42	0.20
(iii)	0.046	0.63	0.30
(iv)	0.055	0.66	0.47
c (v)	0.068	0.20	0.43
(vi)	0.077	0.23	0.53
(vii)	0.097	0.33	0.45

5.2.4 Structural Characteristics

The ternary phase in the Au-Cr-Zn system forms a structurally complex γ-brass related phase belonging to the group of cubic giant cell structures. The phase crystallizes in the acentric space group $F\bar{4}3m$ with approximately 402-412 atoms in the cubic unit cell that are distributed over 15-19 crystallographically independent positions depending on the chemical composition of the phase. The number of atoms in the unit cell changes parallel to the increase of the gold-content. Hence, the lattice parameters vary linearly with mole fraction of gold (x_{Au}) throughout the homogeneity range as shown in the Fig. 5.2.9.

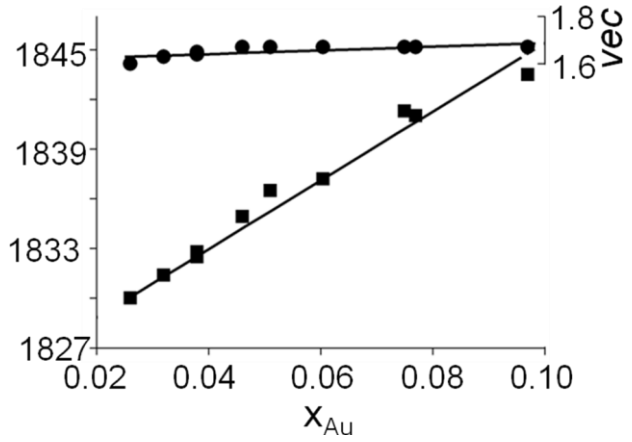

Figure 5.2.9: Lattice parameters vs. mole fraction of Au (x_{Au}) from single crystal X-ray diffraction experiment of Au–Cr–Zn phase. The *vec* observed for the refined compositions is shown at the top of the graph.

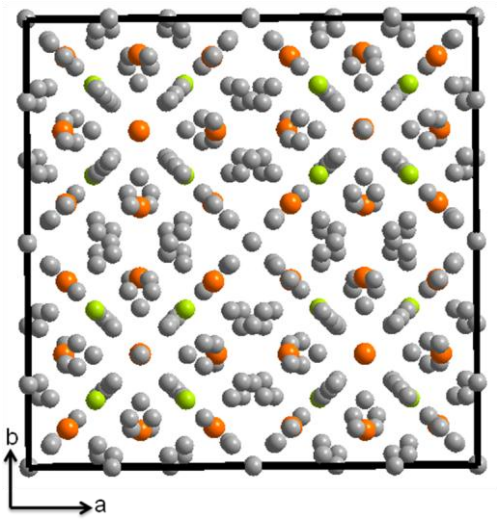

Figure 5.2.10: The projection of the atoms of the $Au_{10}Cr_4Zn_{89}$ structure onto the *ab* plane of the unit cell.

The the volume increment coming along with the increasing number of vacancies with the increasing gold content of the phase is overcompensated by the larger atomic volume of gold (10.2 cm^3 mol^{-1}) compared with that of chromium (7.23 cm^3 mol^{-1}) and zinc (9.2 cm^3 mol^{-1}). The structure of the phases adopts a 6 x 6 x 6 superstructure of a body centered cubic type structure with ordered vacancies, [146] or, alternatively, 2 x 2 x 2 superstructure of a γ-brass related structure.[23]

The structure of these complex cubic structures is fairly complicated (c.f. Fig. 5.2.10). In order to understand them, several approaches have been proposed to organize the atoms into simple, recognizable patterns.

In a first such approach, the structures may be regarded as arrangements of nested polyhedral units, [132, 147] isolated or linked, centered at sites of high symmetry points. Such arrangements of nested polyhedral unit have been termed as ‘clusters’. [131] This is a purely geometric description. The aggregations of atoms are not actually clusters in a chemical sense. They are not separated from the residual part of the structure. The

arbitrary sets of atoms simplify the task of visualizing and memorizing such complicated structures.

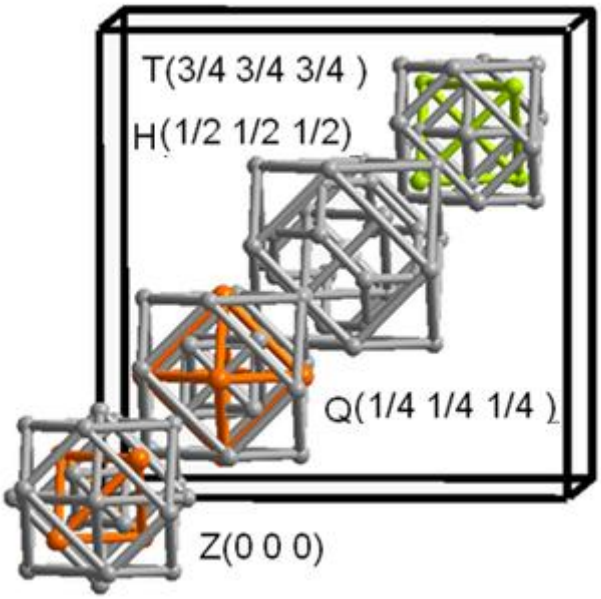

Figure 5.2.11: The arrangement of clusters in the crystal structure of $Au_{10}Cr_4Zn_{89}$ along the body diagonal, clusters are centered about the high symmetry points of the *F*-centered cubic unit cell and their identities are revealed. The clusters are represented by idealized cuboctahedral shells. Constituting zinc atoms are shown in gray (40%), chromium in lime and gold in orange.

In another approach the structures are described in terms of their coordination polyhedra, c.f. Fig. 5.2.12.

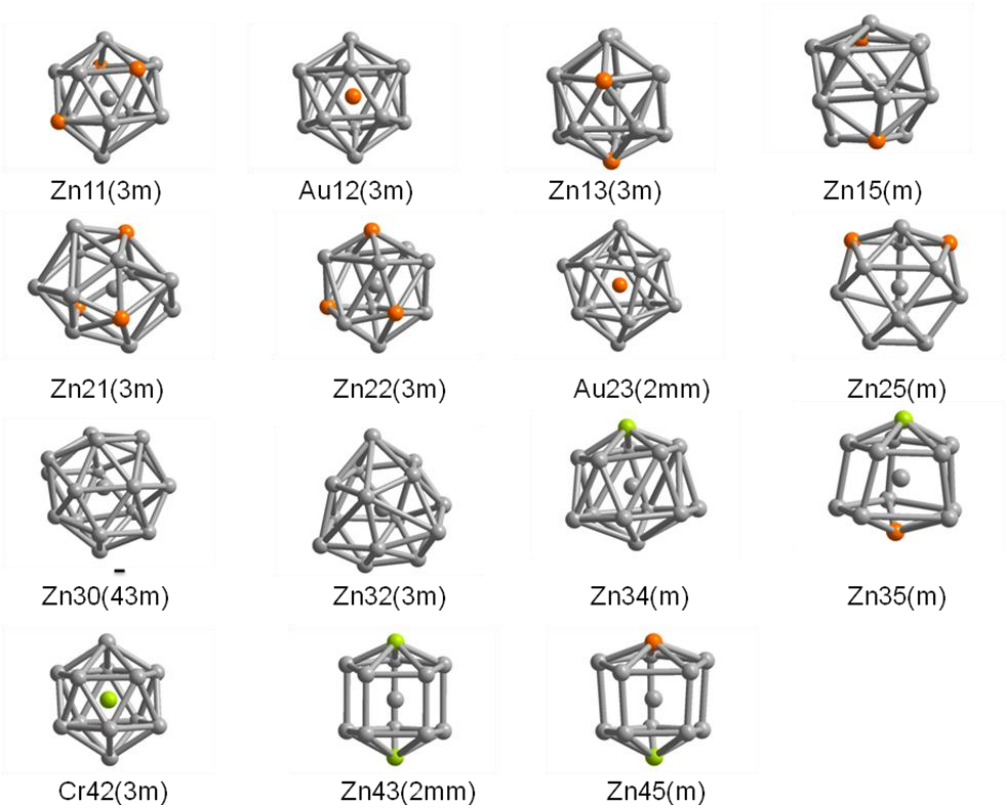

Figure 5.2.12: The coordination polyhedra of the atoms Au, Cr, Zn of the $Au_{10}Cr_4Zn_{89}$ structure is shown. Both gold (Au12 & Au23) sites and the chromium site (Cr42) are coordinated by 12 zinc atoms which form icosahedra. The remaining zinc atoms of $Au_{10}Cr_4Zn_{89}$ occupy 12 atomic sites with coordination numbers varying between 12 and 16. Constituting zinc atoms are drawn in gray (40%), chromium in lime and gold in orange.

In a third approach, the structures can be visualized as consisting of atomic layers, c.f. Fig. 5.2.13.

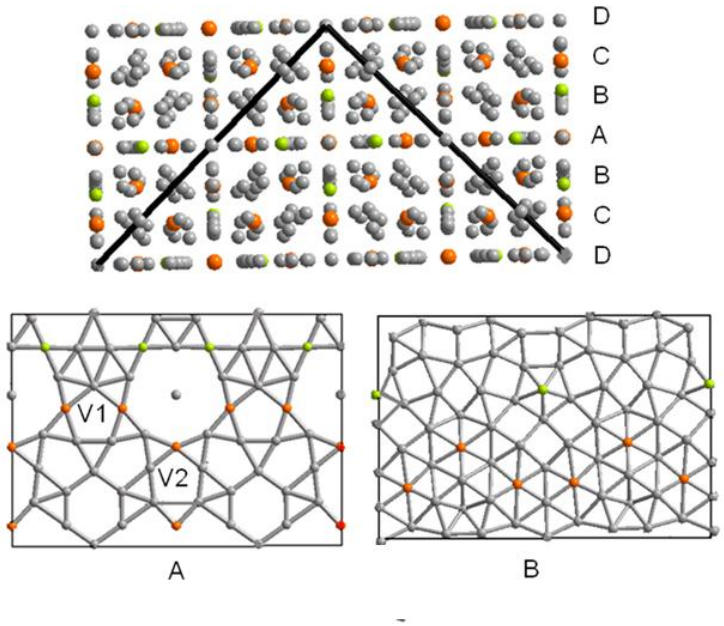

flat layer puckered layer

Figure 5.2.13: The projection of the structure of $Au_{10}Cr_4Zn_{89}$ along [110] has been depicted. Only one-half of the cell are shown. Stacking of four different atomic layers can be discerned; they are labeled as A, B, C, D. The position V1 corresponds to the lattice points (½ 0 ½) and (0 ½ ½) of the fcc lattice. If the origin of the cell is allowed to move at the atomic positions V1, the layers A can be transformed to D and B to C.

Here we choose the first approach for getting insight in some structural characteristics of this new ternary or pseudo-binary system. According to the concept, the four constitutive clusters are located at the high symmetry points of the unit cell: (0 0 0), (¼ ¼ ¼), (½ ½ ½), and (¾ ¾ ¾) and equivalent translational invariant points. So, structures are formed by 4 x 4 clusters. We designate each cluster type by a capital letter indicating the central position of each cluster, i.e., Z for 0, Q for ¼, H for ½, and T for ¾. [133] Furthermore, the clusters will be differentiated by a set of three or four atomic shells composing the clusters. The shells are congruent to one of the various Platonic and Archimedean solids. Each shell corresponds to a distinct crystallographic site and is distinguished by two capital letters. CC designates the centre of a cluster, IT those occupying the vertices of an inner tetrahedron. Accordingly, OT stands for outer

tetrahedron, TT for truncated tetrahedron, also called Friauf polyhedron and CO for cuboctahedron. Furthermore, we numerate atoms of a given cluster according to their distance from the centre of the cluster.

As previously mentioned in Chapter 4 for $CrZn_{17-\delta}$, the atomic arrangement of structures in the Au–Cr–Zn system can be subdivided into two partial structures of similar size and different composition. One part of the structure is completely ordered built up by H and T clusters and made of 204 atoms, hence, compositionally invariant throughout the homogeneity range of the phase. Both the clusters are arranged like carbon atoms in diamond. The second partial structure comprising the Z and Q clusters is partly disordered and variable in composition. They also form a diamond-like arrangement. The two diamond like frameworks shifted by one half of a lattice vector, interpenetrate [148,149] mutually but contactless to each other.

The compositionally invariant partial structure: The H cluster of the compositionally invariant partial structure consists of a central Zn atom, a TT shell of 12 Zn34 with 4 additional OT Zn32 above the hexagonal faces of the truncated tetrahedron. The Zn_{17} units are enclosed by 12 CO Zn35, resulting in a clean Zn_{29} α-Mn-type cluster. The second well-ordered cluster is built up by 22 atoms and grouped about T. The largest portion of the Cr-content of the compound, Cr42, is segregated on T OT sites. 6 OH Zn43 bisect the edges of the Cr42 OT. Twelve surrounding Zn45 CO complement the $NiTi_2$-type Cr_4Zn_{18} cluster (Fig. 5.2.17.2). Clusters H and T remain unaffected from Cr and Zn replacement by Au. Accordingly, the composition of the ordered substructure is Cr_4Zn_{47}. The two clusters H and T are arranged like zinc and sulphur atom in the zinc blende structure.

The compositionally variable partial structure: The second partial structure is formed by the Z and Q clusters. It varies in composition between $Au_{2.64}Cr_{2.36}Zn_{44.72}$ and $Au_{10.0}Zn_{42.0}$. The variation of composition is accompanied by various disorder phenomena.

(i) random vacancies due to partly occupied sites

(ii) mutual substitution of the two components on specific sites

(iii) positional disorder in form of split positions

The Z cluster builds up by partly occupied Zn10 CC and Zn11 IT sites, mixed occupied M12 OT sites, Zn13 OH and an outer Zn15 CO shell. OT sites are mixed occupied by Au and Cr in the ternary Au-Cr-Zn phase. The disorder of type (i) gives rise to a physically meaningless short distance between Zn10 and Zn11. The clear correlation between the independently refined occupation factors f(CC) = 1-f(IT), (c.f. Table 5.2.2) can be rationalized by assuming that either a defect bcc-type cluster with shell sequence CC, OT, OH, CO or a γ-type cluster (IT, OT, OH, CO) is situated about Z. Correspondingly, we can built a bcc-type cluster or γ-brass type cluster on positions Q. The bcc type cluster consists of CC, IT´, OT, OH, CO. Moreover, Zn23 OH sites are occupied and other OH atoms take two symmetrically uncoupled twofold split positions OH' and OH''. Twelve Zn25 form the outermost CO shell.

Structure-composition relations: In this section we will discuss the correlation between the chemical composition and different forms of disorders in clusters Z and Q that gives rise to the width of the phase. Variable mutual substitution of the two distinct chemical constituents occurs on two specific atomic sites-M12 and M23. A clear trend observed for mixing of Au/Cr in cluster Z and Au/Zn in cluster Q. In samples with composition ranging $0.026 \leq x_{Au} \leq 0.032$, Au linearly substitutes Cr in M12 atomic site (c.f. Fig. 5.2.14). Sample starting with a composition of $x_{Au} = 0.038$, Au starts to substitutes for Zn on the M23 (perfect octahedral site) in addition to the M12 site. For specimens with $x_{Au} \geq 046$, the M12 site remains fully occupied by Au while linear substitution continues in M23 site (Fig. 5.2.14). Hence, the depletion of Zn by Au substitution throughout the homogeneity range is essentially limited to cluster Q.

Zn 21´ IT is threefold split and shows random vacancies as well. A closer inspection of the variation of the amount of random vacancies [$V_{Q\ (IT')} = 1\text{-}3 \times f_{Q\ (Zn21')}$] in cluster Q with relative amount of gold (x_{Au}) reveals a linear interrelation between mutual substitution and random vacancy (Fig. 5.2.15).

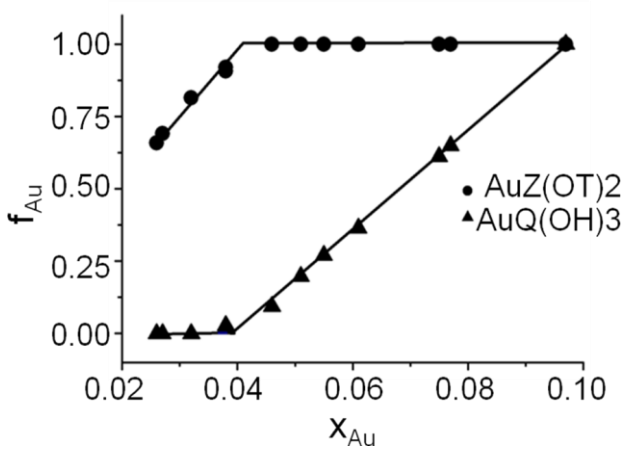

Figure 5.2.14: Representation of substitutional disorder: site occupancy factor of gold (f_{Au}) (at OT site of cluster Z and M23 octahedral site of cluster Q) vs. mole fraction of Au (x_{Au}) in the Au–Cr–Zn system.

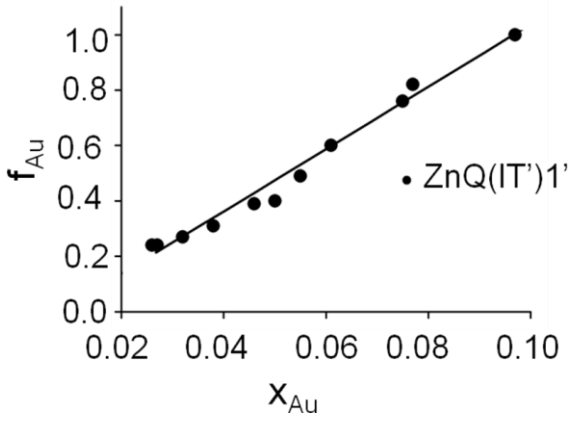

Figure 5.2.15: Random vacancy at IT' site ($V_{Q(IT')}$ = 1-$f_{Q(IT')}$) versus relative amount of gold. (x_{Au}) in the ternary Au-Cr-Zn system.

Cluster Z consists of partly occupied Zn10 CC and Zn11 IT. Furthermore, cluster Q consists of partially occupied Cr20 CC and Zn21 IT. The SOF of Zn10 and Zn11 atoms are linearly dependent. Therefore, vacancies at Zn10 ($V_{Z(CC)}$ = 1-$f_{Z(CC)}$) and Zn11 ($V_{Z(IT)}$ = 1-$f_{Z(IT)}$) in the cluster Z show clear linear interrelation with relative amount of Au (Fig. 5.2.16-i). Correspondingly, vacancy at Cr20 and Zn21 assigned as $V_{Q(CC)}$ and $V_{Q(IT)}$

manifest a further linear interrelation parallel to the relative amount of gold (Fig. 5.2.16-ii).

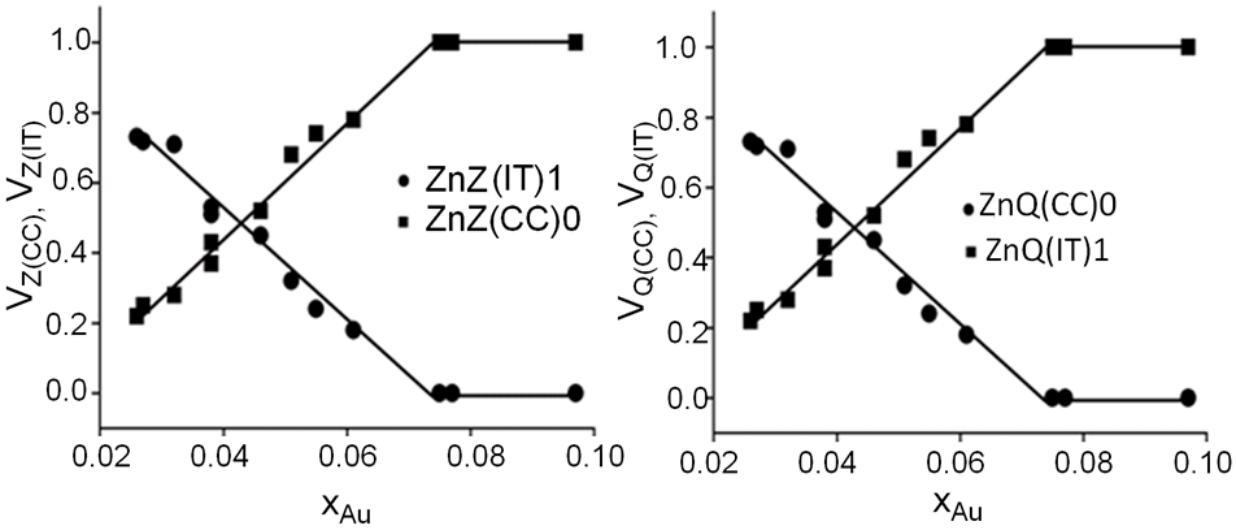

Figure 5.2.16: (i) Vacancy at CC site ($V_{Z(CC)}$ = 1-$f_{Z(CC)}$) and at IT site ($V_{Z(IT)}$ = 1-$f_{Z(IT)}$) of cluster Z and (ii) vacancy at CC site ($V_{Q(CC)}$ = 1-$f_{Q(CC)}$) and at IT site ($V_{Q(IT)}$ = 1-$f_{Q(IT)}$) of cluster Q vs. mole fraction of gold (x_{Au}) in the Au-Cr-Zn system.

Zn10 is uniquely identified with defect bcc-type, where it is situated at the OT site of cluster Z. Correspondingly, Zn11 defines the IT site of γ-brass-type in cluster Z. Furthermore, Cr20 defining the CC site is the characteristics for β-brass-type cluster in Q and Zn21 defining the IT site specify γ-brass-type in Q. Hence, we conclude that cluster Z transmutes from a mixture of a defect bcc-and γ-brass-type clusters to a clean γ-brass-type Au_4Zn_{22} cluster (Fig. 5.2.17.1 left) by progressive replacement of Cr and/or Zn by Au and cluster Q transforms from a β-brass-type cluster to a clean γ-brass-type Au_6Zn_{20} over the mixture of β-and γ-brass types by Au/Cr and/or Au/Zn replacement (Fig. 5.2.17 1 right). Hence, in the phase richest in Au all kinds of disorders are vanished in favour of the formation of perfectly ordered Au_4Zn_{22} and Au_6Zn_{20} γ-brass-type clusters.

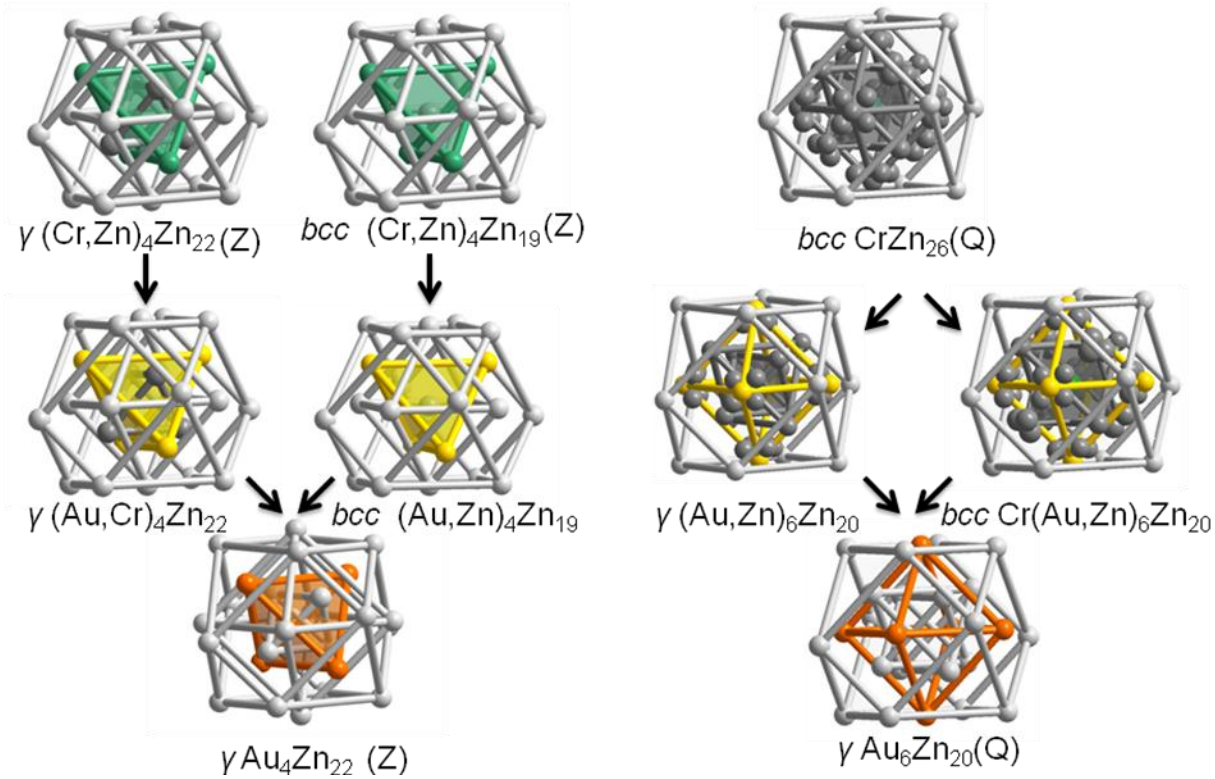

Figure 5.2.17.1: (left) Transmutation of cluster Z at (0 0 0) form a mixture of defect bcc and γ-brass in the crystal structure of $Cr_{1.36}Zn_{23.79}$ to clean γ-type Au_4Zn_{22} in $Au_{10}Cr_4Zn_{89}$ by progressive replacement of Cr and Zn by Au. Constituting zinc atoms have been shown in gray, Cr/Zn in sea green and Au/Cr in gold and gold in orange.

(right) Transmutation of cluster Q at 1/4 1/4 1/4 from a bcc-type cluster to a clean γ-brass-type cluster by replacement of Cr and Zn by Au. Constituting zinc atoms have been depicted in gray, Au/Zn in gold and Au in orange.

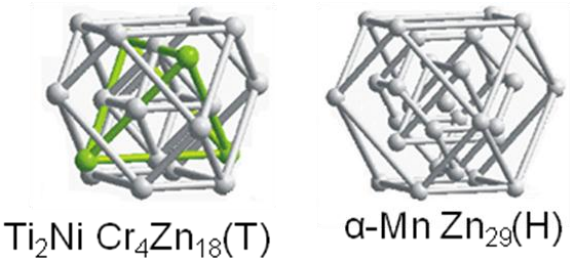

Figure 5.2.17.2: Representation of the cluster H at 1/2 1/2 1/2 α-Mn-type Zn_{29} (right) and cluster T centered at 3/4 3/4 3/4 $TiNi_2$-type Cr_4Zn_{18} (left)-unaffected by Au/Cr and /or Au/Zn replacement.

Positional disorder of OH site in cluster Q arises from physically meaningless short distances between OH' and OH'' atoms (see Fig.4.8 in Chapter 4). Independent refinements of the fractional occupancies for Au-poor samples having composition of x_{Au} = 0.026, 0.027, 0.032 result in the relation f(Zn23) + 2 x f(Zn23') + 2 f(Zn23'') ≈ 1. Correspondingly, Au-rich sample of x_{Au} = 0.077 confirms the relation f(Au23) + 2 x f(Zn23') + 2 f(Zn23'') ≈ 1 and sample of x_{Au} = 0.097, f(Au23) = 1. But, for the crystals of nominal composition ranging from 0.077 > x_{Au} ≥ 0.038, the sum of SOF of three very close sites (OH, OH', OH'') shows considerable deviations from full occupancies. This problem can be resolved if we assume that mutual statistical substitution of two constituents (Au and Zn) on specific perfect octahedral site (OH) obey the previous relation. So all six and not more OH positions per cluster are occupied.

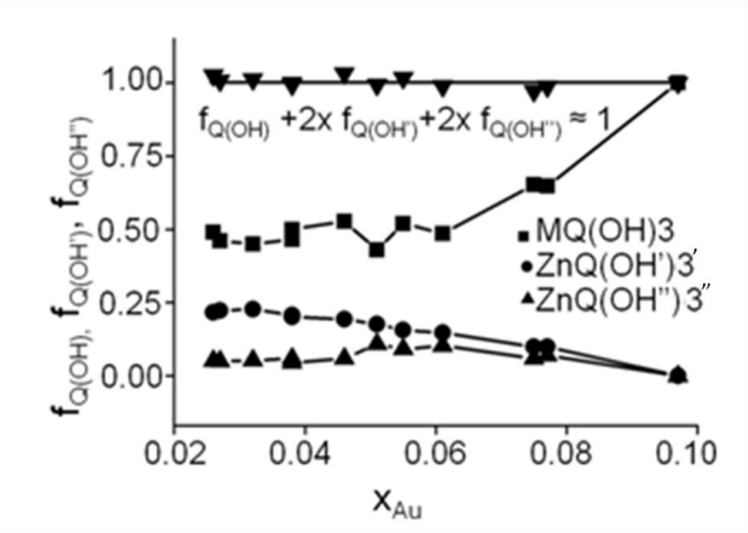

Figure 5.2.18: Representation of positional disorder: site occupancy factors at octahedral sites (f_{OH}, $f_{OH'}$, $f_{OH''}$) of cluster Q vs. mole fraction of Au (x_{Au}) from single crystal X-ray diffraction experiment of the various Au-Cr-Zn samples.

With increasing gold-content a clear increase of $f_{Q(OH)}$ site and a clear decrease of $f_{Q(OH')}$ are observed, accompanying the change from the split octahedral sites (OH, OH', OH'')

to a perfectly ordered octahedral position (OH) accumulating full gold occupancy (Fig. 5.2.18).

An additional correlation between site occupancy factors provide evidence that f(Zn22) + f(Zn23'') ≈ 1. But no clear trend of the change of occupation on the Zn22 and the Zn23'' sites is observed parallel to the overall Au-content of the phase.

Correlations among the SOF of disordered sites indicate that the defect bcc/β-brass-type cluster predominates at the Au-poor phase boundary whereas the clean γ-brass type Au_4Zn_{22}/Au_6Zn_{18} clusters form at the Au-rich phase boundary.

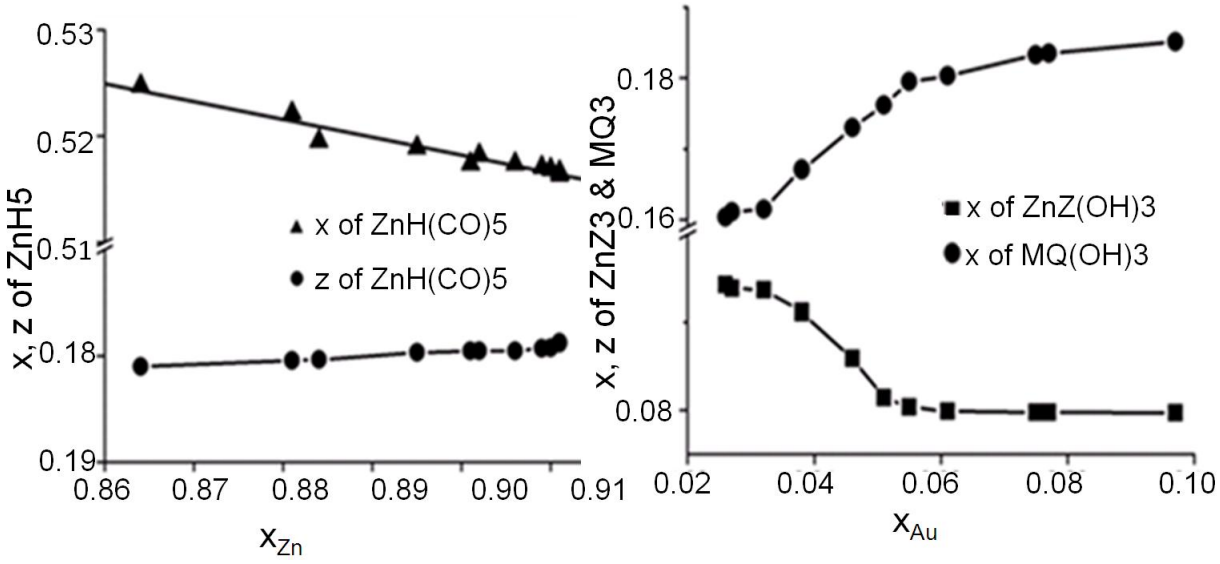

Figure 5.2.19: Positional parameters (x, z) for CO atoms of cluster H vs. mole fraction of Au (x_{Zn}) from single crystal X-ray diffraction experiment of the various samples of the Au-Cr-Zn system (left).

Positional parameters (x) for OT atoms of cluster Z and OH atoms of cluster Q vs. mole fraction of Au (x_{Au}) from single crystal X-ray diffraction experiment of the various Au-Cr-Zn samples (right).

An analysis of positional parameters associated with the Zn35 site reveals a clear trend between (x, z) and mole fraction of zinc within the homogeneity range. With increasing

zinc content, x values of H(CO)5 drop linearly whereas z values increase (Fig. 5.2.19-left), though the H cluster remains compositionally intact throughout the homogeneity range by Cr/Au and/or Zn/Au replacement. Furthermore, x values associated with Zn13 in cluster Z reduce and x value of M23 in cluster Q increases parallel to Au insertion in the phase (Fig. 5.2.19-right).

The correlations among site occupancy factors f (c.f. Table 5.2.2) provide evidence that the various disorder phenomena in various shells are spatially correlated and show flexibility in composition. Some kind of information transfer takes place to those Cr and Zn sites which vary with composition. The gradual increase in Au-content-essentially confined to the mixed occupied OT site of cluster Z and perfect OH site of cluster Q results in a concomitant change of the site occupancy factors: f(Z,Zn11), f(Q, Zn21), f(Q,Zn21´). These factors specify an interrelation between the compositional changes in the cluster types of the compositionally variable partial structure in a structurally complex metallic alloy.

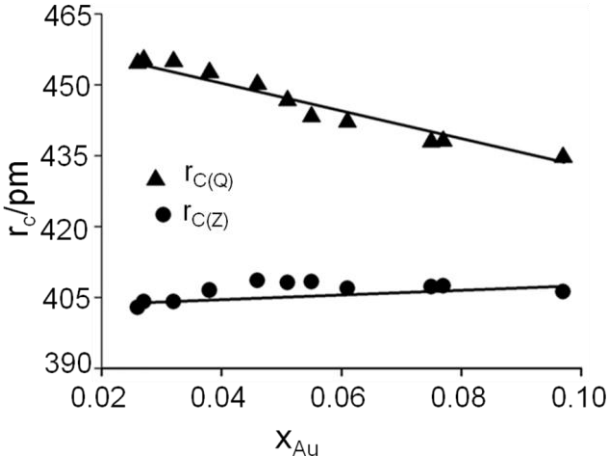

Figure 5.2.20: Effective cluster dimensions ($r_{C(Z)}$, $r_{C(Q)}$) for cluster Z and Q vs. mole fraction of Au (x_{Au}) from single crystal X-ray diffraction experiment of the various Au-Cr-Zn specimens.

We assume that such vacancies as well as partial mixing of Au/Cr and/or Au/Zn on various sites are crucial to keep the *vec* nearly constant in terms of Hume-Rothery stabilisation. If we take for Au 1e, for Cr -4 e and for Zn 2 e into account, we obtain *vec* values covering the range between 1.60 and 1.68 per atom (Fig. 5.2.9). In samples with composition ranging $0.026 \leq x_{Au} \leq 0.032$, Au linearly substitutes Cr on the M12 atomic site. The partial replacement of Cr by Au increases the valence electron concentration. But increase of vacancies at the zinc site (Zn21') with the increasing Au content of the M12 atomic site keeps the *vec* values of the phases close to the expected ideal values for γ-brass-type phases. Moreover, for specimens with $x_{Au} \geq 046$ the M12 site remains fully occupied by Au while substitution of Zn by Au occurs on the M23 site. Substitution of Zn by Au on the M23 site and parallel increase of no of vacancies at Zn21' site reduce the *vec* values from 21/13. But a concomitant increase of the Zn fraction at IT i.e. f(Zn21) and the reduction of the Cr fraction at CC (fCr20) of cluster Q throughout the homogeneity range occur keeping the vec values constant. Noteworthy, the value of the phase at the Cr-rich boundary is close to the expected ideal value of the Hume-Rothery rules for γ-phases, i.e. 21/13 = 1.615. Recent results show that the range can vary between 1.59 and 1.77. [150] In conclusion, the variations in composition associated with the structural changes occurring along the homogeneity range of the Au-Cr-Zn phase are interrelated in such a way that the *vec* value of the phase varies only little.

In the last section, we will discuss the effect of Au substitution on the effective cluster dimension, i.e. circumference radii r_C for respective cuboctahedra, given by the distance between their centre (CC sites) and their vertices (CO sites) throughout the homogeneity range. The dimension of the compositionally conserved clusters (H, T) endures marginal variation. With increasing gold content $r_{C(H)}$ decreases from 496 at gold-poor boundary to 495 pm at Au-rich side whereas $r_{C(T)}$ drops from 375 to 372 pm. On the other hand, cluster Q shows a notable variation in its effective dimension, whereas cluster Z does not change significantly in size, though both Q and Z form

compositionally variable partial structure. With increasing gold content, $r_{C(Q)}$ drops systematically from 455 to 447 finally ending at 435 pm, changing from heavily disordered β-brass-type cluster to clean γ-brass-type Au_6Zn_{20} (Fig. 5.2.20). Finally, for cluster Z, $r_{C(Z)}$ increases from 403 pm (for both defect bcc and γ-brass-type at Au-poor phase) to 406 pm (for clean γ-brass-type Au_4Zn_{20} at Au-rich side). Moreover, γ-bass cluster of composition Au_6Zn_{20} ($r_{C(Q)}$ = 435 pm) shows a volume approximately 20% larger than that of the congeneric Au_4Zn_{22} cluster ($r_{C(Q)}$ = 406 pm).

5.2.5 Summary

The structure of $CrZn_{17-\delta}$ system can be distinctly modified by replacing chromium and zinc by gold. It uncovered $(2a_\gamma)^3$ superstructure of γ-brass-related phase ranging from $Au_{2.6}Cr_{6.4}Zn_{91.7}$ to $Au_{10}Cr_4Zn_{89}$. According to single crystal diffraction experiments, the ternary phase crystallizes in the acentric space group type $F\bar{4}3m$ with approximately 403-412 in the cubic unit cell having a significant phase width. The structure of the cubic phase consists of six distinctive clusters each having 22-29 atoms arranged at 16 high symmetry points of the unit cell. The structure can be divided into two partial structures. One partial structure consists of clean α-Mn-type Zn_{29} (H) and $NiTi_2$-type Cr_4Zn_{18} (T) clusters are ordered and remain unaffected during the replacement of Cr and/or Zn by Au over the homogeneity range. Its complement shows variable composition and hosts three types of disorders such as vacancies (Zn10/Zn11, Cr20/Zn21, Zn21´), substitution (Au and Cr or Au and Zn) and positional disorder (M23/Zn24/Zn26 and Zn21´) in the form of split positions. This variable partial structure endures significant effects by Au/Cr and/or Au/Zn substitution on constituting clusters: mixture of disordered γ-brass-type and defect bcc type clusters transmute to clean γ-brass type Au_4Zn_{22} and disordered bcc type clusters transform to clean γ-brass-type Au_6Zn_{20} over an intermediate mixture of bcc and γ-brass-type clusters.

An extensive study of compositionally different crystals of the solid solution $(Au,Cr)Zn_n$, n = 10.2–6.4 reveals a systematic spatial correlation among the site occupancy factors of vacancy sites, mixed occupied and positional disordered sites. Instead of mutual substitution of chemical constituents on specific atomic sites we can propose a mechanism for a mutual substitution of distinctive constituting clusters. So, the homogeneity range of the structure can be seen as arising from an incoherent intergrowth of distinctive partial structures in variable proportions on a length scale corresponding to small integers of the unit cell. The dependence of various kinds of disorders is controlled by valence electron concentration in term of Hume-Rothery stabilization. The valence electron concentration per atom ranges from 1.60 to 1.68.

Au–Cr–Zn phase shows week metallic behavior and temperature dependent paramagnetic properties for gold-poor samples. Gold-rich samples display moderate electrictrical conductivity and temperature dependent diamagnetic behavior. For samples with intermediate gold content, resistivities decrease parallel to temperature increment, exhibit mainly diamagnetic properties and are temperature independent. The phase melts congruently and the melting point increases parallel to the gold content in the sample.

5.3 Spatially correlated structural disorder phenomena in γ-brass related complex zinc-rich alloys $(Pd,Cr)Zn_n$; n = 14.8-12.3

5.3.1 Introduction

Here, we will discuss the effect of palladium on substituted $CrZn_{17-\delta}$. Palladium is a good choice for substitution because of its heavy scattering power in comparison with chromium and zinc. This fact may permit distinguishing the atomic site of palladium by the results of X-ray single crystal diffraction experiment. Single crystal X-ray diffraction experiments on several specimens in the highly differentiated ternary Pd-Cr-Zn alloy reveal the existence, phase width and structural characteristics associated with spatial interrelation among all kinds of disorders in γ-brass related phases (γ´) formulated as $(Pd,Cr)Zn_n$, n = 14.8–12.3.

5.3.2 Solid State Synthesis

About six reactions were carried out with different Pd/Cr ratio in (Pd_xCr_{1-x}) $Zn_{\sim 17}$ starting from the pure elements: Pd (99.9%, ABCR), Cr (99.995%, Aldrich) and Zn (99.9999%, Chempur). Samples of precisely weighted metals (ca. 0.3 g) are loaded and sealed in previously out-gassed, fused silica ampoules (3 cm long, 0.8 cm in diameter) under a reduced argon pressure of about 0.5 Pa. The metals were heated at a rate of 194.4 $K\ h^{-1}$ up to 1273 K at which the ampoules were kept for 2 h, after that, the temperature was reduced to 703 K at a rate of 114K h^{-1} and annealed at this temperature for 5 days. The samples were either quenched in cold water or cooled to ambient temperature. To avoid possible loss of zinc due to evaporation, the reactants were kept at a lower temperature

than the rest of the ampoule. Products obtained from these reactions were silvery, brittle ingots and were found to be stable in air. In most cases, small amounts of gaseous zinc re-condenses into few tiny globules in close contact to the regular, brittle, silvery, lustrous metallic products.

5.3.3 Single crystal structural determination

Seven single crystals ranging from $0.01 \leq x_{Pd} \leq 0.04$ were selected from different Pd-Cr-Zn reactions were studied by X-ray means. Among all the samples studied, three crystals are discussed in details. Further crystallographic information of other specimens is listed in the appendix. Crystal 1 (C1) was selected from a sample poorest in Pd having x_{Pd} = 0.014 and crystal 5 (C5) was selected from a sample richest in palladium having x_{Pd} = 0.032. Crystal 4 (C4) having an intermediate Pd-content sample but nearest to C5, was taken from a sample having x_{Pd} = 0.030. The diffraction intensities were recorded with an imaging plate diffraction system IPDS (Stoe & Cie) working with $Mo_{K\alpha}$ radiation. [63] The intensities could be indexed on the basis of a 1.8 nm large *F*-centered cubic unit cell. The measured intensities were corrected for Lorentz and polarization effects and were further corrected for absorption by using STOE X-SHAPE and X-RED program. [66,67] The structures were solved in the acentric space group $F\bar{4}3m$ (No. 216) by applying direct methods and refined using the SHELX-97 program package based on full-matrix least-square refinements. [24] The possible position of missing zinc atoms was taken from difference Fourier synthesis maps. At this stage the structure refinement converged at *R* (*F*) < 0.15. Further improvement of the calculations was achieved by partially replacing zinc by palladium on the site which showed lower displacement parameters with respect to normal, assuming those sites to be fully occupied overall. On the other hand those metal sites having relatively large thermal displacement parameters were checked for the partial occupancy and positional disorder. Atoms for which the refined occupancy factors deviated by less than twice the standard from unity were reset to unity in the final refinement cycles. Local structural disorder phenomena were recorded by introducing split positions. All the disorder sites

were refined with non-coupled occupation parameters, except those ones showing mixed occupancy. Each structure was checked for possible twinning by inversion and its absolute configuration. The anisotropic displacement parameters of all the atoms except a few positional disordered sites were refined. The final refinement including an extinction correction and a proper weighting scheme yields R (*F*) values between 0.023 and 0.059. Further details concerning the crystallographic data and structure determination (for C1, C4, C5) are gathered in the Table 5.3.1. Positional and occupational parameters together with the equivalent displacement parameters (U_{eq}) are given in the Table 5.3.2 and 5.3.3. Further details of the crystal structure determination are listed in the appendix (A45, A46, A47, A48 and A49).

5.3.4 Phase analysis and physical properties

The homogeneity range of cubic γ´-brass phases in Pd-Cr-Zn systems was determined by means of preparative methods, calorimetric measurement, X-ray diffraction and EDS analysis.

Chemical composition determined by X-ray single crystal refinement as well as EDS analysis exhibits an extended phase width over $0.014 \leq x_{Pd} \leq 0.032$ and $0.050 \leq x_{Cr} \leq 0.043$, i.e., from $Pd_{1.4}Cr_{5.0}Zn_{94.7}$ to $Pd_{3.3}Cr_{4.5}Zn_{95.4}$. Composition evaluated by EDS and X-ray single crystal refinements matches well to one another. Specimens with $x_{Pd} \leq 0.014$ exhibit a strong tendency to form multiply twinned face-centered cubic lattices of a ~1.8 nm large *F*-centered cubic unit cells. The sample with $x_{Pd} \geq 0.032$, $Pd_{3.3}Cr_{4.5}Zn_{95.4}$ coexists with a competing ternary η-phase (space group $P6_3/mmc$, prototype Mg) as observed by EDX and analysis and X-ray powder diffraction experiment. The η-phase is the primary solid solution of parent Zn (92-94 at.%) metal substituting randomly by Pd (3-4 at%) and Cr (2-4 at.%).

Table 5.3.1: Crystallographic and technical data for the single crystal structure refinements of $Pd_{1.40}Cr_{5.00}Zn_{94.66}$ (C1), $Pd_{3.12}Cr_{4.64}Zn_{95.16}$ (C4), $Pd_{3.28}Cr_{4.48}Zn_{95.36}$ (C5)

	C1	C4	C5
crystallographic data			
chemical formula	$Pd_{1.40}Cr_{5.00}Zn_{94.66}$	$Pd_{3.12}Cr_{4.64}Zn_{95.16}$	$Pd_{3.28}Cr_{4.48}Zn_{95.36}$
Pearson symbol	*cF*404.0	*cF*411.7	*cF*412.5
x_{Pd}	0.014	0.030	0.032
crystal system			
space group type; Z	cubic; $F\bar{4}3m$ (No.216); 4		
a/pm[a]	1830.86(8)	1834.19(5)	1834.2(2)
V/10^6 pm^3 [a]	6137.1(5)	6170.7(3)	6170.8(12)
ρ_{calcd}/g cm^{-3}	7.136	7.312	7.340
μ/mm^{-1}	37.368	37.804	37.909
crystal color	silvery with metallic luster		
data collection			
crystal size/mm^3	0.08x0.08x0.04	0.08x0.08x0.02	0.06x0.04x0.04
Diffractometer	IPDS (Stoe & Cie.)		
Radiation	$Mo_{K\alpha}$		
monochromator	graphite		
distance crystal-IP/mm	80	80	90
T/K	293(2)	293(2)	293(2)
φ_{min}-φ_{max}/°	0-180	0-180	0-180
$\Delta\varphi$	1	1	1
$2\theta_{max}$/°	63.3	63.18	57.68
reflns measured	18248	18617	13004
index range	-27≤*h*≤26 -26≤*k*≤27 -26≤*l*≤26	-25≤*h*≤27 -27≤*k*≤27 -26≤*l*≤26	-24≤*h*≤24 -24≤*k*≤23 -24≤*l*≤24
completeness of data set	1.000	1.000	0.985
data reduction/ absorption correction	IPDS-software,[63] X-RED[66]/numerical, X-SHAPE[67]		
unique reflns	1083	1085	857
R_{int}	0.1246	0.0971	0.0372
Structure solution, refinement			
structure solution	direct methods, SHELXS-97[64]		
structure refinement	full-matrix least squires on F^2 (SHELXL-97[64])		
no. reflns used	1083	1085	857
no. variables	79	81	78
observed reflns (F_o>4σ(F_o))	913	990	847
R(*F*) (F_o>4σ(F_o))	0.0586	0.0370	0.0232
R(*F*) (all data)	0.0706	0.0436	0.0239
weighting factor k_1/k_2 [b]	0.0425/738.4863	0.0253/330.4525	0.0237/313.9543
wR (F^2)(all data)	0.1292	0.0701	0.0542
GOF (F^2)	1.158	1.012	1.078
extinction coefficient	0.000042 (5)	0.000019(3)	0.000027(4)
$\Delta\rho_{min}/\rho_{max}$/$10^{-6}$epm^{-3}	-1.872/2.340	-0.971/1.141	-0.794/1.690

[a] Parameters determined by use of powder diffraction data. [b] Weighting scheme: $1/\omega=\sigma^2(F_O^2)+(k_1.P)^2+k_2.P$ with $P = \frac{1}{3}(\max(F_O^2,0) + .2F_c^2)$.

Table 5.3.2: Structural data for $Pd_{1.40}Cr_{5.00}Zn_{94.66}$ (C1), $Pd_{3.12}Cr_{4.64}Zn_{95.16}$ (C4), $Pd_{3.28}Cr_{4.48}Zn_{95.36}$ (C5)

Cluster	Atom	Site	*x*	*y*	*z*	SOF	*U*eq[a]/pm^2
Z(1)	Zn10	4a CC	0[b]	0	0	0.39(2)	170(4)
						0	-
						0	-
	Zn11	16e IT	0.05436(18)	*x*	*x*	0.577(11)	194(13)
			0.05353(8)				143(5)
			0.05328(6)				109(4)
	M12	16e OT	0.91476(8)	*x*	*x*	0.36 (2)	169(6)
			0.91441(5)			0.78 (3)	101(5)
			0.91434(4)			0.82(2)	72(4)
	Zn13	24f OH	0.1698(2)	0	0	1	360(8)
			0.17852(12)				189(4)
			0.17904(9)				148(3)
	Zn15	48h CO	0.15664(8)	*x*	0.02136(10)	1	207(3)
			0.15682(6)		0.02022(7)		131(2)
			0.15629(4)		0.02021(5)		105(2)
Q(2)	Cr20	4c CC	1/4	1/4	1/4	1	150(15)
						0.63(4)	110(3)
						0.48(3)	10(3)
	Zn21	16e IT	-	-	-	0	-
			0.3093(4)	*x*	*x*	0.35(2)	170(3)
			0.3105(3)			0.58(2)	210(2)
	Zn21´	48h IT´	0.3216(2)	*x*	0.3482(3)	0.227(6)	144(18)
			0.3218(3)		0.3459(7)	0.148(9)	150(4)
			0.3231(4)		0.3457(9)	0.089(7)	60 (4)
	Zn22	16e OT	0.16541(11)	*x*	*x*	0.906(11)	232(8)
			0.16548(8)			0.945(13)	155(8)
			0.16554(6)			1	145(4)
	Zn23	24g OH	0.0932(4)	1/4	1/4	0.412(11)	261(18)
			0.0849(2)			0.688(16)	145(12)
			0.08274(12)			0.835(10)	139(7)
	Zn23´	48h OH´	0.2786(3)	*x*	0.3899(5)	0.230(7)	220(2)
			0.2778(5)		0.3903(6)	0.139(10)	180(4)
			0.2782(5)		0.3891(6)	0.107(7)	190(4)
	Zn23´´	48h OH´´	0.2710(11)	*x*	0.1099(15)	0.061(6)	100(6)
			0.2725(16)		0.110(2)	0.044(11)	140(12)
			-		-	-	-
	Zn25	48h CO	0.07582(10)	*x*	0.26590(11)	1	277(4)
			0.08140(9)		0.26891(9)		269(4)
			0.08333(6)		0.26941(7)		218(3)
H(3)	Zn30	4c CC	1/2	1/2	1/2	1	193(12)
							151(9)
							118(7)
	Zn32	16e OT	0.41256(11)	*x*	*x*	1	186(6)
			0.41418(8)				129(4)
			0.41455(6)				101(3)
	Zn34	48h CO	0.04837(7)	*x*	0.65293(11)	1	188(3)
			0.04827(5)		0.65382(8)		127(3)
			0.04821(4)		0.65397(6)		96(2)
	Zn35	16e OT	0.19090(7)	*x*	0.51705(10)	1	203(4)
			0.19012(6)		0.51969(8)		156(3)
			0.18993(4)		0.52063(6)		126(2)
T(4)	Cr42	16e OT	0.64856(12)	*x*	*x*	1	136(7)
			0.64879(10)				87(5)
			0.64903(7)				77(4)
	Zn43	24g OH	0.64299(14)	1/4	1/4	1	188(5)
			0.64879(10)				87(5)
			0.64421(8)				104(3)
	Zn45	48h CO	0.10593(7)	*x*	0.77647(10)	1	211(4)
			0.10716(5)		0.77694(7)		142(3)
			0.10745(4)		0.77719(6)		105(2)

[a] *U*eq is defined as one third of the trace of orthogonalized U_{ij} tensor. [b] structural data given in the top to bottom lines refer to crystals C1, C4, C6 respectively.[c] SOF(Pd), SOF(Zn)=1-SOF(Pd).

Table 5.3.3.1: Anisotropic thermal displacement parameters U_{ij} (pm^2) for $Pd_{1.40}Cr_{5.00}Zn_{94.66}$ (C1)

Atom	U_{11}	U_{22}	U_{33}	U_{23}	U_{13}	U_{12}
Zn10	170(4)	U_{11}	U_{11}	0	0	0
Zn11	194(13)	U_{11}	U_{11}	18(11)	U_{23}	U_{23}
M12	169(6)	U_{11}	U_{11}	0(5)	U_{23}	U_{23}
Zn13	660(2)	207(8)	U_{22}	-2(10)	0	0
Zn15	209(4)	U_{11}	202(7)	-34(5)	U_{23}	16(6)
Cr20	150(15)	U_{11}	U_{11}	0	0	0
Zn22	232(8)	U_{11}	U_{11}	-22(8)	U_{23}	U_{23}
Zn23	140(3)	320(3)	U_{22}	-110(3)	0	0
Zn25	316(6)	U_{11}	200(9)	70(6)	U_{23}	134(8)
Zn30	193(12)	U_{11}	U_{11}	0	0	0
Zn32	186(6)	U_{11}	U_{11}	3(7)	U_{23}	U_{23}
Zn34	172(4)	U_{11}	220(8)	4(4)	U_{23}	-20(6)
Zn35	190(5)	U_{11}	230(8)	-8(5)	U_{23}	17(6)
Cr42	136(7)	U_{11}	U_{11}	-10(7)	U_{23}	U_{23}
Zn43	206(11)	179(6)	U_{22}	-18(8)	0	0
Zn45	234(5)	U_{11}	167(8)	21(4)	U_{23}	1(7)

Table 5.3.3.2: Anisotropic thermal displacement parameters U_{ij} (pm^2) for $Pd_{3.12}Cr_{4.64}Zn_{95.16}$ (C4)

Atom	U_{11}	U_{22}	U_{33}	U_{23}	U_{13}	U_{12}
Zn11	143(5)	U_{11}	U_{11}	8(5)	U_{23}	U_{23}
Pd12	101(5)	U_{11}	U_{11}	9(3)	U_{23}	U_{23}
Zn12	101(5)	U_{11}	U_{11}	-9(3)	U_{23}	U_{23}
Zn13	171(10)	198(6)	U_{22}	43(8)	0	0
Zn15	134(3)	U_{11}	125(5)	-18(3)	U_{23}	-7(4)
Cr20	110(3)	U_{11}	U_{11}	0	0	0
Zn21	170(3)	U_{11}	U_{11}	120(2)	U_{23}	U_{23}
Zn22	155(8)	U_{11}	U_{11}	-15(5)	U_{23}	U_{23}
Zn23	187(19)	124(13)	U_{22}	-35(13)	0	0
Zn25	331(6)	U_{11}	143(7)	81(5)	U_{23}	194(7)
Zn30	151(9)	U_{11}	U_{11}	0	0	0
Zn32	129(4)	U_{11}	U_{11}	19(5)	U_{23}	U_{23}
Zn34	108(3)	U_{11}	165(6)	-6(3)	U_{23}	-22(4)
Zn35	138(4)	U_{11}	192(7)	-4(4)	U_{23}	0.20(5)
Cr42	87(5)	U_{11}	U_{11}	-15(5)	U_{23}	U_{23}
Zn43	150(9)	127(5)	U_{22}	-7(6)	0	0
Zn45	164(4)	U_{11}	100(6)	08(3)	U_{23}	1(5)

Table 5.3.3.3: Anisotropic thermal displacement parameters U_{ij} (pm^2) for $Pd_{3.28}Cr_{4.48}Zn_{95.36}$ (C5)

Atom	U_{11}	U_{22}	U_{33}	U_{23}	U_{13}	U_{12}
Zn11	109(4)	U_{11}	U_{11}	11(4)	U_{23}	U_{23}
M12	72(4)	U_{11}	U_{11}	-9(2)	U_{23}	U_{23}
Zn13	144(7)	150(4)	U_{22}	52(6)	0	0
Zn15	107(3)	U_{11}	100(4)	-20(3)	U_{23}	9(3)
Cr20	10(3)	U_{11}	U_{11}	0	0	0
Zn21	210(2)	U_{11}	U_{11}	121(16)	U_{23}	U_{23}
Zn22	145(4)	U_{11}	U_{11}	-13(4)	U_{23}	U_{23}
Zn23	153(10)	132(8)	$U22$	-14(7)	0	0
Zn25	265(4)	U_{11}	124(5)	77(4)	U_{23}	150(5)
Zn30	118(7)	U_{11}	U_{11}	0	0	0
Zn32	101(3)	U_{11}	U_{11}	12(4)	U_{23}	U_{23}
Zn34	78(3)	U_{11}	134(5)	-6(2)	U_{23}	-18(3)
Zn35	109(3)	U_{11}	161(5)	0(3)	0(3)	18(4)
Cr42	77(4)	U_{11}	U_{11}	2(5)	U_{23}	U_{23}
Zn43	123(7)	94(4)	U_{22}	-21(5)	0	0
Zn45	122(3)	U_{11}	73(4)	13(3)	U_{23}	-2(3)

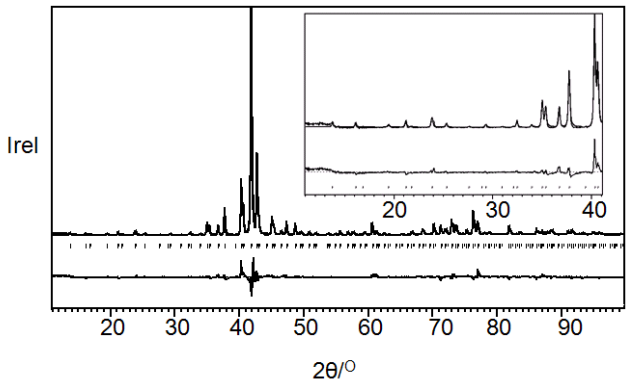

Figure 5.3.1: Observed and calculated X-ray powder diffractogram of $Pd_{3.28}Cr_{4.48}Zn_{95.36}$ (C5) for the 2θ range 10-100^O together with the profile fit, the difference spectrum and the Bragg positions. Insert shows low angle Rietveld profile fit; $Cu_{K\alpha}$, a = 1834.2 (2) pm; R_B = 0.0506, R_P = 0.0900.

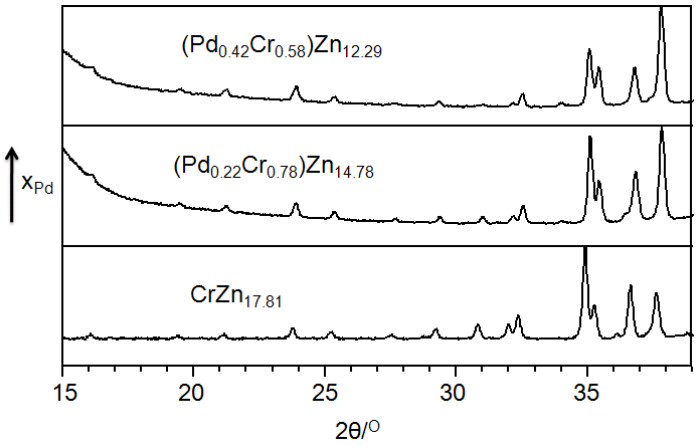

Figure 5.3.2: X-ray powder diffraction patterns in the 2θ range15-40^O observed for $CrZn_{17.81}$, $Pd_{1.40}$ $Cr_{5.00}$ $Zn_{94.66}$ and $Pd_{3.28}Cr_{4.48}Zn_{95.36.}$

A Rietveld refinement [62,127,128] was performed on a single phase sample containing x_{Pd} = 0.032 (x_{Cr} = 0.043). Positional parameters received from the single crystal X-ray structure determination as starting parameters for refinement against X-ray powder data of the corresponding sample. A profile fit is shown in the Fig. 5.3.1. The relevant data concerning the refinements are given in the figure caption. Three diffraction patterns in the 2θ range 15-40^O are shown in the Fig. 5.3.2. Progressively substitution of Zn by Au is reflected in a modified intensity modulation of diffraction peaks becoming most obvious for low angle diffraction intensities.

Thermal analyses show that the phase melts at 795(2) K (Fig. 5.3.3). The decomposition temperatures change according to compositions of the phase throughout the homogeneity range. The peak maxima shift towards higher temperature at the heating rate of 10 K h^{-1} with increase in the palladium content throughout the homogeneity range. Reformation of the phase of Pd-Cr-Zn system is inhibited at a chosen cooling rate of 10 K h^{-1}.

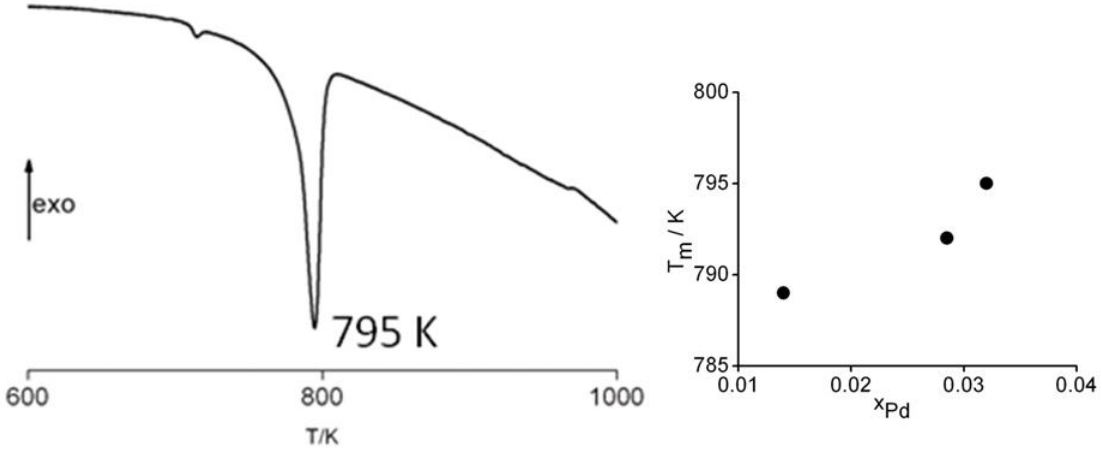

Figure 5.3.3: Thermo-chemical analysis of $Pd_{3.28}$ $Cr_{4.48}$ $Zn_{95.36}$ (left). Note: Small peak at 713 K arises due to the melting of minority portion of elemental zinc. Plot of melting points (T_m) as a function of the molar palladium fraction x_{Pd} (right) of various samples in the Pd-Cr-Zn system.

Susceptibility of palladium poor sample (x_{Pd} = 0.014) is mainly diamagnetic. χT vs T curve is almost linear between 30 and100 K (Fig. 5.3.4). Above 100 K, susceptibility increases with increasing temperature but still behaves diamagnetic up to room temperature. Below 30 K, molar susceptibility exhibits pauli paramagnetic behaviour. The diamagnetic contribution between 30 and 100 K is -1.91(1) x 10^{-10} m^3mol^{-1} which is very close to the calculated diamagnetic contribution from Pascal-constant (-1.98. x 10^{-10} m^3mol^{-1}). The specimen richest in palladium, increasing slope (> 100 K) of χ with T has been suppressed in comparison with the Pd-poor sample. This may be the effect of increasing palladium content as well as decreasing chromium content.

A continuous change from paramagnetic to diamagnetic behavior is observed with increasing temperature. The material exhibits mainly diamagnetic behavior with an additional Curie-like paramagnetic contribution. Moreover, increasing χ with T leads that the material also behaves like antiferromagnet below the ordering temperature.

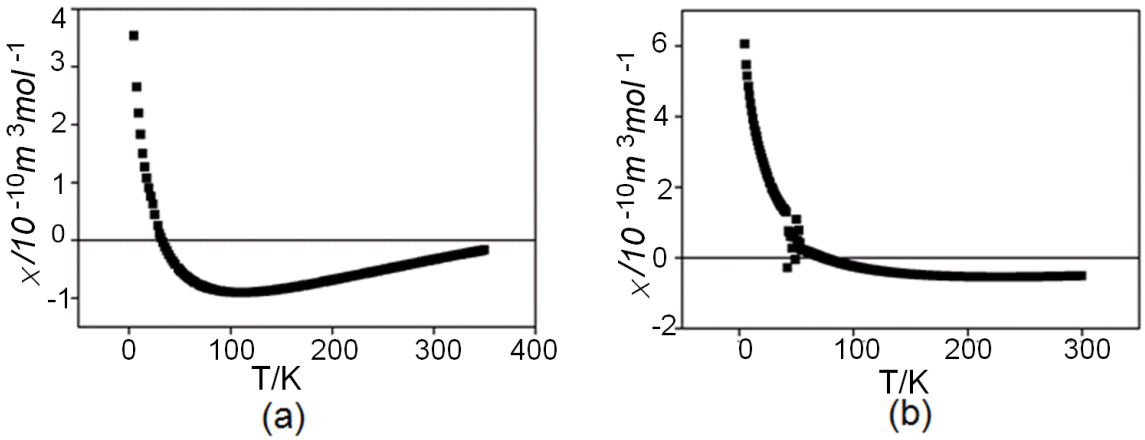

Figure 5.3.4: Magnetic susceptibility of (a) $Pd_{1.40}$ $Cr_{5.00}$ $Zn_{94.66}$ and (b) $Pd_{3.28}Cr_{4.4.48}Zn_{95.36}$ at 1T.

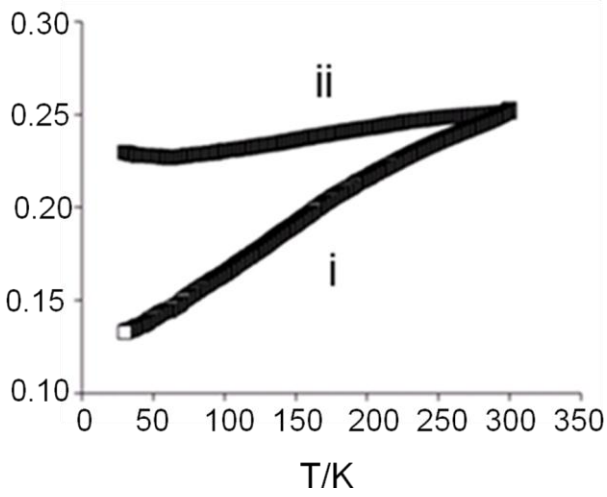

Figure5.3.5: Resistivities ρ of single phase samples $Pd_{1.40}$ $Cr_{5.00}$ $Zn_{94.66}$ (i), $Pd_{3.28}$ $Cr_{4.48}Zn_{95.36}$ (ii), between 30 and 300 K.

The Ternary phase of Pd-Cr-Zn system shows weak metallic behavior (Fig. 5.3.5). Resistivities (ρ) increase with temperature from 30 K to 300 K. Data concerning the resistivities of Pd-Cr-Zn system is listed in Table 5.3.4.

The resistivities of Pd-Cr-Zn ternary phases at 300 K are nearly two orders of magnitude higher than that of the constituent zinc elements–$\rho_{Zn,\ 293K}$ = 5.8 μΩ cm.

Table 5.3.4: A summary of resistivity data for the selected crystalline specimens

x_{Pd}	ρ_{30K} (mΩcm)	ρ_{300K} (mΩcm)
0.014	0.23	0.25
0.032	0.13	0.25

5.3.5 Structural Characteristics

The ternary phase in Pd-Cr-Zn system adopts a structurally complex γ-related phase belonging to the group of cubic giant cell structures and isopointal to the structure of $CrZn_{17-\delta}$. The phase crystallizes in the acentric space group $F\bar{4}3m$ with approximately 404-413 atoms in the cubic unit cell. The number of atoms in the unit cell increases parallel to the increase of palladium-content. Hence, the lattice parameters vary with mole fraction of palladium (x_{Pd}) throughout the homogeneity range.

The crystal structure of the ternary phase can be described by using the cluster concept. [131] The clusters are shown in the Fig. 5.3.6. These clusters are centered at the high symmetry points of the unit cell: (0 0 0), (¼ ¼ ¼), (½ ½ ½), and (¾ ¾ ¾).

As mentioned in Chapter 4 for $CrZn_{17-\delta,}$ the atomic arrangement of structures in the Pd-Cr-Zn system can be subdivided into two topologically similar but chemically distinct partial structures. One partial structure is completely ordered consisted of H and T clusters with 204 atoms and compositionally invariant throughout the homogeneity range of the phase. Moreover, the ordered partial structure forms a hierarchical variant of a zinc blende type structure. Other partial structure comprising of the Z and Q clusters is partly disordered and variable in composition and forms a replica of other zinc blende type substructure which is shifted by half a lattice vector relative to the first one.

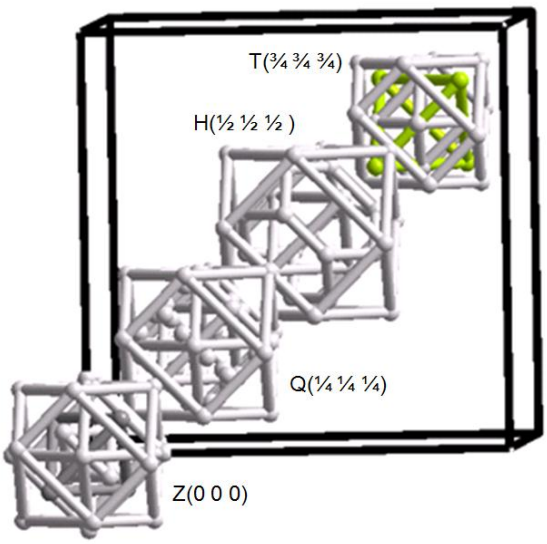

Figure 5.3.6: The arrangement of clusters in the crystal structure of $Pd_{3.3}Cr_{4.5}Zn_{95.4}$ along the body diagonal. Clusters are centered about the high symmetry points of the *F*-centered cubic unit cell and their identities are revealed. Constituting zinc atoms are shown in gray (25%), chromium in lime and Pd/Zn in dark grey (40%).

Structural changes in substituted $CrZn_{17-\delta}$ induced by the replacement of Zn by Pd

The compositionally invariant partial structure: Cluster H at (½ ½ ½) is unaffected from Pd/Zn replacement, always α-Mn-type Zn_{29} cluster. Moreover, cluster T at (¾ ¾ ¾) like cluster H, remains unaffected, always $NiTi_2$-type Cr_4Zn_{18} cluster (Fig. 5.3.7).

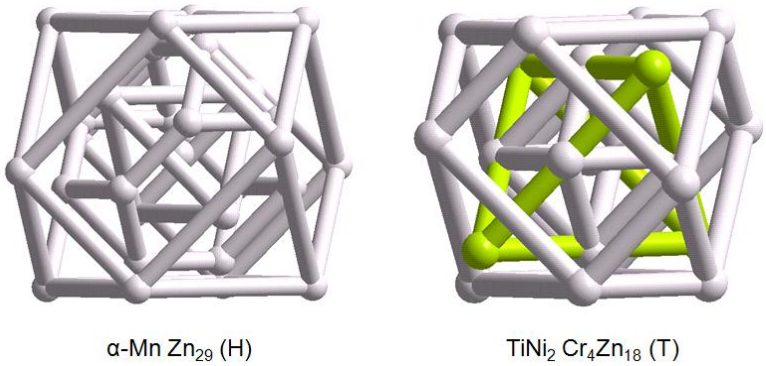

Figure 5.3.7: Representation of the cluster H about (½ ½ ½) α-Mn-type Zn_{29} and cluster T centered at (¾¾¾) $TiNi_2$-type Cr_4Zn_{18}-unaffected by Pd/Zn replacement.

The compositionally variable partial structure: The disordered partial structure varies with composition. The variation of composition is accompanied by various disorder phenomena as typical for complex metallic alloys.

(i) random vacancies

(ii) substitutional disorder

(iii) positional disorder in term of split positions

The Z cluster builds up by partly occupied Zn10 CC and Zn11 IT sites, mixed occupied M12 OT sites, Zn13 OH, and an outer Zn15 CO shell. OT sites are mixed occupied by Pd and Zn in the ternary Pd-Cr-Zn system. The disorder of type (i) gives rise to physically meaningless short distance between Zn10 and Zn11. This problem can be explained if we assume that two different cluster types alternatively are situated about their high symmetry point. Furthermore, independently refined occupation factors of all the specimens show, in no case, the sum of SOF of two very close sites exceeds unity, i.e. f(CC) + f(IT) ≈ 1.00 (c.f. Table 5.3.5). So, we may conclude that either a defect bcc-type cluster with shell sequence CC, OT, OH, CO or a γ-type cluster (IT, OT, OH, CO) is situated about Z. Correspondingly, we can build a bcc-type cluster or γ-brass type cluster on positions Q. The bcc type cluster consists of CC, IT´, OT, OH, CO. Furthermore, independent refinement of fractional occupancies of OH Zn23, two symmetrically uncoupled twofold split positions OH' Zn23' and OH'' Zn23'' exhibits the relation: f(Zn23) + 2 x f(Zn23') + 2 f(Zn23'') ≈ 1. The relation defines all six positions per cluster are occupied. Twelve Zn25 form the outermost CO shell.

Structure-composition relation: Variable mutual substitution of the two distinct chemical constituents occurs on M12. Pd substitute Zn in M12 atomic site (c.f. Table. 5.3.5) with the increasing of x_{Pd} in the cluster Z. Hence, the depletion of Zn by Pd substitution throughout the homogeneity range is essentially limited to cluster Z.

Table 5.3.5: SOF of various sites in cluster Z and Q

No.		Cluster Z		Cluster Q			
	x_{Pd}	$f_{Pd/Zn}$ (OT)	f_{Zn} (CC)/ f_{Zn} (IT)	f_{Cr} (CC)/ f_{Zn} (IT)	f_{Zn}(IT´)	f_{Zn} (OT)/ f_{Zn} (OH´´)	f_{Zn} (OH)/ f_{Zn} (OH´)/ f_{Zn} (OH´´)
C1	0.014	0.36/0.64	0.39/0.61	1/0	0.23	0.91/0.06	0.41/0.23/0.06
C2	0.028	0.74/0.26	0/1	0.79/0.25	0.17	0.95/0.04	0.64/0.16/0.04
C3	0.029	0.73/0.27	0/1	0.72/0.28	0.15	0.95/0.05	0.64/0.15/0.05
C4	0.030	0.78/0.22	0/1	0.63/0.35	0.15	0.94/0.05	0.69/0.14/0.05
C5	0.032	0.82/0.18	0/1	0.48/0.58	0.09	1/0	0.84/0.11/0

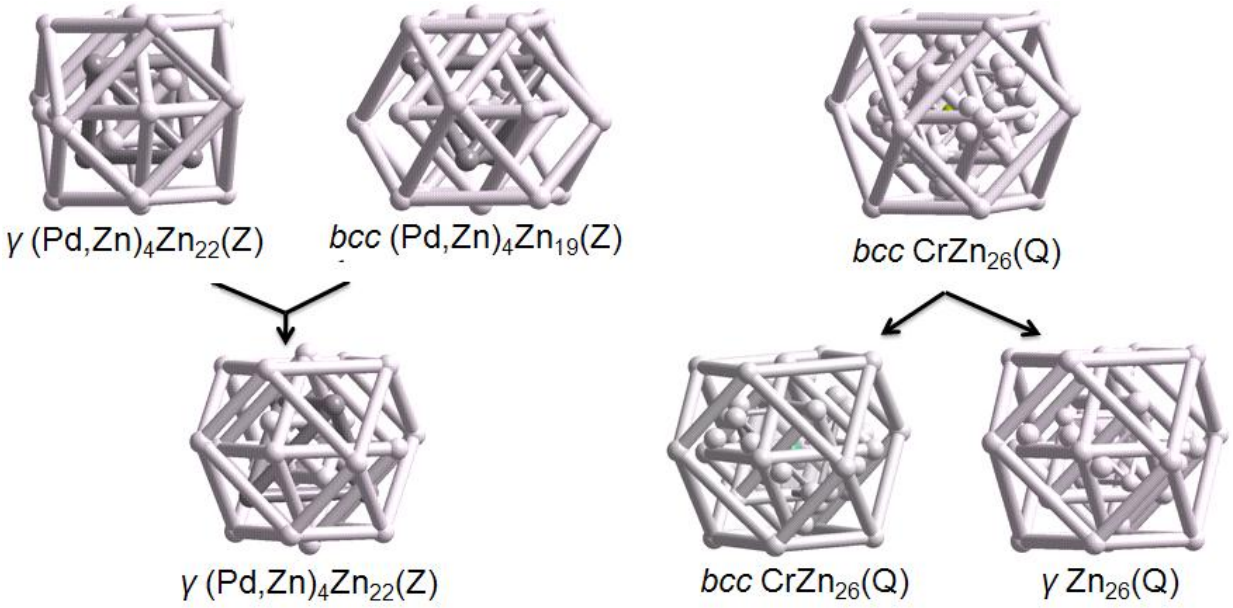

Figure 5.3.8: (Left) Transmutation of cluster Z at (0 0 0) from a mixture of defect bcc and γ-brass in the crystal structure of $Pd_{1.4}Cr_{5.0}Zn_{94.7}$ to γ-type $Pd_{3.3}Zn_{22.7}$ in $Pd_{3.3}Cr_{4.5}Zn_{95.4}$ by the replacement of Zn by Pd. Constituting zinc atoms are shown in gray (20%), mixed occupied Pd/Zn in 50% grey, fully occupied Cr in lime and partly occupied Cr in sea green.

(Right) Transformation of cluster Q at 1/4 1/4 1/4 from a bcc-type cluster to a mixture of γ-brass-type and bcc-type cluster by the replacement of Zn by Pd.

Zn 21´ IT in the cluster Q is threefold split and shows random vacancies as well. The random vacancy [$V_{Q\ (IT')}$ = 1-3 x $f_{Q\ (Zn21')}$] in cluster Q increases with mole fraction of palladium.

The SOF of Zn10 and Zn11 atoms show clear interrelation with mole fraction of Pd. With the increase of palladium content, vacancy at CC Zn10 site increases and vacancy IT Zn11 site decreases in the cluster Z.

Correspondingly, vacancy at Cr20 and Zn21 manifest a further interrelation parallel to the mole fraction of palladium (Table 5.3.5). Zn10 is uniquely identified with defect bcc-type and Zn11 with γ-brass type in the Z cluster. Correspondingly, Cr20 is the characteristics of β-brass type and Zn21 defining the IT site specify γ-brass type in Q. Hence, we conclude that cluster Z transmutes from a mixture of a defect bcc- and γ-brass-type clusters to a γ-brass type $(Pd, Zn)_4Zn_{22}$ cluster (Fig. 5.3.8) by the replacement of Zn by Pd and cluster Q transforms from a β-brass type cluster to the mixture of β-and γ-brass-type clusters by Pd/Zn replacement (Fig. 5.3.8).

With increasing palladium-content a clear increase of f(Zn23) and a clear decrease of f(Zn23') and f(Zn23'') is observed, accompanying the change from the heavily disordered split octahedral positions (OH,OH', OH'') to the partly disordered split octahedral sites (OH, OH') (Fig.5.3,8 & Tab. 5.3.5)

An additional correlations between site occupancy factors provide evidence that f(Zn22) + f(Zn23'') ≈ 1. f(Zn22) increases parallel with the overall Pd-content of the phase (Tab. 5.3.5).

Correlations among site occupancy factors give evidence that the various disorder phenomena in various shells are spatially correlated. Systematic change in disorder phenomena on the Zn sites is an implication of the varying Pd-content. Some kind of information transmits from Pd to Zn sites. The change of the palladium-content restricted to the mixed occupied OT site of cluster Z. The parallel increase of the f(Z,Zn12), the Zn fraction at OT in cluster Z, Zn fraction at IT sites at cluster Q, V(Q,Zn21´) and f(Q,Zn23) exhibits an interrelation between the compositional change in the cluster types of variable partial structure. Moreover, these spatial correlations among all kinds of disorders evolve the phase width of a complex metallic alloy. So, the homogeneity range of the structure arises from an incoherent intergrowth of distinctive

partial structures in variable proportions on a length scale corresponding to small integers of the unit cell.

We believe that such vacancies as well as partial mixing of Pd and Zn atoms are relevant to maintain the *vec* values more or less constant at 1.67-1.68 per atom throughout the entire homogeneity range. If Pd is taken to be zerovalent, Cr tetravalent (negative) and Zn bivalent, partial replacement of Zn by Pd (M12) and parallel increase of vacancies (Zn21') reduce *vec* throughout the entire homogeneity range. But, simultaneous increase of the Zn fraction (fQ,Zn21') at OT site and decreasing site occupancy of Cr (fQ,Cr20) at CC parallel with the overall Pd content of the phase are crucial to keep the *vec* values nearly constant at 1.67-1.68 per atom.

This last chapter deals with a comparison of the structures of the two superstructures of of γ-brass related phases (Au,Cr)Zn_n (n = 10.2-6.4) and (Pd,Cr)Zn_n (n = 14.8-12.3). According to the classical Hume-Rothery concept the structure of γ-brass-type phases is assumed to be decisively controlled by the valence electron concentration irrespective of other distinctive atomic factors. Indeed, the chemistry of 4d (e.g. Pd) and 5d (e.g. Au) block elements frequently differs significantly due to differences in bonding capabilities of the corresponding nd states. The structures of ternary derivatives of $CrZn_{17-\delta}$ share many features in spite of the compositional distinctions and the complexity of the structures. Common features are: (i) The clusters are essentially same in both structures. The composition of the ordered partial structure is Cr_4Zn_{47} for each compound. Ordered partial structures are unaffected by Pd or Au. (ii) Though different in composition, the cluster types of the disordered structures are the same as well. Structural differences concern: (i) Partial structure variable in composition of the Au-Cr-Zn system endures significant effects by Au/Cr and/or Au/Zn substitution on constituting clusters: mixture of disordered γ-brass type and defect bcc type clusters transmute to clean γ-brass type Au_4Zn_{22} and disordered bcc type clusters transform to clean γ-brass-type Au_6Zn_{20} over an intermediate mixture of bcc and γ-brass-type clusters. On the other hand, cluster Z transmutes from a mixture of a defect bcc-and disorder γ-brass-

type clusters to a disorder γ-brass type $(Pd,Zn)_4Zn_{22}$ cluster by the replacement of Zn by Pd and cluster Q transforms from a β-brass type cluster to the mixture of β- and γ-brass-type clusters by Pd/Zn replacement.(ii) Superstructure of γ-brass related phases in the Au-Cr-Zn system occur between 1.60-1.68 e^-/a. The valence electron concentration per atom in the Pd-Cr-Zn system ranges from 1.67 to 1.68 throughout the entire homogeneity range. We conclude that in spite of a close structural resemblance the enormous complexity of these large cell structures provides room for element specific structural differentiations.

5.3.6 Summary

The structure of $CrZn_{17-\delta}$ can be distinctly modified by replacing Zn by Pd. The results of this study show that meaning of homogeneity needs critical reassessment if complex alloys exhibiting homogeneity ranges are considered. Disorder phenomena in the solid solution of $(Pd,Cr)Zn_n$, (n=14.8-12.3) are spatially correlated and confined to one of the two hierarchical substructures of zinc blende-type. The valence electron concentration per atom ranges from 1.67 to 1.68 throughout the entire homogeneity range.

Chapter 6

Structural chemistry of ternary γ-brass type phases in the Au-Pd-Zn system

6.1 Introduction

The γ-brass phases are of particular interest of our investigation for their structural complexity, their chemical and structural relationships with various quasi-crystal approximants and for their stabilisation mechanism. γ-brass phases are part of a special class of intermetallic compounds, in which the formation of a particular structure occurs at certain value of ratio of valence electrons to atom (*vec*), i.e. 21/13, which was first recognised by Hume-Rothery in 1926. [16,18] In fact, the condition is valid irrespective of nature of constituting metals. There are various compounds such as Cu_5Zn_8 [23] and Cu_9Al_4. [34,151] which adopt γ-brass structure at *vec* value at 21/13 per atom. Recently, it has been shown by FLAPW calculations, various binary γ-brass compounds occur at the e/a value of 21/13 e^-/atom. [25,30,111]

Several compounds on γ-brass phases having composition M_2Zn_{11} (M = Ni, [11] Pd, [52] Pt, [130]) occur at the e/a ratio of 21/13 e^- /atom to these compounds, if Zn is assigned valency of two and transition metals to zero. The existence and the compositions of γ-brass type structures have been confirmed by using both X-ray diffraction analysis and neutron diffraction studies in systems such as Fe-Zn (Fe_3Zn_{10}), [56,110] Ni-Zn (Ni_2Zn_{11}), [25,111] Cu-Zn ($Cu_{5-x}Zn_{8+x}$), [23,52,110] Pd-Zn ($Pd_{2+\delta}Zn_{11-\delta}$), [52,53] Rh-Zn ($Rh_2Zn_{11}$), [138] Ir-Zn ($Ir_2Zn_{11}$), [139] and Pt-Zn ($Pt_2Zn_{11-\delta}$). [52,130] However, these binary phase spaces in its close vicinity [53,54,140,141] of the γ-brass region accommodates bundle wise phases with bewildering composition and structural complexity. Among the complex phases, structure most closely related to γ-brass is a 2 x 2x 2 superstructure (space group $F\bar{4}3m$) which is designated as γ´-brass. This phase is reported in various binary systems,

such as $Ir_{7+7\delta}Zn_{97-11\delta}$ [122] and Pt_5Zn_{21} [129] along with γ–brass phase and also occurs in other binary systems such as $CrZn_{17-\delta,}$ [145] $Ir_4Mg_{29,}$ [152] $Ta_{39}Al_{69,}$ [142] $Sm_{11}Cd_{45,}$ [153] $Cu_{45}Sn_{11,}$ [154] and $Li_{21}Si_5$ [146] in which only γ´-brass phase has been observed. But only a few ternary or pseudo binary systems have been reported to date. [143,155] To date there is no γ´-brass phase has been reported in the Pd-Zn binary system.

To get an insight into the structure–composition–property relationship among complex metal–rich phases, we have concentrated on ternary or pseudobinary Hume–Rothery–based system. This work is motivated by the discovery $Pd_{2+x}Zn_{11-x}$ in the γ-brass region i.e. approximately between 75 and 85 atom % Zn. The zinc richest phase accommodates the cubic γ–brass structure, but as the Pd concentration increases, these phases show extraordinary periodicities along a single direction that provide the approximants to potentially one-dimensional quasi-periodic structure. On account of these backgrounds, we investigate the gold substituted $Pd_{2+x}Zn_{11-x}$ to understand how substitution of Pd and Zn by Au atoms can influence the structural stability and chemical compositions of γ–brass phases related to $Pd_{2+x}Zn_{11-x}$. No phase has been reported in the Au-Pd-Zn ternary system to date.

To study the influence of valence electron on γ-brass type phases, we attempted replacing Zn and/or Pd by Au in the parent $Pd_{2+x}Zn_{11-x}$ phase. $Au_{2.89}Pd_{3.44}Zn_{19.68}$ represents the upper limit of Au substitution in the phase $Pd_{2+x}Zn_{11-x}$. Further substitution of Au leads to 2 × 2 × 2 superstructures of γ-brass with lattice parameters ranging from 1816.2(1) to 1816.6(2) pm (Pearson code *cF*402-*cF*405).

6.2 Ternary γ-brass phases in the Au-Pd-Zn system

Here, in this chapter-6.2, we will discuss the existence, phase width, structural features and physical properties of new γ-phases in the ternary Au-Pd-Zn system.

6.2.1 Synthesis and characterization

Single phase samples-$(Au_x,Pd_{1-x})Zn_{\sim 5.5}$ with nominal composition x_{Au} = 0.07 and x_{Au} = 0.11 have been synthesized by conventional solid state synthesis. The preparations were carried out on a 0.3 gm scale from Au (99.99%,ABCR), Pd (99.99%, ABCR) and Zn (99.9999%, Chempur) in previously out-gassed, evacuated quartz glass ampoules (3 cm long, 0.8 cm in diameter). The metals were heated at a rate of 194.4 K h^{-1} up to 1273 K and were kept at this temperature for 2 h, hereafter, the temperature was reduced to 823 K at a rate of 90 K h^{-1} and annealed at this temperature over the course of 5 days after which the ampoules were either quenched in water or cooled to ambient temperature. Products obtained from these reactions were silvery, brittle and stable in air. Products were characterized by powder diffraction and single crystal diffraction methods.

6.2.2 Single crystal structure determination

Crystals for recording X-ray diffraction intensities were selected from the samples having composition of x_{Au} = 0.09 (C1) and x_{Au} = 0.11 (C2). X-ray diffraction intensities were collected on an IPDS instrument at room temperature. [63] Diffraction intensities were collected up to $2\theta_{max} \approx 60\text{-}66^{O}$. The Laue symmetry was m-3m. The systematic extinction h+k+l = 2n+1 pointed to the cubic space group $I\bar{4}3m$ (No. 217). The data was subsequently corrected for Lorentz and polarization effects. A numerical absorption correction based on the shape of the crystal was applied to the data. [66, 67] The initial positional parameters were obtained by direct methods using SHELXS-97. [32] The structure was refined in the cubic space group $I\bar{4}3m$. All the atomic positions were refined anisotropically with the SHELX-97 [64] program package based on full-matrix least-square refinements. Sites having substitutional disorder were assumed to be unity by mutual substitution of two components. The final refinement performed on $|F|^2$

yielded R(F) ($F_O > 4\sigma(F_O)$) between 0.0220 and 0.0354. Details of the data collection, atomic coordinates, equivalent isotropic displacement parameters and anisotropic displacement parameters are given in the Table 6.2.1, 6.2.2, 6.2.3 and 6.2.4, respectively.

6.2.3 Phase analyses and physical properties

A sample of single phase was characterized by means of powder X-ray diffraction. The diffraction profile of the homogeneous sample was quantitatively analyzed by the Rietveld method. [62,127,128] Positional parameters of the single crystal X-ray structure analysis were used as starting parameters for the refinements of the X-ray powder data. The Rietveld fit for a single phase sample of $x_{Au} = 0.068$ is shown the Fig. 6.2.1.

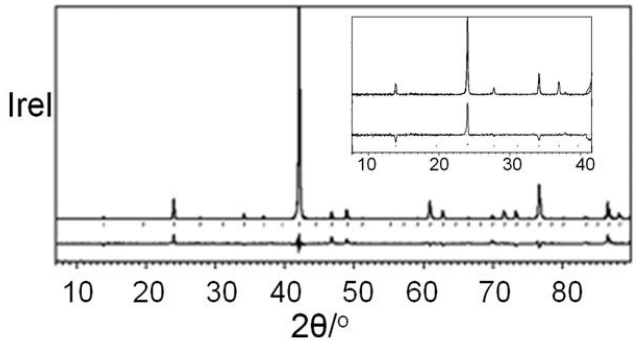

Figure 6.2.1: Observed and calculated X-ray powder diffractogram of $Au_{1.78}Pd_{3.68}Zn_{20.55}$ ($x_{Au} = 0.068$) for the 2θ range 10-90^O together with the profile fit, the difference spectrum and the Bragg positions; $Cu_{K\alpha,}$; $R_B = 0.0653$, $R_P = 0.0933$.

Table 6.2.1: Crystallographic and technical data for the single crystal structure refinements of $Au_{1.78}Pd_{3.68}Zn_{20.55}$ (C1), $Au_{2.89}Pd_{3.44}Zn_{19.68}$ (C2)

	C1	C2
crystallographic data		
chemical formula	$Au_{1.78}Pd_{3.68}Zn_{20.55}$	$Au_{2.89}Pd_{3.44}Zn_{19.68}$
Pearson symbol	*cI*52	*CI*52
x_{Au}	0.068	0.111
crystal system		
space group type; Z	cubic; $I\bar{4}3m$ (No.217); 2	
a/pm[a]	910.3(1)	911.9(1)
V/10^6 pm^3 [a]	754.3(1)	758.3(2)
ρ_{calcd}/g cm^{-3}	9.179	9.729
μ/mm^{-1}	53.402	62.221
crystal color	silvery with metallic luster	
data collection		
crystal size/mm^3	0.08x0.04x0.04	0.10x0.04x0.04
diffractometer	IPDS (Stoe & Cie.)	
radiation	$Mo_{K\alpha}$	
monochromator	Graphite	
distance crystal-IP/mm	90	80
φ_{min}-φ_{max}/^{o}	0-180	0-180
$\Delta\varphi$	1	1
$2\theta_{max}$/^{o}	60.80	66.12
reflns measured	3213	3883
index range	-12≤*h*≤11 -12≤*k*≤12 -12≤*l*≤12	-14≤*h*≤13 -14≤*k*≤13 -12≤*l*≤14
completeness of data set	1.000	0.994
data reduction/ absorption correction	IPDS-software,[63] X-RED[66]/numerical, X-SHAPE[67]	
unique reflns	242	297
R_{int}	0.0469	0.0994
structure solution, refinement		
structure solution	direct methods, SHELXS-97[64]	
structure refinement	full-matrix least squires on F^2 (SHELXL-97[64])	
no. reflns used	242	297
no. variables	22	20
observed reflns (F_o>4σ(F_o))	237	294
R(*F*) (F_o>4σ(F_o))	0.0220	0.0354
R(*F*) (all data)	0.0226	0.0357
weighting factor k_1/k_2 [b]	0.0306/15.8652	0.0465/23.2855
wR (F^2)(all data)	0.0588	0.0814
GOF (F^2)	1.086	1.135
extinction coefficient	0.00206(17)	0.0007(2)
$\Delta\rho_{min}/\rho_{max}$/10^{-6}epm^{-3}	-0.829/0.726	-1.598/4.099

[a] Parameters determined by use of single crystal diffraction data. [b] Weighting scheme: $1/\omega=\sigma^2(F_O^2)+(k_1.P)^2+k_2.P$ with P = ⅓(max (F_O^2,0) +.2F_c^2).

Table 6.2.2: Structural data for $Au_{1.78}Pd_{3.68}Zn_{20.55}$ (C1), $Au_{2.89}Pd_{3.44}Zn_{19.68}$ (C2)

Atom	Site		*x*	*y*	*z*	SOF	*U*eq[a]/pm^2
Zn1	8e	IT	0.89178(11)[b]	*x*	*x*	1	148(4)
			0.89151(13)				104(4)
M2[c]	8e	OT	0.17381(6)	*x*	*x*	0.918(9)	151(4)
			0.17452(6)			0.863(10)	97(4)
M3[d]	12g	OH	0.63833(11)	0	0	0.242(8)	143(4)
			0.63804(9)			0.389(8)	91(3)
Zn4	24h	CO	0.68976(9)	*x*	0.96102(13)	1	153(3)
			0.69033(10)		0.96108(16)		118(4)

[a] *U*eq is defined as one third of the trace of orthogonalized U_{ij} tensor. [b] structural data given in the top to bottom lines refer to C1,C2 respectively. [c] SOF(Pd), SOF(Au)=1-SOF(Pd). [d] SOF(Au), SOF(Zn)=1-SOF(Au).

Table 6.2.3: Anisotropic thermal displacement parameters U_{ij} (pm^2) for $Au_{1.78}Pd_{3.68}Zn_{20.55}$ (C1)

Atom	U_{11}	U_{22}	U_{33}	U_{23}	U_{13}	U_{12}
Zn1	148(4)	U_{11}	U_{11}	7(4)	U_{23}	U_{23}
M2	151(4)	U_{11}	U_{11}	4(3)	U_{23}	U_{23}
M3	166(6)	132(5)	U_{22}	14(4)	0	0
Zn4	159(4)	U_{11}	140(5)	-12(4)	U_{23}	-11(4)

Table 6.2.4: Anisotropic thermal displacement parameters U_{ij} (pm^2) for $Au_{2.89}Pd_{3.44}Zn_{19.68}$ (C2)

Atom	U_{11}	U_{22}	U_{33}	U_{23}	U_{13}	U_{12}
Zn1	104(4)	U_{11}	U_{11}	13(4)	U_{23}	U_{23}
M2	97(4)	U_{11}	U_{11}	2(3)	U_{23}	U_{23}
M3	99(4)	87(3)	U_{22}	7(3)	0	0
Zn4	121(4)	U_{11}	112(5)	-30(3)	U_{23}	8(4)

According to DTA measurement of a sample, $Au_{2.89}Pd_{3.44}Zn_{19\ .68}$ (x_{Au} = 0.11) begins to melt at 1001 K (Fig. 6.2.2). The peak maximum is found at 1097 K. The recrystallizaton of sample occurs at 1086 K. Pre-melting features evolved at approximately at 981 K for the samples of different compositions. We may suggest that this thermal effect is associated with a continuous increase of structural disorder upon heating prior to melting.

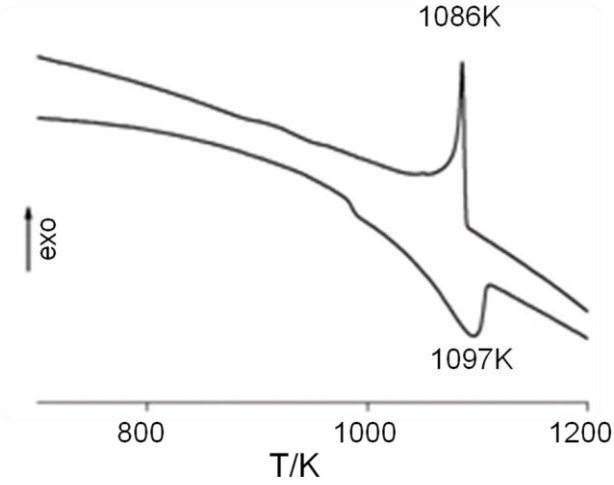

Figure 6.2.2: Thermo-chemical analysis of $Au_{2.89}Pd_{3.44}Zn_{19.68}$ (x_{Au} = 0.11).

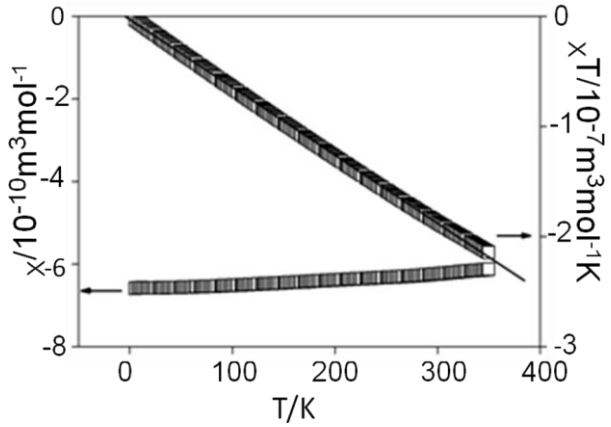

Figure 6.2.3: The molar susceptibility of $Au_{1.78}Pd_{3.68}Zn_{20.55}$ (x_{Au} = 0.068) as a function of temperature.

The magnetic susceptibility of $Au_{1.78}$ $Pd_{3.68}$ $Zn_{20.55}$ was measured at a magnetic flux density of 1Tesla (Fig. 6.2.3). In this case, the Pauli paramagnetism of the metallic conductor was found to be overcompensated by the core diamagnetism of the constituent components of the phase. The temperature independent diamagnetic contribution was obtained from the slope of a χT versus T plot. The value obtained was found to be −6.15 (1) x 10^{-10} m^3mol^{-1} for $Au_{1.78}Pd_{3.68}Zn_{20.55}$ (x_{Au} = 0.068) from linear fit.

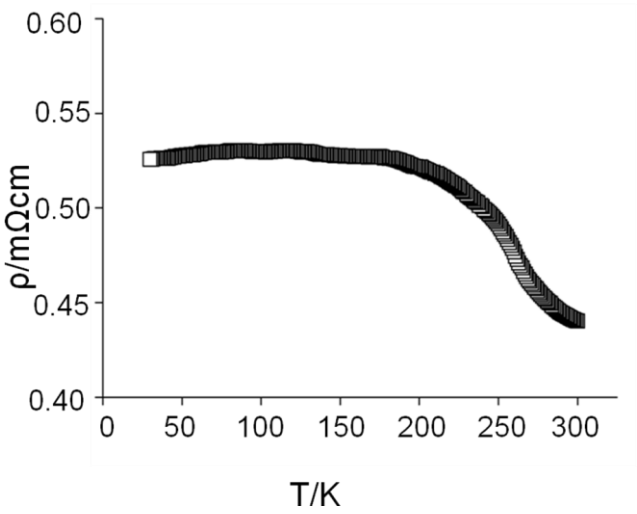

Figure 6.2.4: Resistivity ρ of single phase samples $Au_{2.89}Cr_{3.44}Zn_{19.68}$ (x_{Au} = 0.11) between 30 and 300 K.

The resistivity was determined by applying a four-probe method in the d.c. mode over the temperature range 30–300 K. γ-brass phase in the Au-Pd-Zn system shows decreasing resistivity from 0.53 mΩcm (30 K) to 0.44 mΩcm (300 K) (Fig. 6.2.4). The value is nearly two orders of magnitude higher than that of zinc metal (ρ(293K) = 5.8 μΩ cm).

6.2.4 Structural Characteristics

Ternary Au-Pd-Zn phases containing less gold than palladium (x_{Au} = 0.066, x_{Au} = 0.11) crystallize in the cubic space group $I\bar{4}3m$ containing 52 atoms per unit cell. The phases adopt a γ-brass type structures which are isopointal to the structures of M_5Zn_8 (M = Cu), [23] Fe_3Zn_{10}, [56,110] $Pd_{2+\delta}Zn_{11-\delta}$, [52,53] M_2Zn_{11} (M = Ni [25,111], Rh [138], Ir [139]). Lattice parameters as well as molar volume increase with increasing gold content.

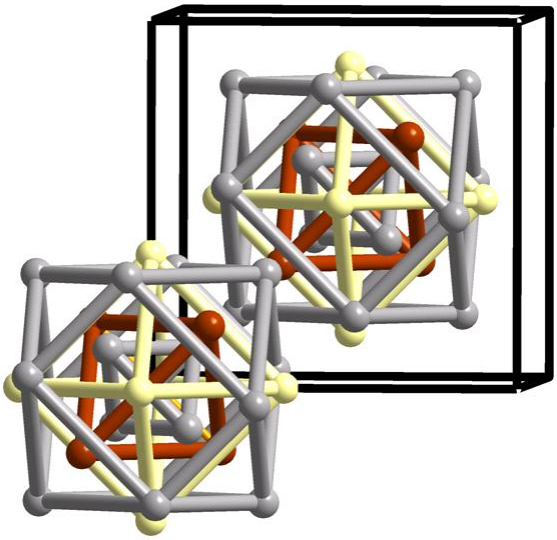

Figure 6.2.5: The arrangement of clusters in the crystal structure of Au-Pd-Zn (C1) along the body diagonal. Clusters are centered at the high-symmetry points of the *I*-centered cubic unit cell. The clusters are represented by idealized exterior cuboctahedron shells. Constituting zinc atoms has been shown by gray (40%), mixed occupied Au and Zn by light yellow and Au/Pd by brown colour.

Various methods have been proposed to describe the cubic γ-brass structure. γ-brass phase is a $(3a_\beta)^3$ superstructure of a β-brass type structure with 2 out of 54 positions being vacant, one at the origin and the other at the center of the triply expanded super cell. This kind of structure is traditionally described by using the cluster concept, an approach first introduced by Bradley and Jones. [131] The cluster view is shown in the Fig. 6.2.5.

According to the cluster concept, the Au-Pd-Zn γ-brass structures consist of 26 atom cluster and their centres are located at the high symmetry points of the unit cell: (0 0 0), (½ ½ ½), and equivalent translational invariant points. Each cluster is built up by four crystallographic distinct sites. One `8c´ site is occupied by eight Zn1 atoms forming two inner tetrahedrons addressed as IT, one grouped around the origin and the other around the centre of the unit cell. The next shell defines outer tetrahedron (OT) built up by M2 (the mixture of Au and Pd atoms) sitting above the faces of inner tetrahedron and

is situated at a second `8c´ site. OT together with its complementary IT forms a distorted, empty cube. The next shell around the distorted empty cube consists of six M3 (the mixture of Au and Zn atoms) atoms situated above the faces of the cube, thus forming an octahedron. Respective '12e' site is occupied by six M3 atoms. A distorted cuboctahedron of Zn4 atoms placed above the edges of the octahedron. The respective '24g' site is occupied by Zn4 complementing the 26 atom unit (Fig. 6.2.6).

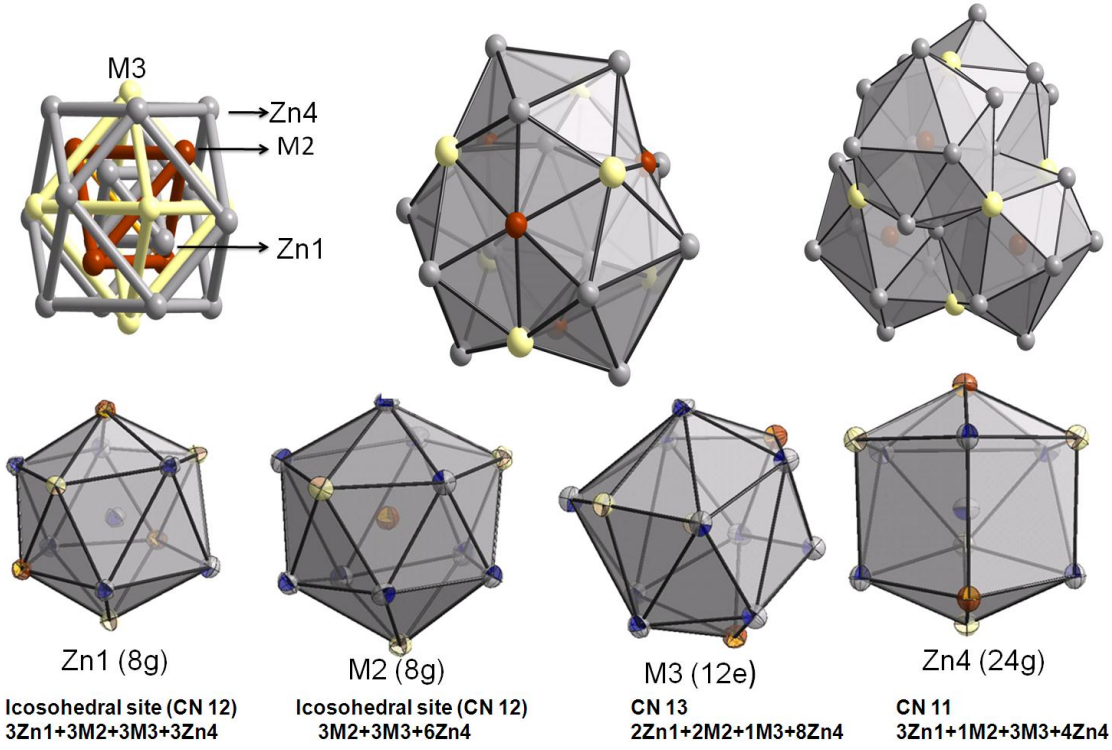

Figure 6.2.6: Representation of the cubic γ-brass structure of $Au_{1.78}Pd_{3.68}Zn_{20.55}$ (x_{Au} = 0.068), representation of 26 atom cluster that forms a bcc-type packing, emphasizing the different nested polyhedral shells (top left). Those 26 atoms compile to form discrete interlocking quadruples of distorted icosahedra about four Zn1 atoms, i.e. Pierce cluster (top middle). Four condensed M2 centered icosohedra (top right) and local environment for each of the four atomic sites of the γ-brass structure (down row) are depicted. Sites with mixed Au/Zn occupation are shown in light yellow, Au/Pd in light yellow, and zinc in grey, respectively.

Another description of this structure involves local environment at each of the four distinct crystallographic sites, of which are depicted in Figure 6.2.6 using a distance cut off 300 pm (Table 6.2.5). The ordered defects give rise to a cooperative displacement of atoms transforming the defect bcc-type dodecahedral coordination of the atoms into three topologically distinct configurations. The Zn1 and M2 sites are surrounded by distorted icosohedra, whereas the M3 and Zn4 sites have 13- and 11-atomic environment, respectively. The γ-cluster is built up by 57 tetrahedra- a configuration of discrete quadruples of interpenetrating distorted icosahedra about IT atoms sharing a common IT, also called Pierce cluster. [121] A similar but expanded 26 atom cluster consisting of 38 atoms forms a quadruple of icosahedra about the OT atoms. Each of the four icosahedra shares with an enclosed IT one of its faces. The final figure is a modified Pierce Cluster (Fig. 6.2.6 top right) consisting of 81 tetrahedra. Clusters of this size partially interpenetrate. Four interpenetrating M2-centred icosahedra can be formulated as $[M2\ (M1_{3/3}\ M3_{3/2}\ Zn4_{6/2})]_{4.}$ The convex vertexes of this cluster are exclusively occupied by Zn atoms whereas the concave vertexes are mixed occupied by gold/zinc. The complexity of the atomic structure and the presence of icosohedra highlight the quasi-crystal approximant character of the phase.

With respect to 26-atom classical γ-brass cluster, chemical composition throughout the homogeneity range varies due to the substitution by Au-restricted to OT and OH shells exclusively forming an adamantine-like cage. Furthermore, inner tetrahedral and cuboctahedra sites are completely occupied by zinc atoms creating a clean Zn_{16}-tetrahedron of tetrahedral (Fig. 6.2.7)-remains unaffected by gold replacement. This construction is chemically suggestive of the experimental site preference in this γ-brass ternary variant.

Vec value-21/13 per atom is generally assumed to be particular for the formation of γ-brass phases. The partial replacement of Au and Pd on the M2 site as well as mixing of Au and Zn on the M3 site keep the valence electron concentration nearly constant at 1.62-1.65 per atom throughout the entire homogeneity range, if Pd, Au and Zn are taken to zero, mono and divalent, respectively for the counting scheme.

This chapter deals with a comparison of the structures of two congeneric γ-phases in the Pd-Zn-Al [98] and Au-Pd-Zn system. In terms of the 26-atom clusters, the inner tetrahedron (IT) and cuboctahedron (CO) are occupied by mixtures of Zn and Al atoms, the outer tetrahedron (OT) is fully occupied by Pd atoms, and the octahedron (OH) is occupied by a mixture of Zn and Pd atoms in the γ-brass phases of the Pd-Zn-Al system. Similar mixing of Zn and Pd atoms on the OH sites is observed in binary $Pd_{2+x}Zn_{11-x.}$ In contrast, in the γ-brass phases of the Au-Pd-Zn system, inner tetrahedron and cuboctahedron sites are solely occupied by zinc atoms and the outer tetrahedron (OT) and octahedron (OH) are occupied by Au/Pd and Au/Zn atoms, respectively, if the structure can be viewed in terms of 26-atom γ-brass clusters.

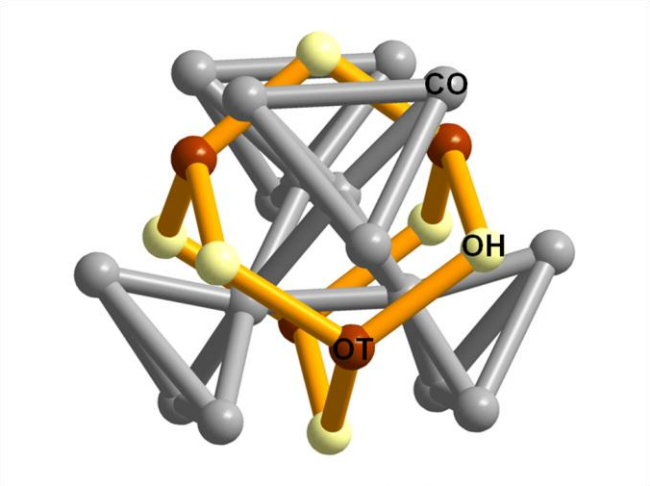

Figure 6.2.7: Representation of the cubic γ-brass cluster seen as a tetrahedron of tetrahedra and an interpenetrating adamantine-type cage. Sites with mixed Au/Zn occupation are shown in light yellow, Au/Pd in light yellow, and zinc in grey, respectively.

Table 6.2.5: Minimum (d_{min}), maximum (d_{max}) and mean interatomic distances (<d>) and coordination numbers (C.N.) for $Au_{1.78}Pd_{3.68}Zn_{20.55}$ (C1), $Au_{2.89}Pd_{3.44}Zn_{19.68}$ (C2)

Cluster	Atoms	Site	C1 d_{min}-d_{max} <d> (pm)	C.N.	C2 d_{min}-d_{max} <d> (pm)	C.N.
γ	Zn2	OT	267.6-278.6 <271.5>	12	267.1-279.8 <272.2>	12
	M2	IT	261.5-281.6 <268.9>	12	261.3-282.6 <269.4>	12
	M3	OH	251.9-292.8 <278.0>	13	251.8-293.8 <278.6>	13
	Zn4	CO	260.5-292.8 <273.8>	11	261.3-293.8 <274.1>	11

6.2.5 Summary

The structure represents the characteristics 3 x 3 x 3 superstructure of an ordinary β-brass-type phase. According to the single crystal diffraction results, this ternary γ-brass-type phase crystallizes in the cubic space group $I\bar{4}3m$ with a significant phase width. The structure comprises of 26 atom γ-brass-type cluster placed at high symmetry points (0 0 0) and (½ ½ ½) in unit cell. Furthermore, γ-brass-type ternary phases in the Au-Pd-Zn system occur at e/a ratio of 1.62-1.65 e^- / atom.

The ternary variant of the γ-phase exhibits a drop of resistivity with increasing temperature and displays diamagnetic properties.

6.3. Structural chemistry of ternary γ'-phases in the Au-Pd-Zn system

Herein, we will discuss the existence, phase width, spatially correlated structural features and physical properties of new γ´-brass phases in the ternary Au-Pd-Zn system.

6.3.1 Solid state synthesis

$(Au_xPd_{1-x})Zn_{\sim 5.5}$ ($0.12 \leq x_{Au} \leq 0.15$) were synthesized starting from pure elements: Pd (99.99%, ABCR), Au (99.99%, ABCR), Zn (99.9999%, Chempur). Samples of precisely weighted metals (ca.0.3 g) were loaded and sealed in previously out-gassed, fused silica ampoules (3 cm long, 0.8 cm in diameter) under a reduced argon pressure of about 0.5 Pa. The metals were heated at a rate of 194.4 K h^{-1} up to 1273 K at which the ampoules were kept for 2 h, hereafter, the temperature was reduced to 823 K at a rate of 90 K h^{-1} and annealed at this temperature for 5 days. The samples were either quenched in cold water or cooled to ambient temperature. To avoid eventual loss of zinc due to evaporation, the reactants were kept at a lower temperature than the rest of the ampoule. Products obtained from these reactions were silvery, brittle ingots and were found to be stable in air.

6.3.2 Single crystal structure determination

Eight single crystals were selected from different compositions ranging $0.13 \leq x_{Au} \leq 0.15$ and $0.79 \leq x_{Zn} \leq 0.76$. The results of six structure refinements unambiguously confirm those of the rest. C1, C2, C3 were selected from the Zn-poor sample (x_{Zn} = 0.77, 0.76, 0.76 respectively). C4, C5, C7 were selected from single phase samples (x_{Zn} = 0.79,

0.79, 0.78, respectively). The diffraction intensities were recorded with an imaging plate diffraction system IPDS (Stoe & Cie, $Mo_{K\alpha}$). [63] The intensities could conclusively be indexed on the basis of a 1.8 nm large *F*-centered cubic unit cell. The collected intensities were corrected for absorption effects. [66, 67] The structures were solved in space group $F\bar{4}3m$ (No. 216) and refined using the SHELX-97 [64] program package based on full-matrix least-square refinements. Sites with mixed occupancy (Zn/Au, Zn/Pd, Au/Pd) were assumed to be unity. Atoms, for which the refined occupancy factors deviated by less than twice the standard deviation from unity, were reset to unity in the final refinement cycles. Local structural disorder phenomena were adequately recorded by introducing split positions. Each structure was checked for possible twinning by inversion and for its absolute configuration. Anisotropic displacement parameters of the atoms were taken into account. The final refinements including an extinction correction and proper weighting scheme yielded residual values R(*F*) between 0.0251 and 0.0530. Further details concerning the crystallographic data and structure determination are given in the Table 6.3.1 and 6.3.2. The positional and equivalent displacement parameters are given in the Table 6.3.3 and 6.4.4 respectively. Further details of the crystal structure investigations are given in the appendix (from A53 to A61).

6.3.3 Phase analyses and physical properties

The homogeneity range of the cubic γ´-phase in the Au-Pd-Zn system was examined by means of preparative methods, calorimetric measurements and by X-ray diffraction. According to X-ray structural analysis the homogeneity range of the γ´-phase was found to range $0.13 \leq x_{Au} \leq 0.14$ and $0.79 \leq x_{Zn} \leq 0.76$, what was confirmed by both EDS and single crystal X-ray diffraction experiments on several crystalline specimens (see Table 6.3.5). Specimens having $x_{Au} \leq 0.13$ and $x_{Au} \geq 0.14$, the γ'-phases coexist with only Au-substituted ternary variants of γ-phases (space group $I\bar{4}3m$, a ≈ 9 Å). Rietveld refinements [62,127,128] were performed on the single phase samples containing x_{Au} = 0.13 and x_{Au} = 0.14 using X'pert Plus programme package.

Table 6.3.1: Crystallographic and technical data for the single crystal structure refinements of $Au_{13.02}Pd_{10.11}Zn_{77.46}$ (C1), $Au_{13.34}Pd_{10.45}Zn_{77.03}$ (C2), $Au_{13.42}Pd_{10.84}Zn_{76.98}$ (C3)

	C1	C2	C3
crystallographic data			
chemical formula	$Au_{13.02}Pd_{10.11}Zn_{77.46}$	$Au_{13.34}Pd_{10.45}Zn_{77.03}$	$Au_{13.42}Pd_{10.84}Zn_{76.98}$
Pearson symbol	*cF*402.4	*cF*403.3	*cF*405.0
x_{Au}	0.129	0.132	0.133
crystal system			
space group type; Z	cubic; $F\bar{4}3m$	(No.216); 4	
a/pm[a]	1816.2(1)	1817.1(1)	1818.6(2)
$V/10^6$ pm^3 [a]	5991.2(5)	5999.3(4)	6014.5(1)
ρ_{calcd}/g cm^{-3}	9.648	9.715	9.750
μ/mm^{-1}	64.964	65.599	65.720
crystal color	silvery with metallic	luster	
data collection			
crystal size/mm^3	0.10x0.06x0.03	0.08x0.06x0.04	0.10x0.04x0.03
diffractometer	IPDS (Stoe & Cie.)		
radiation	$Mo_{K\alpha}$		
monochromator	graphite		
distance crystal-IP/mm	50	70	80
φ_{min}-φ_{max}/^{o}	0-180	0-180	0-180
$\Delta\varphi$	1	1	1
$2\theta_{max}$/^{o}	69.98	60.92	63.78
reflns measured	19987	16477	18246
index range	$-27\le h\le 29$	$-23\le h\le 25$	$-26\le h\le 26$
	$-29\le k\le 29$	$-25\le k\le 25$	$-26\le k\le 26$
	$-29\le l\le 28$	$-24\le l\le 25$	$-26\le l\le 26$
completeness of data set	0.996	1.000	0.990
data reduction/ absorption correction	IPDS-software,[63] X-RED[66]/numerical, X-SHAPE[67]		
unique reflns	1349	955	1071
R_{int}	0.1186	0.0520	0.0777
Structure solution, refinement			
structure solution	direct methods, SHELXS-97[64]		
structure refinement	full-matrix least squires on F^2 (SHELXL-97[64])		
no. reflns used	1349	955	1071
no. variables	79	79	79
observed reflns ($F_o>4\sigma(F_o)$)	1255	908	796
$R(F)$ ($F_o>4\sigma(F_o)$)	0.0530	0.0358	0.0525
$R(F)$ (all data)	0.0569	0.0372	0.0702
weighting factor k_1/k_2 [b]	0.0387/1540.1018	0.0513/765.0313	0.0891/5.8658
wR (F^2)(all data)	0.1359	0.1089	0.1511
GOF (F^2)	1.088	1.144	1.041
extinction coefficient	0.000010(2)	0.000005(2)	0.000017(4)
$\Delta\rho_{min}/\rho_{max}/10^{-6}$epm^{-3}	-3.296/2.791	-1.701/1.861	-2.126/2.598

[a] Parameters determined by use of single crystal diffraction data. [b] Weighting scheme: $1/\omega=\sigma^2(F_O^2)+(k_1.P)^2+k_2.P$ with P = ⅓(max (F_O^2,0) +.2F_c^2).

Table 6.3.2: Crystallographic and technical data for the single crystal structure refinements of $Au_{13.22}Pd_{7.26}Zn_{78.99}$ (C4), $Au_{14.08}Pd_{7.19}Zn_{78.38}$ (C5), $Au_{14.27}Pd_{7.54}Zn_{78.19}$ (C7)

	C4	C5	C7
crystallographic data			
chemical formula	$Au_{13.22}Pd_{7.26}Zn_{78.99}$	$Au_{14.08}Pd_{7.19}Zn_{78.38}$	$Au_{14.27}Pd_{7.54}Zn_{78.19}$
Pearson symbol	*cF*397.9	*cF*398.6	*cF*400.0
x_{Au}	0.133	0.141	0.143
crystal system			
space group type; Z	cubic; $F\bar{4}3m$ (No.216); 4		
a/pm[a]	1813.2(1)	1814.3(5)	1814.3(8)
$V/10^6$ pm^3 [a]	5961.2(6)	5972.2(3)	5972.5(5)
ρ_{calcd}/g cm^{-3}	9.514	9.632	9.702
μ/mm^{-1}	65.550	67.274	67.768
crystal color	silvery with metallic luster		
data collection			
crystal size/mm^3	0.12x0.08x0.04	0.08x0.04x0.03	0.12x0.06x0.05
diffractometer	IPDS (Stoe & Cie.)		
radiation	$Mo_{K\alpha}$		
monochromator	graphite		
distance crystal-IP/mm	50	110	60
φ_{min}-φ_{max}/°	0-180	0-180	0-180
$\Delta\varphi$	1	1	1
$2\theta_{max}$/°	59.86	55.82	63.60
reflns measured	15347	12661	14730
index range	-25≤*h*≤25	-23≤*h*≤23	-26≤*h*≤26
	-23≤*k*≤25	-23≤*k*≤23	-26≤*k*≤19
	-25≤*l*≤25	- 23≤*l*≤23	-26≤*l*≤25
completeness of data set	0.996	0.981	0.998
data reduction/			
absorption correction	IPDS-software,[63] X-RED[66]/numerical, X-SHAPE[67]		
unique reflns	909	752	1063
R_{int}	0.0949	0.0640	0.0770
structure solution, refinement			
structure solution	direct methods, SHELXS-97[64]		
structure refinement	full-matrix least squire on F^2 (SHELXL-97[64])		
no. reflns used	909	752	1063
no. variables	68	68	67
observed reflns (F_o>4σ(F_o))	791	745	951
R(*F*) (F_o>4σ(F_o))	0.0389	0.0251	0.0359
R(*F*) (all data)	0.0480	0.0254	0.0426
weighting factor k_1/k_2 [b]	0.0282/91.9827	0.0290 /468.1170	0.0550/149.6045
wR (F^2)(all data)	0.0683	0.0612	0.0900
GOF (F^2)	1.088	1.088	1.071
extinction coefficient	0.0000131(15)	0. 0000059(17)	0.000013(3)
$\Delta\rho_{min}/\rho_{max}/10^{-6}$epm^{-3}	-2.752/1.493	-1.115/1.232	-1.822/3.254

[a] Parameters determined by use of single crystal diffraction data. [b] Weighting scheme: $1/\omega=\sigma^2(F_O^2)+(k_1.P)^2+k_2.P$ with P = ⅓(max (F_O^2,0) +.2F_c^2).

Table 6.3.3: Structural data for $Au_{13.02}Pd_{10.11}Zn_{77.46}$ (C1), $Au_{13.34}Pd_{10.45}Zn_{77.03}$ (C2), $Au_{13.42}Pd_{10.84}Zn_{76.98}$ (C3)

Cluster	Atom	Site		*x*	*y*	*z*	SOF	*U*eq[a]/pm^2
Z(1)	Zn11	16e	IT	0.0547(7)[b]	*x*	*x*	0.26(2)	200(5)
				0.0540(3)			0.324(17)	110(3)
				0.0542(3)			0.46(2)	140(3)
	Zn11´	16e	IT´	0.94583(18)			0.75(2)	118(14)
				0.94616(15)			0.670(17)	102(14)
				0.9462(2)			0.57(2)	150(2)
	Au12	16e	OT	0.9124(5)	*x*	*x*	0.132(10)	220(4)
				0.9120(2)			0.211(8)	170(2)
				0.9120(2)			0.299(10)	205(19)
	M13[c]	24g	OH	0.18083(6)	0	0	0.886(14)	92(3)
				0.18078(6)			0.808(12)	101(4)
				0.18119(9)			0.732(15)	137(6)
	Zn14	48h	CO	0.14680(12)	*x*	0.02156(18)	1	194(6)
				0.14820(10)		0.02114(14)		197(6)
				0.14956(14)		0.0206(2)		247(8)
Q(2)	Zn21	16e	IT	0.30713(15)	*x*	*x*	1	127(8)
				0.30633(11)				116(7)
				0.30605(15)				141(9)
	M22[d]	16e	OT	0.16509(6)	*x*	*x*	0.522(15)	86(6)
				0.16451(5)			0.540(12)	96(6)
				0.16417(8)			0.530(17)	130(8)
	M23[e]	24f	OH	0.07019(17)	1/4	1/4	0.39(5)	124(11)
				0.07000(14)			0.48(4)	152(10)
				0.06970(18)			0.66(5)	201(13)
	Zn24	48h	CO	0.09260(9)	*x*	0.26617(13)	1	114(5)
				0.09268(8)		0.26654(11)		104(5)
				0.09281(11)		0.26697(16)		139(6)
H(3)	Zn31	16e	IT	0.55416(14)	*x*	*x*	1	108(7)
				0.55389(10)				95(6)
				0.55394(15)				134(8)
	M32[f]	16e	OT	0.41164(9)	*x*	*x*	0.057(16)	84(6)
				0.41146(7)			0.111(14)	76(6)
				0.41173(9)			0.160(19)	127(8)
	M33[g]	24f	OH	0.32230(18)	0	0	0.065(12)	92(9)
				0.32178(14)			0.122(11)	136(10)
				0.32069(18)			0.186(15)	187(12)
	Zn34	48h	CO	0.34482(10)	*x*	0.51942(16)	1	123(5)
				0.34477(8)		0.51950(13)		102(5)
				0.34474(11)		0.51953(18)		146(6)
T(4)	Zn41	16e	IT	0.80249 (14)	*x*	*x*	1	102(7)
				0.80258(10)				96(7)
				0.80274(14)				135(9)
	Pd42	16e	OT	0.66162(9)	*x*	*x*	1	133(6)
				0.66150(7)				110(6)
				0.66187(10)				111(7)
	M43[h]	24f	OH	0.56839(7)	1/4	1/4	0.747(15)	110(4)
				0.56841(4)			0.719(12)	130(5)
				0.56844(9)			0.651(16)	163(7)
	Zn44	48h	CO	0.09689(11)	*x*	0.77801(16)	1	150(5)
				0.09656(9)		0.77655(13)		148(5)
				0.09614(12)		0.77521(18)		187(7)

[a] *U*eq is defined as one third of the trace of orthogonalized U_{ij} tensor. [b] structural data given in the top to bottom lines refer to C1,C2, C3 respectively. [c] SOF(Au), SOF(Zn)=1-SOF(Au). [d] SOF(Au), SOF(Zn)=1-SOF(Au). [e] SOF(Pd), SOF(Zn)=1-SOF(Pd). [f] SOF(Au), SOF(Pd)=1-SOF(Au). [g] SOF(Au), SOF(Zn)=1-SOF(Au). [h] SOF(Au), SOF(Zn)=1-SOF(Au).

Table 6.3.4: Structural data for $Au_{13.22}Pd_{7.26}Zn_{78.99}$ (C4), $Au_{14.08}Pd_{7.19}Zn_{78.38}$ (C5), $Au_{14.27}Pd_{7.54}Zn_{78.19}$ (C7)

Cluster	Atom	Site		*x*	*y*	*z*	SOF	*U*eq[a]/pm^2
Z(1)	Zn11´	16e	IT´	0.94607(14)[b]	*x*	*x*	1	88(8)
				0.94613(9)				92(5)
				0.94623(10)				109(6)
	Au13	24g	OH	0.18071(7)	0	0	1	44(3)
				0.18055(4)				71(2)
				0.18066(5)				89(2)
	Zn14	48h	CO	0.14485(10)	*x*	0.02180(16)	1	116(5)
				0.14453(7)		0.02198(10)		131(4)
				0.14447(8)		0.02186(12)		148(4)
Q(2)	Zn21	16e	IT	0.30728(13)	*x*	*x*	1	68(8)
				0.30790(9)				106(5)
				0.30796(11)				110(6)
	M22[c]	16e	OT	0.16541(7)	*x*	*x*	0.501(13)	28(6)
				0.16539(4)			0.619(10)	59(4)
				0.16542(5)			0.651(12)	87(4)
	Zn23	24f	OH	0.0714(2)	1/4	1/4	1	84(8)
				0.07105(12)				90(6)
				0.07094(15)				106(6)
	Zn24	48h	CO	0.09211(9)	*x*	0.26579(13)	1	57(5)
				0.09186(6)		0.26519(9)		95(4)
				0.09170(7)		0.26510(11)		116(4)
H(3)	Zn31	16e	IT	0.55390(14)	*x*	*x*	1	61(7)
				0.55397(9)				90(5)
				0.55391(11)				115(6)
	M32[d]	16e	OT	0.41130(9)	*x*	*x*	0.052(16)	49(8)
				0.41100(5)			0.113(12)	64(6)
				0.41101(7)			0.115(13)	83(6)
	Zn33	24f	OH	0.3237(2)	0	0	1	38(7)
				0.32426(13)				77(5)
				0.32404(15)				86(5)
	Zn34	48h	CO	0.34521(9)	*x*	0.51947(16)	1	81(5)
				0.34498(6)		0.51958(10)		98(4)
				0.34497(7)		0.51966(12)		93(4)
T(4)	Zn41	16e	IT	0.80222 (13)	*x*	*x*	1	57(7)
				0.80215(8)				80(5)
				0.80212(10)				79(5)
	Pd42	16e	OT	0.66135(10)	*x*	*x*	0.868(14)	74(9)
				0.66080(6)			0.910(10)	93(7)
				0.66029(7)			1	102(5)
	M43[e]	24f	OH	0.56860(7)	1/4	1/4	0.835(14)	78(5)
				0.56841(4)			0.858(9)	100(3)
				0.56776(5)			0.867(11)	128(4)
	Zn44	48h	CO	0.09752(11)	*x*	0.77960(14)	1	93(5)
				0.09759(7)		0.77983(9)		116(4)
				0.09768(9)		0.78001(12)		135(4)

[a] *U*eq is defined as one third of the trace of orthogonalized U_{ij} tensor. [b] structural data given in the top to bottom lines refer to C4,C5,C7 respectively. [c] SOF(Au), SOF(Zn)=1-SOF(Au). [d] SOF(Au), SOF(Pd)=1-SOF(Au). [e] SOF(Au),SOF(Zn)=1-SOF(Au).

Positional parameters of the single crystal X-ray structure determination were used as starting parameters for refinements against bulk sample X-ray powder data. A profile is shown in the Fig. 6.3.1 and 6.3.2.

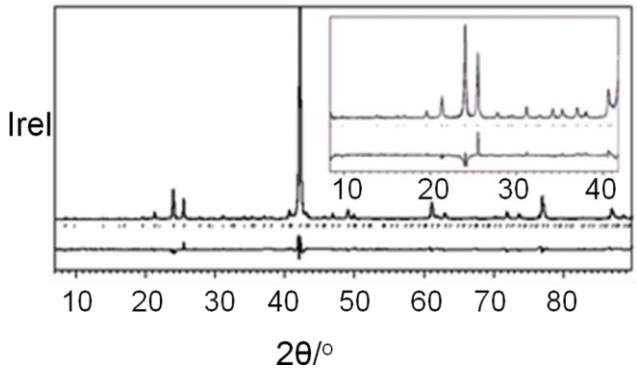

Figure 6.3.1: Observed and calculated X-ray powder diffractogram of $Au_{13.02}$ $Pd_{10.11}$ $Zn_{77.46}$ (x_{Au} = 0.13) for the 2θ range 10-90^{O} together with the profile fit, the difference spectrum and the Bragg positions. Insert shows low angle Rietveld profile fit; $Cu_{K\alpha}$; R_B = 0.0490, R_P = 0.08308.

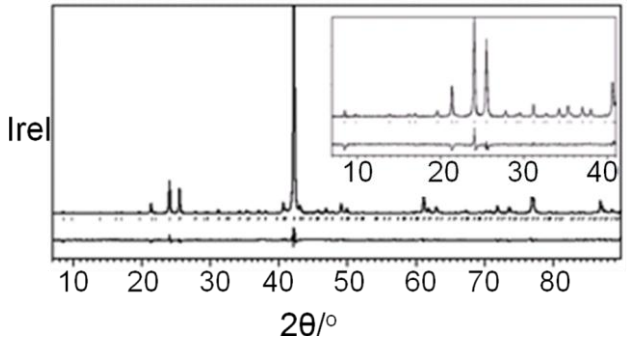

Figure 6.3.2: Observed and calculated X-ray powder diffractogram of $Au_{14.08}Pd_{7.19}Zn_{78.38}$ (x_{Au} = 0.14) for the 2θ range 10-90^{O} together with the profile fit, the difference spectrum and the Bragg positions. Insert shows low angle Rietveld profile fit; $Cu_{K\alpha}$; R_B = 0.0334, R_P = 0.0653.

The composition determined by X-ray diffraction agrees acceptably with the results of 12 EDS analyses from crystals of ternary γ'-brass phases in Au-Pd-Zn system.

Table 6.3.5: A summary of the composition of selected samples as determined by EDS and single crystal-X-ray diffraction

Loaded composition	Crystal designation	Refined composition	EDS composition
$Au_{13.1}Pd_{9.1}Zn_{78.5}$	C1	$Au_{13.0}Pd_{10.1}Zn_{77.5}$	$Au_{14.3(8)}Pd_{10.7(8)}Zn_{76.2(8)}$
$Au_{13.1}Pd_{10.1}Zn_{77.6}$	C2	$Au_{13.3}Pd_{10.5}Zn_{77.0}$	$Au_{14.3(8)}Pd_{9.7(8)}Zn_{76.5(8)}$
$Au_{12.9}Pd_{8.9}Zn_{77.6}$	C4	$Au_{13.2}Pd_{7.3}Zn_{79.0}$	$Au_{12.7(6)}Pd_{7.4(4)}Zn_{80.1(10)}$
$Au_{14.0}Pd_{7.0}Zn_{78.0}$	C5	$Au_{14.1}Pd_{7.2}Zn_{78.4}$	$Au_{14.3(4)}Pd_{7.6(7)}Zn_{76.0(11)}$
$Au_{15.0}Pd_{7.0}Zn_{78.0}$	C6	$Au_{14.1}Pd_{7.6}Zn_{78.3}$	$Au_{14.5(8)}Pd_{7.5(2)}Zn_{78.3(10)}$
$Au_{15.0}Pd_{7.0}Zn_{78.0}$	C7	$Au_{14.3}Pd_{7.5}Zn_{78.2}$	$Au_{15.4(2)}Pd_{7.6(2)}Zn_{76.9(4)}$

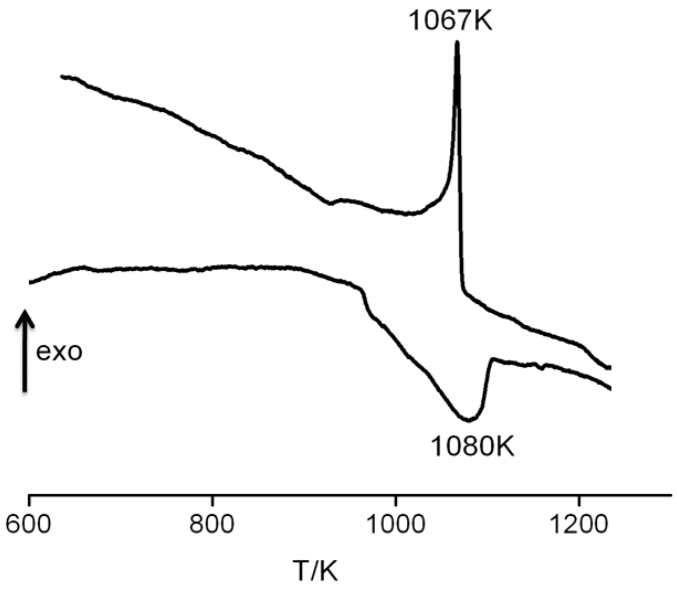

Figure 6.3.3: Thermo-chemical analysis of $Au_{14.27}Pd_{7.54}Zn_{78.19}$ (x_{Au} = 0.14).

According to the DTA measurements of the single phase sample, Au-rich γ'-phase (x_{Au} = 0.14) begins to melt at 988 K (Fig. 6.3.3). The peak maximum is found at 1080 K. The phase starts to reform at 1073 K. For the gold (x_{Au} = 0.13) poor sample, the peak

maxima is found at 1051K. The shift of the peak maxima of melting point is attributed to the phase width of γ´-ternary phase.

Pre-melting features evolved at approximately 963K for the samples of different compositions. We may suggest that this thermal effect is associated with a discontinuous increase of structural disorder upon heating prior to melting.

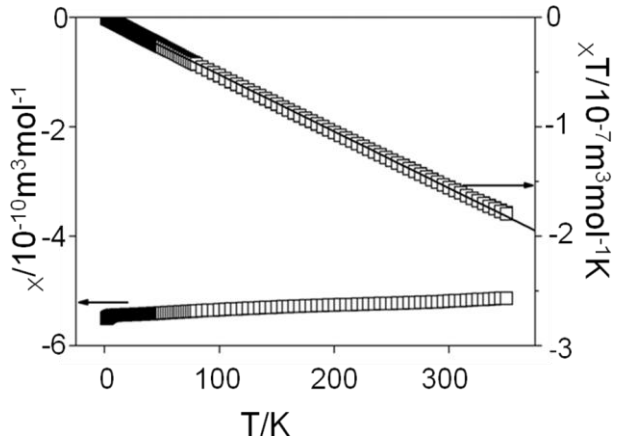

Figure 6.3.4: Magnetic susceptibility as a function of temperature for $Au_{14.27}Pd_{7.54}Zn_{78.19}$ (x_{Au} = 0.14).

Magnetic susceptibilities of the clean crystalline samples were recorded with a SQUID magnetometer in the temperature range 5-300 K at a magnetic flux density of 1-5 Tesla. The data were corrected for diamagnetism of the sample holder made of gelatin. The Pauli paramagnetism of these metallic phases is found to be overcompensated by the core diamagnetism of its constituents (Fig. 6.3.4). The values of magnetic susceptibility for $Au_{14.3}Pd_{7.5}Zn_{78.2}$ and $Au_{14.1}Pd_{7.2}Zn_{78.4}$ are -5.03 (1) $x10^{-10}$ and -5.50 (1) x 10^{-10} m^3 mol^{-1}, respectively. In each case the value refers to an average atom of the formula, i.e. $\frac{1}{(a+b+c)}Au_aCr_bZn_c$.

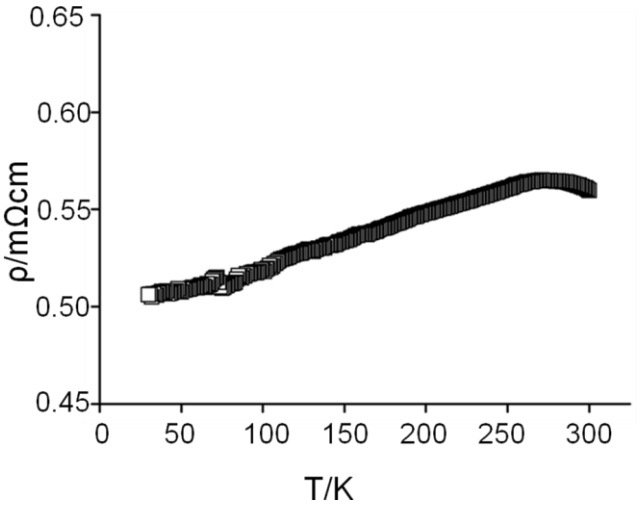

Figure 6.3.5: Resistivities ρ of single phase samples $Au_{13.02}Pd_{10.11}Zn_{77.46}$ (x_{Au} = 0.13) between 30 and 300 K.

γ´-phase in the Au-Pd-Zn system, resistivities grow from 0.50 mΩcm (30 K) to 0.56 mΩcm (300 K) (Fig. 6.3.5). These values are nearly two orders of magnitude higher than that of zinc metal (ρ(293K) = 5.8 μΩ cm).

6.3.4 Structural characteristics

The ternary γ´-phases in the Au-Pd-Zn system form a structurally complex, highly disordered γ-related phase belonging to a cubic giant cell structures. The phase crystallizes in the acentric space group $F\bar{4}3m$ with approximately 398-405 atoms in the cubic unit cell that are distributed over 15-17 crystallographically independent positions depending on the chemical composition. The average number of atoms per cell as well as unit cell volume decreases with the increase of zinc content. The structure of γ´ represents a $(6a_{bcc})^3$ superstructure of β-brass type structure with ordered vacancies. The ordered vacancies are the characteristics of γ-brass type or related structures. Hence, alternatively the structure can be described by the $(2a_{\gamma})^3$ superstructure of

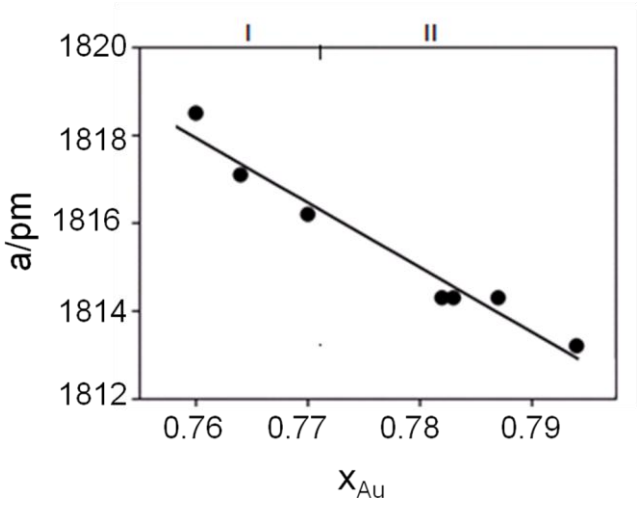

Figure 6.3.6: Lattice parameters vs. mole fraction of Zn (x_{Zn}) from single crystal X-ray diffraction experiment of Au-Pd-Zn γ´phases.

ordinary γ-brass structure. Such kind of structures can be favourably analysed by partitioning them into clusters, [131] also called nested polyhedral units, [132] which are grouped around the high symmetry points of the lattice. Furthermore, it is a geometrical mean to describe the atomic arrangement of structurally complex intermetallic alloy. Chemical bonding is not considered here. The composition of the phase can be obtained from summing up the composition of the constituting clusters. Moreover, it strikingly discloses element-specific structural dissimilarities between γ-brass-related structures having more than 400 atoms in the unit cell. According to the concept, the Au-Pd-Zn γ´-brass structures consist of 4 x 4 clusters per unit cell and their centres are located at the high symmetry points of the *F*-centred unit cell: (0 0 0), (¼ ¼ ¼), (½ ½ ½), (¾ ¾ ¾) and equivalent translational invariant points. We address each cluster type by a capital letter indicating the central position of each cluster, i.e., Z for 0, Q for ¼, H for ½, and T for ¾. [133] Furthermore, the numbers of atoms in each cluster vary between 22 and 26 according to chemical composition. The shells are congruent to one of the

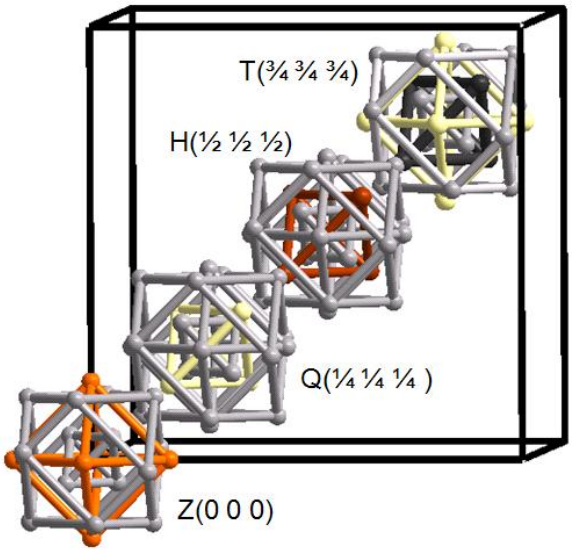

Figure 6.3.7: The arrangement of clusters in the crystal structure of $Au_{14.27}Pd_{7.54}Zn_{78.19}$ (C6) along the body diagonal. Clusters are centered at the high-symmetry points of the *F*centered cubic unit cell and their identities are revealed. The clusters are represented by idealized cuboctahedron shells. Constituting zinc atoms have been shown by gray (40%), palladium by grey (80%), gold by orange, mixed-occupied Au and Zn by light yellow and Au/Pd by brown color.

various Platonic and Archimedean solids. Each shell corresponds to a distinct crystallographic site and is distinguished by two capital letters. CC designates the centre of a cluster, IT those occupying the vertices of an inner tetrahedron. Accordingly, OT stands for outer tetrahedron, CO for cuboctahedron. Furthermore, we numerate atoms of a given cluster according to their distance from the centre of the cluster.

The 26 atoms ideal γ-brass cluster constructed from successive polyhedral shells: (a)IT sites, (b) OT shells-vertices are above the faces of IT, (c) OH sites lying above the edges of OT, and (d) distorted CO sites placed above the edges of the OH sites. All those clusters (Z, Q, H, T) display variable compositions associated with random and substitutional vacancies, mixed (Au/Zn, Au/Pd, Pd/Zn) occupancies demonstrate a considerable phase width. In the region (I)-poor in zinc, the γ´-brass phase occurs. In the Zn-rich region (II) of γ´-phase a slightly modified cubic giant cell intimately related with γ´-brass structure is present (Fig. 6.3.6).

In this section, we will emphasize the variation of chemical composition and structural features in different clusters (Z, Q, H, T). Single crystal X-ray studies in different specimens (C1, C2, C3) in the region I at cluster Z, Zn11(IT) and Zn11´(IT´) display physically meaningless short distances. This problem unravels completely if we assume two different cluster types alternatively grouped about a high symmetry point. This assumption is supported and confirmed by the pair-wise linear dependence of related site occupancy factor of those atomic sites which generate too short interatomic distance as a result of independent refinements (c. f. Table 6.3.3). Hence, we may conclude at Z(0 0 0) either ideal γ-brass type $Au_4(Au, Zn)_6Zn_{16}$ with shell sequence IT, OT, OH,CO or defect γ-brass type $(Au, Zn)_6Zn_{16}$ (IT´, OH, CO) is situated about Z in region I whereas, the structures in region II (C4, C5, C6, C7) display defect γ-type clean Au_6Zn_{16} cluster. There is a gradual increase of zinc concentration on IT´ site and the drop on IT site as we move towards the Zn-rich phase of region I. However, for Zn-rich case (region II), IT´ is solely occupied by zinc. Hence, IT site depletes. Two additional correlations between site occupancy factors f (c.f. Table 6.3.6 & 6.3.7), in Cluster Z (region I) give evidence, that the various disorder phenomena in various shells are interrelated: f(OT, Au12) ≈ f(OH, 1-M13), f(Zn11´) + f(Au12´) ≈ 0.88. A slight increase of gold on the mixed occupied OH (in Z cluster of region I) site results in the drop of gold occupation in OT site parallel to the overall increment of zinc content following the above relation. Further increment of overall zinc content (x_{Zn} = 0.78-0.79) of samples, $f_{OT(Z)}$ = 0 originates from the full occupancy by gold on the OH site of Z. Hence, full occupation of gold on OH site of Z cluster generates a complete vacant OT site which is reflected in the structure of specimens of region II.

It is worthwhile to mention that the IT´ sites (Table 6.3.3 & 6.3.4) in crystals of region II is in close proximity with the OT sites in crystals of region I that is C1, C2 and C3 in which both IT´ and OT sites are partly occupied. However, we addressed this position as IT´ rather than OT because the observed IT´-IT´ distances (275.9(3)-281.0(2) pm) are comparable with IT-IT distances of others crystals.

Table 6.3.6: SOF of Zn and Au on the IT and the IT´ sites in cluster Z

	Region	x_{Zn}	x_{Au}	f_{Zn} (IT)	f_{zn} (IT´)
I	C3	0.76	0.13	0.46	0.57
	C2	0.76	0.13	0.32	0.67
	C1	0.77	0.13	0.26	0.75
II	C7	0.78	0.14	0	1
	C6	0.78	0.14	0	1
	C5	0.78	0.14	0	1
	C4	0.79	0.13	0	1

Table 6.3.7: SOF of Au/Zn on OH and OT sites in cluster Z

	Region	x_{Zn}	x_{Au}	f_{Au}/f_{Zn} (OH)	f_{Au} (OT)
I	C3	0.76	0.13	0.73/0.27	0.30
	C2	0.76	0.13	0.81/0.19	0.21
	C1	0.77	0.13	0.88/0.12	0.13
II	C7	0.78	0.14	1/0	0
	C6	0.78	0.14	1/0	0
	C5	0.78	0.14	1/0	0
	C4	0.79	0.13	1/0	0

Noteworthy, defect γ-type Au_6Zn_{16} cluster shows features of one sort of clusters found in $Ce_{20}Mg_{19}Zn_{81}$ [143] in which the minority component-Mg occupies OH site having clean Mg_6Zn_{16} cluster. This M_6Zn_{16} is also related to Ti_2Ni-type with a similar special orientation of atoms as in Ti_2Ni but different sequence of geometrical form (Fig. 6.3.8). The largest portion of the Au-content of the phase, M13 is segregated on OH. Structural analysis indicates that no accumulation of palladium occurs in the Z cluster over the homogeneity range.

In cluster Q, IT and CO sites remain fully occupied by zinc whereas the OT site is mutually substituted by Au/Zn. Furthermore, at the Zn-rich end (region II), the OH site

has full occupation of zinc but at the Zn-poor region (I) the equivalent site is systematically replaced by palladium with decreasing overall zinc content of the phase. Finally, the occupations of IT site for the crystals (C4, C5, C7) of region II show a clear trend for mixing Au and Zn atoms with zinc in Cluster Q (c.f. Table 6.3.3 & 6.3.4).

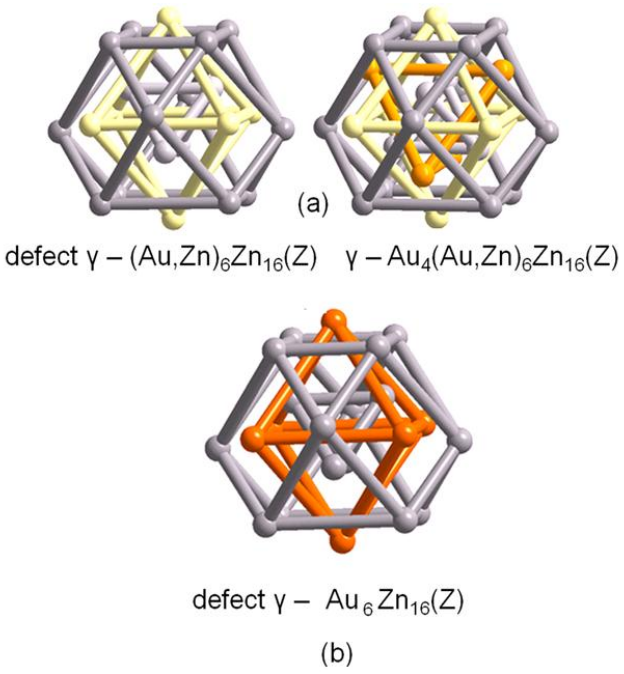

Figure 6.3.8: (a) Representation of two different cluster types (defect-γ /real γ-type) alternatively grown about the origin found in Z(0 0 0) at zinc-poor region of the γ´-phase of Au-Pd-Zn ternary system, (b) representation of clean Au_6Zn_{16} (defect γ-cluster) at Z(0 0 0) as occurring in the zinc-rich region. Sites with mixed Au/Zn occupation are shown in light yellow, gold in orange, and zinc in grey, respectively.

Cluster H contributes to the variation in overall composition as an outcome of mutual substitution of Au/Pd at the OT site and Au/Zn mixing at the OH site. Moreover, mixing of Au and Zn atoms occurs at the OH site for zinc poor cases (C1, C2, C3). However, for Zn-rich samples (C7, C5, C4), the OH site of cluster H is fully occupied by Zn. Furthermore, mixing of Au and Pd on the OT site occurs parallel to the overall zinc

content of the samples in both regions (I and II). IT, CO sites maintain full occupation by zinc atoms over the whole phase width.

Finally, cluster T shows mutual substitution of Au and Zn at OH. Samples of region I are solely occupied by palladium atoms at the OT site. Moreover, for the specimens of the zinc-rich end (C4, C5) of region II, the OT sites are partially occupied whereas samples at the zinc-poor side (of region II-C6 & C7) are fully occupied by palladium. Furthermore, the concentration of vacancy at the OT site increases parallel to the molar fraction of zinc. IT and CO sites are not attacked by any one of the minority components (Au, Pd). The OH and CO sites are solely occupied by zinc. The largest portion of the Pd content of the phase, Pd42, is accumulated on OT site of cluster T.

Table 6.3.8: SOF on the OH and OT sites in cluster T

	Region	x_{Zn}	f_{Pd} (OT)	f_{Au}/f_{Zn} (OH)
I	C3	0.76	1	0.651/0.349
	C2	0.76	1	0.719/0.281
	C1	0.77	1	0.747/0.253
II	C7	0.78	1	0.867/0.133
	C6	0.78	1	0.863/0.137
	C5	0.78	0.91	0.858/0.142
	C4	0.79	0.86	0.835/0.165

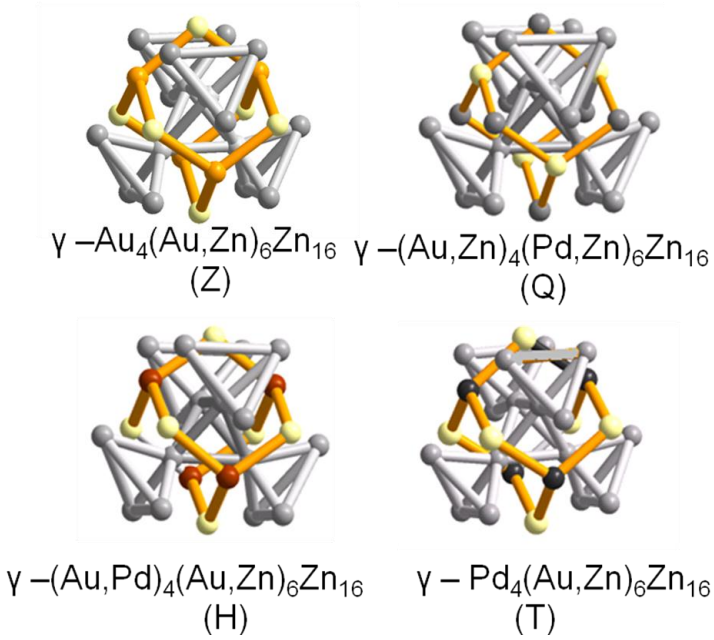

Figure 6.3.9: Representation of four chemically distinct but topologically similar clusters found in the crystal structures of $Au_{13.02}Pd_{10.11}Zn_{77.46}$ (x_{Au} = 0.13). Spheres representing sites with mixed Au/Zn occupation are shown in light yellow, Au/Pd in brown, Pd/Zn in 50% grey, palladium in 80% grey, gold in orange, and zinc in grey (40%), respectively.

Selected shells are labeled with their abbreviations as used in the text. The clusters from left to right are numbered consecutively along the body diagonal starting with cluster Z placed about the origin. Each cluster has been shown by its symbol and composition.

The specific feature of γ´-ternary phase is the occurrence of a single cluster type, the so called γ-brass type. The redistribution of atoms (mixing of Au/Zn, Pd/Zn, Au/Pd) occurs at OT and OH sites and there is no redistribution of atoms among IT and CO sites. Hence, Fig 6.3.9 shows the construction of the γ-brass-type cluster that is both chemically meaningful and geometrically palatable. IT and CO sites are solely occupied by zinc atoms forming a clean Zn_{16} tetrahedron of tetrahedral whereas OT and OH sites together form adamantine-type cage which is responsible for variation in composition.

Partial occupation as well as the mutual substitution of atoms on different crystallographic sites is crucial to keep the valence electron concentration value essentially constant throughout the homogeneity range if we assume that the phase is

stabilised by the Hume-Rothery mechanism. If we consider the conventional counting scheme for Au: 1 electron, Pd: 0 electron and Zn: 2 electrons, the *vec* values range between 1.66 and 1.72 per atom for γ’-brass-type phases in the ternary Au-Pd-Zn system. For the γ’ Au-Pd-Zn phases, *vec* is reduced by a progressive replacement of Zn by Au atoms on various crystallographic sites (M(OH)13, M(OT)22, M(OH)43). But the simultaneous increase of Zn fraction at the M(OH)23 and the M(OH)43 sites, as well as increase of vacancy concentration on the Au(OT)12 site shifts the *vec* towards the expected value of the γ-phases.

According to the observed correlations among chemical composition*,* lattice parameters *and vec* values, there are two different regions of γ´-brass-type phases. γ´ phases of region I with high unit cell volumes, low zinc contents and a *vec* value of approximately 1.66-1.67 per atom, contain no vacancies. On the other hand, γ´-brass-type phases with low cell volumes, high zinc contents and *vec* values (1.71-1.72 per atom), contain the highest content of atomic vacancies in the unit cell. Hence, we conclude that the γ- and γ’-phase may coexist rather than steadily transmute into each other.

This chapter deals with a comparison of the structures of two congeneric γ’-phases in the Pd-Zn-Al [98] and Au-Pd-Zn system. The structures of two γ’-phases share few features in spite of the compositional distinctions and the complexity of the structures. Common features are: (i) Clusters are essentially same in both structures. A specific feature is the occurrence of a single cluster-type, the so-called γ-type. (ii) Though different in composition, the inner tetrahedron (IT) site of the defect γ-cluster is completely vacant at the Al- or Au-rich boundary of the phases. Structural differences concern: (i) Two clusters are completely ordered whereas the other two contain all structural disorder in the γ’ Pd-Zn-Al phases (ii) *vec* is larger: 1.71-1.75 in the case of Pd-Zn-Al.

Table 6.3.9: Minimum (d_{min}), maximum (d_{max}) and mean interatomic distances (<d>) and coordination numbers (C.N.) for $Au_{13.02}Pd_{10.11}Zn_{77.46}$ (C1), $Au_{13.34}Pd_{10.45}Zn_{77.03}$ (C2), $Au_{13.42}Pd_{10.84}Zn_{76.98}$ (C3)

Cluster	Atoms	Site	C1 d_{min}-d_{max} <d> (pm)	C.N.	C2 d_{min}-d_{max} <d> (pm)	C.N	C3 d_{min}-d_{max}	C.N.
Z(1)	Zn11	IT	244.1-281.0 <266.4>	12	249.3-277.5 <267.0>	12	252.8-278.8 <268.5>	12
	Zn11	IT´	268.9-278.3 <274.0>	9	269.0-278.1 <274.6>	9	269.8-281.0 <275.9>	9
	Au12	OT	245.2-281.6 <262.2>	12	247.1-282.1 <263.3>	12	249.6-282.7 <264.6>	12
	M13	OH	256.9-283.9 <272.6>	15	256.2-284.6 <273.3>	15	253.7-285.2 <274.0>	15
	Zn14	CO	244.1-279.4 <268.1>	11	249.3-278.4 <269.0>	11	252.8-281.0 <269.9>	11
Q(2)	Zn21	IT	266.8-293.4 <274.0>	12	267.3-289.5 <273.6>	12	268.0-288.3 <273.8>	12
	M22	OT	261.5-278.0 <268.0>	12	261.6-278.8 <268.2>	12	262.0-279.7 <268.7>	12
	M23	OH	251.7-292.9 <280.5>	13	251.4-292.8 <280.3>	13	251.2-292.8 <280.1>	13
	Zn24	CO	258.8-290.3 <273.2>	11	258.5-290.4 <273.3>	11	257.9-290.6 <273.4>	11
H(3)	Zn31	IT	264.0-278.2 <270.7>	12	265.0-277.0 <270.9>	12	266.9-277.5 <271.4>	12
	M32	OT	260.3-279.0 <269.3>	12	260.6-279.9 <269.4>	12	261.0-281.0 <269.7>	12
	M33	OH	256.9-308.4 <278.9>	13	256.2-305.7 <278.7>	13	253.7-302.6 <278.6>	13
	Zn34	CO	258.8-292.9 <275.2>	11	259.2-292.8 <274.9>	11	259.4-292.8 <274.8>	11
T(4)	Znr41	IT	262.2-272.0 <268.6>	12	263.5-272.5 <269.2>	12	264.8-271.9 <269.7>	12
	Pd42	OT	258.8-283.2 <270.7>	12	258.5-283.5 <270.5>	12	259.4-283.3 <270.3>	12
	M43	OH	251.7-311.4 <280.8>	13	251.4-308.0 <280.3>	13	251.2-304.9 <280.0>	13
	Zn44	CO	245.3-353.5 <313.5>	15	247.1-352.7 <313.9>	15	249.6-352.1 <314.4>	15

Table 6.3.10: Minimum (d_{min}), maximum (d_{max}) and mean interatomic distances (<d>) and coordination numbers (C.N.) for for $Au_{13.22}Pd_{7.26}Zn_{78.99}$ (C4), $Au_{14.08}Pd_{7.19}Zn_{78.38}$ (C5), $Au_{14.27}Pd_{7.54}Zn_{78.19}$ (C7)

Cluster	Atoms	Site	C4 d_{min}-d_{max} <d> (pm)	C.N.	C5 d_{min}-d_{max} <d> (pm)	C.N	C7 d_{min}-d_{max} <d> (pm)	C.N.
Z(1)	Zn11	IT´	268.3-276.6 <271.8>	9	268.2-276.4 <271.6>	9	268.4-275.9 <271.5>	9
	Au13	OH	259.3-282.1 <270.4>	11	260.5-281.3 <270.3>	11	260.1-280.8 <272.9>	11
	Zn14	CO	265.7-315.5 <283.0>	12	265.6-316.4 <282.9>	12	266.0-315.9 <282.8>	12
Q(2)	Zn21	IT	264.5-293.8 <273.4>	12	265.2-297.1 <274.6>	12	265.3-297.4 <274.8>	12
	M22	OT	261.6-275.9 <267.4>	12	261.5-276.5 <267.8>	12	261.7-276.6 <267.9>	12
	Zn23	OH	253.9-294.5 <281.0>	13	253.0-294.0 <281.3>	13	251.7-293.9 <281.3>	13
	Zn24	CO	258.5-290.2 <273.1>	11	258.9-290.7 <273.2>	11	258.5-291.0 <273.2>	11
H(3)	Zn31	IT	261.5-276.4 <269.4>	12	260.7-277.0 <269.7>	12	261.9-276.7 <269.7>	12
	M32	OT	259.2-277.4 <268.5>	12	259.8-277.3 <269.1>	12	260.0-277.6 <269.2>	12
	Zn33	OH	258.5-312.4 <278.5>	13	258.9-313.6 <278.9>	13	258.5-313.8 <278.9>	13
	Zn34	CO	257.8-294.5 <275.2>	11	256.7-294.0 <275.4>	11	255.5-293.9 <275.3>	11
T(4)	Znr41	IT	260.3-272.0 <267.5>	12	260.4-273.5 <268.0>	12	260.2-274.8 <268.5>	12
	Pd42	OT	257.8-282.8 <270.6>	12	256.7-283.7 <271.0>	12	255.5-284.9 <271.3>	12
	M43	OH	253.9-315.5 <281.2>	13	253.0-316.4 <281.5>	13	251.7-315.9 <281.6>	13
	Zn44	CO	260.2-353.7 <296.5>	15	260.4-353.5 <275.7>	15	260.2-353.4 <296.6>	15

6.3.5 Summary

Systematic studies of the ternary Au-Pd-Zn system in the range $0.13 \leq x_{Au} \leq 0.14$ and $0.79 \leq x_{Zn} \leq 0.76$ reveal 2a x 2a x 2a superstructure of ordinary γ-brass-type phases. According to the single crystal diffraction results, these new ternary γ´-brass-type phases crystallize in the cubic acentric space group $F\bar{4}3m$ with a significant phase width. The structure comprises four independent γ-brass-type clusters placed at high

symmetry points in the unit cell. All clusters show some variation in composition as a consequence of the substitution of gold for zinc and/or palladium, host some structural disorder such as mixing of Au and Zn, Au and Pd or Pd and Zn, and accommodate split positions and vacancies. Stabilisation of this ternary γ´-brass phase in terms of Hume-Rothery mechanism occurs from 1.66 to 1.72 per atom. These *vec* values are slightly higher than those expected for γ-brass-type phases.

The new ternary γ´-phases are weak metallic conductors and exhibit diamagnetic properties.

Chapter 7

Spatially correlated structural disorder phenomena in zinc rich alloys $(Au,Ru)Zn_n$; n = 10.7-3.2

7.1 Introduction

The iron-zinc system has been investigated in the zinc-rich domain. Several phases, e.g. cubic γ-$Fe_3Zn_{10,}$ [110] monoclinic ζ-FeZn13, [71] and hexagonal δ-$FeZn_{10}$ [56,156] has been structurally characterized.

Recently, we have structurally identified the congener of hexagonal $FeZn_{10}$ [56,156] in Ru-Zn system, $RuZn_{10}$ [55] exhibiting ~564 atoms in its unit cell. In order to gain an insight into expressions, cause and mechanism of such phases, we investigated the effect of substitution of ruthenium and zinc by gold on the evolution of the structure of ternary derivatives of $RuZn_{10}$.

We have chosen gold for substitution because of its strong scattering factor in comparison with ruthenium and zinc. This fact may permit distinguishing the atomic site of gold by the results of X-ray diffraction experiment. Comprehensive studies by single crystal X-ray diffraction experiments on several specimens in highly differentiated ternary Au-Ru-Zn alloy reveal the existence, phase width and structural characteristics formulated as $(Au,Ru)Zn_n$, n = 10.7-3.2.

7.2 Synthesis and morphological features

About six reactions were carried out with different M/Zn ratio (M = Au, Ru) in $(Au_{0.5}Ru_{0.5})Zn_{n,}$ (n = 11, 5, 6, 4, 3) starting from the pure elements: Au (99.99%, ABCR), Ru (99.8%,ABCR) and Zn (99.9999%, Chempur). Samples of precisely weighted metals (ca. 0.3 g) are loaded and sealed in previously out gassed, fused silica ampoules (3 cm long, 0.8 cm in diameter) under a reduced argon pressure of about 0.5 Pa. The metals

were heated at a rate of 194.4 Kh^{-1} up to 1273 K at which the ampoules were kept for 5h, hereafter, the temperature was reduced to 823 K at a rate of 37.5 K h^{-1} and annealed at this temperature for 5 days. The samples were either quenched in cold water or cooled to ambient temperature. To avoid loss of zinc due to evaporation the reactants were kept at a lower temperature than the rest of the ampoule. Products were silvery, brittle ingots and were air stable.

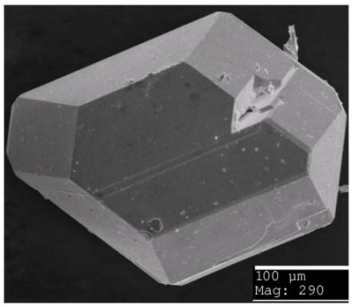

Figure 7.1: Scanning electron micrograph of a regular form of a crystal of in the Au-Ru-Zn system.

7.3 Single crystal structural determination

Four single crystals ranging from $0.76 \leq x_{Zn} \leq 0.91$ were selected from different Au-Ru-Zn reactions were studied by X-ray means. Four crystals are discussed in detail herein. Crystal 1 (C1) was selected from a sample richest in zinc having x_{Zn} = 0.919, x_{Au} = 0.0140 and crystal 4 (C4) was selected from a sample richest in gold-content having x_{Au} = 0.148, x_{Zn} = 0.761. Crystal 3 (C2) and crystal 3 (C3) having a medium Au-content was taken from samples of nominal composition x_{Au} = 0.045, x_{Zn} = 0.871 and x_{Au} = 0.129, x_{Zn} = 0.779, respectively. The diffraction intensities were recorded with an imaging plate diffraction system IPDS (Stoe & Cie) working with $Mo_{K\alpha}$ radiation. [63] The intensities could be indexed on the basic of large primitive hexagonal unit cell. The measured intensities were corrected for Lorentz and polarization effects and were further corrected for absorption by using the STOE X-SHAPE and X-RED programs. [66, 67] The structures were solved in the space group *P* 6_3/mmc (No. 194) by applying direct methods and refined using the SHELX-97 program package based on full-matrix least-square

refinements. [64] The possible positions of missing zinc atoms were taken from difference Fourier synthesis maps. At this stage the structure refinement converged at $R(F) < 0.10$. Further improvement of the calculations was achieved by partially replacing ruthenium and/or zinc by gold on the site which showed lower displacement parameters with respect to normal, assuming those sites to be fully occupied overall by two different atomic species. On the other hand, those metal sites having relatively large thermal displacement parameters were checked for the partial occupancy and positional disorder. Atoms for which the refined occupancy factors deviated by less than twice the standard from unity were reset to unity in the final refinement cycles. Local structural disorder phenomena were recorded by introducing split positions. All the disorder sites were refined with non-coupled occupation parameters except the ones showing mixed occupancy. All the atoms of the structure were refined with anisotropic displacement parameters. The final refinement including an extinction correction and a proper weighting scheme yields R (*F*) values between 0.0268 and 0.0496. Further details concerning the crystallographic data and structure determination (for C1, C2, and C4) are provided in the Table 7.1. Equivalent displacement parameters are given in the Table 7.2.1, 7.2.2, and 7.3.3. Further details of the crystal structure determination are tabulated in the appendix (A63, A64).

7.4 Phase analysis

The homogeneity range and constitutions of large hexagonal phases in the Au-Ru-Zn systems were examined by means of preparative methods, X-ray single crystal diffraction and EDS analysis.

Chemical composition determined by EDS and X-ray single crystal refinement shows an extended homogeneity range over $0.01 \leq x_{Au} \leq 0.15$ and $0.76 \leq x_{Zn} \leq 0.91$, i.e., from $Au_{3.8}Ru_{20.0}Zn_{253.4}$ to $Au_{41.5}Ru_{25.7}Zn_{213.7}$.

Composition evaluated by EDS and X-ray single crystal refinements is in excellent agreement with each other. The loaded composition for different preparation, their corresponding refined composition, from single crystal X-ray diffraction experiments and EDS analysis for selected crystalline specimens are summarized in the Table 7.3.

Table 7.1: Crystallographic and technical data for the single crystal structure refinements of $Au_{3.75}Ru_{20.00}Zn_{253.39}$ (C1), $Au_{12.43}Ru_{23.33}Zn_{242.03}$ (C2), $Au_{41.52}Ru_{25.74}Zn_{213.74}$ (C4)

	C1	C2	C4
crystallographic data			
chemical formula	$Au_{3.75}Ru_{20.00}Zn_{253.39}$	$Au_{12.43}Ru_{23.33}Zn_{242.03}$	$Au_{41.52}Ru_{25.74}Zn_{213.74}$
Pearson symbol	*hP*554.3	*hP*555.6	*hP*562.0
x_{Au}	0.014	0.045	0.148
crystal system			
space group type; Z	hexagonal; $P6_3/mmc$ (194); 2		
a/pm	1285.85(4)	1290.39(3)	1294.53(4)
c/pm	5753.70(18)	5741.60(17)	5791.98(19)
$V/10^6$ pm^3 [a]	8238.7(4)	8279.5(4)	8406(3)
ρ_{calcd}/g cm^{-3}	7.789	8.275	9.779
μ/mm^{-1}	41.132	47.276	68.087
crystal color	silvery with metallic luster		
data collection			
crystal size/mm^3	0.10x0.08x0.04	0.12x0.05x0.04	0.06x0.04x0.03
Diffractometer	IPDS (Stoe & Cie.)		
Radiation	$Mo_{K\alpha}$		
Monochromator	graphite		
distance crystal-IP/mm	140	150	100
φ_{min}-φ_{max}/^{o}	0-180	0-180	0-180
$\Delta\varphi$	1	1	1
$2\theta_{max}$/^{o}	50	50	50
reflns measured	36450	145358	43686
index range	$-15\le h\le 15$	$-15\le h\le 15$	$-15\le h\le 15$
	$-14\le k\le 15$	$-14\le k\le 15$	$-15\le k\le 15$
	$-62\le l\le 67$	$-65\le l\le 67$	$-66\le l\le 67$
completeness of data set	0.998	0.979	0.995
data reduction/ absorption correction	IPDS-software,[63] X-RED[66]/numerical, X-SHAPE[67]		
unique reflns	2683	2649	2732
R_{int}	0.0888	0.1584	0.0886
structure solution, refinement			
structure solution	direct methods, SHELXS-97[64]		
structure refinement	full-matrix least squires on F^2 (SHELXL-97[64])		
no. reflns used	2683	2649	2732
no. variables	325	318	285
observed reflns ($F_o>4\sigma(F_o)$)	1763	2056	1919
$R(F)$ ($F_o>4\sigma(F_o)$)	0.0389	0.0496	0.0268
$R(F)$ (all data)	0.0653	0.0725	0.0490
weighting factor k_1/k_2 [b]	0.0519/0	0.0616 /0	0.0303/0
wR (F^2)(all data)	0.0961	0.1154	0.0576
GOF (F^2)	0.929	1.074	0.805
extinction coefficient	-	-	0.0000096(10)
$\Delta\rho_{min}/\rho_{max}/10^{-6}$epm^{-3}	-0.979/1.807	-1.779/1.844	-1.331/1.710

[a] Parameters determined by use of single crystal diffraction data. [b] Weighting scheme: $1/\omega=\sigma^2(F_O^2)+(k_1.P)^2+k_2.P$ with P = ⅓(max $(F_O^2,0)$ +.2F_c^2)

Table 7.2.1: Anisotropic thermal displacement parameters U_{ij} (pm^2) for $Au_{3.75}$ $Ru_{20.00}$ $Zn_{253.39}$ (C1)

Atom	*U*11	*U*22	*U*33	*U*23	*U*13	*U*12
Ru01	476(11)	*U*11	539(15)	0	*U*23	238(5)
Zn02	523(8)	506(11)	541(8)	-15(8)	-7(4)	253(6)
Zn03	504(11)	536(8)	546(8)	-2(4)	-5(8)	252(6)
Zn04	518(11)	494(8)	574(8)	-10(4)	-19(8)	259(6)
Zn05	524(6)	554(7)	554(6)	-7(5)	7(5)	270(6)
Zn06	533(8)	559(12)	524(8)	22(8)	11(4)	280(6)
Zn07	465(5)	*U*11	497(8)	5(4)	5(4)	247(6)
Ru08	478(5)	473(8)	535(6)	-11(5)	-6(3)	236(4)
Ru09	547(8)	575(6)	609(7)	4(3)	9(6)	273(4)
Zn10	564(8)	639(13)	552(9)	48(9)	24(4)	319(6)
Zn11	494(7)	510(7)	631(6)	9(5)	13(6)	236(6)
Zn12	551(7)	546(7)	551(6)	-5(5)	1(5)	256(6)
Zn13	580(12)	547(9)	648(10)	-17(4)	-34(9)	290(6)
Zn14	534(6)	*U*11	557(9)	-4(4)	4(4)	246(8)
Zn15	543(6)	*U*11	627(9)	-54(4)	*U*23	239(8)
Zn16	548(8)	580(12)	578(9)	-78(8)	-39(4)	290(6)
Zn17	507(11)	*U*11	605(16)	0	*U*23	253(6)
Zn18	505(11)	611(17)	560(12)	0	*U*23	305(9)
Zn19	527(6)	*U*11	544(9)	0(4)	*U*23	272(7)
Ru20	467(7)	*U*11	526(10)	0	*U*23	233(4)
Ru21	470(5)	*U*11	526(8)	0	*U*23	243(7)
Zn22	509(6)	*U*11	562(9)	-13(4)	13(4)	238(7)
Zn23	508(5)	*U*11	521(8)	-12(4)	12(4)	253(7)
Zn24	566(9)	590(12)	588(9)	-96(9)	-48(4)	295(6)
Zn28	577(9)	519(9)	571(8)	0	*U*23	315(8)
Zn26	506(6)	532(7)	547(6)	-9(5)	-17(5)	218(6)
Zn27	518(8)	491(11)	637(9)	4(8)	2(4)	246(6)
Au28/Zn28	489(6)	*U*11	520(7)	0	*U*23	244(3)
Au29/Zn29	502(6)	493(8)	511(6)	-3(5)	-1(3)	246(4)
Zn30/Ru30	443(10)	443(14)	459(10)	0	*U*23	222(7)
Zn31	502(6)	557(6)	497(6)	-17(5)	-29(5)	305(5)
Zn32	529(8)	516(11)	601(9)	28(8)	14(4)	258(6)
Zn33	624(12)	511(8)	575(9)	-7(4)	-14(9)	312(6)
Zn34	519(12)	558(8)	715(10)	-6(5)	-12(9)	260(6)
Zn35	540(12)	526(8)	688(10)	-29(4)	-58(9)	270(6)
Zn36/Ru36	493(11)	*U*11	545(15)	0	*U*23	247(6)
Zn37/Au37	538(11)	538(11)	550(15)	0	0	269(6)
Zn38/Ru38	502(5)	*U*11	530(8)	2(4)	-2(4)	246(7)
Au39/Zn39	516(10)	*U*11	544(13)	0	0	258(5)
Ru40	480(7)	*U*11	518(10)	0	0	240(4)
Zn41	430(3)	*U*11	577(19)	-25(9)	25(9)	231(18)
Zn42	620(3)	*U*11	640(5)	-20(2)	20(2)	270(4)
Zn42´	430(4)	420(4)	440(4)	50(3)	-20(3)	210(3)
Zn43	484(19)	890(2)	535(16)	210(6)	420(13)	242(10)
Zn44	480(5)	440(3)	520(19)	-20(12)	-40(2)	240(3)
Zn45	450(2)	*U*11	630(4)	-19(14)	*U*23	240(2)
Zn45´	520(2)	670(3)	570(2)	-240(17)	-4(16)	334(18)
Zn46	420(4)	470(3)	530(3)	-280(13)	-60(3)	210(19)
Zn46´	690(3)	510(2)	560(2)	33(16)	-12(19)	330(2)
Au47/Zn47	503(5)	*U*11	538(8)	4(3)	-4(3)	254(6)
Au48/Zn48	490(10)	418(7)	480(8)	-31(4)	-63(7)	245(5)
Au49/Zn49	494(6)	426(6)	468(5)	8(4)	4(5)	220(5)
Zn50/Au50	446(10)	*U*11	456(13)	0	*U*23	223(5)

Table 7.2.2: Anisotropic thermal displacement parameters U_{ij} (pm^2) $Au_{12.43}$ $Ru_{23.33}$ $Zn_{242.03}$ (C2)

Atom	*U*11	*U*22	*U*33	*U*23	*U*13	*U*12
Ru01	204(10)	*U*11	208(19)	0	*U*23	102(5)
Zn02	243(7)	233(10)	214(11)	-13(9)	-6(4)	117(5)
Zn03	192(10)	255(7)	244(11)	-4(4)	-8(8)	96(5)
Zn04	252(10)	227(7)	248(11)	-6(4)	-13(9)	126(5)
Zn05	240(6)	263(6)	242(8)	-14(5)	-6(6)	135(5)
Zn06	253(7)	256(11)	241(11)	-1(9)	-1(4)	128(5)
Zn07	222(5)	*U*11	199(11)	1(4)	-1(4)	134(6)
Ru08	217(5)	186(7)	219(8)	-2(6)	-1(3)	93(3)
Ru09	162(6)	194(5)	199(7)	0(3)	-1(5)	81(3)
Zn10	283(8)	317(12)	237(11)	26(9)	13(5)	158(6)
Zn11	214(6)	211(6)	303(8)	11(6)	-10(6)	89(5)
Zn12	273(6)	256(6)	234(8)	-8(6)	0.0001(6)	106(5)
Zn13	285(11)	241(7)	277(12)	-16(5)	-33(9)	143(5)
Zn14	263(5)	*U*11	239(11)	-11(4)	*U*23	131(7)
Zn15	252(5)	*U*11	263(12)	-21(5)	*U*23	109(7)
Zn16	266(7)	273(11)	248(12)	-44(9)	-22(4)	137(5)
Zn17	211(10)	*U*11	270(2)	0	*U*23	106(5)
Zn18	217(10)	308(16)	273(17)	0	*U*23	154(8)
Zn19	264(5)	*U*11	224(11)	16(4)	-16(4)	137(7)
Ru20	202(7)	*U*11	169(12)	0	*U*23	101(3)
Ru21	203(5)	*U*11	197(10)	0	*U*23	116(6)
Zn22	262(5)	*U*11	256(12)	-11(5)	11(5)	105(7)
Zn23	253(5)	*U*11	237(11)	0(4)	0(4)	125(7)
Zn24	272(8)	286(11)	260(12)	-65(9)	-32(5)	143(6)
Zn25	286(9)	225(9)	268(12)	0	*U*23	156(7)
Zn26	215(6)	252(6)	240(8)	-17(6)	-24(6)	83(5)
Zn27	245(8)	204(10)	354(13)	-7(9)	-4(5)	102(5)
Au28/Zn28	209(5)	*U*11	196(8)	0	*U*23	104(2)
Au29/Zn29	211(5)	216(7)	211(7)	-7(5)	-3(3)	108(3)
Zn30/Ru30	230(10)	229(14)	197(14)	0	*U*23	114(7)
Zn31	208(5)	256(6)	160(7)	-35(5)	-47(5)	159(5)
Zn32	258(7)	265(11)	264(12)	31(9)	15(4)	132(5)
Zn33	371(12)	254(7)	253(12)	1(5)	1(10)	186(6)
Zn34	255(11)	305(8)	385(14)	-13(5)	-25(10)	128(6)
Zn35	205(10)	197(7)	346(12)	-32(4)	-65(9)	103(5)
Zn36/Ru36	219(10)	*U*11	240(2)	0	*U*23	110(5)
Zn37/Au37	246(10)	*U*11	208(19)	0	*U*23	123(5)
Zn38/Ru38	213(5)	*U*11	214(11)	3(4)	-3(4)	108(6)
Au39/Zn39	206(7)	*U*11	196(11)	0	*U*23	103(3)
Ru40	226(7)	*U*11	193(13)	0	0	113(4)
Zn41	380(4)	*U*11	210(3)	-21(14)	21(14)	90(3)
Zn41´	250(3)	170(2)	190(3)	-140(18)	-120(2)	74(19)
-						
Zn42´	300(2)	370(2)	270(2)	37(16)	60(16)	198(19)
Zn43	235(18)	600(2)	2402)	240(7)	48(14)	118(9)
Zn44	552(16)	*U*11	210(2)	0	*U*23	276(8)
Zn45	130(2)	*U*11	280(5)	26(16)	-026(16)	70(2)
Zn45´	370(2)	120(4)	390(4)	150(3)	90(2)	540(2)
Zn46	190(4)	420(4)	780(7)	-56(18)	-110(4)	95(18)
Au47/Zn47	213(3)	*U*11	236(7)	-5(2)	*U*23	109(4)
Au48/Zn48	311(7)	248(5)	255(8)	-28(3)	-56(5)	155(4)
Au49/Zn49	280(4)	*U*11	211(5)	5(3)	4(4)	96(3)
Zn50/Ru50	224(11)	*U*11	231(18)	0	*U*23	112(5)

Table 7.2.3: Anisotropic thermal displacement parameters U_{ij} (pm^2) for $Au_{41.52}$ $Ru_{25.74}$ $Zn_{213.74}$ (C4)

Atom	*U*11	*U*22	*U*33	*U*23	*U*13	*U*12
Ru01	306(15)	*U*11	310(2)	0	*U*23	153(8)
Zn02	325(11)	309(15)	292(11)	-9(10)	-4(5)	155(7)
Zn03	310(14)	331(10)	311(11)	-8(5)	-16(10)	155(7)
Zn04	340(15)	309(10)	329(11)	-5(5)	-10(10)	170(7)
Zn05	333(10)	*U*11	319(8)	-4(7)	8(7)	176(8)
Zn06	326(11)	340(15)	305(11)	13(10)	6(5)	170(7)
Zn07	283(10)	*U*11	299(11)	6(5)	-6(5)	142(11)
Ru08	297(7)	303(10)	288(8)	-3(7)	-1(3)	152(5)
Ru09	292(10)	320(7)	290(8)	-4(3)	-8(7)	146(5)
Zn10	352(11)	407(16)	328(12)	51(11)	25(5)	204(8)
Zn11	330(11)	311(11)	384(9)	17(7)	-23(8)	144(9)
Zn12	317(11)	347(10)	325(8)	-8(7)	-12(7)	149(9)
Zn13	350(15)	343(11)	307(11)	-6(5)	-11(10)	175(8)
Zn14	325(10)	*U*11	313(12)	-1(5)	1(5)	146(12)
Zn15	287(10)	*U*11	355(12)	-51(5)	51(5)	111(12)
Zn16	348(11)	357(16)	344(12)	-52(11)	-26(5)	178(8)
Zn17	307(15)	*U*11	360(2)	0	*U*23	154(8)
Zn18	314(15)	320(2)	327(16)	0	*U*23	159(10)
Zn19	341(11)	*U*11	275(11)	8(5)	-8(5)	173(12)
Ru20	287(10)	*U*11	301(14)	0	*U*23	144(5)
Ru21	287(14)	300(10)	284(11)	0	*U*23	144(7)
Zn22	326(10)	*U*11	338(12)	-8(5)	8(5)	174(12)
Zn23	347(11)	*U*11	345(12)	-9(5)	9(5)	175(13)
Zn24	344(11)	356(15)	304(11)	-38(11)	-19(5)	178(8)
Zn25	415(16)	384(16)	309(11)	0	*U*23	266(13)
Zn26	337(10)	327(10)	322(8)	-8(7)	-9(7)	158(9)
Zn27	326(11)	328(15)	337(12)	-7(10)	-3(5)	164(8)
Au28/Zn28	349(9)	*U*11	317(10)	0	*U*23	174(4)
Au29/Zn29	309(10)	318(12)	307(10)	-10(7)	-5(4)	159(6)
Zn30/Ru30	311(14)	360(2)	297(16)	0	*U*23	179(11)
Zn31	323(10)	330(10)	323(8)	-7(7)	0(7)	167(9)
Zn32	311(10)	306(14)	334(12)	17(10)	9(5)	153(7)
Zn33	349(15)	328(10)	318(11)	11(5)	22(11)	174(8)
Zn34	343(15)	314(10)	343(12)	-6(5)	-12(10)	171(8)
Zn35	325(14)	312(10)	313(12)	-7(5)	-14(10)	163(7)
Zn36/Ru36	374(12)	*U*11	389(16)	0	*U*23	187(6)
Zn37/Au37	356(9)	*U*11	416(11)	0	*U*23	178(4)
Zn38/Ru38	341(11)	*U*11	358(12)	-7(4)	7(4)	158(11)
Au39/Zn39	353(5)	*U*11	334(7)	0	*U*23	177(3)
Ru40	315(11)	*U*11	312(14)	0	*U*23	157(5)
Zn41	362(16)	*U*11	270(19)	0	*U*23	181(8)
Zn42	387(11)	*U*11	383(13)	1(6)	-1(6)	199(13)
Zn43	335(15)	349(11)	361(12)	-7(5)	-14(11)	168(8)
Zn44	371(16)	*U*11	310(2)	0	*U*23	186(8)
Au45	353(5)	*U*11	342(5)	-4(2)	4(2)	193(5)
Au46	363(7)	365(5)	368(6)	-9(2)	-18(4)	181(3)
Au47/Zn47	348(4)	*U*11	339(4)	-8(2)	8(2)	174(4)
Au48/Zn48	343(5)	355(4)	368(4)	-2(2)	-3(4)	171(3)
Au49/Zn49	358(4)	344(4)	339(3)	2(3)	-7(3)	170(3)
Zn50/Ru49	310(15)	*U*11	248(19)	0	*U*23	155(7)

Table 7.3: A summary of loaded and obtained composition from single crystal X-ray diffraction and EDS analysis for selected crystalline specimens

Loaded composition	Crystal designation	Refined composition	EDS composition
$Au_{7.0}Ru_{16.2}Zn_{254.0}$	C1	$Au_{3.8}$ $Ru_{20\cdot0}$ $Zn_{253.4}$	$Au_{5.7(3)}Ru_{22.7(5)}Zn_{249.0(7)}$
$Au_{19.8}Ru_{19.8}Zn_{238.0}$	C2	$Au_{12.4}$ $Ru_{23.3}$ $Zn_{242.0}$	$Au_{16.3(9)}Ru_{24.9(2)}Zn_{236.5(8)}$
$Au_{28.0}Ru_{28.0}Zn_{223.9}$	C3	$Au_{36.2}$ $Ru_{25\cdot5}Zn_{218.2}$	$Au_{36.5(4)}Ru_{25.4(5)}Zn_{218.0(9)}$
$Au_{42.0}Ru_{36.5}Zn_{202.2}$	C4	$Au_{41.5}$ $Ru_{25.7}$ $Zn_{213.7}$	$Au_{43.5(6)}Ru_{27.8(6)}Zn_{209.6(8)}$

7.5 Structural characteristics

The ternary phase in the Au-Ru-Zn system forms a structurally complex phase belonging to the group of large hexagonal structures. The phase crystallizes in the space group $P6_3/mmc$ with approximately 554-562 atoms in the hexagonal unit cell depending on the chemical composition. The number of atoms in the unit cell increases parallel to the increase of gold-content.

The structures of these complex hexagonal phases are complicated. In order to understand the structure, several approaches have been proposed to organize the atoms into simple, recognizable patterns. Complex structures of this type have been analysed by decomposing them into interpenetrating clusters, [147] also called nested polyhedral units [131,132] which are grouped around the high symmetry points of the unit cell. According to the concept, the five constitutive clusters are located at the high symmetry points of the unit cell. The clusters are designated by the capital letters-A, B, C, D and E. The atomic arrangement of structures in the Au-Ru-Zn system can be subdivided into two partial structures. One part of the structure is completely ordered built up by clusters A and B and compositionally invariant throughout the homogeneity range of the phase. The second partial structure comprising the clusters C, D and E is partly disordered and variable in composition.

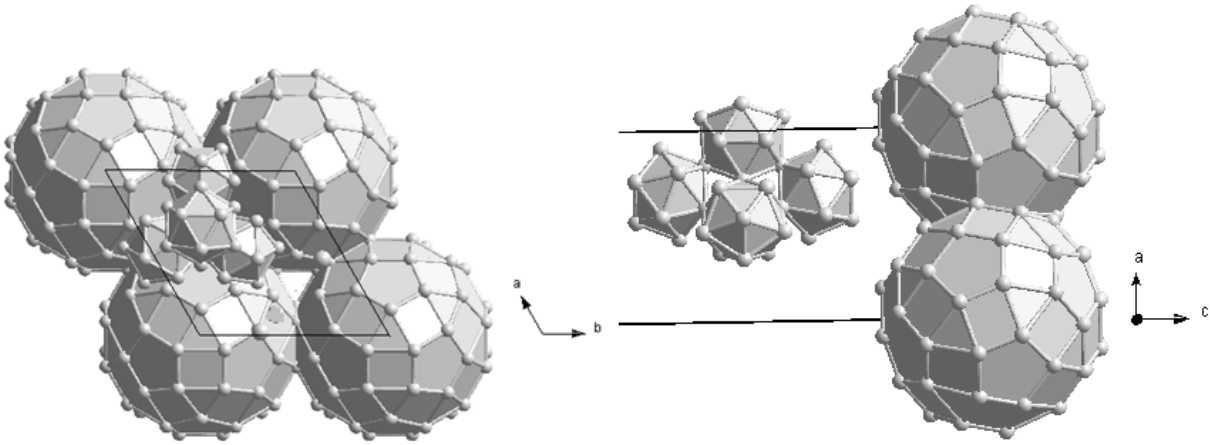

Figure 7.2: Representation of the ordered clusters (A at z = 0 and B at z = 1/4) of the structure $Au_{3.8}$ $Ru_{20.0}$ $Zn_{253.4}$ of the unit cell.

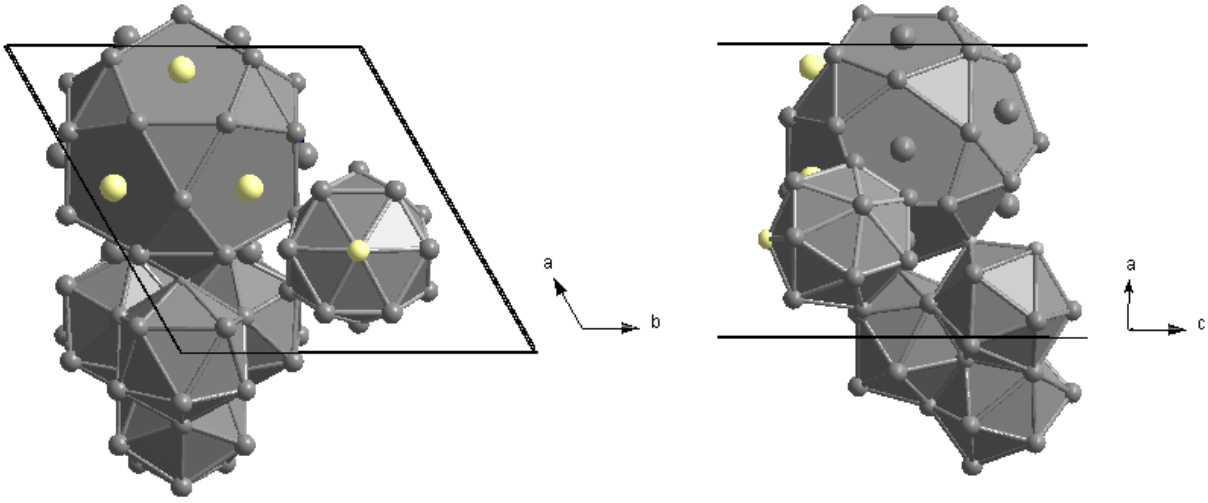

Figure 7.3: Representation of the disordered clusters C, D and E of the structure $Au_{3.8}$ $Ru_{20.0}$ $Zn_{253.4}$ of the unit cell.

The compositionally invariant partial structure: Cluster A of the compositionally invariant partial structure consists of 127 atoms (Table 7.4.1). The central Ru atom of this cluster is located at (0 0 0). The central Ru atom is enclosed by 12 Zn units, resulting in clean Zn_{12} icosahedra (FK CN 12). The vertex configuration is 3^5, i.e. each

vertex is linked with 5 triangular faces. The second shell is an Archimedean icosidodecahedron with twenty triangular faces and twelve pentagonal faces built up by 30 Zn atoms. Vertex configuration is 3.5.3.5. 12 ruthenium atoms above the 12 pentagonal faces of the icosidodecahedron form a clean Ru_{12} icosahedron. Furthermore, $Ru_{12}Zn_{30}$ unit results in a Frank-Kasper polyhedra with 42 vertices and 80 triangular faces. The composition of these three inner Mackay polyhedra is $Ru_{13}Zn_{42}$. Further, well ordered clean Zn_{60} Archimedean rhombicosidodecahedron consists of 20 triangular faces, 30 square faces, 12 pentagonal faces with the vertex configuration 3.4.5.4. Twelve further zinc atoms conform to a second, enlarged icosahedra with its vertices located above the 12 pentagonal faces of the rhombicosidodecahedron. Cluster A at (0 0 0) is unaffected from replacement of Ru and Zn by Au, always $Ru_{13}Zn_{114}$ cluster (Fig. 7.4 (A)).

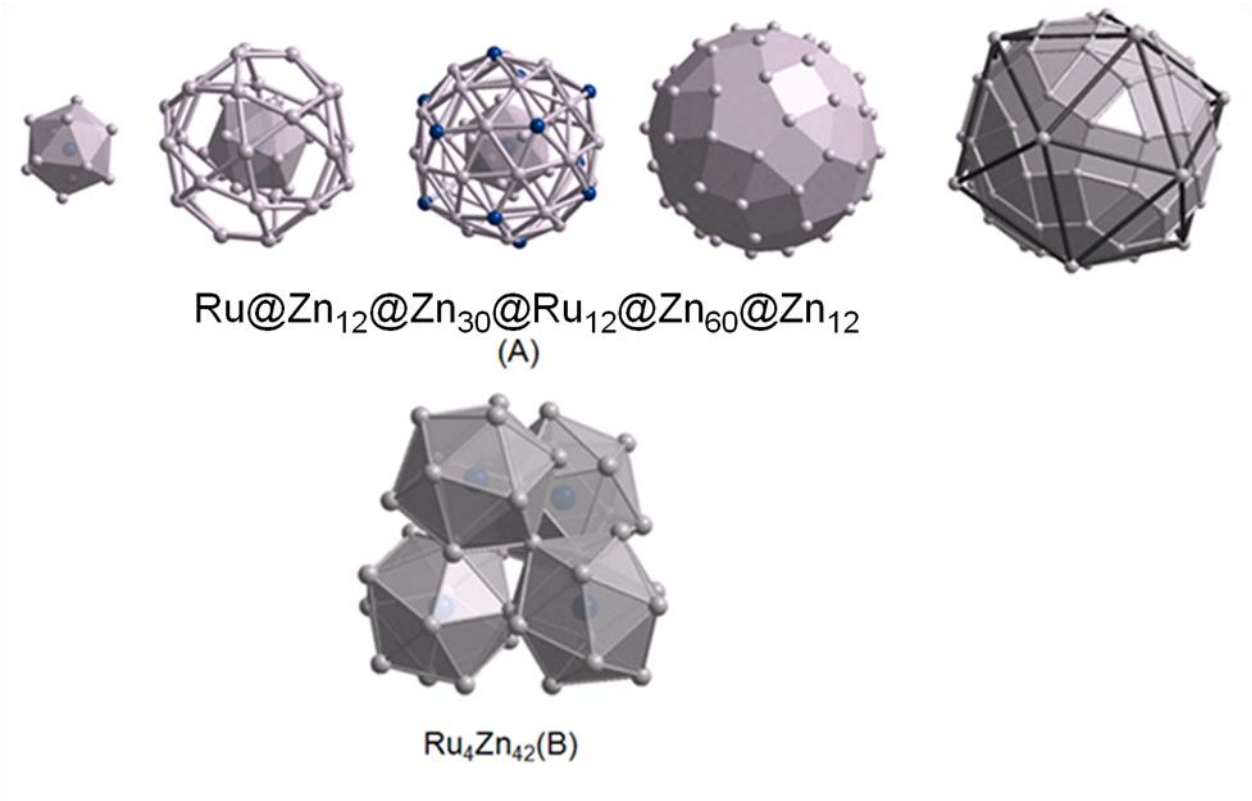

Figure 7.4: Representation of the cluster A about (0 0 0) and cluster B extended $TiNi_2$–type-unaffected by gold increment in the ternary Au-Ru-Zn hexagonal phase.

Table 7.4.1: Structural data for cluster A of $Au_{3.75}$ $Ru_{20.00}$ $Zn_{253.39}$ (C1), $Au_{12.43}$ $Ru_{23.33}$ $Zn_{242.03}$ (C2), $Au_{36.2}$ $Ru_{25.5}$ $Zn_{218.2}$ (C3), $Au_{41.52}$ $Ru_{25.74}$ $Zn_{213.74}$ (C4)

Ru01	2a	0.0000	0.0000	0.0000	1	497(8)
		0.0000	0.0000	0.0000	1	205(8)
		0.0000	0.0000	0.0000	1	350(11)
		0.0000	0.0000	0.0000	1	307(10)
Zn02	12k	0.07109(8)	0.14217(17)	0.03452(3)	1	525(5)
		0.07060(9)	0.14121(18)	0.03456(4)	1	231(5)
		0.07030(14)	0.1406(3)	0.03439(5)	1	354(7)
		0.07035(12)	0.1407(2)	0.03423(4)	1	310(6)
Zn03	12k	0.22692(17)	0.11346(9)	0.00831(3)	1	532(5)
		0.22570(18)	0.11285(9)	0.00834(4)	1	237(5)
		0.2262(3)	0.11311(13)	0.00805(5)	1	362(7)
		0.2266(2)	0.11330(11)	0.00805(4)	1	320(6)
Zn04	12k	0.15028(17)	0.07514(8)	0.07239(3)	1	526(5)
		0.14942(19)	0.07471(9)	0.07287(4)	1	239(5)
		0.1504(3)	0.07522(14)	0.07259(5)	1	367(7)
		0.1518(2)	0.07592(12)	0.07203(4)	1	323(6)
Zn05	24l	0.31596(11)	0.27457(11)	0.045354(19)	1	544(3)
		0.31606(12)	0.27291(12)	0.04534(3)	1	244(3)
		0.31559(19)	0.2711(2)	0.04497(4)	1	373(5)
		0.31610(16)	0.27171(17)	0.04465(3)	1	324(4)
Zn06	12k	0.19609(9)	0.39219(18)	0.02806(3)	1	536(5)
		0.19607(9)	0.39213(19)	0.02790(4)	1	250(5)
		0.19689(14)	0.3938(3)	0.02778(5)	1	364(7)
		0.19689(12)	0.3938(2)	0.02745(4)	1	322(6)
Zn07	12k	0.36548(13)	0.36548(13)	0.0000	1	9(4)
		0.36456(15)	0.36456(15)	0.0000	1	205(4)
		0.3640(2)	0.3640(2)	0.0000	1	362(7)
		0.36570(19)	0.36570(19)	0.0000	1	288(5)
Ru08	12k	0.13626(6)	0.27252(12)	0.069276(19)	1	496(3)
		0.13634(6)	0.27268(12)	0.06878(3)	1	211(3)
		0.13603(9)	0.27206(19)	0.06807(3)	1	342(5)
		0.13588(8)	0.27175(16)	0.06770(3)	1	295(4)
Ru09	12k	0.44219(13)	0.22109(6)	0.01679(2)	1	580(3)
		0.44065(12)	0.22032(6)	0.01649(3)	1	189(3)
		0.44104(18)	0.22052(9)	0.01627(4)	1	327(5)
		0.44060(16)	0.22030(8)	0.01629(3)	1	304(4)
Zn10	12k	0.08315(9)	0.16630(18)	0.10922(3)	1	577(5)
		0.08529(10)	0.17058(19)	0.10937(4)	1	275(5)
		0.08518(14)	0.1704(3)	0.10866(5)	1	392(7)
		0.08296(13)	0.1659(3)	0.10815(4)	1	356(6)
Zn11	24l	0.33962(11)	0.47086(12)	0.06579(2)	1	551(3)
		0.33974(12)	0.47038(12)	0.06560(3)	1	251(4)
		0.3399(2)	0.47001(19)	0.06532(4)	1	382(5)
		0.33960(17)	0.47043(17)	0.06474(3)	1	349(4)
Zn12	24l	0.32037(11)	0.28093(11)	0.092928(19)	1	558(3)
		0.31973(12)	0.28180(13)	0.09280(3)	1	266(4)
		0.3160(2)	0.2838(2)	0.09235(4)	1	408(5)
		0.31275(16)	0.28786(17)	0.09192(3)	1	337(4)
Zn13	12k	0.49800(18)	0.24900(9)	0.06294(3)	1	588(5)
		0.49983(19)	0.24992(10)	0.06216(4)	1	263(5)
		0.5005(3)	0.25025(14)	0.06113(5)	1	366(7)
		0.5015(2)	0.25073(12)	0.06097(4)	1	332(6)
Zn14	12k	0.54517(9)	0.45483(9)	0.03165(3)	1	551(5)
		0.54831(9)	0.45169(9)	0.03175(4)	1	255(5)
		0.55042(13)	0.44958(13)	0.03218(5)	1	368(7)

		0.55016(12)	0.44984(12)	0.03235(4)	1	328(6)
Zn15	12k	0.40969(9)	0.59031(9)	0.01318(3)	1	585(5)
		0.40824(10)	0.59176(10)	0.01268(4)	1	263(5)
		0.40807(14)	0.59193(14)	0.01228(5)	1	362(7)
		0.40882(12)	0.59118(12)	0.01254(4)	1	324(6)
Zn16	12k	0.20348(9)	0.40697(18)	0.10541(3)	1	565(5)
		0.20415(9)	0.40830(19)	0.10502(4)	1	262(5)
		0.20476(14)	0.4095(3)	0.10461(5)	1	381(7)
		0.20447(12)	0.4089(2)	0.10460(4)	1	349(6)
Zn17	4f	0.6667	0.3333	0.02631(5)	1	540(8)
		0.6667	0.3333	0.02574(7)	1	232(8)
		0.6667	0.3333	0.02527(9)	1	369(12)
		0.6667	0.3333	0.02538(7)	1	325(10)

Table 7.4.2: Structural data for cluster B of $Au_{3.75}$ $Ru_{20.00}$ $Zn_{253.39}$ (C1), $Au_{12.43}$ $Ru_{23.33}$ $Zn_{242.03}$ (C2), $Au_{36.2}$ $Ru_{25.5}$ $Zn_{218.2}$ (C3), $Au_{41.52}$ $Ru_{25.74}$ $Zn_{213.74}$ (C4)

Zn18	6h	0.25984(13)	0.5197(3)	0.2500	1	547(7)
		0.26010(14)	0.5202(3)	0.2500	1	256(7)
		0.2613(2)	0.5226(4)	0.2500	1	374(10)
		0.26231(17)	0.5246(3)	0.2500	1	319(8)
Zn19	12k	0.40746(8)	0.59254(8)	0.21151(3)	1	529(4)
		0.40762(9)	0.59238(9)	0.21139(4)	1	249(5)
		0.40768(14)	0.59232(14)	0.21150(5)	1	369(7)
		0.40767(12)	0.59233(12)	0.21150(4)	1	318(6)
Ru20	4f	0.3333	0.6667	0.17679(3)	1	486(5)
		0.3333	0.6667	0.17686(4)	1	191(5)
		0.3333	0.6667	0.17729(6)	1	340(8)
		0.3333	0.6667	0.17774(5)	1	292(7)
Ru21	6h	0.46778(8)	0.53222(8)	0.2500	1	485(4)
		0.46753(8)	0.53247(8)	0.2500	1	194(4)
		0.46668(13)	0.53332(13)	0.2500	1	338(7)
		0.46587(2)	0.53417(11)	0.2500	1	292(5)
Zn22	12k	0.45199(9)	0.54801(9)	0.16744(3)	1	534(4)
		0.45121(10)	0.54879(10)	0.16691(4)	1	272(5)
		0.44771(14)	0.55229(14)	0.16659(5)	1	392(7)
		0.44544(12)	0.55456(12)	0.16674(4)	1	325(6)
Zn23	12k	0.53235(8)	0.46765(8)	0.20913(3)	1	513(4)
		0.53241(9)	0.46759(9)	0.20950(4)	1	248(5)
		0.53188(14)	0.46812(14)	0.21124(6)	1	425(8)
		0.53132(12)	0.46868(12)	0.21270(4)	1	345(6)
Zn24	12k	0.26300(9)	0.52600(18)	0.14108(3)	1	579(5)
		0.26349(10)	0.52698(19)	0.14105(4)	1	271(5)
		0.26296(14)	0.5259(3)	0.14123(5)	1	393(7)
		0.26217(12)	0.5243(2)	0.14150(4)	1	333(6)
Zn25	12j	0.46202(16)	0.32696(16)	0.2500	1	537(4)
		0.46124(17)	0.32657(17)	0.2500	1	247(5)
		0.4586(3)	0.3252(3)	0.2500	1	388(7)
		0.4544(2)	0.3222(2)	0.2500	1	340(6)
Zn26	24l	0.30133(11)	0.35830(11)	0.226317(19)	1	547(3)
		0.30117(12)	0.35913(12)	0.22631(3)	1	251(3)
		0.2991(2)	0.35948(19)	0.22650(4)	1	383(5)
		0.29551(17)	0.35807(16)	0.22661(3)	1	332(4)
Zn27	12k	0.21791(9)	0.43583(17)	0.18466(3)	1	552(5)
		0.21831(9)	0.43661(18)	0.18483(4)	1	272(5)
		0.21847(14)	0.4369(3)	0.18547(6)	1	390(7)
		0.21681(12)	0.4336(2)	0.18612(4)	1	330(6)

The B cluster is an extended $NiTi_2$-type Ru_4Zn_{42} cluster as previously found for $CrZn_{17-\delta}$ (Fig. 4.9 (d)) depicted as a quadruple of icoshedra (Fig. 7.4 (B)). Each of the four icosahedra is condensed to a triangular face of an octahedron (Table 7.4.2). The cluster L-tetrahedra [157] is formulated as Ru_4Zn_{42}. Cluster B (1/3 2/3 z) remains unaffected by the substitution of Au for Ru and Zn atoms, always extended $NiTi_2$-type Ru_4Zn_{42} cluster.

The compositionally variable partial structure: The variable structure is formed by the clusters C, D and E. The variation of composition is accompanied by various disorder phenomena which are typical for complex metallic alloy systems:

(i) random vacancies

(ii) mutual substitution of the two components on specific sites

(iii) positional disorder in form of split positions

The cluster C is depicted as a γ-cluster in Fig. 7.5 (i). The γ-cluster is built up by four atomic shells: an inner tetrahedron (IT) formed by 3 Zn33 and 1 Zn36/Ru36, an outer tetrahedron (OT) consisted of 3 Au29/Zn29 and 1 Au28/Zn28, an octahedron (OH) (made of 3 Zn32 and 3 Zn34) and a distorted cuboctahedron (CO) formed by 3 Zn30/Ru30, 6 Zn31 and 3 Zn35. The γ-cluster can be alternatively described as a discrete quadruple of distorted icosahedra about IT atoms enclosing a common IT, then also called Pierce cluster. [90] An expanded Pierce cluster consisting of 34 atoms forms a quadruple of icosahedra about the OT (Au/Zn) atoms. Each of the four icosahedra shares with atoms of an enclosed IT one of its faces (Tab. 7.4.3).

The shell (in Fig. 7.5 (ii)) represents a Friauf polyhedron (Table 7.4.4) which is described by the formula 3^{28}. The cluster consists of a central Zn37/Au37 atom (CC), a truncated tetrahedron (TT)-shell of formed by 3 Zn16, 6 Zn11 and 3 Zn24 atoms with 4 additional OT atoms (3 Zn38/Ru38 and Au39/Zn39) above the hexagonal faces of TT shell. Cluster D contributes to the variation in the overall composition of mutual substitution of Au/Zn at CC site and mutual substitution of Au/Zn and Zn/Ru at OT site as well.

Table 7.4.3: Structural data for cluster C of $Au_{3.75}$ $Ru_{20.00}$ $Zn_{253.39}$ (C1), $Au_{12.43}$ $Ru_{23.33}$ $Zn_{242.03}$ (C2), $Au_{36.2}$ $Ru_{25.5}$ $Zn_{218.2}$ (C3), $Au_{41.52}$ $Ru_{25.74}$ $Zn_{213.74}$ (C4)

Au28/Zn28	4e	0.0000	0.0000	0.14005(2)	0.671(5)/0.330(5)	499(4)
		0.0000	0.0000	0.13959(3)	0.775(7)/0.225(7)	205(4)
		0.0000	0.0000	0.13900(3)	0/1	369(4)
		0.0000	0.0000	0.13858(3)	0.778(11)/0.222(11)	338(7)
Au29/Zn29	12k	0.11362(6)	0.22724(11)	0.203843(18)	0.240(3)/0.760(3)	503(4)
		0.11384(5)	0.22768(11)	0.20384(2)	0.313(4)/0.687(11)	212(4)
		0.11371(7)	0.22742(15)	0.20358(3)	0.441(9)/0.559(9)	387(7)
		0.11021(8)	0.22043(16)	0.20436(3)	0.221(7)/0.779(7)	310(7)
Zn30/Ru30	6h	0.09344(11)	0.1869(2)	0.2500	1/0	449(6)
		0.09421(11)	0.1884(2)	0.2500	0.68(3)/0.32(3)	219(7)
		0.09300(17)	0.1860(3)	0.2500	0/1	484(8)
		0.08738(17)	0.1748(3)	0.2500	1/0	317(8)
Zn31	24l	0.32739(10)	0.30030(11)	0.182528(17)	1	501(3)
		0.32691(11)	0.30048(12)	0.18248(2)	1	189(3)
		0.32337(19)	0.2977(2)	0.18269(4)	1	375(5)
		0.31972(16)	0.29438(17)	0.18294(3)	1	324(4)
Zn32	12k	0.11619(9)	0.23239(18)	0.15620(3)	1	550(5)
		0.11651(10)	0.23301(19)	0.15651(4)	1	261(5)
		0.11717(11)	0.2343(2)	0.15621(4)	1	318(6)
Zn26	24l	0.30133(11)	0.35830(11)	0.226317(19)	1	547(3)
		0.30117(12)	0.35913(12)	0.22631(3)	1	251(3)
		0.2991(2)	0.35948(19)	0.22650(4)	1	383(5)
		0.29551(17)	0.35807(16)	0.22661(3)	1	332(4)
Zn33	12k	0.14251(19)	0.07126(9)	0.17964(3)	1	557(5)
		0.1424(2)	0.07118(10)	0.17981(4)	1	280(5)
		0.1415(3)	0.07077(14)	0.17937(5)	1	376(7)
		0.1398(2)	0.06989(12)	0.17841(4)	1	329(6)
Zn10		0.08315(9)	0.16630(18)	0.10922(3)	1	577(5)
		0.08529(10)	0.17058(19)	0.10937(4)	1	275(5)
		0.08518(14)	0.1704(3)	0.10866(5)	1	392(7)
		0.08296(13)	0.1659(3)	0.10815(4)	1	356(6)
Zn34	12k	0.23375(18)	0.11687(9)	0.22459(3)	1	602(5)
		0.2335(2)	0.11677(10)	0.22398(4)	1	320(5)
		0.2349(3)	0.11744(14)	0.22300(5)	1	394(7)
		0.2378(2)	0.11892(12)	0.22166(4)	1	330(6)
Zn27	12k	0.21791(9)	0.43583(17)	0.18466(3)	1	552(5)
		0.21831(9)	0.43661(18)	0.18483(4)	1	272(5)
		0.21847(14)	0.4369(3)	0.18547(6)	1	390(7)
		0.21681(12)	0.4336(2)	0.18612(4)	1	330(6)
Zn35	12k	0.24052(18)	0.12026(9)	0.13403(3)	1	583(5)
		0.24146(18)	0.12073(9)	0.13376(4)	1	249(5)
		0.2387(3)	0.11936(13)	0.13341(5)	1	342(7)
		0.2346(2)	0.11730(11)	0.13327(4)	1	315(6)
Zn36/Ru36	4e	0.0000	0.0000	0.21935(5)	1/0	511(8)
		0.0000	0.0000	0.21951(7)	1/0	228(8)
		0.0000	0.0000	0.21918(9)	1/0	273(12)
		0.0000	0.0000	0.21764(5)	0/1	379(8)

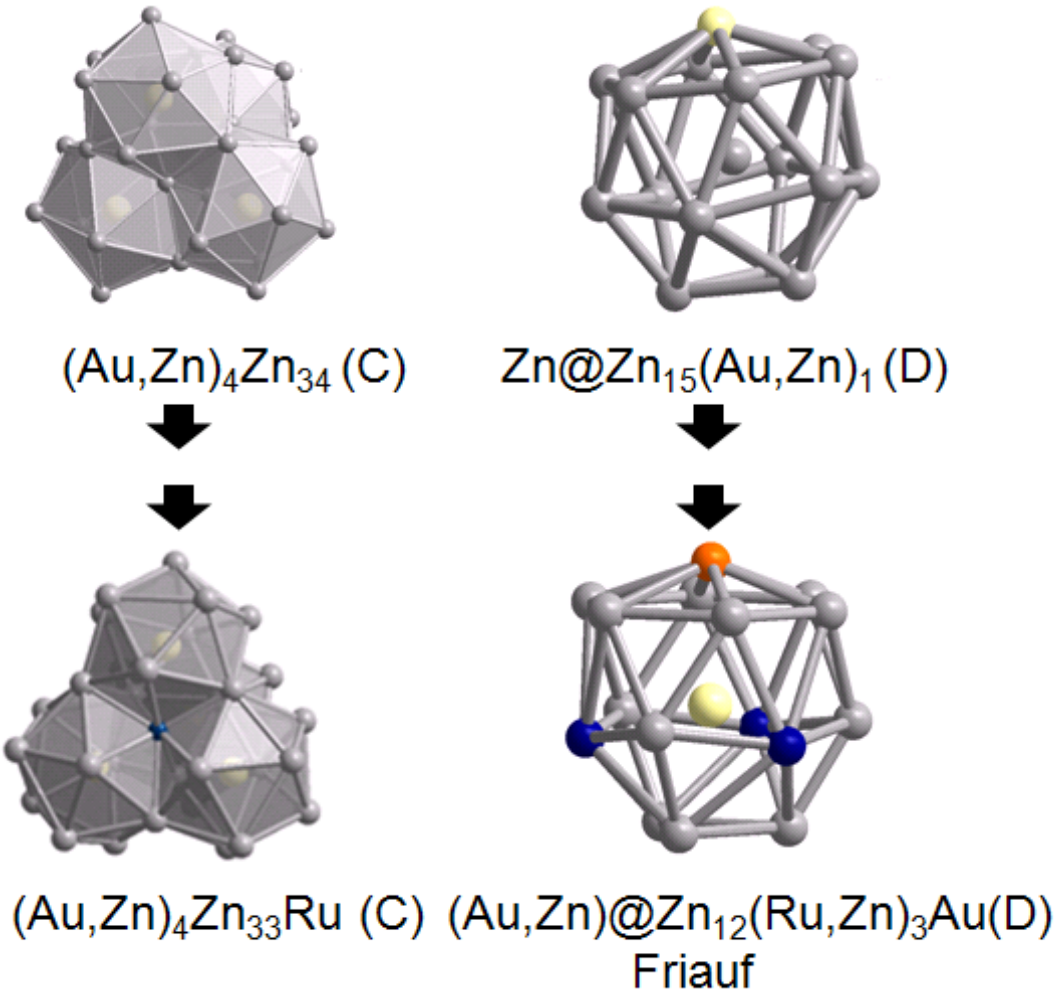

Figure 7.5: (i) Transmutation of cluster C form γ-brass type $(Au,Zn)_4Zn_{34}$ in the crystal structure of $Au_{3.8}Ru_{20.0}Zn_{253.4}$ to γ-type $(Au,Zn)_4Zn_{33}Ru$ in the crystal structure of $Au_{41.5}Ru_{25.7}Zn_{213.7}$ by the replacement of Zn by Au and Ru.
(ii) Transmutation of cluster D from Friauf $(Au,Zn)_1Zn_{15}$ in the crystal structure of $Au_{3.8}Ru_{20.0}$ $Zn_{253.4}$ to Friauf Zn_{12} $(Ru,Zn)_3$ Au in $Au_{41.5}Ru_{25.7}Zn_{213.7}$ by the replacement of Zn by Au and Ru.
Constituting zinc atoms are shown in grey, Ru/Zn in dark blue and Au/Zn by light yellow and gold in orange.

Table 7.4.4: Structural data for cluster D of $Au_{3.75}$ $Ru_{20.00}$ $Zn_{253.39}$ (C1), $Au_{12.43}$ $Ru_{23.33}$ $Zn_{242.03}$ (C2), $Au_{36.2}$ $Ru_{25.5}$ $Zn_{218.2}$ (C3), $Au_{41.52}$ $Ru_{25.74}$ $Zn_{213.74}$ (C4)

Zn37/Au37	4f	0.3333	0.6667	0.09576(5)	1/0	542(8)
		0.3333	0.6667	0.09634(6)	1/0	233(8)
		0.3333	0.6667	0.09878(4)	0.346(15)/0.654(15)	413(10)
		0.3333	0.6667	0.09912(3)	0.178(12)/0.822(12)	376(7)
Zn38/Ru38	12k	0.45020(8)	0.54980(8)	0.11108(3)	1/0	513(4)
		0.44990(8)	0.55010(8)	0.11090(3)	0.765(18)/0.235(18)	213(5)
		0.44808(12)	0.55192(12)	0.11032(5)	0.58(4)/0.42(4)	416(12)
		0.44603(10)	0.55397(10)	0.11010(3)	0.38(3)/0.62(3)	352(9)
Au39/Zn39	4f	0.3333	0.6667	0.04880(4)	0.154(5)/0.846(5)	525(8)
		0.3333	0.6667	0.04933(3)	0.408(7)/0.592(7)	203(6)
	Au	0.3333	0.6667	0.04933(3)	1	383(4)
		0.3333	0.6667	0.04936(2)	1	347(4)
Zn24	12k	0.26300(9)	0.52600(18)	0.14108(3)	1	579(5)
		0.26349(10)	0.52698(19)	0.14105(4)	1	271(5)
		0.26217(12)	0.5243(2)	0.14150(4)	1	333(6)
Zn11	24l	0.33962(11)	0.47086(12)	0.06579(2)	1	551(3)
		0.33974(12)	0.47038(12)	0.06560(3)	1	251(4)
		0.3399(2)	0.47001(19)	0.06532(4)	1	382(5)
		0.33960(17)	0.47043(17)	0.06474(3)	1	349(4)
Zn16	12k	0.20348(9)	0.40697(18)	0.10541(3)	1	565(5)
		0.20415(9)	0.40830(19)	0.10502(4)	1	262(5)
		0.20476(14)	0.4095(3)	0.10461(5)	1	381(7)
		0.20447(12)	0.4089(2)	0.10460(4)	1	349(6)

Table 7.4.5: Structural data for cluster E of $Au_{3.75}$ $Ru_{20.00}$ $Zn_{253.39}$ (C1), $Au_{12.43}$ $Ru_{23.33}$ $Zn_{242.03}$ (C2), $Au_{36.2}$ $Ru_{25.5}$ $Zn_{218.2}$ (C3), $Au_{41.52}$ $Ru_{25.74}$ $Zn_{213.74}$ (C4)

Ru40	4f	0.6667	0.3333	0.14034(3)	1	493(5)
		0.6667	0.3333	0.14027(4)	1	215(5)
		0.6667	0.3333	0.13947(6)	1	0.0364(8)
		0.6667	0.3333	0.13969(5)	1	314(7)
Zn41	12k	0.64906(18)	0.35094(18)	0.18463(7)	0.33	470(2)
		0.6521(3)	0.3479(3)	0.18445(10)	0.339(7)	360(4)
		0.6667	0.3333	0.18345(10)	1	593(17)
	4f	0.6667	0.3333	0.18383(7)	1	331(10)
Zn42	12k	0.5620(5)	0.4380(5)	0.12228(16)	0.273(6)	640(3)
-						
		0.5600(2)	0.4400(2)	0.12404(8)	0.748(16)	550(2)
		0.55906(13)	0.44094(13)	0.12485(4)	1	383(6)
Zn42´	24l	0.5295(6)	0.4033(7)	0.12091(12)	0.198(4)	440(3)
Zn42´		0.5369(3)	0.4114(3)	0.12220(8)	0.343(5)	305(13)
-	-					
Zn43	12k	0.4473(3)	0.22367(14)	0.15798(5)	0.646(5)	683(11)
		0.4453(3)	0.22265(15)	0.15792(6)	0.694(8)	398(12)
		0.4431(3)	0.22153(16)	0.15665(6)	0.926(15)	0.0454(15)
		0.4443(2)	0.22214(12)	0.15559(4)	1	350(6)
Zn44	12k	0.6411(5)	0.3206(3)	0.09457(6)	0.319(4)	480(2)
	4f	0.6667	0.3333	0.09406(8)	1	436(11)
		0.6667	0.3333	0.09324(9)	1	437(13)
		0.6667	0.3333	0.09367(7)	1	350(10)
Zn45	12k	0.5533(3)	0.4467(3)	0.15532(11)	0.296(5)	498(18)
		0.5538(3)	0.4462(3)	0.15552(15)	0.264(7)	180(2)

Au45	Au	0.55750(10)	0.44250(10)	0.17031(10)	0.564(11)	439(12)
Au45		0.55636(5)	0.44364(5)	0.170291(15)	0.934(4)	342(4)
Zn45´	24l	0.5267(3)	0.3797(4)	0.16542(6)	0.330(4)	573(13)
Zn45´		0.5286(4)	0.3855(6)	0.16571(11)	0.358(7)	589(19)
Zn45´	12k	0.5553(7)	0.4447(7)	0.1551(7)	0.23(3)	45(10)
-						
Zn46	12k	0.4499(6)	0.2250(3)	0.12422(10)	0.293(5)	480(18)
		0.4533(6)	0.2266(3)	0.12194(17)	0.360(9)	490(3)
Au46		0.446(2)	0.2231(11)	0.1085(3)	0.15(3)	200(6)
Au46		0.44820(10)	0.22410(5)	0.109488(16)	0.899(4)	366(4)
Zn46´	24l	0.6998(4)	0.5171(4)	0.11479(6)	0.319(4)	573(13)
Zn46´		0.6983(4)	0.5172(4)	0.11518(9)	0.287(5)	217(15)
Zn46´		0.739(4)	0.5339(18)	0.1128(4)	0.42(7)	105(8)
-	-					
Au47/Zn47	12k	0.53844(7)	0.46156(7)	0.07784(2)	0.108(3)/0.892(3)	513(4)
		0.53893(5)	0.46107(5)	0.07837(2)	0.370(4)/0.630(4)	220(3)
		0.53923(5)	0.46077(5)	0.078943(19)	1/0	0.0391(3)
		0.53800(4)	0.46200(4)	0.078793(14)	1/0	345(2)
Au48/Zn48	12k	0.45202(16)	0.22601(8)	0.20687(3)	0/1	455(4)
		0.45454(12)	0.22727(6)	0.20677(2)	0.334(4)/0.666(4)	264(4)
		0.45723(10)	0.22862(5)	0.206893(19)	1/0	419(3)
		0.45958(9)	0.22979(4)	0.206874(14)	1/0	357(2)
Au49/Zn49	24l	0.33239(10)	0.35631(10)	0.137774(17)	0/1	467(3)
		0.02395(7)	0.35551(7)	0.137502(17)	0.330(3)/0.669(3)	249(3)
		0.33118(7)	0.35573(7)	0.137112(13)	1/0	413(2)
		0.02421(6)	0.35630(6)	0.137270(10)	1/0	349(1)
Zn35	12k	0.24052(18)	0.12026(9)	0.13403(3)	1	583(5)
		0.24146(18)	0.12073(9)	0.13376(4)	1	249(5)
		0.2387(3)	0.11936(13)	0.13341(5)	1	342(7)
		0.2346(2)	0.11730(11)	0.13327(4)	1	315(6)
Zn31	24l	0.32739(10)	0.30030(11)	0.182528(17)	1	501(3)
		0.32691(11)	0.30048(12)	0.18248(2)	1	189(3)
		0.32337(19)	0.2977(2)	0.18269(4)	1	375(5)
		0.31972(16)	0.29438(17)	0.18294(3)	1	324(4)
Zn13	12k	0.49800(18)	0.24900(9)	0.06294(3)	1	588(5)
		0.49983(19)	0.24992(10)	0.06216(4)	1	263(5)
		0.5005(3)	0.25025(14)	0.06113(5)	1	366(7)
		0.5015(2)	0.25073(12)	0.06097(4)	1	332(6)
Zn23	12k	0.53235(8)	0.46765(8)	0.20913(3)	1	513(4)
		0.53241(9)	0.46759(9)	0.20950(4)	1	248(5)
		0.53188(14)	0.46812(14)	0.21124(6)	1	425(8)
		0.53132(12)	0.46868(12)	0.21270(4)	1	345(6)
Zn12	24l	0.32037(11)	0.28093(11)	0.092928(19)	1	558(3)
		0.31973(12)	0.28180(13)	0.09280(3)	1	266(4)
		0.3160(2)	0.2838(2)	0.09235(4)	1	408(5)
		0.31275(16)	0.28786(17)	0.09192(3)	1	337(4)
Zn22	12k	0.45199(9)	0.54801(9)	0.16744(3)	1	534(4)
		0.45121(10)	0.54879(10)	0.16691(4)	1	272(5)
		0.44771(14)	0.55229(14)	0.16659(5)	1	392(7)
		0.44544(12)	0.55456(12)	0.16674(4)	1	325(6)
Zn50/Ru50	4f	0.6667	0.3333	0.22806(4)	1/0	450(7)
		0.6667	0.3333	0.22808(5)	0.52(3)/0.48(3)	226(9)
		0.6667	0.3333	0.22849(8)	1/0	325(11)
		0.6667	0.3333	0.22887(6)	1/0	289(9)
Zn38/Ru38	12k	0.45020(8)	0.54980(8)	0.11108(3)	1/0	513(4)
		0.44990(8)	0.55010(8)	0.11090(3)	0.765(18)/0.235(18)	213(5)
		0.44808(12)	0.55192(12)	0.11032(5)	0.58(4)/0.42(4)	416(12)
		0.44603(10)	0.55397(10)	0.11010(3)	0.38(3)/0.62(3)	352(9)

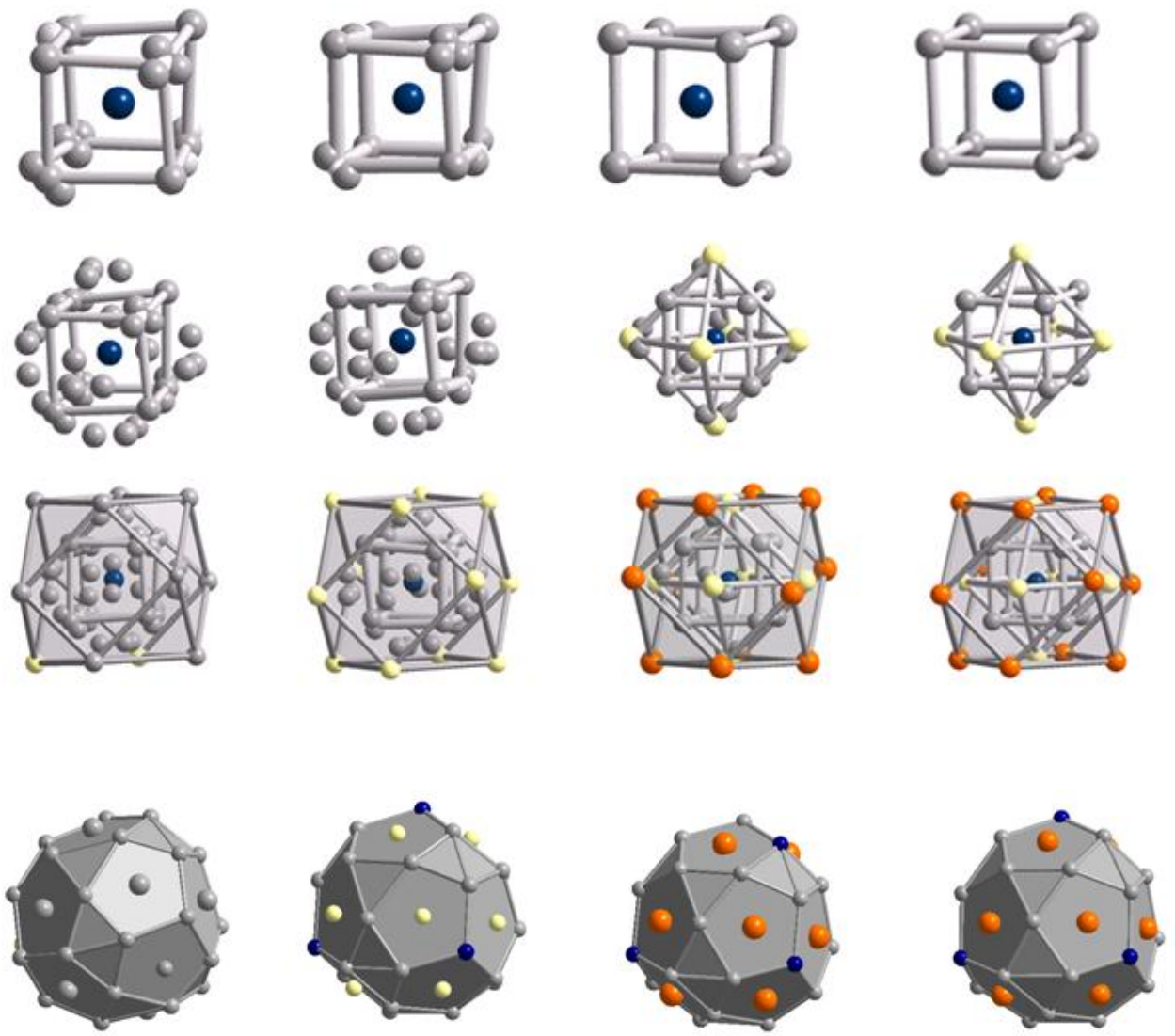

$Ru@Zn_{14}@Zn_{12}@Zn_{28}$ $Ru@Au_6Zn_8@Au_{12}@Zn_{25}(Zn,Ru)_3$

(a) (b) (c) (d)

Figure 7.6: Representation of the cluster E-bcc-type about Ru40 and effect of substitution by Au in the ternary Au-Ru-Zn hexagonal phase. (a), (b), (c) and (d) represent shells of cluster E in the samples of C1, C2, C3 and C4, respectively.

Cluster E is depicted as β-brass-type (Fig. 7.6 & Tab. 7.4.5). Three Zn41atoms and one Zn42 atom form an outer tetrahedron (OT). Furthermore, three Zn43 atoms and one Zn44 atom form another outer tetrahedron (OT). These two outer tetrahedra (OT) together form a distorted cube. Moreover, Zn41 site is three-fold split in the crystals of C1 and C2 as well as Zn44 site in the specimen of C2. Independent refinement of site occupancy factors of Zn41 site for various crystal shows: 3x f(Zn41) ≈ 1 and 3x f(Zn44) ≈ 1. With increasing gold content in the samples, the three-fold split sites (Zn41, Zn44) transmute to an ordered atomic sites accumulating full zinc occupancy. Positional disorder on OH site in cluster E arises from physically meaningless short distances between Zn45 and two-fold split Zn45'. Moreover, Zn46 and two-fold split Zn46' have short distance too. (Zn45, Zn45') and (Zn46, Zn46') form a heavily disordered octahedron (OH) in the specimens of C1 and C2. With the gradual incorporation of gold in the sample, Zn45 and Zn46 sites are occupied by gold accompanying with the disappearance of Zn45' and Zn46' sites.

Twelve atoms (6 x M47, 3 x M48 and 3 x M49) form the next cuboctahedral shell. Variable mutual substitution of the two distinct chemical constituents occur on-M47, M48 and M49. A clear increasing trend of gold occupancy is observed for the mixing of Zn/Au in cuboctahedral forming atomic sites in cluster E and finally those sites end up with full gold occupation. At the zinc-rich boundary, 28 zinc atoms form the outer shell representing a tetrated dodecahedron (polyhedral formula-$3^{16}5^{12}$) with equal number of faces and vertices.

7.6 Summary

Systematic studies of the ternary Au-Ru-Zn system in the range $0.014 \leq x_{Au} \leq 0.148$ and $0.914 \leq x_{Zn} \leq 0.76$, reveals that ternary phases are isotopic with $FeZn_{10}$. According to single crystal diffraction results, these new ternary phases crystallize in the hexagonal space group $P6_3/mmc$, exhibit a significant phase width and contain approximately 554-562 atoms in the hexagonal unit cell which are distributed over 50-53 crystallographically independent positions according to the chemical composition. The

atomic arrangement of structures in the Au-Ru-Zn system can be subdivided into two partial structures. One part of the structure is completely ordered. It is built up by $Ru_{13}Zn_{114}$ cluster and extended $NiTi_2$-type Ru_4Zn_{42} cluster and is compositionally invariant throughout the homogeneity range of the phase. No substitution of Au takes place in this partial structure. The second partial structure comprising extended γ-brass-type M_5Zn_{33}, M_5Zn_{12} (Friauf) and extended β-brass-type $M_{22}Zn_{33}$ clusters is partly disordered, shows variable composition and hosts disorders such as substitutional (Au and Zn or Ru and Zn) and positional disorder (Zn42/Zn42', Zn45/Zn45' and Zn46/Zn46') in form of split positions. Among the five different clusters, extended β-brass-type cluster endures significant effect by Au/Zn or Ru/Zn substitution. Heavily disordered β-brass-type cluster transmutes to partly disordered bcc-type due to the substitution of Ru and/or Zn by Au.

Chapter 8

Summary

A systematic reinvestigation of the zinc-rich region of the binary chromium-zinc system uncovers and identifies a structurally complex intermetallic γ-brass-type phase in brass-like systems, $CrZn_{17-\delta}$ ($-0.8 \leq \delta \leq 1.7$). The information of this zinc-rich phase was first mentioned by Henry Le Chatelier in 1895. Afterthat, the Cr-Zn binary system has been studied by many researchers. The crystal structure of $CrZn_{17}$ was first proposed by Hanemann [49] to be based on hexagonal lattice which eventually turned out to be correspondence to a rhombohedral setting of a cubic lattice as revealed by $a_o = a_c(2\sqrt{2})$, $b_o = a_c/\sqrt{3}$, $c_o = a_c/2$. The crystal structure has been analysed for three distinct compositions including the phases at Cr-rich ($\delta = 1.7$) and Zn-rich ($\delta = -0.8$) boundaries by single crystal X-ray diffraction. The structure of $CrZn_{17-\delta}$ represents a 2 x 2 x 2 superstructure of a γ-brass-related structure with approximately 400 atoms in the cubic unit cell. Partitioning of the structure into various clusters grouped around the 16 high symmetry points reveals that the structure can be subdivided into two partial structures, arranged like two non-intersecting zinc blende type nets shifted relatively to each other by half a lattice parameter a/2. One partial structure comprising clean α-Mn-type Zn_{29} and $NiTi_2$-type Cr_4Zn_{18} clusters is ordered and compositionally invariant over the homogeneity range. Its complement is significantly richer in Zn, $Cr_{1.3}Zn_{47.8}$-$Cr_{2.2}Zn_{47.5}$, and disordered. Three types of disorder can be identified: random vacancies, substitution and positional disorder.

Correlations can be identified between disorder parameters of affected sites indicating a spatial coherence between the various disorder phenomena.

The valence electron concentration of $CrZn_{17-\delta}$ per atom is-at least at the Cr-rich boundary, very close to 21/13 as expected for the *vec*-controlled structure formation of γ-phases. The structure is isopointal to that of congeneric $MoZn_{20.4}$.Though the two structures are very similar in many respects, the enormous structural complexity as expressed by the large

unit cell and numerous symmetrically inequivalent crystallographic sites, provides room for noticeable element specific structural differentiation.

A systematic investigation of chemical substitution in the Cr-Zn system has distinctly modified by replacing chromium and zinc by gold and has uncovered $(2a_\gamma)^3$ superstructure of γ-brass related phase ranging from $Au_{2.6}Cr_{6.4}Zn_{91.7}$ to $Au_{10.0}Cr_{4.0}Zn_{89.0}$. According to the single crystal diffraction experiments, the ternary phase crystallizes in the acentric space group $F\bar{4}3m$ with approximately 403-412 atoms in the cubic unit cell having a significant phase width. The structure of the cubic phase consists of six distinctive clusters each having 22-29 atoms arranged at the high symmetry points of the unit cell. As previously found for $CrZn_{17-\delta}$, the atomic arrangement can be subdivided into two partial structures of similar size and different composition. One partial structure consisting of clean α-Mn-type Zn_{29} and $NiTi_2$-type Cr_4Zn_{18} clusters are ordered and remain unaffected during the replacement of Cr and/or Zn by Au over the homogeneity range. Its complement shows variable composition and hosts three types of disorders such as vacancies, substitution and positional disorder in the form of split position. This variable partial structure endures significant effect by Au/Cr or Au/Zn substitution on constituting clusters: mixture of γ-brass type and defect bcc transmutes to clean γ-brass type Au_4Zn_{22} and bcc type cluster transform to clean γ-brass type Au_6Zn_{20} over an intermediate mixture of bcc and γ-brass type clusters.

An extensive study of compositionally different crystals of solid solution $(Au,Cr)Zn_n$, n=10.2–6.4 reveals a systematic spatial correlation among the site occupancy factors of vacancy sites, mixed occupied and positional disordered sites. Instead of mutual substitution of chemical constituents on specific atomic sites we can propose a mechanism for a mutual substitution of distinctive constituting clusters. So, the homogeneity range of the structure arises from an incoherent intergrowth of distinctive partial structures in variable proportions on a length scale corresponding to small integers of the unit cell. The linear dependence of various kinds of disorders controls valence electron concentration in terms of Hume-Rothery stabilization. Valence electron concentration per atom ranges from 1.60 to 1.68-very close to 21/13 as expected value for Hume-Rothery rule at gold poor structures.

The structure of $CrZn_{17-\delta}$ can also be distinctly modified by replacing Zn by Pd in this work and has uncovered a superstructure of γ-brass-related phase. The results of this study show that the phase ranges from $Pd_{1.40}Cr_{5.0}Zn_{94.7}$ to $Pd_{3.28}Cr_{4.48}Zn_{95.36.}$ Disorder phenomena in the solid solution of $(Pd,Cr)Zn_n$, (n=14.8-12.3) are spatially correlated and confined to one of the two hierarchical substructures of zinc blende-type. The valence electron concentration per atom ranges from 1.67 to 1.68 throughout the entire homogeneity range.

The influence of gold or palladium on the structure of γ-brass-related phase $CrZn_{17-\delta}$ varies as the chemistry of 4d (e.g. Pd) and 5d (e.g. Au) block elements frequently differs significantly due to differences in bonding capabilities of the corresponding nd states. The structures of ternary derivatives of $CrZn_{17-\delta}$ share many features in spite of the compositional distinctions and the complexity of the structures. Common features are: (i) The clusters are essentially same in both of the structures. The composition of the ordered partial structure is Cr_4Zn_{47} for each compound. Ordered partial structures are unaffected by Pd or Au. (ii) Though different in composition the cluster types of the disordered structures are the same as well. Structural differences concern: (i) This variable partial structure of the Au-Cr-Zn system endures significant effects by Au/Cr and/or Au/Zn substitution on constituting clusters: mixture of disordered γ-brass type and defect bcc type clusters transmute to clean γ-brass type Au_4Zn_{22} and disordered bcc type clusters transform to clean γ-brass type Au_6Zn_{20} over an intermediate mixture of bcc and γ-brass type clusters. On the other hand, cluster grouped about (0 0 0) transmutes from a mixture of a defect bcc-and disorder γ-brass-type clusters to a disorder γ-brass type $(Pd,Zn)_4Zn_{22}$ cluster by the replacement of Zn by Pd and cluster Q grouped around (¼ ¼ ¼) transforms from a β-brass type cluster to the mixture of β- and γ-brass-type clusters by Pd/Zn replacement.(ii) Superstructure of γ-brass related phases in the Au-Cr-Zn system occur between 1.60-1.68 e^-/a. Valence electron concentration per atom in the Pd-Cr-Zn system ranges from 1.67 to 1.68 throughout the entire homogeneity range. We conclude that in spite of a close structural resemblance the enormous complexity of these large cell structures provides room for element specific structural differentiations.

We attempted to study the influence of valence electron concentration (vec) on γ-brass type phases replacing Zn and/or Pd by Au (transition-element) in the parent $Pd_{2+x}Zn_{11-x}$ phase. $Au_{2.89}Pd_{3.44}Zn_{19.68}$ represents the upper limit of Au substitution in the γ'-phase $Pd_{2+x}Zn_{11-x}$. Further substitution of Au leads to 2 × 2 × 2 superstructures of γ-brass (γ') with lattice parameters ranging from 1816.2(1) to 1816.6(2) pm (Pearson code *cF*402-*cF*405).

The structure of γ-brass represents the characteristics 3 x 3 x 3 superstructure of an ordinary β-brass phase. According to the single crystal diffraction results, this ternary γ-brass-type phase crystallizes in the cubic space group $I\bar{4}3m$ with a significant phase width. The structure can be described by using 26 atom γ-brass-type cluster placed at high symmetry points (0 0 0) and (½ ½ ½) in unit cell. Furthermore, γ-brass-type ternary phase in the Au-Pd-Zn system occurs at e/a ratio of 1.62-1.65 e^- / atom which is very close to 21/13 as expected for the *vec*-controlled structure formation of γ-phases.

According to new ternary γ´-brass phases in the Au-Pd-Zn system crystallize in the cubic acentric space group $F\bar{4}3m$ with a significant phase width. The structure comprises four independent γ-brass clusters placed at high symmetry points in the unit cell. All the clusters here show variation in composition as a consequence of the substitution of gold in these clusters and host some structural disorder such as mixing of Au and Zn, Au and Pd or Pd and Zn, accommodating split positions and vacancies. Stability of this ternary γ´-brass phase in terms of Hume-Rothery mechanism occurs between 1.66 and 1.72 per atom. These *vec* values are slightly higher than those expected for γ-brass phases.

γ'-phase in the Au-Pd-Zn is congeneric to γ'-phases in the Pd-Zn-Al . The structures of two γ'-phases share few features in spite of the compositional distinctions and the complexity of the structures. Common features are: (i) Clusters are the same in both structures. A specific feature is the occurrence of a single cluster-type, the so-called γ-type. (ii) Though different in composition, the inner tetrahedron (IT) site of the defect γ-cluster is completely vacant at the Al- or Au-rich boundary of the phases. Structural differences are: (i) Two clusters are completely ordered whereas the other two contain

all structural disorder in the γ' Pd-Zn-Al phases. On the contrary, all four different clusters in the γ' Au-Pd-Zn phases show variation in composition and hosts structural disorders. (ii) *vec* in the γ' Pd-Zn-Al phases range between 1.71 and 1.75 / atom whereas it ranges for γ' Au-Pd-Zn phases between 1.66 and 1.72.

In ruthenium-zinc binary system we have structurally identified the congener of hexagonal $FeZn_{10}$, i.e.$RuZn_{10}$. No ternary or pseudobinary systems have been reported to date. To the best of our knowledge, the hexagonal phases in the Au-Ru-Zn system reported herein are the only ternary variants of this family of intermetallic structures. Systematic studies of the ternary Au-Ru-Zn system in the range $0.014 \leq x_{Au} \leq 0.148$ and $0.914 \leq x_{Zn} \leq 0.76$, reveals that ternary phases are isotopic with $FeZn_{10}$. According to the single crystal diffraction results, these new ternary phases crystallize in the hexagonal space group $P6_3/mmc$, exhibit a significant phase width, and contain approximately 554-562 atoms in the hexagonal unit cell which are distributed over 50-53 crystallographically independent positions according to the chemical composition.The structure comprises of five different interpenetrating clusters. Two clusters ($Ru_{13}Zn_{114}$, Ru_4Zn_{42}) are well ordered and remain unaffected by the replacement of Zn by Au and Ru throughout the homogeneity range. Furthermore, other three clusters (M_5Zn_{33}, M_5Zn_{12}, $M_{22}Zn_{33}$), however, show variation in composition and host disorders such as substitution (Au and Zn or Ru and Zn) and positional disorder in the form of split positions. This compositionally variable β-brass-type cluster endures significant effect by Au/Zn or Ru/Zn substitution. Heavily disordered β-brass-type cluster transmutes to partly disordered bcc-type in the course of the replacement Ru and/or Zn by Au.

Chapter 9

Zusammenfassung

Bei einer systematischen Untersuchung der zinkreichen Region des binären Systems Chrom-Zink wurde die strukturell komplexe intermetallische γ-messingartige Phase $CrZn_{17-\delta}$ ($-0.8 \leq \delta \leq 1.7$) identifiziert und charakterisiert. Die ersten Untersuchungen dieser Phase wurden von Henry Le Chatelier in 1985 durchgeführt. Im Anschluss wurde das binäre Cr-Zn-System durch viele weitere Personen studiert. Die Kristallstruktur von $CrZn_{17}$ wurde erstmalig von Hanemann [49] als hexagonale Zelle beschrieben, welche einer rhomboedrischen Aufstellung einer kubischen Zelle gemäß $a_o = a_c(2\sqrt{2})$, $b_o = a_c/\sqrt{3}$, $c_o = a_c/2$ entspricht. Die Phase wurde anhand dreier Einkristalle unterschiedlicher Zusammensetzung, inkl. der Cr- und der Zn-reichen Seite ($\delta = 1.7$ und $\delta = -0.8$) mittels Einkristalldiffraktometrie aufgeklärt. Die Struktur von $CrZn_{17-\delta}$ entspricht einer 2 x 2 x 2 Überstruktur einer γ-messingartigen Phase mit ~400 Atomen pro Elementarzelle. Die Atomlagen lassen sich über die Bildung von Clustern um die 16 höchstsymmetrischen Punkte der Zelle erfassen. Über diese Beschreibung zeigt sich, dass sich die Struktur in zwei Partialstrukturen zerlegen lässt, welche zwei sich nicht überschneidende Netzwerke einer Zinkblendestruktur darstellen mit einer Verschiebung um a/2.

Der erste Strukturteil bildet α-Mn-artige Zn_{29} und $NiTi_2$-artige Cr_4Zn_{18} Cluster aus und ist über die gesamte Phasenbreite vollständig ausgeordnet und ändert seine Zusammensetzung nicht. Die zweite Teilstruktur ist deutlich zinkreicher, $Cr_{1.3}Zn_{47.8}$-$Cr_{2.2}Zn_{47.5}$, und ist fehlgeordnet. Hierbei treten drei Arten der Fehlordnung auf: Positionsfehlordnung, Mischbesetzung und Teilbesetzung der Atomlagen. Es können Korrelationen hergestellt werden zwischen den Fehlordnungsparametern der verschiedenen betroffenen Atome, was eine räumliche Koheränz zwischen den verschiedenen Phänomenen nahelegt.

Die Zahl der Valenzelektronen pro Atom ist, zumindest an der Cr-reichen Seite sehr nahe an 21/13, wie es für eine vec-kontrollierte Phase wie der γ-Messingphase erwartet wird. Die Phase ist ispounktal zu der Phase $MrZn_{20.4}$. Obwohl die beiden Phasen in vielen Bereichen gleich erscheinen bietet die hohe Komplexität, ausgedrückt beispielsweise in der großen Elementarzelle oder der großen Zahl symmetrisch unabhängiger Atomlagen viel Raum für eine im detail unterschiedliche Ausdifferenzierung, welche durch den elementspezifischen Charakter zustande kommt.

Eine systematische Untersuchung der Substitution von Cr und Zn durch Gold ergab eine $(2a_\gamma)^3$-Überstruktur einer ternären γ-messing-artigen Phase der Zusammensetzung zwischen $Au_{2.6}Cr_{6.4}Zn_{91.7}$ und $Au_{10.0}Cr_{4.0}Zn_{89.0}$. Durch Einkristalluntersuchungen wurde die azentrische Raumgruppe $F\bar{4}3m$ ermittelt mit 403-412 Atomen pro Zelle und einer merklichen Phasenbreite. Die Struktur lässt sich über sechs Cluster mit je 22-29 Atomen beschreiben, welche sich um die höchstsymmetrischen Punkte der Elementarzelle aufbauen. Auch hier lässt sich die Struktur in zwei Teilstrukturen gleicher Größe und unterschiedlicher Komposition aufteilen. Eine Teilstruktur bleibt wiederum über die gesamte Phasenbreite ausgeordnet und lässt keine Substition von Zink oder Chrom durch Gold zu. Sie bildet α-Mn-Typ Zn_{29} und $NiTi_2$-Typ Cr_4Zn_{18}-Cluster aus. Die zweite Teilstruktur varriert mit der Zusammensetzung und zeigt drei Typen der Fehlordnung wie Teilbesetzungen, Mischbesetzungen und Positionsfehlordnung in Form von Splitlagen. Dieser Strukturteil toleriert größere Änderungen in der Substitution von Au/Cr bzw. Au/Zn durch Bildung verschiedener Cluster: eine Mischung von einem γ-messing-artigen Cluster und einem defekten bcc-Typ-Cluster geht in einen reinen γ-Messing-Cluster Au_4Zn_{22} über und ein bcc-Typ-Cluster geht in einen γ-messing-artigen Cluster Au_6Zn_{20} über die Zwischenstufe einer Mischung von bcc und γ-Messing über.

Eine umfangreiche Untersuchung der verschiedenen Kristalle der festen Lösung $(Au,Cr)Zn_n$, n=10.2–6.4 offenbart eine systematische räumliche Korrelation zwischen den Besetzungsfaktoren der teilbesetzten Lagen, Mischbesetzungen und Splitlagen. Legierung. Anstelle einer Substitution von Atomsorten auf einer einzelnen Atomlage

wird ein Mechanismus zum Austausch von charakteristisch gebildeten Clustern vorgeschlagen. Damit stellt sich der Homogenitätsbereich der Struktur als inkohärente Verwachsung von Teilstrukturen mit variablen Anteilen dar.

Die lineare Abhängigkeit verschiedener Arten von Fehlordnungen wird durch die Valenzelektronenkonzentration gemäß der Hume-Rothery-Stabilisierung erzeugt. Die Valenzelektronenkonzentration pro Atom variiert zwischen 1.60 und 1.68, sehr nah an 21/13, wie es nach dem Hume-Rothery-Konzept für goldarme Strukturen vorhergesagt wird.

Die Struktur von $CrZn_{17-\delta}$ kann ebenfalls über den Einbau von Pd anstelle von Zn modifiziert werden und bildet ebenfalls eine Überstruktur einer γ-artigen Phase. Die Phasenbreite wurde in der Zusammensetzung zwischen $Pd_{1.40}Cr_{5.0}Zn_{94.7}$ bis $Pd_{3.28}Cr_{4.48}Zn_{95.36}$ bestimmt. Die Fehlordnungsphänomene in der festen Lösung von $(Pd,Cr)Zn_n$ (n=14.8-12.3) sind räumlich korreliert innerhalb einer der zwei Teilstrukturen, welche im Zinkblendetyp beschrieben werden können. Die Valenzelektronenkonzentration pro Atom liegt zwischen 1.67 und 1.68 in der gesamten Phasenbreite.

Der Einfluss von Gold oder Palladium auf die γ-messing-artige Phase $CrZn_{17-\delta}$ unterscheidet sich voneinander, was der Tatsache geschuldet ist, dass die Chemie der 4d (Pd) und 5d (Au)-Elemente sich häufig signifikant aufgrund ihrer Fähigkeit der Bindungsbildung der zugehöigen d-Zustände unterscheidet. Die Struktur der ternären Phasen von $CrZn_{17-\delta}$ teilen trotz der Komplexität der Strukturen viele Gemeinsamkeiten. Dies sind: (i) die beteiligsten Cluster sind in beiden Phasen identisch. Die ausgeordnete Teilstruktur ist jeweils Cr_4Zn_{47}. Diese Teilstruktur bleibt unabhängig von der Zugabe von Pd oder Au erhalten. (ii) Obwohl die Zusammensetzung der ungeordneten Cluster unterschiedlich ist sind sie topologisch identisch. Unterschiede in den Strukturen betreffen: (i) die variable Teilstruktur des Systems Au-Cr-Zn toleriert erhebliche Anteile an Au im Austausch für Cr bzw. Zn bei den sich bildenden Clustern: eine Mischung von einem γ-messing-artigen Cluster und einem defekten bcc-Typ-Cluster geht in einen reinen γ-Messing-Cluster Au_4Zn_{22} über und ein bcc-Typ-Cluster geht in einen γ-

messing-artigen Cluster Au_6Zn_{20} über die Zwischenstufe einer Mischung von bcc und γ-Messing über. Andererseits ändert sich der Cluster um (0 0 0) von einer Mischung aus einem defekten bcc-Cluster und einem fehlgeordneten γ-Messing-Typ-Cluster hin zu einem fehlgeordneten γ-Messing-Typ-Cluster $(Pd,Zn)_4Zn_{22}$ durch den Austausch von Zn mit Pd. Der Cluster um (¼ ¼ ¼) wandelt sich von einem β-Messing-Typ-Cluster zu einer Mischung aus einem β- und einem γ-Messing-Typ-Clusterdurch Austausch von Zn und Pd um. (ii) Die Überstrukturen der γ-messingartigen Phasen im System Au-Cr-Zn treten bei einer vec von 1.60-1.68 auf, wärend sie im System Pd-Cr-Zn bei einer vec von 1.67-1.68 erscheinen. Neben der strukturell großen Ähnlichkeit bietet die hohe Komplexität der Phasen offenbar genug Raum für den Einfluss elementsprzifischer Ausdifferenzierungen.

Wir haben den Einfluss der vec auf γ-messingartige Phasen durch die Substitution von Zn bzw. Pd durch Au in der übergeordneten Phase $Pd_{2+x}Zn_{11-x}$ untersucht. Zunächst erhielten wir das Produkt $Au_{2.89}Pd_{3.44}Zn_{19.68}$, welches den maximalen Substitutionsgrad der γ-Phase darstellt. Weitere Substitution durch Gold führt zu einer 2 x 2 x 2 Überstruktur von γ-Messing (γ') mit Gitterparametern von 1816.2(1) bis 1816.6(2) pm (Pearsonsymbol *cF*402-*cF*405).

Die Struktur des γ-Messings stellt eine 3 x 3 x 3 Überstruktur der β-Messingstruktur dar. Gemäß er Einkristallstudien kristallisiert die ternäre γ-messingartige Phase in der kubischen Raumgruppe $I\bar{4}3m$ mit einer merklichen Phasenbreite. Die Struktur kann über einen 26 Atome umfassenden γ-Messing-Cluster beschrieben werden, welcher um die Punkte (0 0 0) und (½ ½ ½) herum aufgebaut wird. Die ternäre γ-messingartige Phase im System Au-Pd-Zn tritt bei einer vec von 1.62-1.65 auf, was sehr nahe an 21/13 liegt, welches der erwartete Wert für vec-kontrollierte Phasen im γ-Typ ist.

Die neuen ternären γ'-messingartigen Phasen im System Au-Pd-Zn kristallisieren in der kubischen azentrischen Raumgruppe $F\bar{4}3m$ mit einer merklichen Phasenbreite. Die Struktur lässt sich über vier γ-messingartige Cluster beschreiben, welche um die höchstsymmetrischen Punkten in der Raumgruppe aufgebaut werden. Alle Cluster

zeigen Unterschiede in ihrer Zusammensetzung als Folge der Substitution von Gold und beinhalten strukturelle Fehlordnungen wie eine Mischbesetzung von Au und Zn, Au und Pd oder Pd und Zn, zusätzlich Splitpositionen und Leerstellen. Die Stabilität dieser γ'-messingartigen Phasen im Sinne des Hume-Rothery-Systems tritt bei einer vec von 1.66-1.72 auf. Dieser Wert ist etwas höher als für γ-messingartige Phasen erwartet.

Die γ'-Phase im System Au-Pd-Zn ist artverwand zur γ'-Phase im System Pd-Zn-Al. Die Strukturen der beiden γ'-Phasen teilen einige Gemeinsamkeiten: (i) Die gebildeten Cluster sind in beiden Phasen identisch, es werden ausschließlich γ-Typ-Cluster gebildet. (ii) Obwohl die Zusammensetzung unterschiedlich ist wird das innere Tetraeder (IT) des defekten γ-Clusters an der Al- bzw. Au-reichen Seite der Phasenbreite unbesetzt. Strukturelle Unterschiede sind: (i) zwei Cluster bleiben komplett ausgeordnet, während die anderen beiden strukturelle Fehlordnungen in der γ'-Phase im System Pd-Zn-Al aufweisen. Auf der anderen Seite zeigen alle vier Cluster der der γ'-Phase im System Au-Pd-Zn strukturelle Fehlordnungen auf und variieren in ihrer Zusammensetzung innerhalb der Phasenbreite. (ii) die vec der γ'-Phase im System Pd-Zn-Al liegt zwischen 1.71 und 1.75, wärend sie im System Au-Pd-Zn zwischen 1.66 und 1.72 liegt.

Im System RuZn ist die isotype Phase RuZn10 bekannt. Bislang gibt es keine Berichte über eine ternäre oder pseudobinäre Phase der drei Elemente. Nach aktuellem Kenntnisstand sind die hexagonalen Phasen im System Au-Ru-Zn bislang die einzigen ternären Varianten dieser Familie von intermetallischen Strukturen. Systematische Untersuchungen des ternären Systems Au-Ru-Zn im Bereich $0.014 \leq x_{Au} \leq 0.148$ und $0.914 \leq x_{Zn} \leq 0.76$ zeigen, dass die ternären Phasen isotyp zu $FeZn_{10}$ sind. Die Phasen kristallisieren in der Raumgruppe $P6_3/mmc$ mit einer signifikanten Phasenbreite und 554-562 Atomen pro Elementarzelle, welche auf 50-30 kristallographisch unabhängigen Lagen angeordnet sind. Die Struktur lässt sich über fünf verschiedene sich durchdringende Cluster beschreiben. Zwei dieser Cluster bleiben bei dem Austausch von Zn durch Au innerhalb der gesamten Phasenbreite ausgeordnet. Die verbleibenden drei Cluster zeigen eine variable Zusammensetzung und zeigen Fehlordnung wie

Mischbesetzungen (Au/Zn oder Ru/Zn) und Lagenfehlordnungen in Form von Splitpositionen. Die kompositionell variablen β-messingarigen Clustertolerieren einen signifikanten Anteil an Substitution von Zn durch Au oder Ru. Ein stark fehlgeordneter β-messingariger Cluster geht hierbei in einen teilweise fehlgeordneten bcc-artigen Cluster durch die Substitution von Au für Ru oder Zn über.

APPENDIX

All the relevant data are deposited to Prof. Dr. B. Harbrecht, Fachbereich Chemie der Philipps-Universität, Marburg, in the electronic form.

$CrZn_{17-\delta}$ ($-0.8 \leq \delta \leq 1.7$)

A 1: Powder pattern Indexation, 2θobs (<41^{O}) values (measured, $Cu_{K\alpha}$), calculated and observed X - ray intensities for $CrZn_{15.34}$ (x_{Cr} = 0.0540, a = 1824.90 (10) pm)), $I_o > 0.005 I_{max}$

h	*k*	*l*	*2θ(^{O})*	I_{cal}	I_{obs}
1	1	1	8.385	9	9
1	1	3	16.095	7	7
1	3	3	21.204	11	11
2	2	4	23.868	21	20
3	3	3	25.339	6	7
0	4	4	27.628	6	6
2	4	4	29.341	10	11
0	2	6	30.966	19	20
3	3	5	32.137	21	21
2	2	6	32.519	27	29
1	1	7	35.088	52	54
1	5	5	35.088	91	94
0	4	6	35.441	42	43
2	4	6	36.826	75	80
1	3	7	37.836	55	57
3	5	5	37.836	23	24
3	3	7	40.424	399	411
0	2	8	40.738	51	48
4	4	6	40.738	118	112
0	6	6	41.974	1000	977
2	2	8	41.974	712	696

A 2: Crystallographic and technical data for the single crystal structure refinements of $CrZn_{17.15}$ (C4)

crystallographic data		
chemical formula		$Cr_{1.38}Zn_{23.67}$
Pearson symbol		*cF*400.8
x_{Cr}		0.0551
crystal system		
space group type; Z		cubic; $F\bar{4}3m$ (No.216); 16
a/pm[a]		1826.00(8)
V/10^6 pm^3 [a]		6088.4(5)
ρ_{calcd}/g cm^{-3}		7.066
μ/mm^{-1}		37.391
crystal color		silvery with metallic luster
data collection		
crystal size/mm^3		0.10x0.07x0.02
Diffractometer		IPDS (Stoe & Cie.)
Radiation		Mo K_α
Monochromator		Graphite
distance crystal-IP/mm		60
T/K		293(2)
φ_{min}-φ_{max}/^{o}		0-180
$\Delta\varphi$		1
$2\theta_{max}$/^{o}		64.9
reflns measured		19412
index range		-27≤*h*≤27 -27≤*k*≤26 -24≤*l*≤24
completeness of data set		0.997
Data reduction/ absorption correction	IPDS-software,[63] X-RED[66]/numerical, X-SHAPE[67]	
min/max transmission		0.3069/0.6731
unique reflns		1142
R_{int}		0.1148
structure solution, refinement		
structure solution		direct methods, SHELXS-97[64]
structure refinement	full-matrix least squires on F^2 (SHELXL-97[64])	
no. reflns used		1142
no. variables		80
observed reflns (F_o>4σ(F_o))		1067
R(*F*) (F_o>4σ(F_o))		0.0437
R(*F*) (all data)		0.0484
weighting factor k_1/k_2 [b]		0.0170/229.4576
wR (F^2)(all data)		0.0730
GOF (F^2)		1.229
extinction coefficient		0.000022(4)
$\Delta\rho_{min}/\rho_{max}$/10^{-6}epm^{-3}		-1.455/1.755

[a] Parameters determined by use of single diffraction data. [b] Weighting scheme: $1/\omega=\sigma^2(F_O^2)+(k_1.P)^2+k_2.P$ with $P = \frac{1}{3}(\max(F_O^2,0)+.2F_c^2)$.

A 3:.Structural data for $CrZn_{17.15}$ (C4)

Cluster	Atom	Site		*x*	*y*	*z*	SOF	*U*eq[a]/pm^2
Z(1)	Zn10	4a	CC	0[b]	0	0	0.77(3)	130(18)
	Zn11	16e	IT	0.0530(4)	*x*	*x*	0.023(4)	219(13)
	M12[bJ]	16e	OT	0.91537(7)	*x*	*x*	0.88(4)	99(6)
	Zn13	24f	OH	0.16183(16)	0	0	1	287(5)
	Zn15	48h	CO	0.15458(7)	*x*	0.02297(9)	1	234(3)
Q(2)	Cr20	4c	CC	1/4	1/4	1/4	1	60(9)
	Zn21	48h	IT	0.3213(2)	*x*	0.3491(3)	0.245(7)	200(2)
	Zn22	16e	OT	0.16613(9)	*x*	*x*	0.892(14)	272(10)
	Zn23	24g	OH	0.0941(4)	1/4	1/4	0.315(18)	190(3)
	Zn23´	48h	OH´	0.2231(3)	*x*	0.3913(4)	0.246(10)	280(2)
	Zn23´´	48h	OH´´	0.2745(5)	*x*	0.1103(6)	0.104(9)	110(4)
	Zn25	48h	CO	0.07438(8)	*x*	0.26452(8)	1	249(3)
H(3)	Zn30	4c	CC	1/2	1/2	1/2	1	185(9)
	Zn32	16e	OT	0.41191(7)	*x*	*x*	1	154(4)
	Zn34	48h	CO	0.04843(5)	*x*	0.65250(8)	1	160(3)
	Zn35	16e	OT	0.19165(6)	*x*	0.51649(8)	1	178(3)
T(4)	Cr42	16e	OT	0.64837(8)	*x*	*x*	1	66(4)
	Zn43	24g	OH	0.64294(9)	1/4	1/4	1	134(4)
	Zn45	48h	CO	0.10551(6)	*x*	0.77694(7)	1	186(3)

[a] *U*eq is defined as one third of the trace of orthogonalized U_{ij} tensor.[b] SOF(Zn), SOF(Cr)=1-SOF(Zn).

A 4: Anisotropic thermal displacement parameters U*ij* (pm^2) for $CrZn_{17.15}$ (C4)

Atom	U_{11}	U_{22}	U_{33}	U_{23}	U_{13}	U_{12}
Zn10	130(18)	U_{11}	U_{11}	0	0	0
Zn11	230(4)	U_{11}	U_{11}	50(3)	U_{23}	U_{23}
M12	99(6)	U_{11}	U_{11}	0(4)	U_{23}	U_{23}
Zn13	491(14)	185(6)	U_{22}	44(8)	0	0
Zn15	248(4)	U_{11}	207(6)	-91(4)	U_{23}	91(5)
Cr20	60(2)	U_{11}	U_{11}	0	0	0
Zn21	200(2)	U_{11}	210(3)	-118(14)	U_{23}	6(16)
Zn22	272(10)	U_{11}	U_{11}	-63(7)	U_{23}	U_{23}
Zn25	298(5)	U_{11}	150(6)	66(4)	U_{23}	115(6)
Zn30	185(9)	U_{11}	U_{11}	0	0	0
Zn32	154(4)	U_{11}	U_{11}	5(5)	U_{23}	U_{23}
Zn34	114(3)	U_{11}	254(7)	3(3)	U_{23}	-41(5)
Zn35	179(4)	U_{11}	175(6)	5(3)	U_{23}	10(5)
Cr42	66(4)	U_{11}	U_{11}	-17(4)	U_{23}	U_{23}
Zn43	132(8)	135(5)	U_{22}	-51(6)	0	0
Zn45	229(4)	U_{11}	102(5)	41(3)	U_{23}	16(5)

$(Au,Cr)Zn_n$; n = 10.2-6.4

A5: Indexation, $2\theta_{obs}$ (<42^O) values (measured, $Cu_{K\alpha}$), calculated and observed X - ray intensities for $Au_{2.63}Cr_{6.36}Zn_{91.68}$ (C1) (x_{Au} = 0.026, a = 1828.8 (2) pm), $I_o > 0.005 I_{max}$

h	*k*	*l*	$2\theta(^O)$	$I_{calc.}$	$I_{obs.}$
0	2	2	13.678	18	16
1	1	3	16.053	39	33
2	2	2	16.772	13	12
0	0	4	19.390	25	25
1	3	3	21.149	56	53
0	2	4	21.705	9	10
2	2	4	23.806	93	87
1	1	5	25.273	25	26
3	3	3	25.273	44	46
1	3	5	28.846	8	8
0	0	6	29.264	8	8
2	4	4	29.264	46	47
3	3	5	32.053	45	43
2	2	6	32.433	25	24
1	1	7	34.995	47	48
1	5	5	34.995	40	41
0	4	6	35.348	84	88
2	4	6	36.729	39	41
1	3	7	37.736	46	56
3	5	5	37.736	11	13
3	3	7	40.317	318	328
0	2	8	40.630	50	53
4	4	6	40.630	61	65
0	6	6	41.862	1000	944
2	2	8	41.862	872	823

A 6: Indexation, $2\theta_{obs}$ (<42^{O}) values (measured, $Cu_{K\alpha}$), calculated and observed X - ray intensities for $Au_{10.0}Cr_{4.0}Zn_{89.0}$ (C10) (x_{Au} = 0.0097, a = 1843.1 (1) pm), I_o>0.005I_{max}

h	*k*	*l*	$2\theta(^{O})$	$I_{calc.}$	$I_{obs.}$
0	2	2	13.579	14	13
1	1	3	15.936	19	17
2	2	2	16.650	47	39
1	3	3	20.994	185	150
0	2	4	21.546	9	9
2	2	4	23.631	141	121
1	1	5	25.087	74	65
0	0	6	29.047	73	66
2	4	4	29.047	62	57
3	3	5	31.814	53	49
2	2	6	32.192	17	17
1	1	7	34.733	9	9
1	5	5	34.733	84	84
0	4	6	35.083	34	36
2	4	6	36.453	19	21
1	3	7	37.452	82	84
3	5	5	37.452	29	29
3	3	7	40.012	179	201
0	2	8	40.322	37	40
4	4	6	40.322	37	39
0	6	6	41.545	979	1000
2	2	8	41.545	481	491

A 7: Minimum (d_{min}), maximum (d_{max}) and mean interatomic distances (<d>) and coordination numbers (C.N.) for $Au_{2.63}Cr_{6.36}Zn_{91.68}$ (C1), $Au_{3.79}Cr_{5.37}Zn_{91.75}$ (C4), $Au_{10.00}Cr_{4.00}Zn_{89.00}$ (C11)

Cluster	Atoms	Site	C1 d_{min}-d_{max} <d> (pm)	C.N.	C4 d_{min}-d_{max} <d> (pm)	C.N	C11 d_{min}-d_{max} <d> (pm)	C.N.
Z(1)	Zn10	CC	273.0-293.3 <285.2>	10	274.7-306.4 <293.7>	10	- -	- -
	Zn11	IT	239.5-281.4 <264.2>	12	250.2-285.6 <269.0>	12	270.1-279.0 <274.7>	12
	M12	OT	257.7-273.0 <264.8>	13	259.0-274.7 <267.9>	13	259.8-289.0 <272.9>	12
	Zn13	OH	239.5-298.4 <275.4>	13	250.2-306.4 <279.1>	13	270.5-324.1 <291.7>	14
	Zn15	CO	263.1-298.1 <278.6>	12	263.3-297.3 <279.3>	12	268.2-340.5 <243.5>	14
Q(2)	Cr20	CC	258.1-284.7 <271.6>	14	257.3-290.9 <274.3>	14	-	
	Zn21	IT	- -	- -	- -	- -	258.6-309.0 <271.9>	10
	Zn21'	IT'	252.0-335.2 <282.0>	12	252.8-334.0 <282.4>	12	-	
	Zn22	OT	250.5-298.0 <274.4>	13	251.2-301.5 <275.4>	13	266.8-291.5 <276.1>	12
	M23	OH	253.0-284.7 <266.2>	9	250.8-290.9 <266.8>	9	-	
	Zn23'	OH'	244.9-323.9 -	12	246.4-323.6 -	12	- -	
	Zn23''	OH''	245.6-304.5 -	11	240.4-307.2 -	11	249.5-307.6 -	11
	Zn25	CO	258.0-324.0 <282.8>	12	256.6-322.0 <282.3>	12	265.1-308.7 <284.5>	12
H(3)	Zn30	CC	278.9-305.1 <298.6>	16	278.3-305.6 <298.8>	16	271.9-308.9 <299.7>	16
	Zn32	OT	261.2-285.0 <278.5>	11	263.9-285.0 <278.5>	11	265.1-337.7 <292.4>	14
	Zn34	CO	250.2-305.1 <274.8>	12	250.2-305.6 <275.3>	12	250.3-324.1 <281.3>	13
	Zn35	OT	253.0-328.2 <285.7>	14	246.4-328.7 <285.8>	14	249.5-337.7 <284.6>	13
T(4)	Cr42	OT	257.2-265.8 <261.2>	12	256.0-265.0 <261.0>	12	252.0-263.3 <258.9>	12
	Zn43	OH	262.8-277.3 <274.0>	12	263.0-278.4 <273.9>	12	263.3-274.1 <271.9>	12
	Zn45	CO	257.2-305.5 <280.0>	12	256.0-306.4 <280.0>	12	256.9-302.0 <279.0>	12

A 8: Crystallographic and technical data for the single crystal structure refinement of $Au_{2.76}Cr_{6.24}Zn_{91.67}$ (C2)

crystallographic data	
chemical formula	$Au_{2.76}Cr_{6.24}Zn_{91.67}$
Pearson symbol	*cF*402.7
x_{Au}	0.027
crystal system	
space group type; Z	cubic; $F\bar{4}3m$ (No.216); 4
a/pm[a]	1829.62(6)
V/10^6 pm^3 [a]	6124.7(3)
ρ_{calcd}/g cm^{-3}	7.440
μ/mm^{-1}	42.718
crystal color	silvery with metallic luster
data collection	
crystal size/mm^3	0.06x0.05x0.04
Diffractometer	IPDS (Stoe & Cie.)
Radiation	$Mo_{K\alpha}$
Monochromator	Graphite
distance crystal-IP/mm	70
T/K	293(2)
φ_{min}-φ_{max}/^{o}	0-180
$\Delta\varphi$	1
$2\theta_{max}$/^{o}	66.58
reflns measured	13413
index range	-27≤*h*≤23 -25≤*k*≤28 -28≤*l*≤27
completeness of data set	0.986
Data reduction/ absorption correction	IPDS-software,[63] X-RED[66]/numerical, X-SHAPE[67]
unique reflns	1206
R_{int}	0.0998
structure solution, refinement	
structure solution	direct methods, SHELXS-97[64]
structure refinement	full-matrix least squires on F^2 (SHELXL-97[64])
no. reflns used	1206
no. variables	80
observed reflns (F_o>4σ(F_o))	1168
R(*F*) (F_o>4σ(F_o))	0.0411
R(*F*) (all data)	0.0427
weighting factor k_1/k_2 [b]	0.0249/519.0995
wR (F^2)(all data)	0.0821
GOF (F^2)	1.140
extinction coefficient	0.000074(7)
$\Delta\rho_{min}/\rho_{max}$/$10^{-6}$epm^{-3}	-2.519/3.427

[a] Parameters determined by use of single crystal diffraction data. [b] Weighting scheme: $1/\omega=\sigma^2(F_O^2)+(k_1.P)^2+k_2.P$ with P = ⅓(max (F_O^2,0) +.2F_c^2).

A 9: Structural data for $Au_{2.76}$ $Cr_{6.24}Zn_{91.67}$ (C2)

Cluster	Atom	Site	*x*	*y*	*z*	SOF	*U*eq[a]/pm^2
Z(1)	Zn10	4a CC	0	0	0	0.75(3)	192(2)
	Zn11	16e IT	0.0541(3)	*X*	*x*	0.282(13)	210(3)
	M12[b]	16e OT	0.91368(3)	*X*	*x*	0.691(7)	103(2)
	Zn13	24f OH	0.1611(2)	0	0	1	365 (6)
	Zn15	48h CO	0.15514(7)	*X*	0.02327(8)	1	232(3)
Q(2)	Cr20	4b CC	1/4	1/4	1/4	1	86(9)
	Zn21´	48h IT´	0.3211(2)	*X*	0.3486(4)	0.252(7)	300(2)
	Zn22	16e OT	0.16604(8)	*X*	*x*	0.930(14)	225(8)
	ZN23	24g OH	0.0939(3)	1/4	1/4	0.461(18)	270(2)
	ZN23´	48h OH´	0.2224(4)	*X*	0.3911(4)	0.223(9)	280(2)
	Zn23´´	48h OH´´	0.2752(10)	*X*	0.1133(14)	0.050(9)	130(8)
	Zn25	48h CO	0.07453(8)	*X*	0.26507(9)	1	280(4)
H(3)	Zn30	4c CC	1/2	1/2	1/2	1	200(10)
	Zn32	16e OT	0.41188(8)	*X*	*x*	1	179(4)
	Zn34	48h CO	0.04821(5)	*X*	0.65229(8)	1	172(3)
	Zn35	16e OT	0.19119(6)	*X*	0.51663(8)	1	199(3)
T(4)	Cr42	16e OT	0.64832(8)	*X*	*x*	1	80(4)
	Zn43	24g OH	0.64323(10)	1/4	1/4	1	152(3)
	Zn45	48h CO	0.10619(6)	*X*	0.77546(7)	1	199(3)

[a] *U*eq is defined as one third of the trace of orthogonalized U_{ij} tensor. [b] SOF(Au), SOF(Cr)=1-SOF(Au).

A 10: Anisotropic thermal displacement parameters U_{ij} (pm^2) for $Au_{2.76}$ $Cr_{6.24}Zn_{91.67}$ (C2)

Atom	U_{11}	U_{22}	U_{33}	U_{23}	U_{13}	U_{12}
Zn10	190(2)	U_{11}	U_{11}	0	0	0
Zn11	210(3)	U_{11}	U_{11}	57(19)	U_{23}	U_{23}
M12	103(2)	U_{11}	U_{11}	-7(2)	U_{23}	U_{23}
Zn13	710(2)	193(6)	U_{22}	74(8)	0	0
Zn15	244(4)	U_{11}	208(6)	-82(4)	U_{23}	73(5)
Cr20	86 (9)	U_{11}	U_{11}	0	0	0
Zn21´	270(2)	U_{11}	360(4)	-160(2)	U_{23}	33(19)
Zn22	225(8)	U_{11}	U_{11}	-42(5)	U_{23}	U_{23}
Zn25	331(6)	U_{11}	178(6)	81(4)	U_{23}	136(6)
Zn30	200(10)	U_{11}	U_{11}	0	0	0
Zn32	179(4)	U_{11}	U_{11}	13(5)	U_{23}	U_{23}
Zn34	135(3)	U_{11}	244(7)	4(3)	U_{23}	-42(4)
Zn35	197(4)	U_{11}	203(6)	14(4)	U_{23}	7(5)
Cr42	80(4)	U_{11}	U_{11}	-11(4)	U_{23}	U_{23}
Zn43	166(8)	145(5)	U_{22}	-51(6)	0	0
Zn45	244(4)	U_{11}	108(5)	32(3)	U_{23}	16(5)

A 11: Crystallographic and technical data for the single crystal structure refinement of $Au_{3.26}$ $Cr_{5.74}Zn_{91.57}$ (C3)

crystallographic data	
chemical formula	$Au_{3.26}Cr_{5.74}Zn_{91.57}$
Pearson symbol	*cF*402.3
x_{Au}	0.032
crystal system	
space group type; Z	cubic; $F\bar{4}3m$ (No.216); 4
a/pm[a]	1831.4(2)
$V/10^6$ pm^3 [a]	6142.6(12)
ρ_{calcd}/g cm^{-3}	7.490
μ/mm^{-1}	43.657
crystal color	silvery with metallic luster
data collection	
crystal size/mm^3	0.08x0.05x0.04
Diffractometer	IPDS (Stoe & Cie.)
Radiation	$Mo_{K\alpha}$
Monochromator	Graphite
distance crystal-IP/mm	40
T/K	293(2)
φ_{min}-φ_{max}/°	0-199.5
$\Delta\varphi$	1.5
$2\theta_{max}$/°	65.82
reflns measured	22248
index range	$-27 \le h \le 25$ $-26 \le k \le 26$ $-27 \le l \le 27$
completeness of data set	0.994
Data reduction/ absorption correction	IPDS-software,[63] X-RED[66]/numerical, X-SHAPE[67]
unique reflns	1186
R_{int}	0.0998
structure solution, refinement	
structure solution	direct methods, SHELXS-97[64]
structure refinement	full-matrix least squires on F^2 (SHELXL-97[64])
no. reflns used	1186
no. variables	80
observed reflns (F_o>4σ(F_o))	1092
$R(F)$ (F_o>4σ(F_o))	0.0418
$R(F)$ (all data)	0.0451
weighting factor k_1/k_2 [b]	0.0554/431.4415
wR (F^2)(all data)	0.1082
GOF (F^2)	1.090
extinction coefficient	0.000238(18)
$\Delta\rho_{min}/\rho_{max}/10^{-6}$epm^{-3}	-1.753/2.469

[a] Parameters determined by use of powder diffraction data. [b] Weighting scheme: $1/\omega=\sigma^2(F_O^2)+(k_1.P)^2+k_2.P$ with $P = \frac{1}{3}(\max(F_O^2,0) + .2F_c^2)$.

A 12: Structural data for $Au_{3.26}$ $Cr_{5.74}Zn_{91.57}$ (C3)

Cluster	Atom	Site	*x*	*y*	*z*	SOF	*U*eq[a]/pm^2
Z(1)	Zn10	4a CC	0	0	0	0.73(4)	220(3)
	Zn11	16e IT	0.0551(4)	*X*	*x*	0.283(16)	250(3)
	M12[b]	16e OT	0.91353(3)	*X*	*x*	0.815(9)	162(3)
	Zn13	24f OH	0.1615(3)	0	0	1	412 (8)
	Zn15	48h CO	0.15514(9)	*X*	0.02334(10)	1	279(4)
Q(2)	Cr20	4b CC	1/4	1/4	1/4	1	124(10)
	Zn21´	48h IT´	0.3211(3)	*X*	0.3489(4)	0.243(9)	320(3)
	Zn22	16e OT	0.16599(10)	*X*	*x*	0.937(18)	279(11)
	ZN23	24g OH	0.0937(4)	1/4	1/4	0.45(3)	310(3)
	ZN23´	48h OH´	0.2231(5)	*X*	0.3916(5)	0.228(12)	340(3)
	Zn23´´	48h OH´´	0.2733(12)	*X*	0.1112(15)	0.050(11)	140(9)
	Zn25	48h CO	0.07468(10)	*X*	0.26503(11)	1	329(5)
H(3)	Zn30	4c CC	1/2	1/2	1/2	1	264(12)
	Zn32	16e OT	0.41206(9)	*X*	*x*	1	223(5)
	Zn34	48h CO	0.04832(6)	*X*	0.65216(10)	1	222(4)
	Zn35	16e OT	0.19117(6)	*X*	0.51656(10)	1	240(4)
T(4)	Cr42	16e OT	0.64850(11)	*X*	*x*	1	127(5)
	Zn43	24g OH	0.64309(12)	1/4	1/4	1	189(4)
	Zn45	48h CO	0.10624(7)	*X*	0.77537(9)	1	241(4)

[a] *U*eq is defined as one third of the trace of orthogonalized U_{ij} tensor. [b] SOF(Au), SOF(Cr)=1-SOF(Au).

A 13: Anisotropic thermal displacement parameters U_{ij} (pm^2) for $Au_{3.26}Cr_{5.74}Zn_{91.57}$ (C3)

Atom	U_{11}	U_{22}	U_{33}	U_{23}	U_{13}	U_{12}
Zn10	220(3)	U_{11}	U_{11}	0	0	0
Zn11	250(3)	U_{11}	U_{11}	120(2)	U_{23}	U_{23}
M12	162(3)	U_{11}	U_{11}	-5(2)	U_{23}	U_{23}
Zn13	760(2)	241(8)	U_{22}	66(10)	0	0
Zn15	298(6)	U_{11}	242(8)	-92(5)	U_{23}	88(7)
Cr20	124 (10)	U_{11}	U_{11}	0	0	0
Zn21	300(3)	U_{11}	340(4)	-160(2)	U_{23}	30(2)
Zn22	279(11)	U_{11}	U_{11}	-47(7)	U_{23}	U_{23}
Zn25	387(6)	U_{11}	214(8)	67(5)	U_{23}	145(8)
Zn30	264(12)	U_{11}	U_{11}	0	0	0
Zn32	223(5)	U_{11}	U_{11}	8(6)	U_{23}	U_{23}
Zn34	191(4)	U_{11}	284(8)	4(4)	U_{23}	-51(5)
Zn35	239(5)	U_{11}	244(8)	12(4)	U_{23}	15(6)
Cr42	127(5)	U_{11}	U_{11}	0(6)	U_{23}	U_{23}
Zn43	211(10)	179(6)	U_{22}	-52(7)	0	0
Zn45	287(6)	U_{11}	149(7)	33(4)	U_{23}	15(6)

A 14: Crystallographic and technical data for the single crystal structure refinement of $Au_{3.80}Cr_{5.32}Zn_{91.75}$ (C4a)

crystallographic data	
chemical formula	$Au_{3.80}Cr_{5.32}Zn_{91.75}$
Pearson symbol	*cF*403.5
x_{Au}	0.038
crystal system	
space group type; Z	cubic; $F\bar{4}3m$ (No.216); 4
a/pm[a]	1832.5(2)
V/10^6 pm^3 [a]	6153.6(12)
ρ_{calcd}/g cm^{-3}	7.580
μ/mm^{-1}	44.850
crystal color	silvery with metallic luster
data collection	
crystal size/mm^3	0.10x0.06x0.04
Diffractometer	IPDS (Stoe & Cie.)
Radiation	$Mo_{K\alpha}$
Monochromator	Graphite
distance crystal-IP/mm	40
T/K	293(2)
φ_{min}-φ_{max}/^{o}	0-100.0
$\Delta\varphi$	1.0
$2\theta_{max}$/^{o}	66.16
reflns measured	22811
index range	-28≤*h*≤27 -28≤*k*≤27 -27≤*l*≤28
completeness of data set	0.995
Data reduction/ absorption correction	IPDS-software,[63] X-RED[66]/numerical, X-SHAPE[67]
unique reflns	1108
R_{int}	0.1120
structure solution, refinement	
structure solution	direct methods, SHELXS-97[64]
structure refinement	full-matrix least squires on F^2 (SHELXL-97[64])
no. reflns used	1204
no. variables	80
observed reflns (F_o>4σ(F_o))	1108
R(*F*) (F_o>4σ(F_o))	0.0515
R(*F*) (all data)	0.0557
weighting factor k_1/k_2 [b]	0.0884/391.7215
wR (F^2)(all data)	0.1377
GOF (F^2)	1.078
extinction coefficient	0.00019(2)
$\Delta\rho_{min}/\rho_{max}$/$10^{-6}$epm^{-3}	-2.308/2.728

[a] Parameters determined by use of powder diffraction data. [b] Weighting scheme: $1/\omega=\sigma^2(F_O^2)+(k_1.P)^2+k_2.P$ with $P = ⅓(\max(F_O^2,0) + .2F_c^2)$.

A 15: Structural data for $Au_{3.80}Cr_{5.32}Zn_{91.75}$ (C4a)

Cluster	Atom	Site	*x*	*y*	*z*	SOF	*U*eq[a]/pm^2
Z(1)	Zn10	4a CC	0	0	0	0.63(5)	270(4)
	Zn11	16e IT	0.0549(3)	*X*	*x*	0.47(2)	270(2)
	M12[b]	16e OT	0.91344(3)	*X*	*x*	0.920(11)	151(3)
	Zn13	24f OH	0.1670(4)	0	0	1	528 (14)
	Zn15	48h CO	0.15600(10)	*X*	0.02320(13)	1	276(5)
Q(2)	Cr20	4b CC	¼	1/4	1/4	1	148(13)
	Zn21´	48h IT´	0.3210(4)	*X*	0.3478(5)	0.229(11)	300(3)
	Zn22	16e OT	0.16612(12)	*X*	*x*	0.937(18)	279(11)
	ZN23	24g OH	0.0911(4)	1/4	1/4	0.481(16)	310(3)
	Au23	24g OH	0.0911(4)	1/4	1/4	0.019(16)	330(3)
	ZN23´	48h OH´	0.2225(5)	*X*	0.3909(7)	0.201(14)	300(4)
	Zn23´´	48h OH´´	0.2737(19)	*X*	0.113(2)	0.046(14)	210(15)
	Zn25	48h CO	0.07574(13)	*X*	0.26590(14)	1	347(6)
H(3)	Zn30	4c CC	1/2	1/2	1/2	1	247(14)
	Zn32	16e OT	0.41232(11)	*X*	*x*	1	212(6)
	Zn34	48h CO	0.04837(7)	*X*	0.65233(11)	1	210(4)
	Zn35	16e OT	0.19071(9)	*X*	0.51703(12)	1	235(4)
T(4)	Cr42	16e OT	0.64852(12)	*X*	*x*	1	118(6)
	Zn43	24g OH	0.64339(14)	1/4	1/4	1	190(5)
	Zn45	48h CO	0.10678(9)	*X*	0.77522(11)	1	233(5)

[a] *U*eq is defined as one third of the trace of orthogonalized U_{ij} tensor. [b] SOF(Au), SOF(Cr)=1-SOF(Au).

A 16: Anisotropic thermal displacement parameters U_{ij} (pm^2) for $Au_{3.80}Cr_{5.32}Zn_{91.75}$ (C4a)

Atom	U_{11}	U_{22}	U_{33}	U_{23}	U_{13}	U_{12}
Zn10	270(4)	U_{11}	U_{11}	0	0	0
Zn11	270(2)	U_{11}	U_{11}	75(17)	U_{23}	U_{23}
M12	151(3)	U_{11}	U_{11}	-9(2)	U_{23}	U_{23}
Zn13	1100(4)	243(10)	U_{22}	74(12)	0	0
Zn15	282(7)	U_{11}	264(10)	-76(6)	U_{23}	78(8)
Cr20	148 (13)	U_{11}	U_{11}	0	0	0
Zn21	310(4)	U_{11}	290(5)	-120(3)	U_{23}	-10(3)
Zn22	263(13)	U_{11}	U_{11}	-31(8)	U_{23}	U_{23}
Zn25	405(9)	U_{11}	232(10)	85(7)	U_{23}	178(10)
Zn30	247(14)	U_{11}	U_{11}	0	0	0
Zn32	212(6)	U_{11}	U_{11}	8(7)	U_{23}	U_{23}
Zn34	178(5)	U_{11}	274(9)	5(4)	U_{23}	-47(6)
Zn35	233(6)	U_{11}	237(9)	15(5)	U_{23}	12(7)
Cr42	118(6)	U_{11}	U_{11}	-11(6)	U_{23}	U_{23}
Zn43	221(11)	175(6)	U_{22}	-58(8)	0	0
Zn45	280(7)	U_{11}	141(8)	25(4)	U_{23}	-3(7)

A 17: Crystallographic and technical data for the single crystal structure refinement of $Au_{4.59}Cr_{4.85}Zn_{91.33}$ (C5)

crystallographic data	
chemical formula	$Au_{4.59}Cr_{4.85}Zn_{91.33}$
Pearson symbol	*cF*403.1
x_{Au}	0.046
crystal system	
space group type; Z	cubic; $F\bar{4}3m$ (No.216); 4
a/pm[a]	1835.91(9)
$V/10^6$ pm^3 [a]	6188.1(5)
ρ_{calcd}/g cm^{-3}	7.650
μ/mm^{-1}	46.240
crystal color	silvery with metallic luster
data collection	
crystal size/mm^3	0.08 x 0.04 x 0.03
Diffractometer	IPDS (Stoe & Cie.)
Radiation	$Mo_{K\alpha}$
Monochromator	Graphite
distance crystal-IP/mm	40
T/K	293(2)
φ_{min}-φ_{max}/^{o}	0-200.2
$\Delta\varphi$	1.3
$2\theta_{max}$/^{o}	65.82
reflns measured	22560
index range	$-27 \le h \le 28$ $-27 \le k \le 27$ $-28 \le l \le 27$
completeness of data set	0.995
Data reduction/ absorption correction	IPDS-software,[63] X-RED[66]/numerical, X-SHAPE[67]
unique reflns	1197
R_{int}	0.1076
structure solution, refinement	
structure solution	direct methods, SHELXS-97[64]
structure refinement	full-matrix least squires on F^2 (SHELXL-97[64])
no. reflns used	1197
no. variables	81
observed reflns (F_o>4σ(F_o))	975
$R(F)$ (F_o>4σ(F_o))	0.0387
$R(F)$ (all data)	0.0525
weighting factor k_1/k_2 [b]	0.0508/0
wR (F^2)(all data)	0.0882
GOF (F^2)	1.001
extinction coefficient	0.000036(5)
$\Delta\rho_{min}/\rho_{max}$/10^{-6}epm^{-3}	-2.425/2.657

[a] Parameters determined by use of powder diffraction data. [b] Weighting scheme: $1/\omega=\sigma^2(F_O^2)+(k_1.P)^2+k_2.P$ with $P = \frac{1}{3}(\max(F_O^2,0) + .2F_c^2)$.

A 18: Structural data for $Au_{4.59}Cr_{4.85}Zn_{91.33}$ (C5)

Cluster	Atom	Site	*x*	*y*	*z*	SOF	*U*eq[a]/pm^2
Z(1)	Zn10	4a CC	0	0	0	0.48(4)	220(5)
	Zn11	16e IT	0.05512(19)	*X*	*x*	0.55	150(10)
	Au12	16e OT	0.91340(3)	*X*	*x*	1	87(2)
	Zn13	24f OH	0.1730(3)	0	0	1	450(11)
	Zn15	48h CO	0.15655(9)	*X*	0.02268(11)	1	205(4)
Q(2)	Cr20	4b CC	¼	¼	1/4	0.89(4)	50(2)
	Zn21	16e IT	0.312(3)	*X*	*x*	0.09(3)	500(3)
	Zn21´	48h IT´	0.3218(4)	*X*	0.3477(7)	0.203(11)	210(3)
	Zn22	16e OT	0.16615(12)	*X*	*x*	0.943(17)	200(11)
	ZN23	24g OH	0.0859(3)	¼	1/4	0.435(11)	216(17)
	Au23	24g OH	0.0859(3)	¼	1/4	0.093(11)	216(17)
	ZN23´	48h OH	0.2227(5)	*X*	0.3905(7)	0.192(11)	300(4)
	Zn23´´	48h OH	0.2730(13)	*X*	0.1136(18)	0.045(10)	70(11)
	Zn25	48h CO	0.07706(11)	*X*	0.26693(11)	1	283(5)
H(3)	Zn30	4c CC	1/2	½	1/2	1	175(13)
	Zn32	16e OT	0.41273(10)	*X*	*x*	1	161(5)
	Zn34	48h CO	0.04830(6)	*X*	0.65254(10)	1	152(3)
	Zn35	16e OT	0.19043(7)	*X*	0.51739(11)	1	179(4)
T(4)	Cr42	16e OT	0.64866(11)	*X*	*x*	1	60(6)
	Zn43	24g OH	0.64361(12)	¼	1/4	1	130(4)
	Zn45	48h CO	0.10696(7)	*X*	0.77481(10)	1	167(4)

[a] *U*eq is defined as one third of the trace of orthogonalized U_{ij} tensor.

A 19: Anisotropic thermal displacement parameters U_{ij} (pm^2) for $Au_{4.59}Cr_{4.85}Zn_{91.33}$ (C5)

Atom	U_{11}	U_{22}	U_{33}	U_{23}	U_{13}	U_{12}
Zn10	220(5)	U_{11}	U_{11}	0	0	0
Zn11	150(10)	U_{11}	U_{11}	68(12)	U_{23}	U_{23}
Au12	87(2)	U_{11}	U_{11}	-8(2)	U_{23}	U_{23}
Zn13	910(4)	218(10)	U_{22}	80(13)	0	0
Zn15	221(5)	U_{11}	171(8)	-86(5)	U_{23}	60(7)
Cr20	50(2)	U_{11}	U_{11}	0	0	0
Zn21	500(3)	U_{11}	U_{11}	700(2)	U_{23}	700(2)
Zn22	200(11)	U_{11}	U_{11}	-23(7)	U_{23}	U_{23}
Zn25	338(8)	U_{11}	175(8)	96(6)	U_{23}	172(9)
Zn30	175(13)	U_{11}	U_{11}	0	0	0
Zn32	161(5)	U_{11}	U_{11}	17(7)	U_{23}	U_{23}
Zn34	124(4)	U_{11}	209(9)	15(5)	U_{23}	11(7)
Zn35	163(5)	U_{11}	209(9)	15(5)	U_{23}	11(7)
Cr42	60(6)	U_{11}	U_{11}	-19(6)	U_{23}	U_{23}
Zn43	146(11)	122(6)	U_{22}	-63(8)	0	0
Zn45	210(5)	U_{11}	80(7)	37(4)	U_{23}	1(6)

A 20: Crystallographic and technical data for the single crystal structure refinement of $Au_{5.15}Cr_{4.73}Zn_{91.93}$ (C6)

crystallographic data		
chemical formula		$Au_{5.15}Cr_{4.73}Zn_{91.93}$
Pearson symbol		*cF*407.2
x_{Au}		0.051
crystal system		
space group type; Z		cubic; $F\bar{4}3m$ (No.216); 4
a/pm[a]		1836.53(7)
V/10^6 pm^3 [a]		6194.3(5)
ρ_{calcd}/g cm^{-3}		7.796
μ/mm^{-1}		47.715
crystal color		silvery with metallic luster
data collection		
crystal size/mm^3		0.07 x 0.04 x 0.03
Diffractometer		IPDS (Stoe & Cie.)
Radiation		$Mo_{K\alpha}$
Monochromator		Graphite
distance crystal-IP/mm		50
T/K		293(2)
φ_{min}-φ_{max}/^{o}		0-165
$\Delta\varphi$		1.0
$2\theta_{max}$/^{o}		64.86
reflns measured		17464
index range		-27≤*h*≤24
		-27≤*k*≤27
		-28≤*l*≤27
completeness of data set		0.985
Data reduction/		
absorption correction	IPDS-software,[63]	X-RED[66]/numerical, X-SHAPE[67]
unique reflns		1138
R_{int}		0.0512
structure solution, refinement		
structure solution		Direct methods, SHELXS-97[64]
structure refinement	full-matrix least	squires on F^2 (SHELXL-97[64])
no. reflns used		1138
no. variables		85
observed reflns (F_o>4σ(F_o))		1114
R(*F*) (F_o>4σ(F_o))		0.0273
R(*F*) (all data)		0.0282
weighting factor k_1/k_2 [b		0.0077 /387.3427
wR (F^2)(all data)		0.0538
GOF (F^2)		1.126
extinction coefficient		0.000043(3)
$\Delta\rho_{min}/\rho_{max}$/10^{-6}epm^{-3}		-2.239/1.756

[a] Parameters determined by use of powder diffraction data. [b] Weighting scheme: $1/\omega=\sigma^2(F_O^2)+(k_1.P)^2+k_2.P$ with $P=\frac{1}{3}(\max(F_O^2,0)+.2F_c^2)$.

A 21: Structural data for $Au_{5.15}Cr_{4.73}Zn_{91.93}$ (C6)

Cluster	Atom	Site	*x*	*y*	*z*	SOF	*U*eq[a]/pm^2
Z(1)	Zn10	4a CC	0	0	0	0.32(2)	140(4)
	Zn11	16e IT	0.05454(10)	*X*	*x*	0.71(1)	204(9)
	Au12	16e OT	0.913397(17)	*X*	*x*	1	110(1)
	Zn13	24f OH	0.17620(18)	0	0	1	427(7)
	Zn15	48h CO	0.15627(6)	*X*	0.02322(7)	1	227(2)
Q(2)	Cr20	4b CC	1/4	¼	1/4	0.74(3)	46(16)
	Zn21	16e IT	0.3113(15)	*X*	*x*	0.23(4)	320(9)
	Zn21´	48h IT´	0.3206(3)	*X*	0.3474(10)	0.204(13)	360(4)
	Zn22	16e OT	0.16664(8)	*X*	*x*	0.901(11)	229(7)
	ZN23	24g OH	0.08147(11)	¼	1/4	0.231(7)	153(8)
	Au23	24g OH	0.08147(11)	¼	1/4	0.193(7)	153(8)
	ZN23´	48h OH	0.2247(4)	*X*	0.3916(5)	0.176(9)	300(3)
	Zn23´´	48h OH	0.2703(7)	*X*	0.1113 (8)	0.109(10)	340(5)
	Zn25	48h CO	0.07847(7)	*X*	0.26787(7)	1	322(3)
H(3)	Zn30	4c CC	1/2	½	1/2	1	233(9)
	Zn32	16e OT	0.41320(7)	*X*	*x*	1	191(3)
	Zn34	48h CO	0.04821(4)	*X*	0.65268(7)	1	175(2)
	Zn35	16e OT	0.19046(5)	*X*	0.51819(7)	1	219(3)
T(4)	Cr42	16e OT	0.64871(7)	*X*	*x*	1	86(4)
	Zn43	24g OH	0.64369(8)	¼	1/4	1	162(3)
	Zn45	48h CO	0.10718(5)	*X*	0.77504(6)	1	197(2)

[a] *U*eq is defined as one third of the trace of orthogonalized U_{ij} tensor.

A 22: Anisotropic thermal displacement parameters U_{ij} (pm^2) for $Au_{5.15}Cr_{4.73}Zn_{91.93}$ (C6)

Atom	U_{11}	U_{22}	U_{33}	U_{23}	U_{13}	U_{12}
Zn10	140(4)	U_{11}	U_{11}	0	0	0
Zn11	204(9)	U_{11}	U_{11}	58(6)	U_{23}	U_{23}
Au12	110(11)	U_{11}	U_{11}	-9(1)	U_{23}	U_{23}
Zn13	820(2)	230(6)	U_{22}	81(8)	0	0
Zn15	240(3)	U_{11}	201(5)	-73(3)	U_{23}	41(5)
Cr20	46(16)	U_{11}	U_{11}	0	0	0
Zn21	320(9)	U_{11}	U_{11}	240(8)	U_{23}	U_{23}
Zn21´	320(3)	U_{11}	450(10)	-170(3)	U_{23}	60(3)
Zn22	229(7)	U_{11}	U_{11}	-29(5)	U_{23}	U_{23}
Zn25	381(5)	U_{11}	204(5)	103(4)	U_{23}	163(6)
Zn30	233(9)	U_{11}	U_{11}	0	0	0
Zn32	191(3)	U_{11}	U_{11}	31(5)	U_{23}	U_{23}
Zn34	141(3)	U_{11}	243(5)	-7 (3)	U_{23}	-46(3)
Zn35	194(3)	U_{11}	269(6)	-2 (3)	U_{23}	3(4)
Cr42	86 (4)	U_{11}	U_{11}	-17(4)	U_{23}	U_{23}
Zn43	184(7)	151(4)	U_{22}	-55(5)	0	0
Zn45	240(4)	U_{11}	110(4)	30(3)	U_{23}	1(4)

A 23: Crystallographic and technical data for the single crystal structure refinements of $Au_{5.62}Cr_{4.57}Zn_{92.25}$ (C7)

crystallographic data		
Chemical formula		$Au_{5.62}Cr_{4.57}Zn_{92.25}$
Pearson symbol		*cF*409.8
x_{Au}		0.055
crystal system		
space group type; Z		cubic; $F\bar{4}3m$ (No.216); 4
a/pm[a]		1838.6(1)
V/10^6 pm^3 [a]		6215.3(1)
ρ_{calcd}/g cm^{-3}		7.882
μ/mm^{-1}		48.756
crystal color		silvery with metallic luster
data collection		
crystal size/mm^3		0.12x0.08x0.06
Diffractometer		IPDS (Stoe & Cie.)
Radiation		$Mo_{K\alpha}$
Monochromator		Graphite
distance crystal-IP/mm		40
T/K		293(2)
φ_{min}-φ_{max}/^{o}		0-100.0
$\Delta\varphi$		1.0
$2\theta_{max}$/^{o}		66.28
reflns measured		11457
index range		-28≤*h*≤28
		-23≤*k*≤28
		-28≤*l*≤11
completeness of data set		0.994
Data reduction/		
absorption correction	IPDS-software,[63]	X-RED[66]/numerical, X-SHAPE[67]
unique reflns		1214
R_{int}		0.2075
structure solution, refinement		
structure solution		direct methods, SHELXS-97[64]
structure refinement	full-matrix least	squires on F^2 (SHELXL-97[64])
no. reflns used		1031
no. variables		84
observed reflns (F_o>4σ(F_o))		1031
R(*F*) (F_o>4σ(F_o))		0.0509
R(*F*) (all data)		0.0591
weighting factor k_1/k_2 [b]		0.0685/108.7566
wR (F^2)(all data)		0.1395
GOF (F^2)		1.051
extinction coefficient		0.000106(15)
$\Delta\rho_{min}/\rho_{max}$/10^{-6}epm^{-3}		-2.128/3.489

[a] Parameters determined by use of powder diffraction data. [b] Weighting scheme: $1/\omega=\sigma^2(F_O^2)+(k_1.P)^2+k_2.P$ with $P = \frac{1}{3}(\max(F_O^2,0) + .2F_c^2)$.

A 24: Structural data for $Au_{5.62}Cr_{4.57}Zn_{92.25}$ (C7)

Cluster	Atom	Site	*x*	*y*	*z*	SOF	*U*eq[a]/pm^2
Z(1)	Zn10	4a CC	0	0	0	0.22(5)	330(11)
	Zn11	16e IT	0.05416(17)	*X*	*x*	0.82(2)	373(15)
	Au12	16e OT	0.91344(3)	*X*	*x*	1	284(2)
	Zn13	24f OH	0.1795(3)	0	0	1	527(11)
	Zn15	48h CO	0.15616(11)	*X*	0.02333(13)	1	396(5)
Q(2)	Cr20	4b CC	1/4	1/4	1/4	0.57(5)	200(4)
	Zn21	16e IT	0.3107(15)	*X*	*x*	0.34(7)	420(9)
	Zn21´	48h IT´	0.3219(7)	*X*	0.345(5)	0.20(3)	610(11)
	Zn22	16e OT	0.16712(16)	*X*	*x*	0.0.89(2)	399(15)
	ZN23	24g OH	0.08038(15)	1/4	1/4	0.250(13)	307(12)
	Au23	24g OH	0.08038(15)	1/4	1/4	0.270(13)	307(12)
	ZN23´	48h OH´	0.2239(9)	*X*	0.3923(11)	0.156(17)	500(7)
	Zn23´´	48h OH´´	0.2695(12)	*X*	0.1097(15)	0.092(17)	360(9)
	Zn25	48h CO	0.08002(14)	*X*	0.26841(15)	1	483(6)
H(3)	Zn30	4c CC	1/2	1/2	1/2	1	426(18)
	Zn32	16e OT	0.41369(12)	*X*	*x*	1	365(7)
	Zn34	48h CO	0.04824(8)	*X*	0.65280(13)	1	348(4)
	Zn35	16e OT	0.19044(11)	*X*	0.51893(15)	1	404(5)
T(4)	Cr42	16e OT	0.64898(14)	*X*	*x*	1	259(7)
	Zn43	24g OH	0.64385(17)	1/4	1/4	1	344(6)
	Zn45	48h CO	0.10745(10)	*X*	0.77529(12)	1	368(5)

[a] *U*eq is defined as one third of the trace of orthogonalized U_{ij} tensor.

A 25: Anisotropic thermal displacement parameters U_{ij} (pm^2) for $Au_{5.62}Cr_{4.57}Zn_{92.25}$ (C7)

Atom	U_{11}	U_{22}	U_{33}	U_{23}	U_{13}	U_{12}
Zn10	330(11)	U_{11}	U_{11}	0	0	0
Zn11	373(15)	U_{11}	U_{11}	42(10)	U_{23}	U_{23}
Au12	284(2)	U_{11}	U_{11}	-6(2)	U_{23}	U_{23}
Zn13	780(4)	403(11)	U_{22}	57(14)	0	0
Zn15	405(7)	U_{11}	377(10)	-70(6)	U_{23}	21(9)
Cr20	200(4)	U_{11}	U_{11}	0	0	0
Zn21	420(9)	U_{11}	U_{11}	80(6)	U_{23}	U_{23}
Zn21´	310(4)	U_{11}	290(5)	-120(3)	U_{23}	-10(3)
Zn22	399(15)	U_{11}	U_{11}	-8(9)	U_{23}	U_{23}
Zn25	536(9)	U_{11}	377(11)	92(8)	U_{23}	152(13)
Zn30	426(18)	U_{11}	U_{11}	0	0	0
Zn32	365(7)	U_{11}	U_{11}	36(9)	U_{23}	U_{23}
Zn34	317(6)	U_{11}	411(11)	-3(5)	U_{23}	-50(7)
Zn35	378(7)	U_{11}	454(12)	-1(7)	U_{23}	21(8)
Cr42	259(7)	U_{11}	U_{11}	10(8)	U_{23}	U_{23}
Zn43	357(14)	328(8)	U_{22}	-54(10)	0	0
Zn45	414(7)	U_{11}	278(9)	29(5)	U_{23}	0(8)

A 26: Crystallographic and technical data for the single crystal structure refinement of $Au_{6.19}Cr_{4.50}Zn_{91.19}$ (C8)

crystallographic data	
chemical formula	$Au_{6.19}Cr_{4.50}Zn_{91.19}$
Pearson symbol	*cF*407.5
x_{Au}	0.061
crystal system	
space group type; Z	cubic; $F\bar{4}3m$ (No.216); 4
a/pm[a]	1839.0(1)
$V/10^6$ pm^3 [a]	6219.4(1)
ρ_{calcd}/g cm^{-3}	7.917
μ/mm^{-1}	49.634
crystal color	silvery with metallic luster
data collection	
crystal size/mm^3	0.08 x 0.06 x 0.03
Diffractometer	IPDS (Stoe & Cie.)
Radiation	$Mo_{K\alpha}$
Monochromator	Graphite
distance crystal-IP/mm	40
T/K	293(2)
φ_{min}-φ_{max}/^{o}	0-110.0
$\Delta\varphi$	1.0
$2\theta_{max}$/^{o}	65.70
reflns measured	12360
index range	-28≤*h*≤27 -27≤*k*≤20 -19≤*l*≤27
completeness of data set	0.995
Data reduction/ absorption correction	IPDS-software,[63] X-RED[66]/numerical, X-SHAPE[67]
unique reflns	1197
R_{int}	0.0873
structure solution, refinement	
structure solution	direct methods, SHELXS-97[64]
structure refinement	full-matrix least squires on F^2 (SHELXL-97[64])
no. reflns used	1197
no. variables	82
observed reflns (F_o>4σ(F_o))	1110
R(*F*) (F_o>4σ(F_o))	0.0323
R(*F*) (all data)	0.0358
weighting factor k_1/k_2 [b]	0.0485/148.2826
wR (F^2)(all data)	0.0783
GOF (F^2)	1.016
extinction coefficient	0.00011(4)
$\Delta\rho_{min}/\rho_{max}$/$10^{-6}$epm^{-3}	-2.268/2.705

[a] Parameters determined by use of powder diffraction data. [b] Weighting scheme: $1/\omega=\sigma^2(F_O^2)+(k_1.P)^2+k_2.P$ with $P = ⅓(\max(F_O^2,0) + .2F_c^2)$.

A 27: Structural data for $Au_{6.19}Cr_{4.50}Zn_{91.19}$ (C8)

Cluster	Atom	Site	*x*	*y*	*z*	SOF	*U*eq[a]/pm^2
Z(1)	Zn10	4a CC	0	0	0	0.18(2)	70(6)
	Zn11	16e IT	0.05406(9)	*X*	*x*	0.820(12)	204(8)
	Au12	16e OT	0.913371(17)	*X*	*x*	1	123(1)
	Zn13	24f OH	0.18028(16)	0	0	1	356(6)
	Zn15	48h CO	0.15565(6)	*X*	0.02373(7)	1	237(3)
Q(2)	Cr20	4b CC	1/4	1/4	1/4	0.50(3)	50(2)
	Zn21	16e IT	0.3142(6)	*X*	*x*	0.48(3)	390(4)
	Zn21´	48h IT´	0.3211(4)	*X*	0.3474(10)	0.132(12)	230(4)
	Zn22	16e OT	0.16744(9)	*X*	*x*	0.873(14)	247(9)
	ZN23	24g OH	0.07989(7)	1/4	1/4	0.122(7)	149(5)
	Au23	24g OH	0.07989(7)	1/4	1/4	0.364(7)	149(5)
	ZN23´	48h OH	0.2238(5)	*X*	0.3900(6)	0.148(9)	330(4)
	Zn23´´	48h OH	0.2723(6)	*X*	0.1120(7)	0.103(9)	220(5)
	Zn25	48h CO	0.08043(8)	*X*	0.26902(8)	1	317(3)
H(3)	Zn30	4c CC	1/2	1/2	1/2	1	257(10)
	Zn32	16e OT	0.41379(7)	*X*	*x*	1	206(4)
	Zn34	48h CO	0.04818(4)	*X*	0.65284(7)	1	190(2)
	Zn35	16e OT	0.19029(6)	*X*	0.51954(8)	1	249(3)
T(4)	Cr42	16e OT	0.64892(7)	*X*	*x*	1	94(4)
	Zn43	24g OH	0.64402(9)	1/4	1/4	1	181(3)
	Zn45	48h CO	0.10742(5)	*X*	0.77519(7)	1	215(3)

[a] *U*eq is defined as one third of the trace of orthogonalized U_{ij} tensor.

A 28: Anisotropic thermal displacement parameters U_{ij} (pm^2) for $Au_{6.19}Cr_{4.50}Zn_{91.19}$ (C8)

Atom	U_{11}	U_{22}	U_{33}	U_{23}	U_{13}	U_{12}
Zn10	70(6)	U_{11}	U_{11}	0	0	0
Zn11	204(8)	U_{11}	U_{11}	50(6)	U_{23}	U_{23}
Au12	123(1)	U_{11}	U_{11}	-7(1)	U_{23}	U_{23}
Zn13	579(16)	245(6)	U_{22}	63(8)	0	0
Zn15	242(4)	U_{11}	226(6)	-71(4)	U_{23}	23(5)
Cr20	50(2)	U_{11}	U_{11}	0	0	0
Zn21	390(4)	U_{11}	U_{11}	250(3)	U_{23}	U_{23}
Zn22	247(9)	U_{11}	U_{11}	-13(5)	U_{23}	U_{23}
Zn25	368(5)	U_{11}	218(6)	94(4)	U_{23}	138(7)
Zn30	257(10)	U_{11}	U_{11}	0	0	0
Zn32	206(4)	U_{11}	U_{11}	25(5)	U_{23}	U_{23}
Zn34	161(3)	U_{11}	249(6)	-11(3)	U_{23}	-42(4)
Zn35	217(4)	U_{11}	317(7)	-8(4)	U_{23}	12(5)
Cr42	95(4)	U_{11}	U_{11}	-14(8)	U_{23}	U_{23}
Zn43	204(8)	170(4)	U_{22}	-63(5)	0	0
Zn45	262(4)	U_{11}	121(5)	26(3)	U_{23}	-10(4)

A 29: Crystallographic and technical data for the single crystal structure refinement of $Au_{7.69}Cr_{4.30}Zn_{91.03}$ (C9)

crystallographic data	
chemical formula	$Au_{7.69}Cr_{4.30}Zn_{91.03}$
Pearson symbol	*cF*412.1
x_{Au}	0.075
crystal system	
space group type; Z	cubic; $F\bar{4}3m$ (No.216); 4
a/pm[a]	1841.2(2)
V/10^6 pm^3 [a]	6241.7(12)
ρ_{calcd}/g cm^{-3}	8.183
μ/mm^{-1}	52.890
crystal color	silvery with metallic luster
data collection	
crystal size/mm^3	0.10 x 0.06 x 0.04
Diffractometer	IPDS (Stoe & Cie.)
Radiation	$Mo_{K\alpha}$
Monochromator	Graphite
distance crystal-IP/mm	40
T/K	293(2)
φ_{min}-φ_{max}/°	0-120.0
$\Delta\varphi$	1.0
$2\theta_{max}$/°	65.94
reflns measured	13080
index range	-28≤*h*≤26 -24≤*k*≤28 -25≤*l*≤26
completeness of data set	0.995
Data reduction/ absorption correction	IPDS-software,[63] X-RED[66]/numerical, X-SHAPE[67]
unique reflns	1208
R_{int}	0.1483
structure solution, refinement	
structure solution	direct methods, SHELXS-97[64]
structure refinement	full-matrix least squires on F^2 (SHELXL-97[64])
no. reflns used	1208
no. variables	78
observed reflns (F_o>4σ(F_o))	876
R(*F*) (F_o>4σ(F_o))	0.0451
R(*F*) (all data)	0.0714
weighting factor k_1/k_2 [b]	0.0526/27.5692
wR (F^2)(all data)	0.1181
GOF (F^2)	1.042
extinction coefficient	0.000004(3)
$\Delta\rho_{min}/\rho_{max}$/$10^{-6}$epm^{-3}	-1.734/2.105

[a] Parameters determined by use of powder diffraction data. [b] Weighting scheme: $1/\omega=\sigma^2(F_O^2)+(k_1.P)^2+k_2.P$ with $P = \frac{1}{3}(\max(F_O^2,0) + .2F_c^2)$.

A 30: Structural data for $Au_{7.69}Cr_{4.30}Zn_{91.03}$ (C9)

Cluster	Atom	Site	*x*	*y*	*z*	SOF	*U*eq[a]/pm^2
Z(1)	Zn11	16e IT	0.05364(16)	*X*	*x*	1	283(9)
	Au12	16e OT	0.91347(4)	*X*	*x*	1	190(3)
	Zn13	24f OH	0.1833(3)	0	0	1	344(9)
	Zn15	48h CO	0.15550(12)	*X*	0.02370(15)	1	293(6)
Q(2)	Cr20	4b CC	¼	1/4	1/4	0.28(6)	20(8)
	Zn21	16e IT	0.3156(11)	*X*	*x*	0.66(9)	380(6)
	Zn21´	48h IT´	0.345(4)	*X*	0.3188(16)	0.08(3)	260(11)
	Zn22	16e OT	0.16854(18)	*X*	*x*	0.92(3)	285(16)
	ZN23	24g OH	0.07977(10)	1/4	1/4	0.040(13)	222(6)
	Au23	24g OH	0.07989(7)	1/4	1/4	0.612(13)	222(6)
	ZN23´	48h OH	0.2210(17)	*X*	0.385(2)	0.10(2)	520(14)
	Zn23´´	48h OH	0.2784(15)	*X*	0.116(2)	0.060(15)	220(13)
	Zn25	48h CO	0.08241(13)	*X*	0.26991(17)	1	346(6)
H(3)	Zn30	4c CC	½	1/2	1/2	1	300(2)
	Zn32	16e OT	0.41417(15)	*X*	*x*	1	270(7)
	Zn34	48h CO	0.04830(10)	*X*	0.65331(16)	1	271(5)
	Zn35	16e OT	0.18963(12)	*X*	0.52192(18)	1	325(6)
T(4)	Cr42	16e OT	0.64926(16)	*X*	*x*	1	161(9)
	Zn43	24g OH	0.64456(19)	1/4	1/4	1	232(6)
	Zn45	48h CO	0.10775(10)	*X*	0.77568(15)	1	276(5)

[a] *U*eq is defined as one third of the trace of orthogonalized U_{ij} tensor.

A 31: Anisotropic thermal displacement parameters U_{ij} (pm^2) $Au_{7.69}Cr_{4.30}Zn_{91.03}$ (C9)

Atom	U_{11}	U_{22}	U_{33}	U_{23}	U_{13}	U_{12}
Zn11	283(9)	U_{11}	U_{11}	28(10)	U_{23}	U_{23}
Au12	190(3)	U_{11}	U_{11}	-5(3)	U_{23}	U_{23}
Zn13	390(2)	319(13)	U_{22}	31(16)	0	0
Zn15	291(7)	U_{11}	298(13)	-53(7)	U_{23}	3(10)
Cr20	20(8)	U_{11}	U_{11}	0	0	0
Zn21	380(6)	U_{11}	U_{11}	190(4)	U_{23}	U_{23}
Zn22	285(16)	U_{11}	U_{11}	1(10)	U_{23}	U_{23}
Zn25	378(10)	U_{11}	283(12)	29(8)	U_{23}	77(12)
Zn30	300(2)	U_{11}	U_{11}	0	0	0
Zn32	270(7)	U_{11}	U_{11}	8(10)	U_{23}	U_{23}

Zn34	244(7)	U_{11}	327(13)	-6(6)	U_{23}	-57(9)
Zn35	320(9)	U_{11}	336(15)	-16(8)	U_{23}	-15(12)
Cr42	161(9)	U_{11}	U_{11}	-12(9)	U_{23}	U_{23}
Zn43	249(17)	224(9)	U_{22}	-37(11)	0	0
Zn45	317(8)	U_{11}	193(10)	21(6)	U_{23}	-11(9)

A 32: Crystallographic and technical data for the single crystal structure refinements of $Au_{7.88}Cr_{4.29}Zn_{90.42}$ (C10)

crystallographic data		
chemical formula		$Au_{7.88}Cr_{4.29}Zn_{90.42}$
Pearson symbol		*cF*410.4
x_{Au}		0.077
crystal system		
space group type; Z		cubic; $F\bar{4}3m$ (No.216); 4
a/pm[a]		1840.7(2)
V/10^6 pm^3 [a]		6236.6(12)
ρ_{calcd}/g cm^{-3}		8.186
μ/mm^{-1}		53.141
crystal color		
data collection		
crystal size/mm^3		0.12x0.08x0.04
Diffractometer		IPDS (Stoe &Cie.)
Radiation		$Mo_{K\alpha}$
Monochromator		Graphite
distance crystal-IP/mm		40
T/K		293(2)
φ_{min}-φ_{max}/^{o}		0-100
$\Delta\varphi$		1
$2\theta_{max}$/^{o}		66.00
reflns measured		13656
index range		-28≤*h*≤27 -20≤*k*≤27 -22≤*l*≤28
completeness of data set		0.997
Data reduction/ absorption correction	IPDS-software,[63] X-RED[66]/numerical, X-SHAPE[67]	
unique reflns		1211
R_{int}		0.1786
structure solution, refinement		
structure solution		Direct methods, SHELX-97 [64]
structure refinement	full-matrix least squires on F^2 (SHELXL-97[64])	
no. reflns used		1211
no. variables		78
observed reflns (F_o>4σ(F_o))		1027
R(*F*) (F_o>4σ(F_o))		0.0507
R(*F*) (all data)		0.0608
weighting factor k_1/k_2 [b]		0.0587/568.9284
wR (F^2)(all data)		0.1416
GOF (F^2)		1.099
extinction coefficient		0.000039(7)
$\Delta\rho_{min}/\rho_{max}$/$10^{-6}$epm^{-3}		-2.221/2.715

[a] Parameters determined by use of powder diffraction data. [b] Weighting scheme: $1/\omega=\sigma^2(F_O^2)+(k_1.P)^2+k_2.P$ with $P = \frac{1}{3}(\max(F_O^2,0) + .2F_c^2)$.

A 33: Structural data for $Au_{7.88}Cr_{4.29}Zn_{90.42}$ (C10)

Cluster	Atom	Site	*x*	*y*	*z*	SOF	*U*eq[a]/pm^2
Z(1)	Zn11	16e IT	0.05380(16)	*x*	*x*	1	271(8)
	Au12	16e OT	0.91350(3)	*x*	*x*	1	187(3)
	Zn13	24f OH	0.1835(3)	0	0	1	340(9)
	Zn15	48h CO	0.15557(12)	*x*	0.02369(15)	1	291(6)
Q(2)	Cr20	4c CC	1/4	1/4	1/4	0.29(6)	40(8)
	Zn21	16e IT	0.3167(7)	*x*	*x*	0.77(7)	420(5)
	Zn21´	48h OT´	0.3206(16)	*x*	0.349(4)	0.05(2)	70(14)
	Zn22	16e OT	0.16877(18)	*x*	*x*	0.92(3)	288(16)
	Au23	24f OH	0.07981(9)	*x*	*x*	0.647(9)	224(6)
	Zn23´	48h OH´	0.222(2)	*x*	0.390(3)	0.10(3)	600(2)
	Zn23´´	48h OH´´	0.275(2)	*x*	0.117(3)	0.07(2)	440(18)
	Zn25	48h CO	0.08232(13)	*x*	0.27010(17)	1	345(6)
H(3)	Zn30	4c CC	1/2	1/2	1/2	1	319(19)
	Zn32	16e OT	0.41416(14)	*x*	*x*	1	272(8)
	Zn34	48h CO	0.04822(9)	*x*	0.65334(15)	1	249(5)
	Zn35	16e OT	0.18957(12)	*x*	0.52214(16)	1	305(6)
T(4)	Cr42	16e OT	0.64905(15)	*x*	*x*	1	262(5)
	Zn43	24g OH	0.64454(19)	1/4	1/4	1	245(6)
	Zn45	48h CO	0.10792(10)	*x*	0.77557(14)	1	262(5)

[a] *U*eq is defined as one third of the trace of orthogonalized U_{ij} tensor.

A 34: Anisotropic thermal displacement parameters U_{ij} (pm^2) $Au_{7.88}Cr_{4.29}Zn_{90.42}$ (C10)

Atom	U_{11}	U_{22}	U_{33}	U_{23}	U_{13}	U_{12}
Zn11	272(9)	U_{11}	U_{11}	33(10)	U_{23}	U_{23}
Au12	186(3)	U_{11}	U_{11}	-11(2)	U_{23}	U_{23}
Zn13	410(2)	297(12)	U_{22}	29(15)	0	0
Zn15	289(8)	U_{11}	289(12)	-41(7)	U_{23}	-14(10)
Cr20	70(8)	U_{11}	U_{11}	0	0	0
Zn21	420(5)	U_{11}	420(5)	200(4)	U_{23}	U_{23}
Zn22	283(16)	U_{11}	U_{11}	14(10)	U_{23}	U_{23}
Zn25	371(10)	U_{11}	290(13)	45(8)	U_{23}	64(12)
Zn30	320(2)	U_{11}	U_{11}	0	0	0
Zn32	269(8)	U_{11}	U_{11}	21(10)	U_{23}	U_{23}
Zn34	211(7)	U_{11}	321(12)	-7(6)	U_{23}	-45(8)
Zn35	295(8)	U_{11}	324(14)	29(7)	U_{23}	3(10)
Cr42	158(8)	U_{11}	U_{11}	-20(9)	U_{23}	U_{23}
Zn43	251(16)	237(9)	U_{22}	-55(12)	0	0
Zn45	304(8)	U_{11}	175(10)	19(6)	U_{23}	-24(9)

A 35: Crystallographic and technical data for the single crystal structure refinement of $Au_{10.0}Cr_{4.0}Zn_{89.0}$ (C11a)

crystallographic data		
chemical formula		$Au_{10.0}Cr_{4.0}Zn_{89.0}$
Pearson symbol		*cF*412.0
x_{Au}		0.0971
crystal system		
space group type; Z		cubic; $F\bar{4}3m$ (No.216); 4
a/pm[a]		1843.0(1)
$V/10^6$ pm^3 [a]		6259.9(4)
ρ_{calcd}/g cm^{-3}		8.484
μ/mm^{-1}		57.308
crystal color		silvery with metallic luster
data collection		
crystal size/mm^3		0.10x0.08x0.04
Diffractometer		IPDS (Stoe & Cie.)
Radiation		$Mo_{K\alpha}$
Monochromator		Graphite
distance crystal-IP/mm		50
T/K		293(2)
φ_{min}-φ_{max}/^{o}		0-180
$\Delta\varphi$		1.0
$2\theta_{max}$/^{o}		64.98
reflns measured		20193
index range		$-24 \le h \le 27$ $-27 \le k \le 27$ $-24 \le l \le 25$
completeness of data set		0.997
Data reduction/ absorption correction	IPDS-software,[63] X-RED[66]/numerical, X-SHAPE[67]	
unique reflns		1170
R_{int}		0.2019
Structure solution, refinement		
structure solution		direct methods, SHELXS-97[64]
structure refinement	full-matrix least squires on F^2 (SHELXL-97[64])	
no. reflns used		1170
no. variables		63
observed reflns (F_o>4σ(F_o))		1077
$R(F)$ (F_o>4σ(F_o))		0.0517
$R(F)$ (all data)		0.0573
weighting factor k_1/k_2 [b]		0.0000/772.9188
wR (F^2)(all data)		0.0834
GOF (F^2)		1.188
extinction coefficient		0.000040(4)
$\Delta\rho_{min}/\rho_{max}$/10^{-6}epm^{-3}		-3.220/2.262

[a] Parameters determined by use of powder diffraction data. [b] Weighting scheme: $1/\omega=\sigma^2(F_O^2)+(k_1.P)^2+k_2.P$ with $P = \frac{1}{3}(\max(F_O^2,0) + .2F_c^2)$.

A 36: Crystallographic and technical data for the single crystal structure refinement of $Au_{10.0}Cr_{4.0}Zn_{89.0}$ (C11a) (T = 100K)

crystallographic data		
chemical formula		$Au_{10.0}Cr_{4.0}Zn_{89.0}$
Pearson symbol		*cF*412.0
x_{Au}		0.0971
crystal system		
space group type; Z		cubic; $F\bar{4}3m$ (No.216); 4
a/pm[a]		1843.1(1)
$V/10^6$ pm^3 [a]		6260.9(4)
ρ_{calcd}/g cm^{-3}		8.482
μ/mm^{-1}		57.299
crystal color		silvery with metallic luster
data collection		
crystal size/mm^3		0.10x0.08x0.04
Diffractometer		IPDS (Stoe & Cie.)
Radiation		$Mo_{K\alpha}$
Monochromator		Graphite
distance crystal-IP/mm		50
T/K		100(2)
φ_{min}-φ_{max}/^{o}		0-180
$\Delta\varphi$		1.0
$2\theta_{max}$/^{o}		65.72
reflns measured		20085
index range		-26≤*h*≤28
		-28≤*k*≤28
		-26≤*l*≤28
completeness of data set		0.988
Data reduction/		
absorption correction	IPDS-software,[63] X-RED[66]/numerical, X-SHAPE[67]	
unique reflns		1199
R_{int}		0.0483
structure solution, refinement		
structure solution		direct methods, SHELXS-97[64]
structure refinement	full-matrix least squires on F^2 (SHELXL-97[64])	
no. reflns used		1199
no. variables		63
observed reflns (F_o>4σ(F_o))		1189
R(*F*) (F_o>4σ(F_o))		0.0272
R(*F*) (all data)		0.0276
weighting factor k_1/k_2 [b]		0.0297/604.8721
wR (F^2)(all data)		0.0677
GOF (F^2)		1.182
extinction coefficient		0.000054(3)
$\Delta\rho_{min}/\rho_{max}$/$10^{-6}$epm^{-3}		-3.448/3.408

[a] Parameters determined by use of powder diffraction data. [b] Weighting scheme: $1/\omega=\sigma^2(F_O^2)+(k_1.P)^2+k_2.P$ with $P= ⅓(\max(F_O^2,0)+.2F_c^2)$.

A 37: Structural data for $Au_{10.0}Cr_{4.0}Zn_{89.0}$ (C11a)

Cluster	Atom	Site	*x*	*y*	*z*	SOF	*U*eq[a]/pm^2
Z(1)	Zn11	16e IT	0.05336(12)	*x*	*x*	1	110(6)
	Au12	16e OT	0.91349(3)	*x*	*x*	1	70(2)
	Zn13	24f OH	0.1845(2)	0	0	1	175(6)
	Zn15	48h CO	0.15491(10)	*x*	0.02414(12)	1	165(4)
Q(2)	Zn21	16e IT	0.3177(2)	*x*	*x*	1	248(10)
	Zn22	16e OT	0.16931(15)	*x*	*x*	1	158(7)
	Au23	24g OH	0.07963(5)	1/4	1/4	1	141(2)
	Zn25	48h CO	0.08394(10)	*x*	0.27100(13)	1	188(4)
H(3)	Zn30	4c CC	1/2	1/2	1/2	1	189(16)
	Zn32	16e OT	0.41484(12)	*x*	*x*	1	128(6)
	Zn34	48h CO	0.04799(8)	*x*	0.65341(13)	1	149(4)
	Zn35	16e OT	0.18896(9)	*x*	0.52447(12)	1	164(4)
T(4)	Cr42	16e OT	0.64890(13)	*x*	*x*	1	49(7)
	Zn43	24g OH	0.64522(15)	1/4	1/4	1	108(5)
	Zn45	48h CO	0.10831(9)	*x*	0.77576(12)	1	145(4)

[a] *U*eq is defined as one third of the trace of orthogonalized U_{ij} tensor.

A 38: Structural data for $Au_{10.0}Cr_{4.0}Zn_{89.0}$ (C11a) (T = 100K)

Cluster	Atom	Site	*x*	*y*	*z*	SOF	*U*eq[a]/pm^2
Z(1)	Zn11	16e IT	0.05319(7)	*x*	*x*	1	45(3)
	Au12	16e OT	0.91348(2)	*x*	*x*	1	27(1)
	Zn13	24f OH	0.18412(12)	0	0	1	70(3)
	Zn15	48h CO	0.15460(6)	*x*	0.02482(7)	1	58(2)
Q(2)	Zn21	16e IT	0.31913(9)	*x*	*x*	1	105(4)
	Zn22	16e OT	0.17068(8)	*x*	*x*	1	76(4)
	Au23	24g OH	0.07970(3)	1/4	1/4	1	78(13)
	Zn25	48h CO	0.08333(5)	*x*	0.27075(7)	1	71(2)
H(3)	Zn30	4c CC	1/2	1/2	1/2	1	69(8)
	Zn32	16e OT	0.41477(6)	*x*	*x*	1	31(3)
	Zn34	48h CO	0.04801(5)	*x*	0.65311(7)	1	53(2)
	Zn35	16e OT	0.18897(5)	*x*	0.52433(7)	1	74(2)
T(4)	Cr42	16e OT	0.64900(9)	*x*	*x*	1	32(4)
	Zn43	24g OH	0.64514(9)	1/4	1/4	1	44(3)
	Zn45	48h CO	0.10815(5)	*x*	0.77585(7)	1	60(4)

[a] *U*eq is defined as one third of the trace of orthogonalized U_{ij} tensor.

A 39: Anisotropic thermal displacement parameters U_{ij} (pm^2) for $Au_{10.0}Cr_{4.0}Zn_{89.0}$ (C11a)

Atom	U_{11}	U_{22}	U_{33}	U_{23}	U_{13}	U_{12}
Zn11	110(6)	U_{11}	U_{11}	22(7)	U_{23}	U_{23}
Au12	70(2)	U_{11}	U_{11}	-7(2)	U_{23}	U_{23}
Zn13	179(15)	173(10)	U_{22}	29(12)	0	0
Zn15	174(6)	U_{11}	149(10)	-53(5)	U_{23}	-26(8)
Zn21	249(10)	U_{11}	U_{11}	127(13)	U_{23}	U_{23}
Zn22	159(7)	U_{11}	U_{11}	21(7)	U_{23}	U_{23}
Au23	91(4)	166(3)	U_{22}	-15(4)	*0*	*0*
Zn25	207(7)	U_{11}	153(9)	22(6)	U_{23}	1(9)
Zn30	190(16)	U_{11}	U_{11}	0	0	0
Zn32	128(6)	U_{11}	U_{11}	14(8)	U_{23}	U_{23}
Zn34	122(6)	U_{11}	205(10)	-7(5)	U_{23}	-53(7)
Zn35	188(7)	U_{11}	119(9)	31(5)	U_{23}	-19(8)
Cr42	49(7)	U_{11}	U_{11}	-14(7)	U_{23}	U_{23}
Zn43	115(12)	105(7)	U_{22}	-36(10)	0	0
Zn45	175(6)	U_{11}	87(9)	9(5)	U_{23}	-9(7)

A 40: Anisotropic thermal displacement parameters U_{ij} (pm^2) for $Au_{10.0}Cr_{4.0}Zn_{89.0}$ (C11a) at T = 100K

Atom	U_{11}	U_{22}	U_{33}	U_{23}	U_{13}	U_{12}
Zn11	45(3)	U_{11}	U_{11}	9(4)	U_{23}	U_{23}
Au12	27(1)	U_{11}	U_{11}	-3(1)	U_{23}	U_{23}
Zn13	76(7)	68(5)	U_{22}	13(6)	0	0
Zn15	63(3)	U_{11}	49(5)	-21(3)	U_{23}	-7(4)
Zn21	106(4)	U_{11}	U_{11}	39(5)	U_{23}	U_{23}
Zn22	77(4)	U_{11}	U_{11}	9(4)	U_{23}	U_{23}
Au23	60(2)	87 (2)	U_{22}	-9(2)	*0*	*0*
Zn25	77(3)	U_{11}	60(5)	11(3)	U_{23}	7(5)
Zn30	69(8)	U_{11}	U_{11}	0	0	0
Zn32	31(3)	U_{11}	U_{11}	4(4)	U_{23}	U_{23}
Zn34	44(3)	U_{11}	73(5)	1(3)	U_{23}	-25(4)
Zn35	70(3)	U_{11}	82(5)	1(3)	U_{23}	-7(4)
Cr42	32(4)	U_{11}	U_{11}	-7(5)	U_{23}	U_{23}
Zn43	60(7)	36(4)	U_{22}	-10(5)	0	0
Zn45	74(3)	U_{11}	33(5)	6(3)	U_{23}	-10(4)

A 41: Crystallographic and technical data for the single crystal structure refinement of $Au_{10.0}Cr_{4.0}Zn_{89.0}$ (C11b)

crystallographic data	
chemical formula	$Au_{10}Cr_4Zn_{89}$
Pearson symbol	*cF*412
x_{Au}	0.0971
crystal system	
space group type; Z	cubic; $F\bar{4}3m$ (No.216); 4
a/pm[a]	1843.1(1)
V/10^6 pm^3 [a]	6261.0(6)
ρ_{calcd}/g cm^{-3}	8.482
μ/mm^{-1}	57.298
data collection	
crystal size/mm^3	0.06x0.04x0.04
Diffractometer	IPDS(Stoe &Cie)
Radiation	$Mo_{K\alpha}$
Monochromator	Graphite
distance crystal-IP/mm	40
T/K	293(2)
φ_{min}-φ_{max}/°	0-180
$\Delta\varphi$	1
$2\theta_{max}$/°	70.36
reflns measured	19618
index range	-29≤*h*≤23 -29≤*k*≤25 -29≤*l*≤29
completeness of data set	0.996
Data reduction/ absorption correction	IPDS-software,[63] X-RED[66]/numerical, X-SHAPE[67]
unique reflns	1424
R_{int}	0.2314
structure solution, refinement	
structure solution	direct methods, SHELX-97[64]
structure refinement	full-matrix least squire on F^2 (SHELXL-97[64])
no. reflns used	1424
no. variables	63
observed reflns (F_o>4σ(F_o))	1214
R(*F*) (F_o>4σ(F_o))	0.0540
R(*F*) (all data)	0.0672
weighting factor k_1/k_2 [b]	0.0/594.4132
wR (F^2)(all data)	0.0911
GOF (F^2)	1.113
extinction coefficient	0.000135(7)
$\Delta\rho_{min}/\rho_{max}$/$10^{-6}$epm^{-3}	-2.321/2.853

[a] Parameters determined by use of powder diffraction data. [b] Weighting scheme: $1/\omega=\sigma^2(F_O^2)+(k_1.P)^2+k_2.P$ with $P = \frac{1}{3}(\max(F_O^2,0) + .2F_c^2)$.

A.42: Structural data for $Au_{10.0}Cr_{4.0}Zn_{89.0}$ (C11b)

Cluster	Atom	Site	*x*	*y*	*z*	SOF	*U*eq[a]/pm^2
Z(1)	Zn11	16e IT	0.05323(13)	*x*	*x*	1	150(7)
	Au12	16e OT	0.91343(4)	*x*	*x*	1	99(2)
	Zn13	24f OH	0.1851(2)	0	0	1	178(6)
	Zn15	48h CO	0.15479(11)	*x*	0.02439(13)	1	185(5)
Q(2)	Zn21	16e IT	0.3178(2)	*x*	*x*	1	257 (10)
	Zn22	16e OT	0.17017(16)	*x*	*x*	1	169(8)
	Au23	24g OH	0.07971(5)	1/4	1/4	1	142(2)
	Zn25	48h CO	0.08405(10)	*x*	0.27099(13)	1	204 (5)
H(3)	Zn30	4c CC	1/2	1/2	1/2	1	207(17)
	Zn32	16e OT	0.41507(13)	*x*	*x*	1	136(5)
	Zn34	48h CO	0.04808(9)	*x*	0.65321(14)	1	177(4)
	Zn35	16e OT	0.18899(10)	*x*	0.52473(13)	1	183(4)
T(4)	Cr42	16e OT	0.64902(14)	*x*	*x*	1	73(7)
	Zn43	24g OH	0.64531(16)	1/4	1/4	1	132(5)
	Zn45	48h CO	0.10814(9)	*x*	0.77584(13)	1	169(4)

[a] *U*eq is defined as one third of the trace of orthogonalized U_{ij} tensor.

A 43: Anisotropic thermal displacement parameters U_{ij} (pm^2) for $Au_{10.0}Cr_{4.0}Zn_{89.0}$ (C11b)

Atom	U_{11}	U_{22}	U_{33}	U_{23}	U_{13}	U_{12}
Zn11	150(7)	U_{11}	U_{11}	20(8)	U_{23}	U_{23}
Au12	99(2)	U_{11}	U_{11}	-7(2)	U_{23}	U_{23}
Zn13	187(15)	172(9)	U_{22}	1(11)	0	0
Zn15	194(6)	U_{11}	166(10)	-39(6)	U_{23}	-19(9)
Zn21	256(10)	U_{11}	U_{11}	116(13)	U_{23}	U_{23}
Zn22	168(8)	U_{11}	U_{11}	25(8)	U_{23}	U_{23}
Au23	96(4)	165(3)	U_{22}	-12(4)	*0*	*0*
Zn25	217(7)	U_{11}	176(10)	24(6)	U_{23}	5(10)
Zn30	207(17)	U_{11}	U_{11}	0	0	0
Zn32	135(5)	U_{11}	U_{11}	8(8)	U_{23}	U_{23}
Zn34	140(6)	U_{11}	250(11)	-14(5)	U_{23}	-40(7)
Zn35	208(7)	U_{11}	133(9)	39(6)	U_{23}	-17(9)
Cr42	73(7)	U_{11}	U_{11}	-9(8)	U_{23}	U_{23}
Zn43	154(12)	120(7)	U_{22}	-18(10)	0	0
Zn45	204(6)	U_{11}	98(8)	23(5)	U_{23}	-22(8)

A 44: Magnetic data of (Au,Cr)Zn_n n = 6.4-10.2

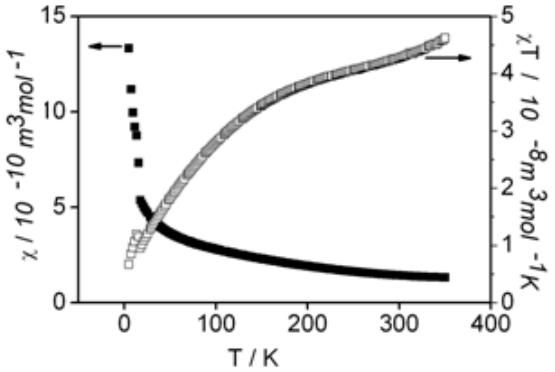

Fig A. 44.1: Magnetic Susceptibility as a function of temperature for $Au_{3.26}Cr_{5.74}Zn_{91.57}$

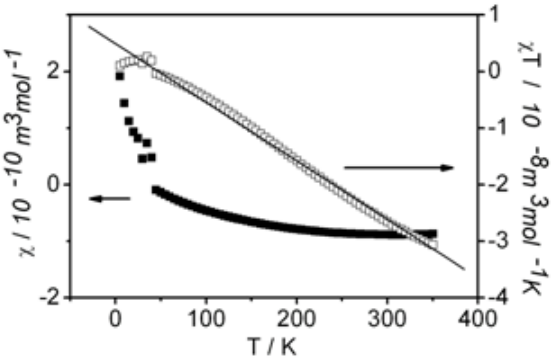

Fig A 44.2: Magnetic susceptibility as a function of temperature for $Au_{5.62}Cr_{4.57}Zn_{92.25}$

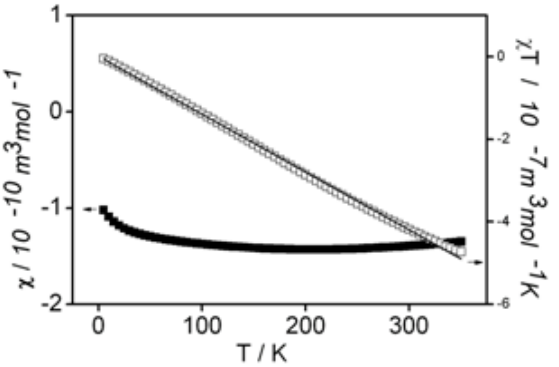

Fig A 44.3: Magnetic susceptibility as a function of temperature for $Au_{6.19}Cr_{4.50}Zn_{92.19}$

$(Pd,Cr)Zn_n$; n = 14.8-12.3

A 45: Crystallographic and technical data for the single crystal structure refinement of $Pd_{2.94}Cr_{4.78}Zn_{95.19}$ (C2)

crystallographic data	
chemical formula	$Pd_{2.94}Cr_{4.78}Zn_{95.19}$
Pearson symbol	*cF*411.7
x_{Pd}	0.028
crystal system	
space group type; Z	cubic; $F\bar{4}3m$ (No.216); 4
a/pm[a]	1831.62(5)
V/10^6 pm^3 [a]	6144.8(3)
ρ_{calcd}/g cm^{-3}	7.333
μ/mm^{-1}	37.947
crystal color	silvery with metallic luster
data collection	
crystal size/mm^3	0.10x0.08x0.05
Diffractometer	IPDS (Stoe & Cie.)
Radiation	$Mo_{K\alpha}$
Monochromator	graphite
distance crystal-IP/mm	80
T/K	293(2)
φ_{min}-φ_{max}/^{o}	0-180
$\Delta\varphi$	1
$2\theta_{max}$/^{o}	63.12
reflns measured	18560
index range	-22≤*h*≤26 -27≤*k*≤27 -27≤*l*≤25
completeness of data set	1.000
data reduction/ absorption correction	IPDS-software,[63] X-RED[66]/numerical, X-SHAPE[67]
unique reflns	1085
R_{int}	0.0617
structure solution, refinement	
structure solution	direct methods, SHELXS-97[64]
structure refinement	full-matrix least squires on F^2 (SHELXL-97[64])
no. reflns used	1085
no. variables	79
observed reflns (F_o>4σ(F_o))	1054
R(*F*) (F_o>4σ(F_o))	0.0282
R(*F*) (all data)	0.0298
weighting factor k_1/k_2 [b]	0.0425/738.4863
wR (F^2)(all data)	0.0669
GOF (F^2)	1.152

extinction coefficient	0.000045 (5)
$\Delta\rho_{min}/\rho_{max}/10^{-6}$epm^{-3}	-1.154/1.466

[a] Parameters determined by use of powder diffraction data.[b] Weighting scheme: $1/\omega=\sigma^2(F_O^2)+(k_1.P)^2+k_2.P$ with $P = \frac{1}{3}(\max(F_O^2,0) + .2F_c^2)$.

A 46: Structural data for $Pd_{2.94}Cr_{4.78}Zn_{95.19}$ (C2)

Cluster	Atom	Site	*x*	*y*	*z*	SOF	*U*eq[a]/pm^2
Z(1)	Zn11	16e IT	0.05386(6)[b]	*x*	*x*	1	142(3)
	M12[b]	16e OT	0.91442(4)	*x*	*x*	0.74(2)	88(4)
	Zn13	24f OH	0.17818(9)	0	0	1	198(3)
	Zn15	48h CO	0.15720(4)	*x*	0.02016(5)	1	120(2)
Q(2)	Cr20	4c CC	1/4	1/4	1/4	0.79(3)	99(18)
	Zn21	16e IT	0.3097(4)	*x*	*x*	0.251(16)	210(4)
	Zn21´	48h IT´	0.3220(2)	*x*	0.3462(4)	0.164(7)	130(2)
	Zn22	16e OT	0.16537(6)	*x*	*x*	0.946(10)	141(6)
	Zn23	24g OH	0.08709(15)	1/4	1/4	0.638(12)	153(9)
	Zn23´	48h OH´	0.2771(3)	*x*	0.3903(4)	0.163(7)	180(2)
	Zn23´´	48h OH´´	0.2744(11)	*x*	0.1131(15)	0.039(7)	120(9)
	Zn25	48h CO	0.08030(7)	*x*	0.26863(7)	1	265(3)
H(3)	Zn30	4c CC	1/2	1/2	1/2	1	136(6)
	Zn32	16e OT	0.41387(6)	*x*	*x*	1	118(3)
	Zn34	48h CO	0.04831(4)	*x*	0.65361(6)	1	116(2)
	Zn35	16e OT	0.19014(4)	*x*	0.51929(6)	1	133(2)
T(4)	Cr42	16e OT	0.64880(7)	*x*	*x*	1	79(4)
	Zn43	24g OH	0.64356(8)	1/4	1/4	1	119(3)
	Zn45	48h CO	0.10709(4)	*x*	0.77684(5)	1	128(2)

[a] *U*eq is defined as one third of the trace of orthogonalized U_{ij} tensor. [b] SOF(Pd), SOF(Zn)=1-SOF(Pd).

A 47: Anisotropic thermal displacement parameters U_{ij} (pm^2) for $Pd_{2.94}Cr_{4.78}Zn_{95.19}$ (C2)

Atom	U_{11}	U_{22}	U_{33}	U_{23}	U_{13}	U_{12}
Zn11	142(3)	U_{11}	U_{11}	14(4)	U_{23}	U_{23}
M12	88(4)	U_{11}	U_{11}	-6(2)	U_{23}	U_{23}
Zn13	199(7)	197(4)	U_{22}	47(6)	0	0
Zn15	123(3)	U_{11}	112(4)	-10(2)	U_{23}	2(3)
Cr20	99(18)	U_{11}	U_{11}	0	0	0
Zn21´	210(4)	U_{11}	U_{11}	130(3)	U_{23}	U_{23}
Zn22	141(6)	U_{11}	U_{11}	-15(4)	U_{23}	U_{23}
Zn25	328(4)	U_{11}	138(5)	96(4)	U_{23}	197(5)
Zn30	136(6)	U_{11}	U_{11}	0	0	0
Zn32	118(3)	U_{11}	U_{11}	16(4)	U_{23}	U_{23}
Zn34	96(3)	U_{11}	157(4)	-5(2)	U_{23}	U_{23}
Zn35	122(3)	U_{11}	175(5)	1(3)	U_{23}	10(3)
Cr42	79(4)	U_{11}	U_{11}	-12(4)	U_{23}	U_{23}
Zn43	145(6)	106(4)	U_{22}	-15(4)	0	0
Zn45	147(3)	U_{11}	89(4)	14(2)	U_{23}	5(3)

A 48: Crystallographic and technical data for the single crystal structure refinement of $Pd_{2.95}Cr_{4.70}Zn_{95.11}$ (C3)

crystallographic data	
chemical formula	$Pd_{2.95}Cr_{4.70}Zn_{95.11}$
Pearson symbol	*cF*411.0
x_{Pd}	0.029
crystal system	
space group type; Z	cubic; $F\bar{4}3m$ (No.216); 4
a/pm[a]	1833.99(6)
$V/10^6$ pm^3 [a]	6168.7(3)
ρ_{calcd}/g cm^{-3}	7.296
μ/mm^{-1}	37.761
crystal color	silvery with metallic luster
data collection	
crystal size/mm^3	0.08x0.07x0.04
Diffractometer	IPDS (Stoe & Cie.)
Radiation	$Mo_{K\alpha}$
Monochromator	Graphite
distance crystal-IP/mm	80
T/K	293(2)
φ_{min}-φ_{max}/^{o}	0-180
$\Delta\varphi$	1
$2\theta_{max}$/^{o}	63.18
reflns measured	18553
index range	-22≤*h*≤27 -27≤*k*≤27 -23≤*l*≤27
completeness of data set	0.998
data reduction/ absorption correction	IPDS-software,[63] X-RED[66]/numerical, X-SHAPE[67]
unique reflns	1083
R_{int}	0.0588
Structure solution, refinement	
structure solution	direct methods, SHELXS-97[64]
structure refinement	full-matrix least squires on F^2 (SHELXL-97[64])
no. reflns used	1083
no. variables	81
observed reflns (F_o>4σ(F_o))	1033
R(*F*) (F_o>4σ(F_o))	0.0294
R(*F*) (all data)	0.0322
weighting factor k_1/k_2 [b]	0.0162/224.5816
wR (F^2)(all data)	0.0531
GOF (F^2)	1.096
extinction coefficient	0.000034 (2)
$\Delta\rho_{min}/\rho_{max}/10^{-6}$epm^{-3}	-1.296/1.080

[a] Parameters determined by use of powder diffraction data. [b] Weighting scheme: $1/\omega=\sigma^2(F_O^2)+(k_1.P)^2+k_2.P$ with $P= \frac{1}{3}(\max(F_O^2,0)+.2F_c^2)$.

A 49: Structural data for $Pd_{2.95}Cr_{4.70}Zn_{95.11}$ (C3)

Cluster	Atom	Site	*x*	*y*	*z*	SOF	*U*eq[a]/pm^2
Z(1)	Zn11	16e IT	0.05382(6) [b]	*x*	*x*	1	129(3)
	M12[b]	16e OT	0.91443(4)	*x*	*x*	0.74(2)	84(4)
	Zn13	24f OH	0.17836(10)	0	0	1	187(3)
	Zn15	48h CO	0.15708(4)	*x*	0.02013(6)	1	113(2)
Q(2)	Cr20	4c CC	1/4	1/4	1/4	0.73(3)	90(2)
	Zn21	16e IT	0.3096(4)	*x*	*x*	0.285(16)	190(4)
	Zn21´	48h IT´	0.3218(3)	*x*	0.3461(5)	0.152(7)	90(2)
	Zn22	16e OT	0.16536(6)	*x*	*x*	0.949(10)	136(6)
	Zn23	24g OH	0.08631(17)	1/4	1/4	0.639(13)	129(10)
	Zn23´	48h OH´	0.2777(3)	*x*	0.3900(4)	0.151(8)	160(3)
	Zn23´´	48h OH´´	0.2726(14)	*x*	0.1079(17)	0.045(9)	170(10)
	Zn25	48h CO	0.08064(7)	*x*	0.26870(7)	1	257(3)
H(3)	Zn30	4c CC	1/2	1/2	1/2	1	135(7)
	Zn32	16e OT	0.41397(6)	*x*	*x*	1	112(3)
	Zn34	48h CO	0.04824(4)	*x*	0.65366(6)	1	110(2)
	Zn35	16e OT	0.19014(4)	*x*	0.51929(6)	1	133(2)
T(4)	Cr42	16e OT	0.64879(7)	*x*	*x*	1	73(4)
	Zn43	24g OH	0.64377(8)	1/4	1/4	1	117(3)
	Zn45	48h CO	0.10712(4)	*x*	0.77691(6)	1	124(2)

[a] *U*eq is defined as one third of the trace of orthogonalized U_{ij} tensor. [b] SOF(Pd), SOF(Zn)=1-SOF(Pd).

A 50: Anisotropic thermal displacement parameters U_{ij} (pm^2) for $Pd_{2.95}Cr_{4.70}Zn_{95.11}$ (C3)

Atom	U_{11}	U_{22}	U_{33}	U_{23}	U_{13}	U_{12}
Zn11	129(3)	U_{11}	U_{11}	9(4)	U_{23}	U_{23}
M12	84(4)	U_{11}	U_{11}	-8(2)	U_{23}	U_{23}
Zn13	179(8)	192(5)	*U*22	49(6)	0.000	0.000
Zn15	116(3)	U_{11}	108(4)	-15(2)	U_{23}	-4(3)
Cr20	90(2)	U_{11}	U_{11}	0	0	0
Zn21	190(4)	U_{11}	U_{11}	170(3)	U_{23}	U_{23}
Zn22	136(6)	U_{11}	U_{11}	-13(4)	U_{23}	U_{23}
Zn23	178(15)	105(11)	U_{22}	-45(11)	0	0
Zn25	321(4)	U_{11}	129(5)	91(4)	U_{23}	203(6)
Zn30	135(7)	U_{11}	U_{11}	0	0	0
Zn32	112(3)	U_{11}	U_{11}	13(4)	U_{23}	U_{23}
Zn34	89(3)	U_{11}	153(5)	-3(2)	U_{23}	-18(3)
Zn35	110(3)	U_{11}	178(5)	-5(3)	U_{23}	19(4)
Cr42	73(4)	U_{11}	U_{11}	-16(4)	U_{23}	U_{23}
Zn43	145(7)	104(4)	U_{22}	-11(5)	0	0
Zn45	144(3)	U_{11}	85(4)	10(2)	U_{23}	4(4)

A 51: Minimum (d_{min}), maximum (d_{max}) and mean interatomic distances (<d>) and coordination numbers (C.N.) for $Pd_{1.40}Cr_{5.00}Zn_{94.66}$ (C1), $Pd_{3.12}Cr_{4.64}Zn_{95.16}$ (C4), $Pd_{3.28}Cr_{4.48}Zn_{95.36}$ (C5)

Cluster	Atoms	Site	C1 d_{min}-d_{max} <d> (pm)	C.N.	C4 d_{min}-d_{max} <d> (pm)	C.N	C5 d_{min}-d_{max} <d> (pm)	C.N.
Z(1)	Zn10	CC	270.3-310.9 <294.7>	10	- -	-	- -	- -
	Zn11	IT	253.9-281.5 <268.7>	12	268.0-277.7 <272.2>	12	268.3-276.4 <271.9>	12
	M12	OT	258.8-270.3 <266.6>	13	258.3-279.9 <268.6>	13	257.8-280.6 <268.4>	12
	Zn13	OH	253.9-347.9 <288.4>	15	268.0-332.0 <289.1>	14	268.9-330.8 <289.5>	14
	Zn15	CO	264.7-300.5 <278.7>	12	267.4-296.5 <279.9>	12	267.0-298.3 <280.1>	12
Q(2)	Cr20	CC	258.9-287.1 <273.5>	14	256.2-302.8 <279.7>	14	258.4-306.8 <282.0>	14
	Zn21	IT	- -	- -	247.6-333.2 <284.1>	- -	251.0-330.6 <284.7>	13
	Zn21´	IT´	253.8-336.3 -	12	242.3-332.6 -	12	236.9-331.8	12
	Zn22	OT	255.8-296.1 <275.5>	13	264.4-288.4 <273.2>	13	266.6-286.0 <273.3>	12
	M23	OH	253.3-287.1 <266.6>	9	246.9-311.3 <275.1>	12	245.4-307.8 <274.5>	12
	Zn23´	OH´	245.8-325.2 -	12	251.5-328.7 -	12	251.8-303.5 -	12
	Zn23´´	OH´´	247.9-311.8 -	11	246.4-312.3 -	11	- -	-
	Zn25	CO	255.0-321.8 <307.2>	12	266.7-311.3 <284.6>	12	266.3-307.8 <284.2>	12
H(3)	Zn30	CC	277.3-306.7 <299.4>	16	272.6-308.7 <299.7>	16	271.5-308.9 <299.5>	16
	Zn32	OT	263.4-285.2 <276.1>	13	266.7-284.2 <276.1>	11	266.3-283.8 <275.3>	13
	Zn34	CO	250.5-306.7 <275.3>	12	250.4-308.7 <276.9>	12	250.1-308.9 <277.4>	12
	Zn35	OT	253.3-329.2 <285.3>	14	246.9-332.7 <285.4>	14	245.4-333.6 <285.6>	14
T(4)	Cr42	OT	258.9-264.6 <261.5>	12	258.7-262.7 <260.5>	12	258.3-261.7 <260.2>	12
	Zn43	OH	262.9-277.1 <274.5>	12	262.7-275.5 <273.2>	12	262.1-275.1 <272.5>	12
	Zn45	CO	258.8-304.5 <279.1>	12	258.3-300.6 <277.7>	12	257.8-299.2 <277.4>	12

γ'-brass phases in the Au-Pd-Zn system

A 52: Powder pattern indexation, 2θobs (≤ 90°) values (measured CuKα), calculated and observed X-ray intensities for $Au_{13.02}Pd_{10.11}Zn_{77.46}$ (xAu = 0.13, a = 1816.2(1) pm)), $I_0 \geq 0.02 I_{max}$

h	*k*	*l*	*2θ(°)*	I_{cal}	I_{obs}
1	3	3	21.237	73	63
2	2	4	23.905	205	213
1	1	5	25.379	112	106
3	3	3	25.379	66	62
0	2	6	31.015	25	25
4	4	4	34.062	19	20
2	4	6	36.885	23	24
3	3	7	40.489	88	91
0	6	6	42.042	980	1000
2	2	8	42.042	665	678
5	5	5	42.951	44	46
2	4	8	45.592	19	21
4	6	6	46.728	41	44
4	4	8	48.938	82	87
3	3	9	49.748	35	35
0	0	12	60.967	66	67
4	8	8	60.967	95	96
1	5	11	61.668	42	41
4	6	10	62.825	49	48
2	6	12	69.981	26	24
3	3	13	70.633	23	22
8	8	8	71.715	73	69
0	10	10	73.432	59	52
2	4	14	76.823	125	127
6	6	12	76.823	119	122
2	8	14	86.767	120	125
0	4	16	88.407	30	31

A 53: Anisotropic thermal displacement parameters U_{ij} (pm^2) $Au_{13.02}Pd_{10.11}Zn_{77.46}$ (C1)

Atom	U_{11}	U_{22}	U_{33}	U_{23}	U_{13}	U_{12}
Zn11	140(3)	U_{11}	U_{11}	40(4)	U_{23}	U_{23}
Zn11´	117(14)	U_{11}	U_{11}	15(10)	U_{23}	U_{23}
Au12	220(4)	U_{11}	U_{11}	-10(2)	U_{23}	U_{23}
M13	98(5)	89(4)	U_{22}	-2(4)	0	0
Zn14	210(8)	U_{11}	162(11)	-46(7)	U_{23}	71(10)
Zn21	127(8)	U_{11}	U_{11}	49(8)	U_{23}	U_{23}
M22	86(5)	U_{11}	U_{11}	9(3)	U_{23}	U_{23}
M23	144(16)	114(11)	U_{33}	14(9)	0	0
Zn24	124(7)	U_{11}	95(10)	18(5)	U_{23}	-7(8)
Zn31	108(7)	U_{11}	U_{11}	18(7)	U_{23}	U_{23}
M32	84(6)	U_{11}	U_{11}	7(4)	U_{23}	U_{23}
M33	118(14)	80(10)	U_{22}	-7(9)	0	0
Zn34	139(7)	U_{11}	92(9)	11(5)	U_{23}	-21(8)
Zn41	102(7)	U_{11}	U_{11}	12(7)	U_{23}	U_{23}
Pd42	133(6)	U_{11}	U_{11}	18(5)	U_{23}	U_{23}
M43	92(6)	120(5)	U_{22}	-18(4)	0	0
Zn44	134(7)	U_{11}	183(11)	30(6)	U_{23}	-28(8)

A 54: Anisotropic thermal displacement parameters U_{ij} (pm^2) for $Au_{13.34}Pd_{10.45}Zn_{77.03}$ (C2)

Atom	U_{11}	U_{22}	U_{33}	U_{23}	U_{13}	U_{12}
Zn11	110(3)	U_{11}	U_{11}	-20(2)	U_{23}	U_{23}
Zn11´	102(14)	U_{11}	U_{11}	0(10)	U_{23}	U_{23}
Au12	170(2)	U_{11}	U_{11}	-20(12)	U_{23}	U_{23}
M13	107(5)	98(4)	U_{22}	3(3)	0	0
Zn14	224(8)	U_{11}	142(10)	-67(6)	U_{23}	125(9)
Zn21	116(7)	U_{11}	U_{11}	20(7)	U_{23}	U_{23}
M22	95(6)	U_{11}	U_{11}	4(3)	U_{23}	U_{23}
M23	162(14)	146(10)	U_{33}	13(9)	0	0
Zn24	103(6)	U_{11}	104(9)	14(5)	U_{23}	-9(7)
Zn31	95(6)	U_{11}	U_{11}	-3(6)	U_{23}	U_{23}
M32	76(6)	U_{11}	U_{11}	4(4)	U_{23}	U_{23}
M33	155(13)	126(10)	U_{22}	-13(8)	0	0
Zn34	104(6)	U_{11}	98(9)	8(4)	U_{23}	-18(6)
Zn41	96(7)	U_{11}	U_{11}	-15(6)	U_{23}	U_{23}
Pd42	110(6)	U_{11}	U_{11}	6(4)	U_{23}	U_{23}
M43	109(6)	139(5)	U_{22}	-17(4)	0	0
Zn44	119(7)	U_{11}	206(10)	34(5)	U_{23}	-27(7)

A 55: Anisotropic thermal displacement parameters U_{ij} for $Au_{13.42}Pd_{10.84}Zn_{76.98}$ (C3)

Atom	U_{11}	U_{22}	U_{33}	U_{23}	U_{13}	U_{12}
Zn11	210(5)	U_{11}	U_{11}	-19(18)	U_{23}	U_{23}
Zn11´	150(2)	U_{11}	U_{11}	-37(16)	U_{23}	U_{23}
Au12	205(19)	U_{11}	U_{11}	-18(12)	U_{23}	U_{23}
M13	150(8)	131(6)	U_{22}	-7(5)	0	0
Zn14	273(12)	U_{11}	194(14)	-69(9)	U_{23}	130(12)
Zn21	141(9)	U_{11}	U_{11}	26(9)	U_{23}	U_{23}
M22	130(8)	U_{11}	U_{11}	4(4)	U_{23}	U_{23}
M23	212(19)	196(14)	U_{33}	5(12)	0	0
Zn24	136(8)	U_{11}	145(12)	14(6)	U_{23}	-7(9)
Zn31	134(8)	U_{11}	U_{11}	0(9)	U_{23}	U_{23}
M32	127(8)	U_{11}	U_{11}	-3(4)	U_{23}	U_{23}
M33	204(18)	178(13)	U_{22}	-26(11)	0	0
Zn34	155(9)	U_{11}	129(12)	16(6)	U_{23}	-26(9)
Zn41	135(9)	U_{11}	U_{11}	-16(9)	U_{23}	U_{23}
Pd42	111(7)	U_{11}	U_{11}	3(6)	U_{23}	U_{23}
M43	147(10)	172(7)	U_{22}	-19(6)	0	0
Zn44	154(9)	U_{11}	253(15)	34(7)	U_{23}	-39(9)

A 56: Anisotropic thermal displacement parameters U_{ij} (pm^2) for $Au_{13.22}Pd_{7.26}Zn_{78.99}$ (C4)

Atom	U_{11}	U_{22}	U_{33}	U_{23}	U_{13}	U_{12}
Zn11´	88(8)	U_{11}	U_{11}	15(9)	U_{23}	U_{23}
Au13	40(5)	45(4)	U_{22}	-1(4)	0	0
Zn14	112(7)	U_{11}	125(11)	-41(6)	U_{23}	41(8)
Zn21	68(8)	U_{11}	U_{11}	34(8)	U_{23}	U_{23}
M22	28(6)	U_{11}	U_{11}	-3(3)	U_{23}	U_{23}
Zn23	70(18)	91(11)	U_{33}	30(14)	0	0
Zn24	68(7)	U_{11}	35(10)	20(5)	U_{23}	-9(8)
Zn31	61(7)	U_{11}	U_{11}	11(8)	U_{23}	U_{23}
M32	49(8)	U_{11}	U_{11}	2(5)	U_{23}	U_{23}
Zn33	49(15)	33(9)	U_{22}	-14(12)	0	0
Zn34	96(8)	U_{11}	51(10)	7(5)	U_{23}	-25(8)
Zn41	57(7)	U_{11}	U_{11}	-27(8)	U_{23}	U_{23}
M42	74(9)	U_{11}	U_{11}	16(7)	U_{23}	U_{23}
M43	53(7)	91(6)	U_{22}	-22(5)	0	0
Zn44	92(7)	U_{11}	95(11)	13(6)	U_{23}	-24(8)

A 57: Anisotropic thermal displacement parameters U_{ij} (pm^2) for $Au_{14.08}Pd_{7.19}Zn_{78.38}$ (C5)

Atom	U_{11}	U_{22}	U_{33}	U_{23}	U_{13}	U_{12}
Zn11´	92(5)	U_{11}	U_{11}	4(5)	U_{23}	U_{23}
Au13	67(3)	73(2)	U_{22}	-1(4)	0	0
Zn14	132(5)	U_{11}	128(7)	-51(4)	U_{23}	57(6)
Zn21	106(5)	U_{11}	U_{11}	29(6)	U_{23}	U_{23}
M22	59(4)	U_{11}	U_{11}	-2(2)	U_{23}	U_{23}
Zn23	72(10)	98(7)	U_{33}	21(8)	0	0
Zn24	105(5)	U_{11}	73(8)	14(4)	U_{23}	-16(6)
Zn31	90(5)	U_{11}	U_{11}	8(5)	U_{23}	U_{23}
M32	64(6)	U_{11}	U_{11}	1(3)	U_{23}	U_{23}
Zn33	59(9)	86(6)	U_{22}	-13(8)	0	0
Zn34	105(5)	U_{11}	84(7)	15(3)	U_{23}	-17(6)
Zn41	80(5)	U_{11}	U_{11}	-11(5)	U_{23}	U_{23}
M42	93(7)	U_{11}	U_{11}	18(4)	U_{23}	U_{23}
M43	70(5)	116(4)	U_{22}	-25(3)	0	0
Zn44	121(5)	U_{11}	107(7)	8(4)	U_{23}	-26(6)

A 58: Anisotropic thermal displacement parameters U_{ij} (pm^2) for $Au_{14.27}Pd_{7.54}Zn_{78.19}$ (C7)

Atom	U_{11}	U_{22}	U_{33}	U_{23}	U_{13}	U_{12}
Zn11´	108(6)	U_{11}	U_{11}	17(7)	U_{23}	U_{23}
Au13	90(4)	88(3)	U_{22}	4(3)	0	0
Zn14	147(6)	U_{11}	144(8)	-50(5)	U_{23}	51(7)
Zn21	109(6)	U_{11}	U_{11}	28(7)	U_{23}	U_{23}
M22	86(4)	U_{11}	U_{11}	-4(2)	U_{23}	U_{23}
Zn23	92(12)	112(8)	U_{33}	32(14)	0	0
Zn24	128(6)	U_{11}	88(8)	12(4)	U_{23}	-23(7)
Zn31	114(6)	U_{11}	U_{11}	19(6)	U_{23}	U_{23}
M32	83(6)	U_{11}	U_{11}	00(4)	U_{23}	U_{23}
Zn33	57(11)	99(7)	U_{22}	-23(9)	0	0
Zn34	103(5)	U_{11}	71(8)	15(4)	U_{23}	-13(6)
Zn41	78(5)	U_{11}	U_{11}	-18(6)	U_{23}	U_{23}
M42	101(5)	U_{11}	U_{11}	18(4)	U_{23}	U_{23}
M43	85(5)	148(4)	U_{22}	-26(3)	0	0
Zn44	138(6)	U_{11}	130(9)	7(6)	U_{23}	-41(7)

A 59: Crystallographic and technical data for the single crystal structure refinements of $Au_{14.13}Pd_{7.59}Zn_{78.29}$ (C6)

	C6
crystallographic data	
chemical formula	$Au_{14.13}Pd_{7.59}Zn_{78.29}$
Pearson symbol	*cF*400.0
x_{Au}	0.14
crystal system	
space group type; Z	cubic; $F\bar{4}3m$ (No.216); 4
a/pm[a]	1814.3(1)
$V/10^6$ pm^3 [a]	5972.4(5)
ρ_{calcd}/g cm^{-3}	9.684
μ/mm^{-1}	67.471
crystal color	silvery with metallic luster
data collection	
crystal size/mm^3	0.11x0.06x0.04
diffractometer	IPDS (Stoe & Cie.)
radiation	$Mo_{K\alpha}$
monochromator	graphite
distance crystal-IP/mm	50
φ_{min}-φ_{max}/^{o}	0-180
$\Delta\varphi$	1
$2\theta_{max}$/^{o}	61.22
reflns measured	15903
index range	-25≤*h*≤25 -25≤*k*≤25 -25≤*l*≤25
completeness of data set	0.985
data reduction/ absorption correction	IPDS-software,[63] X-RED[66]/numerical, X-SHAPE[67]
unique reflns	956
R_{int}	0.0496
structure solution, refinement	
structure solution	direct methods, SHELXS-97[64]
structure refinement	full-matrix least squires on F^2 (SHELXL-97[64])
no. reflns used	956
no. variables	67
observed reflns (F_o>4σ(F_o))	929
R(*F*) (F_o>4σ(F_o))	0.0313
R(*F*) (all data)	0.0338
weighting factor k_1/k_2 [b]	0.0303/662.6765
wR (F^2)(all data)	0.0758
GOF (F^2)	1.149
extinction coefficient	0.0000219(19)
$\Delta\rho_{min}/\rho_{max}$/$10^{-6}$epm^{-3}	-2.106/2.468

[a] Parameters determined by use of single crystal diffraction data. [b] Weighting scheme: $1/\omega=\sigma^2(F_O^2)+(k_1.P)^2+k_2.P$ with $P = ⅓(\max(F_O^2,0) + .2F_c^2)$.

A 60: Structural data for $Au_{14.13}Pd_{7.59}Zn_{78.29}$ (C6)

Cluster	Atom	Site		*x*	*y*	*z*	SOF	*U*eq[a]/pm^2
Z(1)	Zn11´	16e	IT´	0.94592(11)	*x*	*x*	1	155(6)
	Au13	24g	OH	0.18070(4)	0	0	1	102(2)
	Zn14	48h	CO	0.14480(9)	*x*	0.02198(13)	1	231(5)
Q(2)	Zn21	16e	IT	0.30796(12)	*x*	*x*	1	168(7)
	M22[b]	16e	OT	0.16545(4)	*x*	*x*	0.633(11)	87(4)
	Zn23	24f	OH	0.07099(15)	1/4	1/4	1	123(6)
	Zn24	48h	CO	0.09182(7)	*x*	0.26513(11)	1	162(4)
H(3)	Zn31	16e	IT	0.55412(11)	*x*	*x*	1	131(6)
	M32[c]	16e	OT	0.41099(6)	*x*	*x*	0.103(12)	84(6)
	Zn33	24f	OH	0.32394(15)	0	0	1	116(5)
	Zn34	48h	CO	0.34495(7)	*x*	0.51960(12)	1	153(4)
T(4)	Zn41	16e	IT	0.80207 (10)	*x*	*x*	1	108(5)
	Pd42	16e	OT	0.66019(6)	*x*	*x*	1	108(4)
	M43[d]	24f	OH	0.56774(5)	1/4	1/4	0.863(10)	158(4)
	Zn44	48h	CO	0.09748(8)	*x*	0.77982(12)	1	197(4)

[a] *U*eq is defined as one third of the trace of orthogonalized U_{ij} tensor. [b] SOF(Au), SOF(Zn)=1-SOF(Au). [c] SOF(Au), SOF(Pd)=1-SOF(Au). [d] SOF(Au),SOF(Zn)=1-SOF(Au).

A 61: Anisotropic thermal displacement parameters U_{ij} (pm^2) for $Au_{14.13}Pd_{7.59}Zn_{78.29}$

Atom	U_{11}	U_{22}	U_{33}	U_{23}	U_{13}	U_{12}
Zn11´	155(6)	U_{11}	U_{11}	39(7)	U_{23}	U_{23}
Au13	91(4)	108(3)	U_{22}	4(3)	0	0
Zn14	249(7)	U_{11}	196(9)	-97(6)	U_{23}	116(8)
Zn21	168(7)	U_{11}	U_{11}	78(8)	U_{23}	U_{23}
M22	87(4)	U_{11}	U_{11}	-4(2)	U_{23}	U_{23}
Zn23	92(12)	139(8)	U_{33}	2(10)	0	0
Zn24	193(6)	U_{11}	100(8)	26(5)	U_{23}	-57(7)
Zn31	131(6)	U_{11}	U_{11}	27(7)	U_{23}	U_{23}
M32	84(6)	U_{11}	U_{11}	6(3)	U_{23}	U_{23}
Zn33	66(10)	141(7)	U_{22}	-56(10)	0	0
Zn34	167(6)	U_{11}	124(9)	35(4)	U_{23}	-56(7)
Zn41	108(5)	U_{11}	U_{11}	-6(6)	U_{23}	U_{23}
M42	108(4)	U_{11}	U_{11}	22(4)	U_{23}	U_{23}
M43	94(5)	191(4)	U_{22}	-70(4)	0	0
Zn44	189(6)	U_{11}	212(10)	28(5)	U_{23}	-70(7)

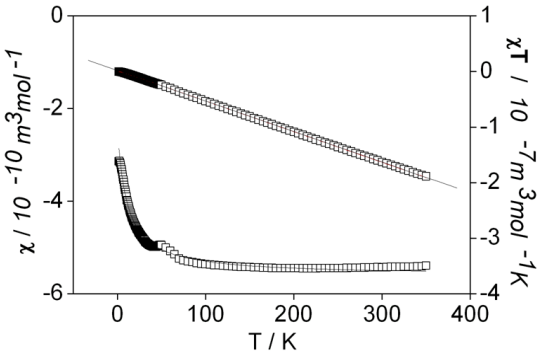

Fig A.62: Magnetic susceptibility as a function of temperature for $Au_{14.1}Ru_{7.2}Zn_{78.4}$

$(Au,Ru)Zn_n$; n = 10.7-3.2

A 63: Crystallographic and technical data for the single crystal $Au_{36.23}Ru_{25.55}Zn_{218.20}$ (C3)

	C3
crystallographic data	
chemical formula	$Au_{36.23}Ru_{25.55}Zn_{218.20}$
Pearson symbol	*hP*560
x_{Au}	0.129
crystal system	
space group type; Z	hexagonal; $P6_3/mmc$ (194); 2
a/pm	1294.70(3)
c/pm	5778.7(3)
$V/10^6$ pm^3 [a]	8389.1(4)
ρ_{calcd}/g cm^{-3}	9.494
μ/mm^{-1}	64.223
crystal color	silvery with metallic luster
data collection	
crystal size/mm^3	0.08x0.06x0.03
Diffractometer	IPDS (Stoe & Cie.)
Radiation	$Mo_{K\alpha}$
Monochromator	graphite
distance crystal-IP/mm	140
φ_{min}-φ_{max}/°	0-180
$\Delta\varphi$	1
$2\theta_{max}$/°	50
reflns measured	40740
index range	-12≤*h*≤15 -15≤*k*≤14 -67≤*l*≤67
completeness of data set	0.978
data reduction/ absorption correction	IPDS-software,[63] X-RED[66]/numerical, X-SHAPE[67]
unique reflns	2700
R_{int}	0.1096
structure solution, refinement	
structure solution	direct methods, SHELXS-97[64]
structure refinement	full-matrix least squires on F^2 (SHELXL-97[64])
no. reflns used	2700
no. variables	302
observed reflns (F_o>4σ(F_o))	2117
R(*F*) (F_o>4σ(F_o))	0.0441
R(*F*) (all data)	0.0636
weighting factor k_1/k_2 [b]	0.0683/0
wR (F^2)(all data)	0.1090

GOF (F^2)	0.982
$\Delta\rho_{min}/\rho_{max}/10^{-6}$epm^{-3}	-1.964/1.862

[a] Parameters determined by use of single crystal diffraction data. [b] Weighting scheme: $1/\omega=\sigma^2(F_O^2)+(k_1.P)^2+k_2.P$ with P = ⅓(max $(F_O^2,0)$ +.2F_c^2)

A 64: Anisotropic thermal displacement parameters U_{ij} (pm^2) for $Au_{36.2}$ $Ru_{25.5}$ $Zn_{218.2}$ (C3)

Atoms	*U*11	*U*22	*U*33	*U*23	*U*13	*U*12
Ru01	279(17)	*U*11	490(3)	0	*U*23	139(8)
Zn02	329(12)	306(16)	420(15)	-15(12)	-8(6)	153(8)
Zn03	298(16)	337(12)	437(16)	-10(6)	-20(12)	149(8)
Zn04	335(17)	323(12)	446(15)	-9(6)	-18(13)	168(8)
Zn05	314(12)	338(12)	483(11)	-20(9)	-11(9)	175(10)
Zn06	340(12)	324(17)	424(16)	16(13)	8(6)	162(8)
Zn07	312(12)	*U*11	471(16)	4(6)	-4(6)	163(13)
Ru08	304(8)	288(11)	429(11)	2(9)	1(4)	144(6)
Ru09	262(11)	282(8)	430(11)	-4(4)	-7(8)	131(6)
Zn10	360(13)	363(18)	456(16)	22(13)	11(7)	181(9)
Zn11	327(12)	294(12)	506(11)	13(9)	-18(9)	140(10)
Zn12	351(13)	351(12)	466(12)	-25(9)	3(9)	134(10)
Zn13	343(17)	324(12)	436(15)	-1(6)	-1(13)	172(8)
Zn14	320(12)	*U*11	471(17)	-5(6)	5(6)	165(14)
Zn15	314(12)	*U*11	443(15)	-13(7)	13(7)	144(14)
Zn16	354(13)	370(18)	426(16)	-57(13)	-29(7)	185(9)
Zn17	304(18)	*U*11	500(3)	0	*U*23	152(9)
Zn18	315(17)	350(2)	470(2)	0	*U*23	173(12)
Zn19	340(13)	*U*11	448(16)	13(6)	-13(6)	184(14)
Ru20	301(12)	*U*11	418(19)	0	*U*23	150(6)
Ru21	275(11)	*U*11	453(16)	0	*U*23	128(13)
Zn22	349(12)	*U*11	472(17)	-10(6)	10(6)	171(14)
Zn23	340(13)	*U*11	598(19)	-5(7)	5(7)	173(15)
Zn24	356(13)	359(18)	464(15)	-33(13)	-17(7)	180(9)
Zn25	394(18)	337(18)	478(16)	0	*U*23	215(15)
Zn26	334(12)	317(12)	468(12)	-22(9)	-27(9)	141(10)
Zn27	321(12)	304(17)	540(18)	-17(13)	-8(7)	152(9)
Au28/Zn28	327(6)	*U*11	452(10)	0	*U*23	163(3)
Au29/ Zn29	319(9)	347(11)	503(11)	-28(7)	-14(4)	174(6)
Zn30/Ru30	445(15)	480(2)	539(18)	0	*U*23	240(10)
Zn31	345(12)	336(12)	464(12)	-12(9)	-17(9)	185(10)
Zn32	355(13)	319(17)	474(17)	20(13)	10(6)	160(9)
Zn33	388(18)	323(12)	439(15)	8(7)	15(13)	194(9)
Zn34	0.0310(17)	356(13)	501(17)	-4(6)	-7(13)	155(8)
Zn35	287(16)	278(11)	464(16)	-10(6)	-20(12)	143(8)
Zn36/Ru36	327(18)	*U*11	470(3)	0	*U*23	163(9)
Zn37/Au37	366(12)	*U*11	505(16)	0	*U*23	183(6)
Zn38/Ru38	369(15)	*U*11	488(18)	-10(6)	10(6)	169(14)
Au39/Zn39	341(6)	*U*11	468(10)	0	*U*23	171(3)
Ru40	327(13)	*U*11	440(2)	0	*U*23	164(6)
Zn41	680(3)	*U*11	430(3)	0	*U*23	338(14)
Zn42	670(3)	*U*11	500(3)	12(10)	-12(10)	500(3)
Zn43	370(2)	450(2)	520(2)	-8(8)	-17(15)	184(12)
Zn44	440(2)	*U*11	440(3)	0	*U*23	218(10)
Au45	424(11)	*U*11	510(3)	-4(5)	4(5)	239(10)
Zn45’	390(8)	*U*11	600(3)	-40(4)	40(4)	230(7)
Au46	240(6)	80(8)	350(6)	-25(19)	-50(4)	120(3)
Zn46’	220(2)	580(7)	790(7)	-120(5)	-450(10)	970(10)
Au47	343(4)	*U*11	492(6)	-7(2)	7(2)	174(5)

Au48	380(6)	366(5)	514(6)	-13(2)	-27(5)	190(3)
Au49	397(5)	349(4)	480(4)	3(3)	5(3)	177(4)
Zn50	295(17)	295(17)	38(3)	0.	*U*23	148(8)

References

[1] H. J. Westbrook, L. R. Fleischer, *Intermetallic Compounds*: *Principles and Practice*; John Wiley & Sons: West Sussex, **1995**; Vol. 1-2.

[2] P. Villars, L. D. Calvert, *Pearson's Handbook of Crystallographic data for Intermetallic Phases*, 2nd ed.; ASM International: Metals Park, OH, **1991**.

[3] R. Nesper, *Angew Chem*. **1991**,*103*, 805-834; *Angew. Chem.*, *Int. Ed. Engl.* **1991**, *30* (7), 789-817.

[4] G. J. Miller, *Eur. J. Inorg. Chem.* **1998,** 523-536.

[5] C. Lee, G. J. Miller; *J. Am. Chem. Soc.* **2000**, *122*, 4937-4947.

[6] R. Nesper, *Prog. Solid State Chem.***1990**, *20*, 1-45.

[7] C .Belin, M. Thillard-Charbonnel, *Coord. Chem. Rev.* **1998**, *178-180*, 529-564.

[8] F. Studt, F. Abild-Pedersen, T. Bligaard, R. Z. SØrensen, C. H. Christensen, J. K. NØrskov, *Science*, **2008**, *320*, 1320-1322.

[9] J. D. Corbett, *Struct. Bonding (Berlin)* **1997**, *87*,157 - 193.

[10] C. H. E. Belin, R. C. H. Belin, *J. Solid State Chem*. **2000** *151*, 85.

[11] A. Johansson, H. Ljung, S. Westman, *Acta Chem. Scand*. **1968**, *22*, 2743.

[12] G. Nover, K. Schubert, *J. Alloys Comp*. **1980**, 75, 51.

[13] A. Johansson, S. Westman, *Acta Chem. Scand* **1970**, *24*, 3471.

[14] G. P. Tiwari, R. V. Ramanujan, *J. Mater. Sci*. **2001**, 36, 271-283.

[15] T. B. Massalski and H. Mizutani, *Prog. Mat. Sci*. **1978**, *22*, 151.

[16] W. Hume-Rothery, *J. Inst. Metals* **1926**, *35*, 295.

[17] W.Hume-Rothery, G. W. Mabbott and K. M. Channel-Evans, *Phil. Trans. R. Soc. A*, **1934**, *233*, 1.

[18] W. Hume-Rothery, G. V. Raynor, *The Structure of Metals and Alloys* (Institute of Metals, London, **1954**).

[19] L. Pauling, J. Ewing, *Reviews of Modern Physics* **1948**, 20, 112.

[20] G. D. Preston, *Phil. Mag*. **1928**, *5*, 1207.

[21] A. Westgren, G. Phragmen, *Phil. Mag*. **1928**, *5*, 280.

[22] K. H. J. Buschow, P. van Engen, R. Jongebreur, *J. Mag. Mater*. **1983**, *38*, 1.

[23] A. J. Bradley, J. Thewlis, *Proc. Roy. Soc. London* **1926**, *112A*, 678.

[24] A. Westgren, G. Phragmen, *Z. Metallkde* **1926**, *18*, 279.

[25] A. Westgren, G. Phragmen, *Trans. Faraday Soc*. **1929**, 25, 379.

[26] H. Jones, *Proc. Phys. Soc*. **1937**, *49*, 250.

[27] N. F. Mott, H. Jones, *The Theory of the Properties of Metals and Alloys* (Dover, New York, **1958**).

[28] T. Takeuchi, H. Sato, U. Mizutani, *J. Alloys Comp*. **2002**, *342*, 355.

[29] H. Sato, R. S. Toth, *Phys. Rev. Letters* **1962**, *8*, 239.

[30] R. Asahi, H. Sato, T. Takeuchi, U. Mizutani, *Phys. Rev*. 2005, *B71*, 165103.

[31] A. T. Paxton, M. Methfessel, D. G. Pettifor, *Proc. Roy. Soc. Lond.***1997**, *A453,* 1493*.*

[32] G. T. de Laissardi`ere, D. N. Manh, L. Magaud, J. P. Julien, F. Cyrot-Lackmann, D. Mayou, *Phy. Rev*. **1995**, *B52*, 7920.

[33] U. Mizutani, T. Takeuchi, H. Sato, *Prog. Mat. Sci*. **2004**, *49*, 227.

[34] R. Asahi, H. Sato, T. Takeuchi, U. Mizutani, *Phys. Rev*. **2005**, *B72*, 125102.

[35] A. J. Morton, *Phys. Status Solidi (a)* **1977**, *44*, 205.

[36] A. J. Morton, *Phys. Status Solidi (a)* **1976**, *33*, 395.

[37] A. J. Morton, *Acta Metallurgica* **1979**, *27*, 863.

[38] S. Thimmaiah, *Dissertation, Philipps-Universitat Marburg*, **2005**.

[39] Y. Koyama, J. Yoshida, H. Hoshiya, Y. Nakamura, Phy. Rev. **1989**, *B40*, 5378.

[40] Y. Koyama, M. Hatano, M. Tanimura*, Phy. Rev*. **1996**, *B53*, 11462.

[41] B. Grushko, E. Kowalska - Strzęciwilk, B. Przepiórzyński, M. Surowiec, *J. Alloys Comp*. **2005**, *402*, 98.

[42] Z. Moser, L. A. Heldt, *J. Phase Equilib*. **1992**, *13(2)*, 172.

[43] H. Le Chaterier, *Comp. Rend. Acad. Sci*. **1895**,*120*, 835-837.

[44] N. -Y. Tang, X. B. Yu, *J. Phase Equilib*. **2005**, *26(1)*, 50.

[45] G. Reumont, P. Perrot, *J. Phase Equilib*. **2003**, *24(1)*, 50.

[46] H. Hartmann, W. Hofmann, D. Müller Abandl, *Braunschweig. Wiss. Ges*. **1955**, *7*,100 (in German).

[47] A. R. Harding, G. V. Raynor, *J. Inst. Met.* **1952**, *80*, 446.

[48] T. Heumann, *Z. Metallkd*. **1948**, *39*, 45(in German).

[49] H. Hanemann, *Z. Metallkd* **1940**, *32*, 91(in German).

[50] Y. Liu, X. P. Su, F. C. Yin, *et al*., Int. *J. Mater. Res*. **2008**, *06*, 669.

[51] M. R. Ai, F. C. Yin, Y. Liu, *et al*., *Int. J. Mater. Res*. **2008**, *02*, 138.

[52] V.-H Edström, S. Westman, *Acta Chem. Seand*. **1969**, *23*, 279-285.

[53] O. Gourdon, G. J. Miller, *Chem. Mater*. **2006**, *18*, 1848-1856.

[54] O. Gourdon, Z. Izaola, L. Elcoro, V. Petricek, G. J. Miller Philos. Mag. **2006**, *86*, 419 -425.

[55] C. Allio, *Dissertation, Philipps-Universitat Marburg*, **2010**.

[56] C. H. E. Belin, R. C. H. Belin, *J. Solid State Chem*. **2000**, *151*, 85-95.

[57] P. C. Canfield, Z. Fisk*, Phil. Mag*.**1992**, *B65*, 1125.

[58] M. G. Kanatzidis, R. Pöttgen, W. Jeitschko, *Angew. Chem*, *Int. Ed. Engl*.**2005**, *44*, 6996.

[59] M. Boström, S. Hovmöller *J. Alloys Comp*. **2001,** *314*,154.

[60] M. A. Zhuravleva, X. Wang, A. J. Schultz, T. Bakas, M. G. Kanatizidis, *Inorg. Chem*. **2002**, *41*, 6056.

[61] R. Belin, M. Tillard, L. Monconduit, *Acta Crystallogr.* **2000**, *C56*, 267.

[62] Philips Analytical, X'Pert Plus (1.0) **1999** (Almelo).

[63] Program Package for X-ray Diffraction. Version 2.75, Stoe & Cie., Darmstadt (Germany) **1996**.

[64] G. M. Sheldrick, SHELX-97-A Program Package for the Solution and Refinement of Crystal Structures, Universität Göttingen (Germany) **1997**.

[65] V. Petricek, M. Dusek, L. Palatinus, JANA2000. The Crystallographic Computing System,Institute of Physics, Praha, Czech Republic, **2000**.

[66] X-RED (1.02)–Data Reduction Program, Stoe & Cie., Darmstadt (Germany) **2001**.

[67] X-SHAPE (2.01)–Crystal Optimization for Numerical Absorption Correction, Stoe & Cie., Darmstadt (Germany) **2001**.

[68] W. Massa, Crystal Structure Determination (Springer-Verlag, Germany, **2004**), second edn.

[69] Voyager (4,0), Thermo Noran (USA), **1999**.

[70] M. Hansen, *Constitution of Binary Alloys*, McGraw-Hill, **1958**, 572.

[71] P. J. Brown, *Acta Cryst*. **1962**, *15*, 608.

[72] H. Okamoto, T. B. Massalski, *Bull. Alloy Phase Daigrams* **1989**,*10*, 59.

[73] W. B. Pearson *J. Less-Common Metals* **1979**, *68*, 9.

[74] J. P. Pemsler, E. J. Rapperport *Metall. Trans.* **1971**, *2*, 79.

[75] T. B. Massalski, W. H. King. *Acta Metall.* **1962**, *10*, 1171.

[76] H. Iwasaki, M. Hirabayashi, K. Fujiwara, D. Watanabe, S. Ogawa. *J. Phys. Soc. Jpn*. **1960**, *15*, 1771.

[77] R. J. Vogel. *Anorg. Chem.* **1906**, *48*, 319.

[78] H. Iwasaki, *J. Phys. Soc. Japs.* **1962**, *17*, 1620-1633.

[79] E. A. Owen, E. A. O'Donnell Roberts, *J. Inst. Met*. **1945**, *71*, 213-254.

[80] M. Wilkens, K. Schubert, *Z. Metallkd.***1958**, *49*, 633-646.

[81] H. Iwasaki, *J. Phys. Soc. Japs.* **1959**, *14*, 1456.

[82] H. Ipser, A. Mikula, P. Terzieff,. *Monatsh. Chem.* **1983**, *114*, 1177-1184.

[83] E. A. Owen, G. D. Preston, *Philos. Mag*. **1926**, *2*, 1266-1270

[84] Y. H. Liu, C. C. Hsu, *Sci. Sin.* **1957**, *6*, 1013-1030.

[85] Y. Matsuo, S. Minamigawa, K. Katada,. *Trans. Jpn. Met.* **1981**, 22, 367-368.

[86] K. Krompholz, A. Weiss, *J. Less-Common Met*. **1976**, *50*, 213-222.

[87] H. Iwasaki, T. Uesugi, *J. Phys. Soc. Japs.* **1968**, *25*, 1640-1646.

[88] E. Günzel, K. Schubert, *Z. Metallkd.* **1958**, *49*, 234-235.

[89] D. A. Davies, E. A. Owen, *Br. J. Appl. Phys.* **1964**, 15, 1309-1314.

[90] R. Prasad, M. Bienzle, F. Sommer *J. Alloy Compd.* **1993**, *200*, 69.

[91] H. Ipser, R. Krachler. *Scripta Metall.* **1988**, *22*, 1651.

[92] H. S. Liu, K. Ishida, Z. P. Jin, Y. Du *Intermetallics* **2003** *11* 987-994.

[93] W. Köster, U. Zwicker, in: "*Festschrift aus Anlaß des 100-jährigen Jubiläums der Firma* W.C. Heraeus GmbH", Hanau, **1951**, 76.

[94] H. Nowotny, E. Bauer, A. Stempfl *Monatsh*. *Chem*. **1951**, *82*, 1086-1093.

[95] K. M. Alasafi, T. Chattopadhyay, K. Schubert *J. Less-Common Met*. **1978**, *59*, 41-50.

[96] T. B. Massalski, *Binary Alloy Phase Diagrams*, ASM International, Ohio, USA **1996**, CD-version.

[97] M. Armbrüster, *diploma thesis*, Philipps-Universität Marburg, **2001**.

[98] S. Thimmaiah, G. J. Miller, *Chem. Eur. J.* **2010**, *16*, 5461-5471.

[99] O. Gourdon, Z. Izaola, L. Elcoro, V. Petricek, G. J. Miller, *Inorganic Chem*. **2009**, *48*, 9715-9722.

[100] H. Nowotny, H. Bittner, *Monatsh*. *Chem*. **1950**, *81*, 679-680.

[101] H. Nowotny,E. Bauer, A. Stempfl, *Monatsh*. *Chem*. **1950**, *81*, 679-680.

[102] H. H. Stadelmaier, W. K. Hardy, *Z. Metallkd*. 1961, 52, 391-396.

[103] Y. Miyoshi, H. Odasima, Y. Shindho, M. Yoshida, T. Kamanaru, *Nippon Steel Technical Report No. 57*, **1993**, 16 - 21 April, pp.16-21

[104] T. Ichida, *Galvatech'95 Conference Proceedings*, *Iron and Steel Society*, Chicago, **1995**, pp. 359-369.

[105] L. Guzman, M. Adami, W. Gissler, S. Klose, S. De Rossi, *Surf. Coat. Technol*. **2000**, *125*, 218-222.

[106] Tz. Boiadjieva, K. Petrov, H. Kronberger, A. Tomandl, G. Avdeev, W. Artner, T. Lavric, M. Monev, *J. Alloys Compd.* **2009**, *480*, 259-264.

[107] *US Patent* **1996**, 5, 510, 196.

[108] *US Patent* **2004**, 6, 682, 828 B2.

[109] C. Scott, C. Oliver, A. Lamande, P. Choquet, D. Chaleix, *Thin Solid Films* **2003**, *436*, 232-237.

[110] J. K. Brandon, R. Y. Brizard, P.C. Chieh, R. K. McMillam, W. B. Pearson, *Acta Crystallogr*. *Sect*. *A***1974**, *30*, 1412-1417.

[111] S. Westman, *Acta Chem. Scand*. **1965**, *19*, 1411-1419.

[112] (a) A.J. Bradley, S. S. Lu, *Z. Kristallogr*. **1937**, *96*, 20-37;

(b) J. W. Visser, *Acta Cryst*. **1977**, *B33*, 316;

(c) Y. Koyama, J. Yoshida, H. Hoshiya, Y. Nakamura, *Phys. Rev*. **1989**, *B40*, 5378 -5386.

[113] C. Janot, *Quasicrystals: A Premier, Clarendon Press, Oxford*, **1994**.

[114] N. Tamura, *Philos. Mag. A* **1997**, *76*, 337-356.

[115] F. C. Frank, J. S. Kasper, Acta Cryst. **1958**, *11*, 184-190.

[116] F. C. Frank, J. S. Kasper, *Acta Cryst*. **1959**, *12*, 483-499.

[117] S. Samson, *Nature* **1962**, *195*, 259-263.

[118] S. Samson, *Acta Crys*. **1965**, *19*, 401-413.

[119] S. Samson, *Acta Crys*. **1967**, *23*, 686-600.

[120] T. Weber, J. Dshemuchadse, M. Kobas, M. Conrad, B. Harbrecht, W. Steurer. *Acta Cryst*. **2009**, *B65*, 1-10.

[121] P. Pearce, *Structure in Nature is a Strategy for Design*, **1978**. MIT Press.

[122] W. Hornfeck, S. Thimmaiah, S. Lee, B. Harbrecht, *Chem. Eur. J*. **2004**, *10*, 4616-4626.

[123] E. H. Kisi, J. D. Browne, *Acta Crys*. **1991**, *B47*, 835-843.

[124] J. Braun, M. Ellner, B. Predel, *J. Alloys Compd*. **1992**,*183*, 444-448.

[125] W. Hornfeck, S. Freistein, B. Harbrecht, *Z. Anorg. Allg. Chem*. **2004**, *630*, 1730.

[126] J. T. Schmidt, S. Lee, D. C. Fredrickson, M. Conrad, J. Sun, B. Harbrecht, *Chem. Eur. J*. **2007**, *13*, 1394-1410.

[127] H. M. Rietveld*, Acta Crystallogr*. **1967**, *22*,151-152.

[128] H. M. Rietveld, *J. Appl. Crystallogr*. **1969**, *2*, 65-71.

[129] S. Thimmaiah, K. W. Richter, S. Lee, B. Harbrecht, *Solid State Sci*. **2003**, *5*, 1309-1317.

[130] B. Harbrecht , S. Thimmaiah, M. Armbrüster, S. Lee, C. Pietzonka, *Z. Anorg. Allg. Chem*. **2002**, *628*, 2744-2749.

[131] A. J. Bradley, P. Jones, *J. Inst. Met*. **1933**, *51*, 131-162.

[132] B. Chabot, K. Cenzual, E. Parthe, *Acta Crys*. **1981**, *A37*, 6-11.

[133] R. F.Berger, S. Lee, J. Johnson, B. Nebgen, A.C.Y. So, *Chem. Eur. J*. **2008**, *14*, 6627-6639.

[134] T. Nasch, W. Jeitschko, *J. Solid State Chem*. **1999**, *143*, 95-103.

[135] W. B. Pearson, *The Crystal Chemistry and Physics of Metals and Alloys*, Wiley – Interscience: New York, **1972**, pp80 - 133.

[136] D. G. Pettifor, *Bonding and Structure of Molecules and Solids*, Oxford Science Publications: Oxford, **1995**.

[137] O. Gourdon, D. Gout, J. Williams, T. Proffen, S. Hobbs, G. J. Miller, *Inorg. Chem.* **2007**, *46*, 251-259.

[138] N. Gross, G. Kotzyba, B. Kunnen, W. Jeitschko, *Z. Anorg. Allg. Chem*. **2001**, *627*, 155.

[139] L. Arnberg, S. Westman, *Acta Chem. Scand*. **1972**, *26*, 513.

[140] A. J. Morton, *Phys. Status Solidi A* **1974**, *23*, 275.

[141] S. Thimmaiah, M. Conrad, S. Lee, B. Harbrecht, *Z. Anorg. Allg. Chem*. **2004**, *630*, 1762.

[142] S. Mahne, B. Harbrecht, *J. Alloys Compd*. **1994**, *203*, 271-279.

[143] V. Pavlyuk, P. Solokha, O. Zelinska, V. Paul-Boncour, A. Nowik-Zajak, *Acta Crys. C* **2008**, *C64*, i50 - i52.

[144] A. S. Koster, J. C. Schoone, *Acta Crystallogr. Sect. A* **1981**, *37*, 1905-1907.

[145] P. P.Jana, O. Zelinska, L. Gulay, Cl. Pietzonka, B. Harbrecht, *Unpublished results*.

[146] R. Nesper, H. -G. von Schnering, *J. Solid State Chem*. **1987**, *70*, 48-57.

[147] E. Hellner, E. Koch, *Acta Crystallogr. Sect. A* **1981**, *37*, 1-6.

[148] H. A. Schwarz, *Gesammelte mathematische Abhandlungen I*, Springer, Berlin, **1980**.

[149] D. C. Fredrickson, S. Lee, R. Hoffmann, *Angew. Chem*. **2007**, *119*, 2004-2023; *Angew. Chem. Int. Ed*. **2007**, *46*, 1958-1976.

[150] A. F. Wells, *Structural Inorganic Chemistry,* 5th ed., 1332, Oxford University

Press(Clarendon), London **1984,** p. 1312.

[151] A. Westgren, G. Phragme´n, *Metallwirtsch.Metallwiss. Metalltech*. **1928**, *7*, 700–703.

[152] F. Bonhomme, K. Yvon, *J. Alloys Compd*. **1995**, *227*, L1–L3.

[153] M. L. Fornasini, B. Chabot, E. Parthe, *Acta Crys. B* **1978**, *34*, 2093–2099.

[154] L. Arnberg, A. Jonsson, S. Westman, *Acta Chem. Scand*. **1976**, *30*,187–192.

[155] S. Lidin, M. Jacob, A.-K. Larsson, *Acta Crystallogr. Sect. A* **1994**, 50, 340-342.

[156] G. F. Bastin, F. J. J. van Loo, and G. D. Rieck, *Z. Metall*. **1974**, *65*, 656.

[157] G. Kreiner, H. F. Franzen, *J. Alloys Compd.* **1995**, *221*, 15–36.

Acknowledgments

I would like to express my heartfelt gratitude to Prof. Dr. B. Harbrecht for giving me the opportunity to join his group, for his essential scientific and personal support, and for his participation in the preparation of this thesis.

I would also thank Prof. Dr. W. Massa for taking on the task of co-examiner.

My sincere thanks go to Dr. L. D. Gulay for introducing me into broad field of crystallography and essential support and suggestions he gave me whenever I encountered problems in this domain.

My best thanks go to my co-workers for being friendly during this project.
I would like to thank C. Pietzonka for magnetic susceptibility and S. Zöreb for resistivity measurement.
Special thanks to A. Authmann for giving me helpful comments.
I express a very special gratitude to my friends Aurab Chakrabarty, Bidraha Bagh, Pradipta Mandal for giving me important advices.

Last but not the least I thank undergraduate students, especially for partial experimental support for this project.

“DFG for my financial support”.

Declaration

I declare that I myself wrote this study and carried out the experimental work described in it, without using any other sources and aids than those that are stated.

Marburg, July, 2011

Curriculum Vitae
Partha Pratim Jana

Personal Data:

Permanent Address

Date of Birth: 21st, April 1983.

Gender: Male

Nationality: Indian

Language: English, Hindi, Bengali.

Fachbereich Chemie

Philipps-Universit¨at

Hans-Meerwein-Straße

D-35032 Marburg

janap@staff.uni-marburg.de

Education:

2007,Nov.-2011,June	Ph D:Philipps Universität,Marburg Advisor: Prof. Dr. Bernd Harbrecht, Institute of Inorganic Chemistry, University of Marburg, Germany.
(Jan.-May.) 2007:	M. Sc. Project Thesis Title: ``**Reduction of α, β-unsaturated carbonyl compounds by palladium(II) and nickel(II) complexes having nitrogen-containing ligands´´** **Advisor:** Prof. Dr. Jubaraj B. Baruah, Department of Inorganic Chemistry, Indian Institute of Technology Guwahati (IITG), India**.**
2005-2007:	M. Sc. (Chemistry), Indian Institute of Technology Guwahati (IITG), India.
2001-2005:	B. Sc. (Honours in Chemistry, 1st Class), University of Calcutta, India.

Publications:

1. Reduction of α, β-unsaturated carbonyl compounds by palladium (II) and nickel(II) complexes having nitrogen-containing ligands

Partha P. Jana, Rupam Sarma and Jubaraj B. Baruah

Journal of Molecular Catalysis A. **2008**, *289*, 57-60.

2. Spatially correlated disorder phenomena inbinary complex metal alloy

Partha Pratim Jana, Oksana Zelinska, Lubomir Gulay, Clemens Pietzonka**,** Bernd Harbrecht manuscript in preparation.

Poster Presentation:

1. "Spatially Correlated structural Disorder Phenomena in the Complex Zinc-Rich Alloy"

Partha P. Jana, Lubomir Gulay, Bernd Harbrecht

6_{th} International Conference on Inorganic Materials, **2008**, Dresden, Germany.

Fellowships & Awards:

PhD fellowship, University of Marburg (November 2007 to June 2011)

Summer internship:

(30_{th} August-12_{th} Sept 2009)

The Zürich School of Crystallography, University of Zürich, Switzerland

(26_{th} September-02_{th} Oct 2010)

International School on Aperiodic crystals, Carqueiranne, France